Lubricated MEMS

Effects of Boundary Slippage and Texturing

Mohammad Tauviqirrahman

De promotiecomissie is als volgt samengesteld:

prof.dr. G.P.M.R. Dewulf	Universiteit Twente	voorzitter en secretaris
prof.dr.ir. D.J. Schipper	Universiteit Twente	Promotor
dr.ir. J. Jamari	University of Diponegoro	Assistent-Promotor
prof.dr.ir. A.J. Huis in ‘t Veld	Universiteit Twente	
prof.dr. J.G.E. Gardeniers	Universiteit Twente	
prof.dr.ir. R. Larsson	Luleå University of Technology, Sweden	
prof.dr.ir. S. Franklin	University of Sheffield, UK	

LUBRICATED MEMS: EFFECTS OF BOUNDARY SLIPPAGE AND TEXTURING
Tauviqirrahman, Mohammad
Ph.D. Thesis, University of Twente, Enschede, The Netherlands
November 2013

ISBN: 978-90-365-1916-8

Keywords: lubrication, MEMS, slip, texturing

Printed by Ipskamp Drukkers B.V., Enschede, The Netherlands

LUBRICATED MEMS

EFFECTS OF BOUNDARY SLIPPAGE AND TEXTURING

PROEFSCHRIFT

ter verkrijging van
de graad van doctor aan de Universiteit Twente,
op gezag van de rector magnificus,
prof.dr. H. Brinksma,
volgens besluit van het College voor Promoties
in het openbaar te verdedigen
op donderdag 7 november 2013 om 14.45 uur

door

Mohammad Tauviqirrahman
geboren op 20 Mei 1981
te Rembang, Indonesia

Dit proefschrift is goedgekeurd door:
de promotor: prof.dr.ir. D.J. Schipper
de assistent-promotor: dr.ir. J. Jamari

Summary

Many types of micro-electro-mechanical-system (MEMS) based products are currently employed in a variety of applications. Recently, there has been an increase in the demand for higher reliability of MEMS which incorporate moving parts for each intended application. This is because the reliability of MEMS containing moving parts is poor and has a limited lifetime. Applying a lubricant to these systems to avoid wear hampers the movement due to the adhesive/surface forces, leading to stiction. By modifying the contacting surfaces, one is able to enhance the behavior of surfaces in a controlled way and thus alter the flow pattern in the liquid lubricating film for an enhanced performance. In this thesis, the concept of complex slip surface (CSS) as an artificial (deterministic) boundary slip surface is introduced. The thesis examines the exploitation of the artificial boundary slip to improve the performance of liquid lubricated-MEMS, with the emphasis on increasing the load support and reducing the coefficient of friction. Therefore, it is of great importance to get a clear view of the concept of the artificial boundary slip with respect to the performance of lubricated-MEMS.

A main principle of fluid film lubrication, as well as a touchstone of the Reynolds equation, is that there is no boundary slip of the liquid lubricant along the two solid surfaces. As a result, lubrication with boundary slip cannot be analyzed by the classical Reynolds equation, which specifically excludes the possibility of slip. The aim of the present work is to build a modified form of the Reynolds equation in which boundary slip is allowed to occur on both of the opposing surfaces. Two different models of boundary slip are discussed, namely: the two-component slip model and the critical shear stress model. The first model assumes that boundary slip will occur when the shear stress at the surface reaches a critical value, and, once the slip begins, that it takes place at a constant slip length. This model is adopted to incorporate some possible slip directions, as well as slip velocities directly.

The second model, the critical shear stress model, is based on the assumption that there is a critical shear stress on the liquid-solid interface. No slip occurs at the interface if the surface shear stress is less than the critical shear stress, but the slip takes place if the shear stress reaches the point of critical shear stress. The modified Reynolds equation with the critical shear stress model that was developed in the current work is based on the assumption that a slip is treated to occur both at the stationary and the moving surface. The model is converted to a finite volume form and solved by tri-diagonal-matrix-algorithm (TDMA) combined with alternating-direction-implicit (ADI) scheme. In this way, the model is able to incorporate the influence of boundary slip on the lubrication performance of MEMS, while keeping the computational time within a reasonable range. The model is validated through experimental work published in the literature.

In the present work, the artificial boundary slip is developed both for smooth and artificial textured surfaces. In order to find an optimal artificial slip configuration for a hydrodynamic contact with respect to the maximum load support, two optimization procedures are examined for various film height distributions. The first is conducted using a genetic algorithm search/optimization method, so that the geometrical parameter of the

optimum slip is obtained. A second approach is performed using a parametric study, in which slip parameters are varied over a large range of values considering different performance parameters. This research also investigates the interplay of slippage and texturing interaction with respect to lubrication performance. A range of parameters such as critical shear stress, slip zone, slip length, texturing zone and texture cell aspect ratio are analyzed.

It is shown that a surface with an optimized complex slip surface (CSS) pattern in a lubricated contact is beneficial compared to a surface without slip, i.e. high hydrodynamic pressure (and thus the load support) and low friction. The effect of an optimized CSS pattern on the hydrodynamic performance is most effective with respect to the maximum load support for parallel sliding surfaces if (1) the critical shear stress on the slip surface is designed as low as possible (2) slip is applied only on the stationary surface. In the case of combined textured slip pattern, it is shown that the load support hardly depends on the texture cell aspect ratio. Slip is much more effective in generating pressure than texturing. The numerical analysis also shows that there is a unique threshold value of the critical shear stress for every texture cell aspect ratio. It is also demonstrated that partial texturing gives better improvement in lubrication performance than full texturing. In general, in the absence of the wedge effect, if compared to a complex slip smooth surface, a partially textured surface is still less efficient at enhancing load support and/or at decreasing friction coefficient, even if this textured configuration is combined with a slip condition.

This thesis is divided into two parts. The first part concerns the modeling aspects and the methodology used to derive a modified form of the Reynolds equation capable of including wall slip boundary conditions. The second part is devoted to the details of individual research papers. This enables the reader is able to obtain a clear understanding of the overall purpose of the research by reading the first part while the second part elucidates the details.

Samenvatting

Verschillende soorten producten, voorzien van een micro-elektro-mechanisch-systeem (MEMS), worden toegepast in velerlei gebieden. De eisen met betrekking tot de betrouwbaarheid van MEMS met bewegende onderdelen neemt meer en meer toe. Tot op heden is de betrouwbaarheid van een MEMS met bewegende onderdelen slecht. Ook heeft een MEMS voorzien van contact makende onderdelen vaak een korte levensduur. Het gebruik van een smeermiddel in dergelijke systemen met als doel slijtagevermindering beperkt de beweging van de onderdelen als gevolg van oppervlakte krachten. Dit resulteert in een probleem dat stictie wordt genoemd. Door de oppervlakken te modificeren kan dit op controleerbare wijze worden voorkomen. In dit proefschrift wordt het concept van een complexe slip oppervlak (CSS), een kunstmatig deterministisch slip oppervlak, geïntroduceerd. De toepassing van een dergelijk CSS is onderzocht met betrekking tot de prestaties van vloeistof gesmeerde MEMS. Hierbij ligt de nadruk op het verhogen van het belasting dragend vermogen en verlagen van de wrijvingscoëfficiënt.

Een basis principe van de volle film smering, en de basis voor de Reynolds vergelijking, is dat er geen slip tussen de vloeistof en de twee oppervlakken optreedt. Dientengevolge, kan smering met oppervlakte slip niet worden geanalyseerd met de klassieke Reynolds vergelijking, omdat deze de mogelijkheid van slip aan het oppervlak uitsluit. In dit onderzoek is een gemodificeerde Reynolds vergelijking afgeleid waarbij oppervlakte slip is toegestaan aan beide oppervlakken. Twee verschillende modellen van oppervlakte slip zijn besproken, te weten het twee componenten slip model en het kritische schuifspanningsmodel. Het eerste model neemt aan dat oppervlakte slip zal optreden wanneer de schuifspanning aan het oppervlak een kritische waarde bereikt. Verder wordt er aangenomen dat, als oppervlakte slip begint, deze gaat plaats vinden met een constante slip lengte. Dit model is toegepast om mogelijke slip richtingen en oppervlakte slip snelheden te integreren. Het tweede model, het kritische schuifspanningsmodel, is gebaseerd op de aanname dat er een kritische schuifspanning aanwezig is op de interface tussen de vloeistof en het oppervlak. Er zal geen oppervlakte slip optreden wanneer de schuifspanning aan het oppervlak lager is dan de kritische schuifspanning. Oppervlakte slip zal wel optreden als de schuifspanning hoger wordt dan de kritische schuifspanning. De, in dit werk afgeleide gemodificeerde Reynolds vergelijking op basis van het kritische schuifspanning model, is gebaseerd op de aanname dat oppervlakte slip plaats kan vinden aan zowel het bewegende en stilstaande oppervlak. Het model is omgezet naar een model op basis van eindige volume elementen en opgelost middels een tridiagonaal-matrix-algoritme (TMDA) gecombineerd met het alternating-direction-implicit (ADI) schema. Met dit model is het mogelijk de invloed van oppervlakte slip op de prestaties van gesmeerde MEMS mee te nemen terwijl de rekentijden binnen de perken blijven. Het model is gevalideerd met experimentele resultaten gepubliceerd in de literatuur.

In het huidige werk is het model toegepast op gladde en getextureerde oppervlakken. Voor het vaststellen van een optimale configuratie van het CSS voor een hydrodynamisch gesmeerd contact met betrekking tot maximaal draagvermogen zijn er twee optimalisatietechnieken onderzocht voor verschillende filmhoogte verdelingen. De eerste optimalisatiemethode maakt gebruik van genetische algortihmen (GA). Hierbij wordt een geometrische parameter vastgesteld, zodanig dat de oppervlakte slip optimaal is voor het creëren van draagvermogen. De tweede methode is een parameter studie waarin de oppervlakte slip parameters zijn gevarieerd met betrekking tot de smeringsprestaties. In dit onderzoek is ook het samenspel tussen oppervlakte slip en texturering met betrekking tot de smeringsprestaties onderzocht. In de parameterstudie is de invloed van verschillende parameters is onderzocht zoals de kritische schuifspanning, slip zone, slip lengte, textuur zone en de afmetingen van de eenheidscel van de textuur op het oppervlak.

Het is aangetoond dat een oppervlak met een geoptimaliseerd complex slip oppervlak (CSS) in een gesmeerd contact gunstig is met betrekking tot hydrodynamische drukopbouw (meer draagvermogen) en lagere wrijving in vergelijking met een oppervlak zonder oppervlakte slip. Het effect van een geoptimaliseerd CSS op de hydrodynamisch prestatie (draagvermogen) is het meest effectief voor parallel glijdende oppervlakken als 1) de kritische schuifspanning op het slip oppervlak zo laag mogelijk is en 2) dat de oppervlakte slip enkel wordt gerealiseerd op het stilstaande oppervlak. Bij een combinatie van oppervlakte slip en texturering blijkt het draagvermogen nauwelijks afhankelijk te zijn van de afmetingen van de eenheidscel van de textuur. Tevens blijkt oppervlakte slip veel effectiever in het genereren van drukopbouw dan texturering. De numerieke analyse geeft aan dat er een unieke drempelwaarde is voor de kritische schuifspanning bij een bepaalde afmeting van de eenheidscel van de textuur. Ook is aangetoond dat een gedeeltelijke texturering een beter smeringsgedrag tot gevolg heeft dan volledige texturering van het oppervlak. In het algemeen, bij afwezigheid van het wig effect, kan gesteld worden dat een glad CSS beter presteert dan een gedeeltelijk getextureerd oppervlak met betrekking tot draagvermogen en lage wrijving, zelf als dit getextureerde oppervlak voorzien wordt van oppervlakte slip.

Dit proefschrift is opgedeeld in twee delen. Het eerste deel betreft modelleringsaspecten en de gehanteerde methode om de gemodificeerde Reynolds vergelijking, rekening houdend met oppervlakte slip, af te leiden. Het tweede deel van het proefschrift is gewijd aan gepubliceerde papers waarin in detail op aspecten, behandeld in het eerste deel, wordt ingegaan. Hierdoor is de lezer in staat om inzicht te verkrijgen in de behaalde resultaten.

Contents

Part I

Part II List of Appended Papers

Paper A:

M. Tauviqirrahman, R. Ismail, Jamari, D.J. Schipper, 2013, "Optimization of the complex slip surface and its effect on the hydrodynamic performance of two-dimensional lubricated contacts", Computers and Fluids, Volume 79, pp. 27 – 43.
doi: 10.1016/j.compfluid.2013.02.021.

Paper B:
M. Tauviqirrahman, R. Ismail, Jamari, D.J. Schipper, 2013, "Study of surface texturing and boundary slip on improving the load support of lubricated parallel sliding contacts", Acta Mechanica, Volume 224, Issue 2, pp. 365 – 381. doi: 10.1007/s00707-012-0752-7.

Paper C:
M. Tauviqirrahman, Muchammad, Jamari, D.J. Schipper, 2013, "Numerical study of the load carrying capacity of lubricated parallel sliding textured surfaces including wall slip", accepted for publication in STLE Tribology Transactions.

Paper D:
M. Tauviqirrahman, R. Ismail, Jamari, D.J. Schipper, 2013, "Computational analysis of the lubricated-sliding contact with artificial slip boundary", International Journal of Applied Mathematics and Statistics, Volume 35, Issue 5, pp. 67 – 80.

Paper E:
M. Tauviqirrahman, R. Ismail, Jamari, D.J. Schipper, 2011, "Optimization of partial slip surface at lubricated-MEMS", Proceedings of 2nd International Conference on Instrumentation, Control and Automation, Issue date: 15-17 Nov., pp. 375 – 379, ISBN: 978-1-4577-1460-3, IEEE Catalog Number: CFP1179P-DVD.
doi: 10.1109/ICA.2011.6130190.

Paper F:
M. Tauviqirrahman, R. Ismail, Jamari, D.J. Schipper, 2011, "Effect of boundary slip on the load support in a lubricated sliding contact", AIP (American Institute of Physics) Conference Proceedings, Volume 1415, Issue 51, pp. 51 – 54. ISBN: 978-0-7354-0992-7. doi:10.1063/1.3667218.

Paper G:
M. Tauviqirrahman, Muchammad, Jamari, D.J. Schipper, 2013, "CFD analysis of artificial slippage and surface texturing in lubricated sliding contact", accepted for publication in Tribology International.

Paper H:
M. Tauviqirrahman, R. Ismail, Jamari, D.J. Schipper, 2013, "Combined effects of texturing and slippage in lubricated parallel sliding contact", Tribology International, Volume 66, pp. 274 – 281. doi: 10.1016/j.triboint.2013.05.014.

Nomenclature

Roman Symbols

b	slip length	[m]
d_c	cell length	[m]
d_h	dimple depth	[m]
d_l	dimple length	[m]
f	friction force per unit width	[N/m]
h	fluid film thickness	[m]
h_F	land film thickness	[m]
h_i	inlet film thickness	[m]
h_o	outlet film thickness	[m]
H	slope incline ratio	[-]
k	proportionality coefficient	[-]
l	total length of lubricated surface	[m]
l_s	length of the slip zone	[m]
l_{ts}	length of the textured slip zone	[m]
p	hydrodynamic pressure	[Pa]
u_w	sliding velocity	[m/s]
u_s	slip velocity	[m/s]
w	load support (or load carrying capacity) per unit width	[N/m]
x	coordinate parallel to surface	[m]
z	cross-film coordinate	[m]

Greek Symbols

α	slip coefficient	[m^2s/kg]
γ	shear rate	[1/s]
ε	relative dimple depth	[-]
η	dynamic viscosity	[kg/(m.s)]
λ	texture cell aspect ratio	[-]
μ	coefficient of friction	[-]
τ_c	critical shear stress	[Pa]
τ_{oc}	initial critical shear stress	[Pa]
ρ_T	texture density	[-]

Sub/Superscripts

i	input
o	output
a	top surface
b	bottom surface

Abbreviations

ADI	Alternating-Direction-Implicit
CSS	Complex Slip Surface
CSSM	Critical Shear Stress Model
HL	Hydrodynamic Lubrication
MEMS	Micro-Electro-Mechanical-System
SLM	Slip Length Model
TDMA	Tri-Diagonal-Matrix-Algorithm
1D	One-Dimensional
2D	Two-Dimensional

Dimensionless Parameters

B	b/h_o
F	$f\ h_o / (u_w \eta l)$
H	h_i/h_o
L_s	l_s/l
L_{ts}	l_{ts}/l
P	$p\, h_o^2 / \eta l u_w$
T_c	$\tau_c\, h_o / \eta u_w$
W	$w\, h_o^2 / (u_w \eta l^2)$
X	x/l
ε	d_h/h_F
λ	d_l/d_h
μ^*	F/W
ρ_T	d_l/d_c

Part I

Chapter 1

Introduction

Today, miniaturization and the rapid development of micro-electro-mechanical-systems (MEMS) have attracted a great deal of attention among worldwide researchers. MEMS based devices have offered significant technological advancement and have played important roles in many significant areas such as information/communication, electro-mechanical, chemical and biological applications. However, one main factor that limits the widespread development and reliability of MEMS is a high level of friction and wear [1, 2]. Furthermore, every type of MEMS device is susceptible to stiction [3].

Stiction is a problem which currently limits the development of MEMS devices and has limited the development of such devices ever since the advent of surface micromachining in the 1980s. In particular, stiction forces are created between moving parts that come into contact with one another, either intentionally or accidentally. As the overall size of a device is reduced, the applied force is not sufficient to overcome surface adhesion, as well as the capillary action of condensed liquid, which introduces 'high friction' in sliding. Consequently, the surfaces of these parts either temporarily or permanently adhere to each other causing malfunction or failure in the device.

Several approaches to solving the stiction problem between two opposing surfaces have been presented in the literature. The basic approaches to prevent stiction include increasing the surface roughness (topography) and/or lowering the solid surface energy by coating the surface with low surface energy materials. This includes self-assembled molecular (SAM) coatings, hermetic packaging and the use of reactive materials in the package [4].

Another promising way of tackling the stiction problem is by using a liquid lubricant between the interacting components of the device to separate the two surfaces and thus reduce the chance of stiction-type failures. However, it was initially believed that the hydrodynamic friction in small-scale devices was so high that it would make the liquid lubrication of MEMS unfeasible. In order for liquid lubrication to be effective in MEMS, the boundary friction must be controlled. Recently, the feasibility of lubrication using liquid in sliding MEMS was demonstrated both numerically and experimentally by some

researchers; see for an example [5-9]. Regarding the liquid lubrication of MEMS, it should be noted that the lubricant film should satisfy two requirements. First, it should be strong enough to carry the entire applied load to prevent direct contact between the surfaces and thus wear. Second, it should have low shear strength for low hydrodynamic friction. In this work the main focus will be on how to maximize the performance of lubrication, i.e. reducing the friction, as well as increasing the load support.

As is commonly known, based on classical hydrodynamic lubrication theory, the governing equations in a full fluid region can be described by the well-known Reynolds equation derived by Osborn Reynolds in 1886 [10] which, given the gap between the surfaces, combines the equations of momentum and continuity into a single equation for fluid pressure. This theory is well established and some important mechanisms for the generation of hydrodynamic pressure have been clearly revealed [11]. The hydrodynamic behavior of lubricated contacts is largely governed by the boundary conditions of the fluid flow. A main principle of fluid film lubrication is that there is no boundary slip condition, i.e. full wetting. In MEMS, this wetting is actually an unwanted effect because it can lead to the occurrence of liquid stiction and, as a result, the micro-parts cannot move [3].

A significant challenge to the development of MEMS lubrication is the problem of achieving proper tribological performance of their contacting and sliding parts [6, 12]. This is because the lubricant behavior is different at the micro-scale when compared to the macro-scale. There is a small clearance between the stationary and the moving components in the lubrication of MEMS devices, which induces the failure of the use of the classical lubrication theory. At the macroscopic level, it is well accepted that in most situations the boundary condition for a viscous fluid at a solid surface is no-slip, that is, the fluid velocity matches the velocity of the solid boundary. While the no-slip condition is accepted almost universally as the appropriate boundary condition to impose at a liquid-solid interface, it remains an assumption that is not based on physical principles. Recently, researchers have suggested that the generally accepted no-slip boundary condition may not be suitable at the micro-scale, for example, see [7, 8]. Thus, one point to be considered when analyzing liquid flows in MEMS is related to the liquid-solid boundary slip or the wettability of the bounding surface. Slip occurs when there is an adhesion failure between the lubricant and the bounding surface.

Boundary slip, which is an active research subject in physical and chemical sciences, has long been studied and recently has attracted tremendous interest from researchers. The concept of a boundary slip condition was first proposed by Navier [13] and is shown schematically in Figure 1.1. In the so-called slip length condition (or 'Navier' condition), the magnitude of the slip velocity, u_s, is proportional to the magnitude of the shear rate experienced by the fluid at the solid surface:

$$u_s = b \left. \frac{\partial u}{\partial z} \right|_{\text{surface}} \tag{1.1}$$

where $\partial u / \partial z$ is the local shear rate and b is the slip length which represents the level of boundary slip. Experimental observations [14-18], however, show that Eq. (1.1) cannot quantitatively describe the interfacial slip velocity. The experimental manifestation of boundary slip shows the existence of a critical shear stress. When the surface shear stress is below the critical shear stress, no slip occurs. When the surface shear stress reaches the

critical value, boundary slip occurs. Hence, it is more reasonable to adopt the critical shear stress criterion in modeling lubrication with boundary slip.

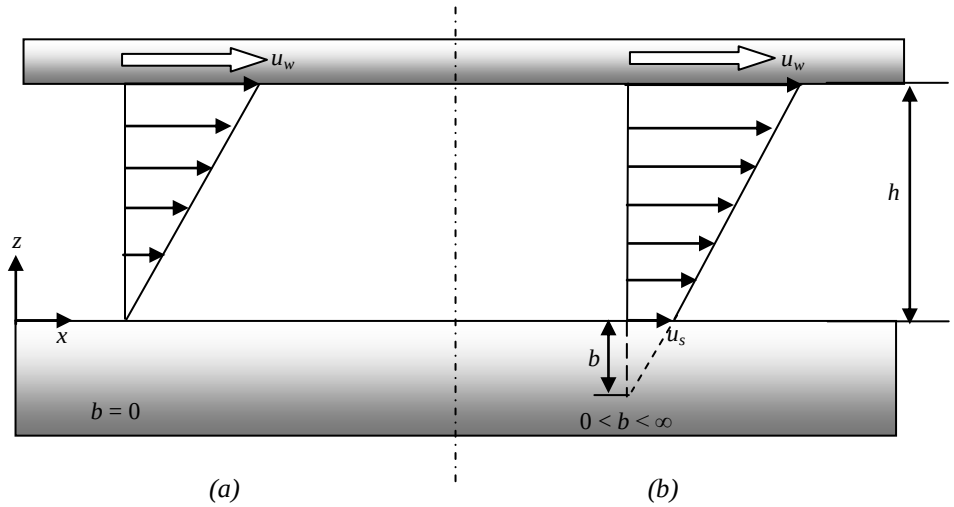

FIGURE 1.1: *Couette velocity profiles between parallel sliding surfaces: (a) no-slip, the shear rate is u_w/h (b) slip at a lubricant-solid interface with slip length, b, at the stationary surface.*

In light of studies on stiction, one approach to the solution of this problem is to achieve control of lubrication through modifying lubricated surfaces in such a way that lubricant boundary slip occurs. In other words, in a controlled way one is able to prevent stiction by introducing boundary slip at the surfaces. Surfaces with this feature are called non-wettable or hydrophobic (or even ultra-hydrophobic) surfaces. However, in such newly lubricated devices, the solution for the lubrication problem with boundary slip cannot be analyzed by the classical Reynolds equation, which specifically excludes the possibility of boundary slip. This thesis proposes a novel approach for hydrodynamic lubricated sliding MEMS devices, including those running with boundary slip, by developing a new modified Reynolds equation with a critical shear stress criterion for boundary slip. The critical (sometimes quoted as 'limiting') shear stress criterion, which is utilized as the boundary slip characteristic, means the shear stress that can be sustained at the liquid-solid interface and can only be up to a critical threshold value. It indicates that when the shear stress is larger than the critical shear stress, boundary slip occurs. This point of view is supported by recent experimental work [7, 8].

The potential use of the boundary slip of a liquid in a low load lubricated contact, as well as in MEMS based devices, was initially explored by Spikes [5, 6] through an analytical solution of the positive effect of variable slip profiles, mainly on friction reduction, in the development of the "half-wetted bearing" principle. The author derived an extended Reynolds equation based on the critical shear stress criterion. In subsequent work, this criterion of slippage was developed by assuming slip to occur when the shear stress on the surface reaches a critical value and above this critical value, the slip length model is

applicable, where the magnitude of shear stress is proportional to the slip velocity [19]. This theory is referred to as the two-component slip model and validated experimentally [7, 8]. Figure 1.2 shows, for example, the comparison between measured results and predicted values for the case of ball-on-flat [8]. It was claimed that there is reasonably good agreement between slip theory and measurements. The two-component slip model is adopted in the present study focusing on a complex boundary slip situation (see appended Paper A). It is noted that main drawback of the two-component slip model presented in [7, 8] is the omission of the possibility of the occurrence of boundary slip on two surfaces, i.e. stationary and moving surface in lubricated sliding contacts. Of the two-component slip model, it was assumed that slip only takes place on one surface, i.e. the stationary surface. Furthermore, the main advantage of that model is that the magnitude of the slip velocity as a function of the critical shear stress, as well as the direction of the slip velocity, can be predicted. In this thesis, using this model, the objective is to find the optimal slip parameters and design rules for reducing the friction and improving the load support in tribological contacts. The extent of an optimal slip zone of a complex slip/no-slip stationary surface with respect to the hydrodynamic load support is of interest. In fact, based on an extensive literature review, the majority of optimization rules are mostly based on a trial-and-error approach. To deal with this issue, a numerical analysis was developed and applied in the model discussed in appended Paper A. Using a genetic algorithm search/optimization method, the optimum slip zone promoting the maximum load support for various film thickness profiles has been obtained.

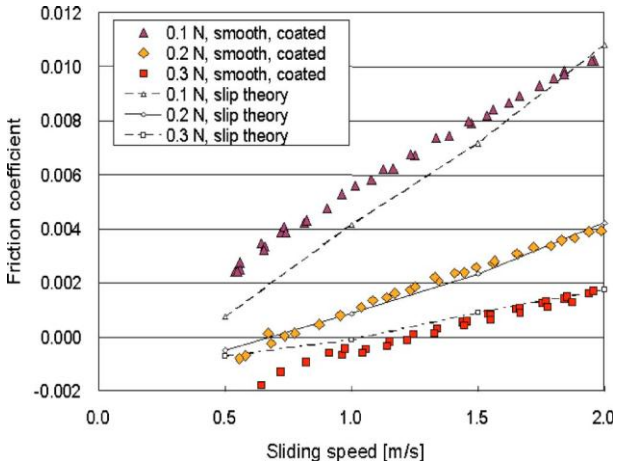

FIGURE 1.2: *Coefficient of friction versus sliding velocity between calculated and measured results: a study case by Choo et al.* [8] *which shows the validity of the two-component slip model.*

The results discussed so far only apply to boundary slip employed on stationary surfaces. For boundary slip at the stationary and moving surface of lubricated sliding contacts, a mathematical model is derived and discussed in Chapter 3 and Papers B, C and H. In this model, the criterion of the occurrence of slip in lubricated sliding contacts is determined by two criteria. Firstly, slip may only occur in those areas where both the

stationary and moving surface have been treated to allow it. Secondly, the shear stress on both surfaces must exceed a critical threshold of the shear stress value. When both criteria are met, the resulting slip velocity is proportional to the difference between the shear stress and the critical value.

Boundary slip on a surface may be of random or deterministic (artificial) nature depending on the magnitude of the critical shear stress at the lubricant-solid interface. Two deterministic boundary slip modes are used: homogeneous slip (the slip zone is applied everywhere along the contact length) and complex slip (the slip zone which covers only a specific zone on the surface) mode. Such modes will be discussed further in the next section and within the appended Papers (A, B, D, E, F and G). It is worth mentioning that the concept of the homogeneous slip is also studied in the work of Spikes [5, 6]. It was analytically demonstrated that such a slip is of satisfactory benefit to low friction behavior. On this issue, the numerical simulations predicted by the developed model here matched well with this finding, see Fig. 1.3. However, another effect emerges, i.e. the reduction in pressure generation, resulting in a lower load support, see Figure 1.4, for example. In this context, to compensate for such a negative effect, a prescribed slip/no-slip surface as an artificial complex boundary slip mode may be introduced. The numerical simulation shows that introducing an artificially created boundary slip onto the sliding surfaces can generate a satisfactory combination of a high load support and a low-friction behavior as shown in detail in the appended Papers A, D, E, F and G. Hence, it is reasonable to anticipate a promising utilization of the complex slip surface in liquid lubricated-MEMS devices.

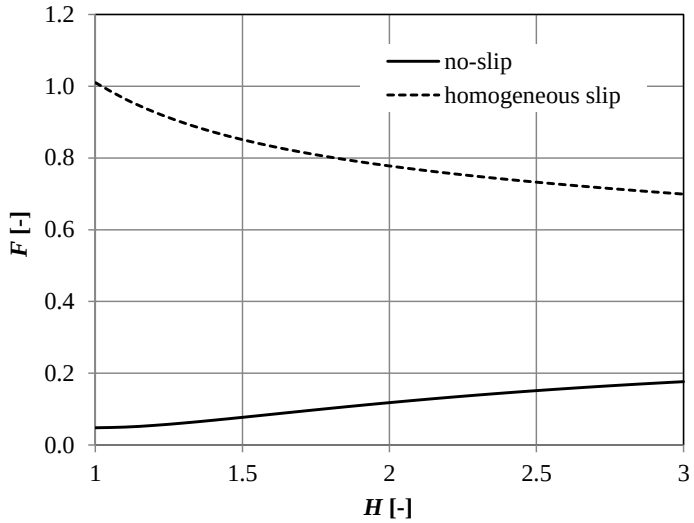

FIGURE 1.3: *Effect of homogeneous slip on the dimensionless friction force, F, under different slope incline ratios, H.* (*Note: H is referred to as the inlet over outlet film thickness ratio in lubricated sliding contacts*).

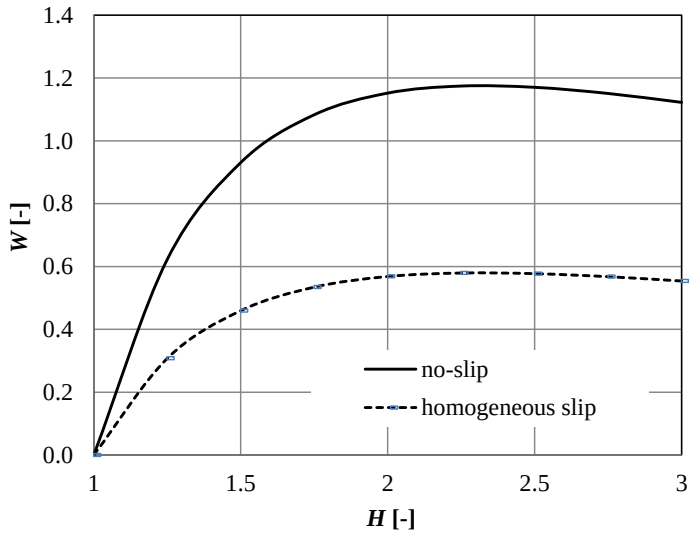

FIGURE 1.4: *Effect of homogeneous slip on the dimensionless load support, W, under different slope incline ratios, H.*

Another major issue investigated in the present work is the presence of surface texturing. It is known that the wettability of a surface is a function of its roughness [20, 21]. Therefore, the importance of taking the roughness effect into account is demonstrated. However, the rough surface considered here is of artificial (deterministic) nature, i.e. surface texture pattern. As is well known, the artificial surface roughness has a great influence on the enhancement of the tribological performance of a lubricated contact and thus is a key parameter that needs to be considered. Surface texturing is considered as an important method to decrease the adhesion and stiction in MEMS devices [22].

Surface texturing (often referred to as "physical roughness") and artificial boundary slip (referred to as "chemical surface treatment") are closely related (with respect to the manufacturing process and gain in expected performance). This is of particular interest because it is believed that the surface modification, including surface texturing and boundary slip, will lead to improved sliding contact characteristics. Therefore, a second point of interest is the interaction of boundary slip with artificial surface roughness as a new, effective means of controlling friction in MEMS. In this thesis, efforts are made to determine the optimal texturing parameters, with or without boundary slip, that would maximize the load support (equivalent to maximizing the fluid film thickness) and/or minimize the coefficient of friction. Two types of texturing, i.e. partial texturing and full texturing, are investigated. However, first, the general theory of the lubrication mechanism with slip on a smooth surface is presented. In summary, the effect of boundary slip and surface texturing on the lubrication of sliding hydrodynamic contact is researched.

Chapter 2

Lubrication with slip

In sliding contacts there are two main kinds of fluid film lubrication: hydrodynamic lubrication and elasto-hydrodynamic lubrication. In hydrodynamic lubrication, the surfaces form a shallow, converging wedge so that as their relative motion causes lubricant entrainment into the contact, the lubricant becomes pressurized and therefore able to support the load. This way, the hydrodynamic action of the lubricant fully separates the surfaces and the load is carried solely by the lubricant film. The film thickness depends on the surface shapes, the surface velocities and the properties of the lubricant. In elasto-hydrodynamic lubrication, the shape of the wedge changes due to deformation of the pressure generated, and as a result the film thickness changes. Generally, the film thickness in lubricated-MEMS is of the order of nano- to micro-meters, supporting the applied pressure of the order of Mega Pascals [6]. This pressure is not high enough either to significantly deform the mating surfaces or to increase the lubricant viscosity. It means that any piezoviscous contribution can be neglected. Therefore, the hydrodynamic lubrication principle is valid in this study.

2.1. Reynolds equation

When hydrodynamic lubrication (HL) is simulated numerically, the hydrodynamic pressure generated in the lubricant film is normally modeled with the aid of the Reynolds equation [10]. The Reynolds equation, see Eq. (2.1), is the commonly used partial differential equation for modeling fluid flow, or more accurately the fluid pressure, given the shape of the gap and the operational conditions, in a full film lubricated contact. The equation is derived by combining two conservation equations of momentum and continuity into a single equation for the fluid pressure, assuming a small film thickness relative to the contact length, non-varying pressure across the film thickness, and the dominance of certain viscous terms. When the derivation is conducted, inertia may be omitted for small Reynolds numbers in combination with the thin film in the contact region, see for example [23]. The

equation obtained relates the fluid pressure to the rate of convergence of the wedge, surface velocities and lubricant viscosity. Eq. (2.1) shows the general formulation:

$$\frac{u_m}{2}\frac{\partial(\rho h)}{\partial x_i} - \nabla\cdot\left(\frac{\rho h^3}{12\eta}\nabla p\right) = 0 \tag{2.1}$$

where ρ density of the lubricant
η dynamic viscosity of the lubricant
h lubricant film thickness
p hydrodynamic pressure across the film thickness
u_m average surface velocity in the direction of motion
x_i coordinate directions

A derivation of the Reynolds equation for an assumed isoviscous incompressible fluid can be found in Hamrock [11].

2.2. Previous studies in hydrodynamic lubrication with slip

The Reynolds lubrication theory has become a useful tool in both analysis and design of lubricated contacts. In the derivation of the classical Reynolds equation, it is assumed that there is no boundary slip at a liquid-solid interface. This is the so-called no-slip boundary condition. On micro-scale, however, due to the progress in micrometer measurement technology, it is possible to observe boundary slip of fluid flow over a solid surface, and therefore the traditional boundary no-slip condition can break down. Under such circumstances, the classical Reynolds equation is no longer applicable.

In lubricated-MEMS, proper lubrication is a key issue in reducing the liquid stiction and hence has received a great deal of attention in the relevant literature recently [1, 5-9, 24]. The classical Reynolds equation is a useful tool in bearing analysis and design. Therefore, in order to make a good design and analysis of the fluid film lubricated-contact, researchers have extended the classical Reynolds equation by taking into account boundary slip.

A solution for the modified Reynolds equation was given by Spikes [5]. The classical theory is extended, based on the critical shear stress criterion of boundary slip, to consider the sliding hydrodynamic lubrication condition where the lubricant has a no-slip boundary condition along the moving solid surface, but can slip at a critical shear stress along the stationary surface. In this configuration, a bearing with a slope incline ratio can generate load support and low friction resulting from fluid entrainment. Later, an equation for Newtonian slip flow was developed by Spikes and Granick [19]. In this model, slip is envisaged to occur only when a critical surface shear stress is reached, and once slip begins, it takes place at a constant slip length. It was also shown that this model was able to reconcile results from some experimental investigations [7, 8]. Boundary slip usually results in a low friction force, but also decreases the hydrodynamic pressure. If the lubricated contact exhibits a perfect slip property (zero critical shear stress), it was found that the load support was only half of that without slip [5, 6, 25]. For non-zero critical shear stress cases, the hydrodynamic lubrication performance is controlled by the critical shear

stress of the two lubricated surfaces, especially by the smaller critical shear stress. However, one can remark that all these studies suggest that load support comes from the physical (i.e. convergent geometrical) wedge.

A lot of work has been carried out to study the influence of boundary slip on HL with the emphasis on the (slightly) parallel sliding configuration. The earliest work on artificial complex slip/no-slip, lubricated parallel sliding devices was reported by Salant and Fortier [26, 27]. They focused on the ability of artificial slip to improve the load support and the friction force in the absence of the wedge effect. Subsequently, several studies were published confirming the findings of Salant and Fortier [26, 27]. Guo and Wong [28] confirmed that the introduction of the so-called tailored boundary slip on the stationary surface of a slider with a diverging gap leads to a net pressure build-up. Similarly, Wu *et al.* [25] studied the behavior of a slider bearing with a mixed slip surface condition and their results indicated that convergent, parallel, and divergent wedges can provide hydrodynamic load support.

Another key issue is cavitation in lubricated parallel sliding contacts with an artificial slip surface. It was shown that the choice of the cavitation model has a significant influence on the performance of the load support value [29].

In the aforementioned numerical studies, hydrodynamic lubrication films with slip conditions were studied for a smooth moving surface against a smooth stationary surface. When performing a literature survey, one will find that the amount of research about the combined effect of boundary slip and artificial rough surface with respect to lubrication is still very limited. This is of particular interest because it is believed that surface modification, including surface texturing (i.e. physical roughness) and slippage (chemical surface treatment), will lead to improved hydrodynamic performance characteristics. As is well known, mainly based on experimental work, the texturing pattern could result in a higher load support for a low convergence wedge and for parallel sliding surfaces. In essence, a textured surface is able to entrain more lubricant (and thus form a thicker film) than a smooth surface.

Rao [30], in the case of one-dimensional slider and journal bearing, evaluated the effect of the artificial slip and texturing combination on the improvement in hydrodynamic performance characteristics. One noteworthy observation is that in using such a configuration, the pressure distribution (and thus the load support) is higher compared to the conventional bearing with no-slip, especially if the uniform film thickness is employed. This is also reported in a later paper [31].

In the case of a journal bearing, Aurelian *et al.* [32] investigated the influence of the boundary slip on the load support and the power loss in hydrodynamic bearings with and/or without texturing conditions. The main conclusion of their study was that choosing the textured/slip zone geometry should be made carefully because an inappropriate choice can lead to a drastic deterioration of the bearing performance, especially in relation to the load support.

Even though major progress has been made in recent decades in modeling lubrication with slip, the majority of work is still based on the slip length criterion of slippage. Boundary slip that exceeds a critical shear stress continues to be neglected.

2.3. Slip models

Early studies [33, 34] have found experimental evidence of boundary slip occurring at a liquid-solid interface. During the past decade, with the development of advanced experimental techniques, numerous experiments have shown that boundary slip can occur at both a hydrophobic surface [14, 18, 35-38] and a hydrophilic surface [15, 16, 38, 39]. For most hydrophilic surfaces, however, no slip occurs.

The great challenge for a hydrophobic surface from the perspective of a numerical simulation is choosing a model for boundary slip. This is because the hydrodynamic behavior of lubricated contacts is mainly affected by the boundary conditions of the lubricant that will provide lubrication. From a numerical point of view, there are two main wall slip models which have been adopted to describe the boundary slip, i.e. the slip length model (SLM) and the critical shear stress model (CSSM). In this section, an overview of these two boundary slip models is presented.

2.3.1. Slip length model (SLM)

The slip length model (SLM), as mentioned in the previous section, predicts that the slip velocity is proportional to the local shear rate and that the proportionality constant is called slip length; the distance below the solid surface where the velocity extrapolates linearly to zero (see Fig. 1.1). In other words, in the slip length model, the velocity at which the liquid slips along the solid surface u_s, the shear stress τ and the slip length b are related by the following equation

$$\tau = \frac{u_s}{b}\eta \tag{2.2}$$

Here, the larger the value of b, the larger the slip. The SLM implies that the slip length is independent of the shear rate, which was not, however, supported by some of the experiments [15, 16, 18, 40] and molecular dynamic simulations [41-43]. First, it was reported that the slip velocity increases in a strong nonlinear manner with the shear rate, especially at high shear rates. In fact, the slip length model can only describe the slip behavior when the shear rate is moderate. Second, it was found that there exists a critical shear stress at the solid/liquid interface, and only after the surface shear stress exceeds that critical shear stress will boundary slip occur.

2.3.2. Critical shear stress model (CSSM)

The experimental manifestation of boundary slip at high shear rates shows the existence of a critical shear stress, i.e. the critical shear stress model. Figure 2.1 shows an ideal critical shear stress model. This concept was first proposed by Smith [44, 45] for lubricants, and later was confirmed by Bair and Winer [46-49] in which the solid surface is a metal (hydrophilic). The critical shear stress assumes that boundary slip takes place only after the surface shear stress, τ, reaches the critical value, τ_c, where the surface shear stress is constant (shear rate independent) but the apparent shear rate can reach any value (the true

shear rate equals the critical threshold). When the surface shear stress is below the critical shear stress, no slip occurs.

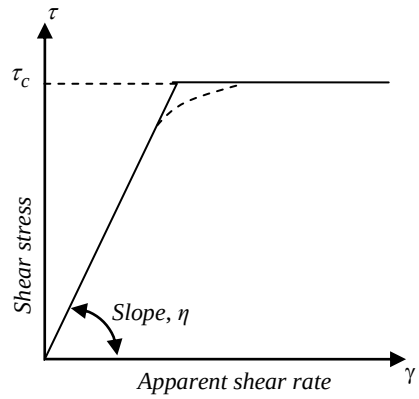

FIGURE 2.1: *Schematic of a stress-rate curve of the critical shear stress model.*

The critical shear stress was found to depend on surface wettability, surface roughness, fluid viscosity, etc. The roughness effect on the critical shear stress is not so clear. Some researchers [14, 18, 49] demonstrated that surface roughness inhibits boundary slip or increases the critical shear stress, but others [50] reported that it increases boundary slip. The critical shear stress may decrease with the surface contact angle [49]. With respect to the surface wettability property, usually the better the surface hydrophobicity, the lower the critical shear stress. The critical shear stress of a superhydrophobic surface is as low as 0.33 Pa [18, 49, 17, 51], which can be considered as a perfect (ideal) slip surface. This value is much lower than the reported critical shear stress of the interface for oil and steel which ranges from 0.16 to 8 MPa [52]. There are two kinds of critical shear stress criteria. The first is the so-called two-component slip model; the model proposed by Spikes & Granick [19] for slip in which the critical shear stress criterion is broadened to incorporate both a critical shear stress and a constant slip length criterion. Slip is envisaged as only occurring when a critical surface shear stress is reached, and once slip begins, it takes place at a constant slip length. In this case, the shear stress occurring when boundary slip takes place is given by

$$\tau_c = \tau_{oc} + \frac{\eta}{b} u_s \tag{2.3}$$

where τ_{oc} is the critical threshold shear stress for slip, η is the dynamic viscosity of the liquid, b is the slip length (once slip begins), and u_s is the slip velocity. This model is quite similar to the concept proposed by Salant and Fortier [26]. They assumed that slip occurs when the critical shear stress is exceeded and the resulting slip velocity is proportional to the difference between the shear stress and the critical value.

The second critical shear stress model is the slip model as a function of the local fluid pressure. This model was investigated by several groups [46-48, 53-57] and given as

$$\tau_c = \tau_{oc} + kp \tag{2.4}$$

where τ_c is the critical shear stress ($\tau_c = \eta\left(\partial u/\partial z\right)_c$ for a Newtonian fluid), τ_{oc} is the initial shear strength when the film pressure equals zero, p is the fluid pressure, and k is the critical, local, interfacial friction coefficient (sometimes quoted as the proportionality coefficient). The parameters τ_{oc} and p depend on the chemical composition of the fluid and the temperature. The proportionality coefficient, k, has been investigated in several ways by a few researchers [54-57] with results that range from about 0.007 to 0.15 and the variation is found to be temperature dependent. This type of CSSM was used for flow analysis in lubrication simulations based on the finite difference method [58] and the finite element method [25, 49, 51, 52, 59-61, 62-65].

2.4. Types of boundary slip

2.4.1. Random slip

Random slip is referred to as boundary slip in which slip occurs due to the effect of the existence of a critical shear stress. In this way, slip can occur at the whole surface or only at a small area depending on the local surface shear stress. One of the earliest works with this type of slip was carried out by Spikes [5], who studied the effect of critical shear stress on the half-wetted bearing system. Later, many works [59, 62, 63, 65] were dedicated to the study of the influence of this slip parameter on hydrodynamically lubricated sliding contacts.

2.4.2. Artificial slip

Recently, the discussion on potential applications of boundary slip to various lubricating devices became of great interest. It is believed that careful choice of a prescribed pattern of an artificial slip region will lead to more efficient hydrodynamic performance characteristics. Efforts have been made in recent years to explore the artificial slip concept. Adjusting some geometrical parameters, such as the shape and the size of the slip zone, is the main core of the development of concepts with the aim of optimizing the hydrodynamic characteristics. Attempts were made to determine the optimal slip zone that gives a satisfactory combination of fair load support and low friction behavior.

In the case of a one-dimensional lubricated sliding contact with an artificial slip configuration, the most lively research in this field has been proven by a significant number of studies published in recent years [5, 6, 25, 28, 29, 60, 66, 67]. Most of the researchers have focused their work on the determination of the length of the slip region for obtaining the best hydrodynamic performance, especially in the absence of the geometrical wedge effect (i.e. slope incline ratio, $H = 1$). As illustrated in Fig. 2.2, a schematic representation of 1D lubricated sliding contact with artificial slip on the stationary surface is shown (with

$H > 1$). Part AB of the stationary surface is fully non-wetted or partially wetted and has a critical shear stress for slippage. Part BC of the stationary surface is fully wetted, which means no boundary slip. Research efforts have been made to identify the optimal length of part AB with respect to maximum load support, for example, see [25, 28] and appended Papers B, D, E and G.

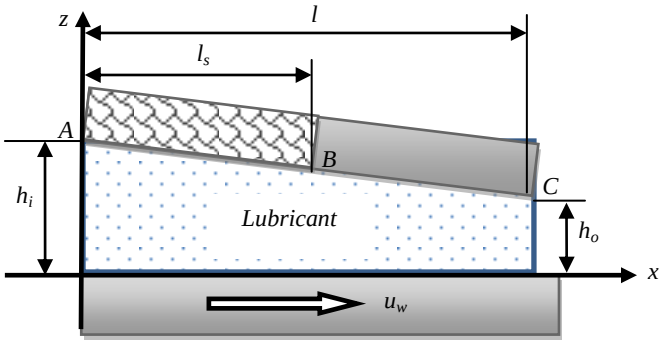

FIGURE 2.2: *Schematic representation of 1D lubricated sliding contact with artificial complex slip surface (CSS) pattern with length l_s.*

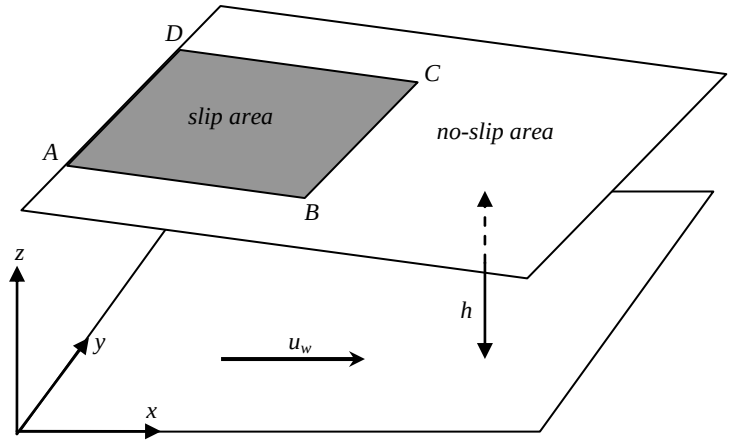

FIGURE 2.3: *Schematic representation of 2D lubricated sliding contact with localized artificial complex slip surface (CSS).*

On the other hand, in the two-dimensional situation (see Fig. 2.3), only a few groups investigated the flow behavior of the lubricated sliding contact containing an artificial slip area, see for example [26, 63, 64, 68], and appending Papers A and F. Various researchers employed a patterned surface for artificial slip with various geometries. Several

shapes of the slip zone area of the lubricated sliding contact were proposed, but the rectangular [26, 27] and trapezoidal [63, 68] shapes are the most common ones mentioned in the literature.

Salant and Fortier [26, 27] were pioneers with respect to introducing and showing the advantage of a complex slip surface in mechanical lubricated systems. They constructed a complex bearing surface on which slip occurs in a certain region of a rectangular shape. It was reported that the slider/journal bearing performance can be improved with respect to friction reduction and enhancement in load support. However, in the numerical solution an instability problem was met when the critical shear stress is non-zero, and therefore they concluded that the bearing operated in an unstable condition in some range of sliding velocities.

In later works, Ma and his co-authors [63] took a closer look at the possible improvement of the performance of lubricated sliding contacts by means of a patterned trapezoidal slip zone area. Optimization of the shape and size of the slip area was conducted in order to obtain many advanced properties of the lubricated contacts. A similar analysis was recently made by Wang *et al*. [68]. Using a modified slip length model in the Reynolds equation, the load support and the end leakage rate can be optimized significantly. It was also reported that the use of an artificial complex slip surface in lubricated contact breaks the classical Reynolds theory, which posits that a convergent geometry-wedge is the first important condition for the generation of hydrodynamic pressure.

By means of new technologies such as surface texturing (for instance, using a laser) and chemical treatment, it is possible to control surface properties in order to improve the overall tribological performance including friction reduction and reliability.

Chapter 3

Modeling

3.1. Modified Reynolds equation

In hydrodynamic lubrication, the important output parameters are friction and load support, which can directly be related to the performance of the lubricated sliding contact. Most often a small coefficient of friction is desired in a lubricated contact.

The lubrication model developed in the current study is based upon the hypothesis that the molecular nature of the fluid can be neglected and the lubricant can be treated as a continuum. With the proviso that the continuum hypothesis holds for MEMS devices, the equations (with a modified boundary condition) for microlubrication can be derived. This way the hydrodynamic lubrication can be governed by the Reynolds equation. In this thesis, a hydrodynamic lubrication model was developed to describe the flow and pressure in a lubricated-MEMS, in which the lubricant can slip on both interfaces (i.e. sliding and stationary surfaces) at a critical shear stress criterion.

In a classical hydrodynamic lubrication problem, the governing equations in a full fluid region can be described by the well-known Reynolds equation. The isoviscous Newtonian one-dimensional Reynolds equation is derived from a simple form of the *x*-component of the Navier-Stokes equation that assumes an incompressible flow and neglects the convective effects in the film:

$$\frac{\partial^2 u}{\partial z^2} = \frac{1}{\eta}\frac{\partial p}{\partial x} \tag{3.1}$$

In order to obtain the velocity distribution by the integration of Eq. (3.1), it is necessary to define the surface boundary conditions. Let us consider a lubricated contact equivalent to a lower plane moving in the *x*-direction with a surface velocity u_w and an upper stationary surface. In this study, the occurrence of slip in the lubricated sliding

contact is determined by two criteria. Firstly, slip may only occur in those areas where both stationary and moving surface have been treated to allow it. Secondly, the shear stress on both surfaces must exceed a critical shear stress value, referred to as τ_{ca} for the stationary surface, and τ_{cb} for the moving surface. When both criteria are met, the resulting slip velocity is proportional to the difference between the shear stress and the critical value, with proportionality factors referred to as α_a for the stationary surface and α_b for the sliding surface. It means that each of the sliding faces has a unique slip property. The product of the slip coefficient with the viscosity, $\alpha\eta$, is commonly named 'slip length'. The surface boundary conditions are proposed as follows:

$$\begin{aligned}
&\text{at } z = h && u = \alpha_a\left(-\eta\frac{\partial u}{\partial z} - \tau_{ca}\right) && \text{for } \tau_a \geq \tau_{ca} \\
& && u = 0 && \text{for } \tau_a < \tau_{ca} \\
&\text{at } z = 0 && u = u_w + \alpha_b\left(\eta\frac{\partial u}{\partial z} + \tau_{cb}\right) && \text{for } \tau_b \geq \tau_{cb} \\
& && u = u_w && \text{for } \tau_b < \tau_{cb}
\end{aligned} \tag{3.2}$$

The solution of Eq. (3.1) yields the distribution of the fluid velocity, subject to the boundary equations, Eq. (3.2). It reads:

$$\begin{aligned}
u = {} & \frac{1}{2\eta}\frac{\partial p}{\partial x}z^2 - \left(\frac{h}{2\eta}\frac{\partial p}{\partial x}\frac{h+2\alpha_a\eta}{h+\eta(\alpha_a+\alpha_b)} + \frac{u_w}{h+\eta(\alpha_a+\alpha_b)} + \frac{\alpha_a\tau_{ca}+\alpha_b\tau_{cb}}{h+\eta(\alpha_a+\alpha_b)}\right)z \\
& + u_w\frac{h+\alpha_a\eta}{h+\eta(\alpha_a+\alpha_b)} - \frac{h}{2\eta}\frac{\partial p}{\partial x}\frac{\alpha_b\eta(h+2\alpha_a\eta)}{h+\eta(\alpha_a+\alpha_b)} + \frac{\alpha_b\tau_{cb}(h+\alpha_a\eta)-\alpha_b\alpha_a\eta\tau_{ca}}{h+\eta(\alpha_a+\alpha_b)}
\end{aligned} \tag{3.3}$$

The modified Reynolds equation is derived by expressing the integrated continuity equations. If the fluid density is assumed to be a mean density across the film, it is convenient to express the continuity equation in integral form as follows [11]:

$$\int_0^h \frac{\partial}{\partial x}u\,dz = -(u)_{z=h}\frac{\partial h}{\partial x} + \frac{\partial}{\partial x}\left(\int_0^h u\,dz\right) = 0 \tag{3.4}$$

Therefore, the modified form of the one-dimensional Reynolds equation with slip reads:

$$\frac{\partial}{\partial x}\left(h^3 \frac{h^2 + 4h\eta\left(\alpha_a + \alpha_b\right) + 12\eta^2\alpha_a\alpha_b}{h\left(h + \eta\left(\alpha_a + \alpha_b\right)\right)} \frac{\partial p}{\partial x} \right) = 6\eta u_w \frac{\partial}{\partial x}\left(\frac{h^2 + 2h\alpha_a\eta}{h + \eta\left(\alpha_a + \alpha_b\right)} \right)$$

$$-6\eta\tau_{ca}\frac{\partial}{\partial x}\left(\frac{\alpha_a h(h + 2\alpha_b\eta)}{h + \eta\left(\alpha_a + \alpha_b\right)} \right) + 6\eta\tau_{cb}\frac{\partial}{\partial x}\left(\frac{\alpha_b h(h + 2\alpha_a\eta)}{h + \eta\left(\alpha_a + \alpha_b\right)} \right) - 12\eta u_w \frac{\alpha_a\eta}{h + \eta\left(\alpha_a + \alpha_b\right)}\frac{\partial h}{\partial x}$$

$$+6h\frac{\partial p}{\partial x}\frac{\partial h}{\partial x}\frac{h\alpha_a\eta + 2\alpha_a\alpha_b\eta^2}{h + \eta\left(\alpha_a + \alpha_b\right)} + 12\eta\tau_{ca}\left(\frac{\alpha_a(h + \alpha_b\eta)}{h + \eta\left(\alpha_a + \alpha_b\right)}\frac{\partial h}{\partial x} \right)$$

$$-12\eta\tau_{cb}\left(\frac{\alpha_a\alpha_b\eta}{h + \eta\left(\alpha_a + \alpha_b\right)}\frac{\partial h}{\partial x} \right) \tag{3.5}$$

The modified form of the Reynolds equation presented here is different from that used in the studies presented previously [25-32, 68]. The developed model includes the critical shear stress terms and the possibility of slip that may occur on both moving surfaces. It must be pointed out that the present model, see Eq. (3.5), can be used to solve the cases in which (1) the zero or non-zero critical shear stress is present, and/or (2) slip occurs either at both surfaces (stationary and moving surface) or at one of the surfaces, by setting α_a, α_b, τ_{ca} and τ_{cb} to its specified value according to the appropriate boundary condition of the lubricated sliding contact. In the present study, the lubricated sliding contact is operating under steady state conditions.

Based on Eq. (3.5), if α_a, α_b, τ_{ca} and τ_{cb} are set to zero, the modified Reynolds equation developed becomes the classical Reynolds equation. Thus, the mechanism to yield the pressure distribution is based on the wedge effect in which the pressure generation is due to the fluid being driven through the wedge-shaped gap because of surface movement. From the analytical solution described by Cameron [69], it is known that a convergent gap is the main requirement to generate the hydrodynamic pressure based on the classical Reynolds theory, and at a slope incline ratio ($H = h_i / h_o$) of 2.2, the hydrodynamic pressure gives the highest value.

The Reynolds equation is normally solved by using numerical methods, which means that the computational domain is divided into a relatively large number of elements both for smooth and rough surfaces. In this work, the modified Reynolds equation is solved numerically using finite difference equations obtained by means of the micro-control volume approach [70]. By employing a discretization scheme, the computed domain is divided into a number of control volumes. The modified Reynolds equation is solved using a TDMA (Tri-Diagonal-Matrix-Algorithm), [70, 71]. The TDMA is actually a direct method for the one-dimensional situation, but it can be applied iteratively, in a line-by-line way with a minimum amount of storage [71]. In the two-dimensional case as described in the appending Paper A, in addition to TDMA, the Reynolds equation is solved using the ADI (Alternating-Direction-Implicit) method [70, 71].

3.2. Lubrication performance

Factors such as lubrication performance (i.e. load support and friction), service life, etc., are important when designing any type of lubricated sliding contacts, including MEMS devices. The performance of a hydrodynamically lubricated contact is certainly affected by the operating conditions, the choice of lubricant and the surface topography. However, as previously mentioned, the artificial chemical surface treatment (i.e. boundary slip) and physical roughness (i.e. texturing) are of main interest here.

Load support, *w*, is obtained by integration of the pressure:

$$w = \int_0^l p dx \tag{3.6}$$

The friction force generated in a lubricated system is due to shearing the fluid. By integrating interface shear stress over the interface surface area, the friction force, *f*, is obtained:

$$f = \int_0^l \tau dx \tag{3.7}$$

where the shear stress at the bottom surface being:

$$\tau = \eta \left(\frac{\partial u}{\partial z} \right)_{z=0} \tag{3.8}$$

The coefficient of friction is defined as the ratio between the total friction and the total normal load:

$$\mu = f / w \tag{3.9}$$

3.3. General considerations

Surface texturing as a predefined roughness was introduced as a surface engineering technique to reduce friction. As previously mentioned, with respect to the friction, the potentially useful implication of boundary slip was also suggested by recent researchers. Knowledge about slip parameters, as well as surface texturing parameters, is essential for achieving friction reduction in lubricated-MEMS devices.

3.3.1. Slip parameters

One of the developed treatments to eliminate stiction is the development of new materials or design of surfaces and interfaces with hydrophobic behavior [21, 22]. Non-wetting (hydrophobicity) is a critical surface behavior for materials in devices for micro-applications. The hydrophobicity of a surface is generally presented in terms of a slippage length, which quantifies the extent to which the fluid near the surface is affected by the surface energy [41].

3.3.1.1. Slip length

Owing to the application of sliding surfaces with very narrow-gap conditions and the emergence of hydrophobic materials, the classical no-slip boundary condition can break down. When lubricant slips along a solid-liquid interface, the slip length, *b*, is generally used to address the relation between the slip velocity and the surface shear rate, that is

$$u_s = b \left. \frac{\partial u}{\partial z} \right|_{\text{surface}} \tag{3.10}$$

where u_s indicates the streamwise slip velocity at the hydrophobic surface, *b* denotes the slip length, and $\partial u / \partial z|_{\text{surface}}$ is the surface shear rate. It is usually postulated that a large value of *b* implies larger slippage. Furthermore, it is also conventionally implied that a large slip is also associated with a large friction force reduction. Numerous works have demonstrated that chemical treatment of a surface generates a slip length in the order of 1 μm [36], whereas a longer slip length of up to 100 μm can be obtained through a combination of a textured pattern with a hydrophobic surface [8, 72, 73]. In the present study, the slip length of a hydrophobic surface is assumed to be uniform in space.

3.3.1.2. Critical shear stress

As mentioned earlier, the better the surface hydrophobicity, the lower the critical shear stress. In this thesis, the effect of artificial surface roughness (i.e. texturing) on the critical shear stress is investigated. The interest in this analysis is heightened by the contradiction between the roughness effects in inhibiting slip observed by Granick *et al.* [49] and the roughness effects in promoting the slip observed by Bonaccurso *et al.* [50].

3.3.2. Surface texture

The use of artificial surface texturing is becoming popular in oil lubricated devices because of its potential benefits in terms of load support and friction force both experimentally and theoretically. It was shown experimentally that such texturing enhances the load support and reduces the hydrodynamic friction force in, for instance, systems with two parallel sliding surfaces [74-76], and in reciprocating (cylinder-liner) contacts [77]. The shapes of

the surface features are usually dimples or grooves, see Fig. 3.1. In the hydrodynamically lubricated sliding contact in particular, artificial surface texturing supports the formation of a lubricating oil film.

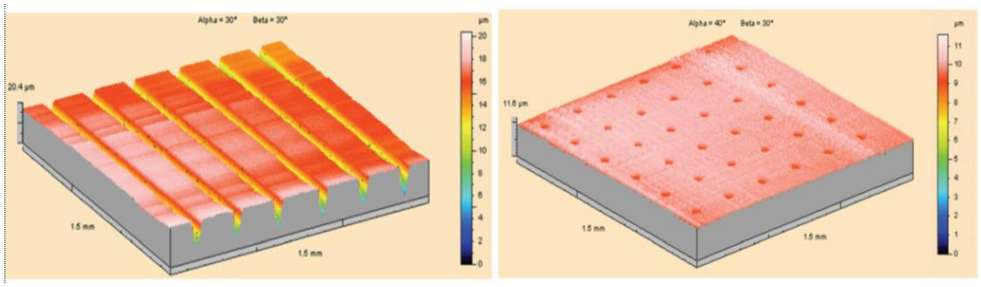

(a) *(b)*

FIGURE 3.1: *Example of laser textured surfaces with (a) grooves and (b) dimples* [78].

Full and partial texturing are two extreme cases of an artificial arrangement of textured areas on a contact surface. It is worth mentioning the early work of Tonder [79] who analyzed partial texturing by theoretical studies with respect to the positive effect of a series of dimples or roughness at the inlet of a sliding surface. A comparison of partially and fully textured surfaces comprising micro-roughness in parallel thrust bearings was given by Brizmer *et al*. [80] through a numerical approach. They demonstrated that full width texturing is not useful for developing a large load support. Subsequently, several studies were published [81-85] confirming the work of Brizmer *et al*. [80]. One emerging conclusion of these studies is that there is an advantage of partial texturing over full texturing.

In addition, attention has been paid to the optimization of texturing parameters. Various surface texture models (elliptical, sinusoidal, rectangular, cylindrical, etc.) were investigated and it is concluded that surface texturing improves the tribological performance. Efforts were made in several works to establish the optimal texturing parameters such as texture depth, width, number of textures and location of the texture that would maximize the load support. The previously-mentioned models and simulation results also provide an excellent set of guidelines for an optimum design of a surface texture in some application fields like in thrust bearings.

Recently, in addition to surface texturing, the use of an artificial slip surface is also of great interest with respect to lubrication [7, 8, 30-32, 51, 68]. Such a surface was introduced in lubricated sliding contacts with the help of microfabrication techniques. Thus, the artificial slip surface and the surface texturing are closely related with respect to the manufacturing process and gain in expected performance. On the micro-scale level such as in lubricated MEMS devices, the boundary condition, i.e. slip or no-slip situation, will play a very important role in determining the hydrodynamic lubrication behavior.

Chapter 4

Results

4.1. Beneficial surface of slip

The use of an artificial slip surface has become common with respect to lubrication since this type of surface improvement gives better tribological performance. However, the big question with respect to the tribological performance of lubricated-MEMS is at which wall boundary slip should be applied; at the stationary surface, the moving surface, or both of them.

Besides, the type of slip zone pattern is of importance. The great challenge for an artificial slip surface, from the perspective of numerical simulation, is choosing the optimal slip zone geometry with respect to lubrication performance. As mentioned in the previous chapter, two artificial slip surface modes have currently been employed: a homogeneous slip surface and a complex slip surface.

Regarding the homogeneous slip condition, numerous simulations have been conducted to investigate the influence of such slip condition on the lubrication performance. It was concluded that the friction force can be reduced significantly. However, another influence emerges; homogeneous slip produces a reduced load support which reduces the positive effect of slip on the friction force, see Figs. 1.3 and 1.4, and appending Papers A, B, D, E, F and G.

In order to answer the issue "at which wall" boundary slip should be applied, as mentioned earlier, several simulations have been carried out. Here, two kinds of artificial slip surfaces were employed, i.e. homogeneous slip (see Fig. 4.1. and appending Paper D), and complex slip (Paper B). In conclusion, it is found that by applying the artificial slip on the stationary surface while the no-slip situation is present on the moving surface, pressure is generated, and thus, load support can be achieved. If the boundary slip is applied on the moving surface or employed both on the moving and stationary surfaces, the load support will be close to zero. Therefore, in the following design for the maximal lubrication performance, the lubricant has a no-slip boundary condition at the moving solid surface but can slip along the stationary surface.

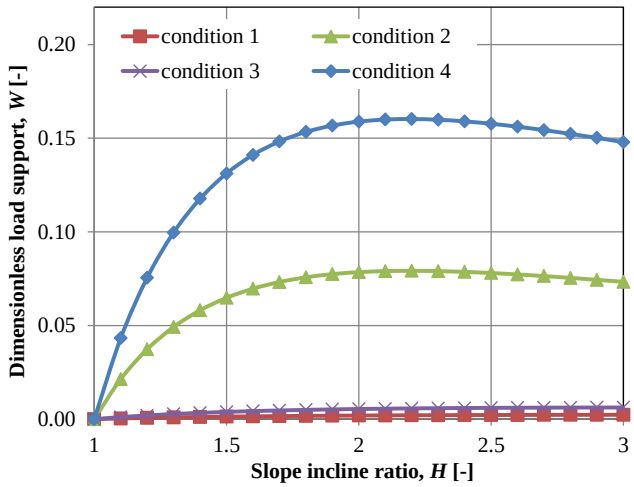

FIGURE 4.1: *Dimensionless load support, W, versus slope incline ratio, H, for several homogeneous boundary slip conditions. Note: slip on stationary and moving surfaces (condition 1); slip on stationary surface (condition 2); slip on moving surface (condition 3); traditional no-slip (condition 4).*

4.2. Artificial slip surface

As is known, the artificial homogeneous slip surface has a very beneficial effect with respect to friction reduction. However, if the performance is related to load support, homogeneous slip is not recommended because of the deterioration of the load support. Generally, related to lubricated-MEMS, the reduction in pressure generation and resulting lower load support is often unwanted because it can lead to failure of the system. For this reason, various geometries of the slip region (ABCD zone of the stationary surface, see Fig. 2.3) are investigated and optimized with respect to hydrodynamic performance. In this way, a high load support combined with a low friction force can be obtained.

In the present work, the term complex slip surface pattern (CSS pattern) is used to address a non-homogeneous engineered slip/no-slip pattern, i.e. a surface consisting of a slip area and a no-slip area. It means that, with such a pattern, a surface can be divided into two regions having different properties. One region with a specific geometry can have a very high critical shear stress, and thus the no-slip condition can be assumed, and the remaining region has a low critical shear stress, so slip may occur. It is believed that a judicious choice of a CSS pattern can alter the flow pattern in the liquid lubricating film so that it will lead to enhanced MEMS characteristics and improved operational stability. As depicted in Figs. 4.2 and 4.3, compared to the classical no-slip contact and the homogeneous slip contact, the CSS pattern gives an advanced pressure distribution even in the absence of the wedge effect. This situation is very beneficial in designing lubricated-MEMS devices which frequently exhibit parallel surfaces.

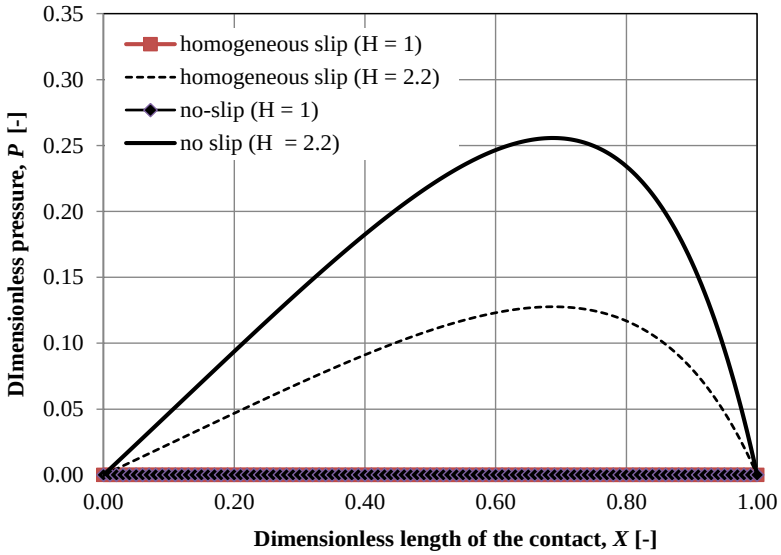

FIGURE 4.2: *Pressure distribution of a lubricated sliding contact for two types of surfaces; (a) no-slip and (b) homogeneous slip. The profiles are predicted for parallel sliding surfaces (H = 1) and the corresponding optimal slope incline ratio (H = 2.2).*

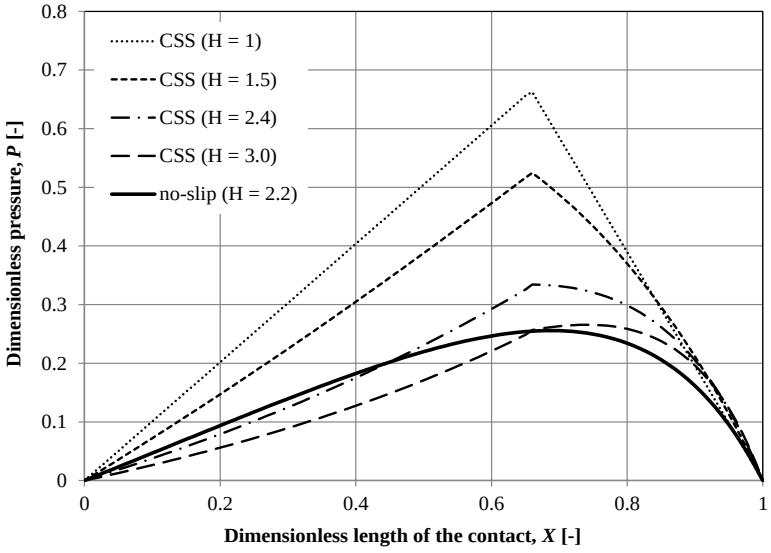

FIGURE 4.3: *Pressure distribution of a lubricated contact for CSS pattern (L_s = 0.65, see Fig. 2.2) with varying slope incline ratio, H.*

In real lubricated contact problems, the number of lubrication parameters can be very large and their influence on the lubrication performance can be very complicated. In order to obtain an optimal or group of sub-optimal solutions, this thesis proposes two approaches of optimization, i.e. parametric study and genetic algorithm. A genetic algorithm is basically an algorithm that is based on natural biological evolutions [86]. In a parametric study, some parameters are varied over a large range of values for different conditions.

The objective of optimization is to maximize the hydrodynamic load support. The load support satisfies two main functional purposes: (1) to carry the load, and (2) to minimize the contact between the solids, thereby reducing wear. The optimization analysis attempts to satisfy both functional requirements with various design parameters, i.e. slip zones (CSS pattern) and film height of the lubricated sliding contact. A parametric study of lubricated sliding contacts with artificial slip surface is presented in Part 1 of the thesis, whereas the optimization analysis by genetic algorithm is discussed in appending Paper A (in Part 2 of the thesis) in more detail.

Paper A, in particular, explores the amount of hydrophobicity and the ratio of hydrophilic to hydrophobic area for a complex slip surface in generating a maximum load support for systems in which the wedge effect is not present. The two-component slip model is adopted to analyze the lubrication behavior with slip in a two-dimensional way, such that the variation of slip areas in both x- and y-direction can be conducted. By employing such a genetic algorithm, the optimized complex slip surface (CSS) pattern, as well as an optimized slope incline ratio, can be solved simultaneously.

4.2.1. Location of slip zone

Figure 4.4 gives the variation of the dimensionless load support, W, with different dimensionless critical shear stress, T_c, and dimensionless length of the slip zone, L_s, according to Eq. (3.5). It can be clearly seen that the load support increases with decreasing critical shear stress. Setting the critical shear stress value to zero (i.e. the perfect slip surface), the highest load support can be achieved for parallel moving surfaces. When the dimensionless critical shear stress is 1, no load support takes place. It means that for a very high critical shear stress, the lubricated contact with an artificial slip surface behaves like a traditional one.

Figure 4.4 also shows that two parallel moving surfaces with an optimized complex slip surface with a perfect slip condition can also provide the fluid load support. Based on the optimization calculation, the complex slip surface with a slip zone that covers 0.65 times the length of the contact (L_s = 0.65) gives the highest load support. It must be noted that for all values of the dimensionless critical shear stress, T_c, if the stationary surface is designed as a homogeneous slip surface (L_s = 1), the numerical results show that there is no load support at parallel sliding surfaces. Another interesting result is shown in Fig. 4.5; the maximum pressure distribution for parallel surfaces with a perfect slip surface using the optimized complex slip surface (L_s = 0.65) is very high and approximately three times as large as the maximum pressure obtained from a no-slip wedge with the optimized slope incline ratio, H = 2.2. For more detailed information on the optimum length of the slip zone, the reader is referred to the appending Papers B, D, and E.

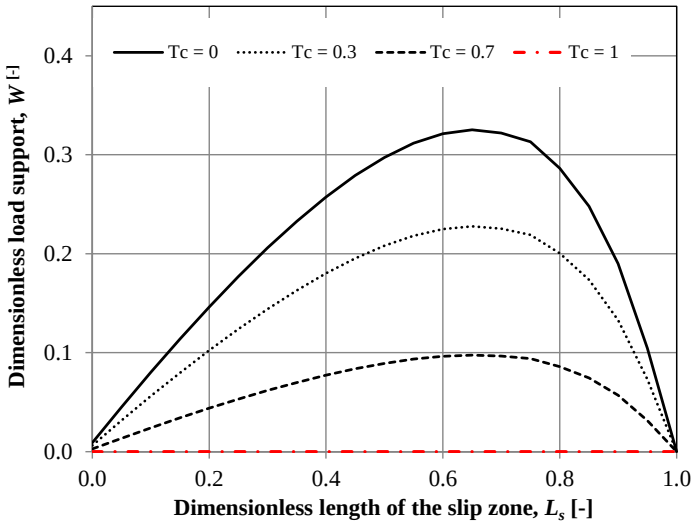

FIGURE 4.4: *Effect of the dimensionless length of slip zone, L_s, on the dimensionless load support, W, of an artificial slip surface at several dimensionless critical shear stress values, T_c, for two parallel moving surfaces.*

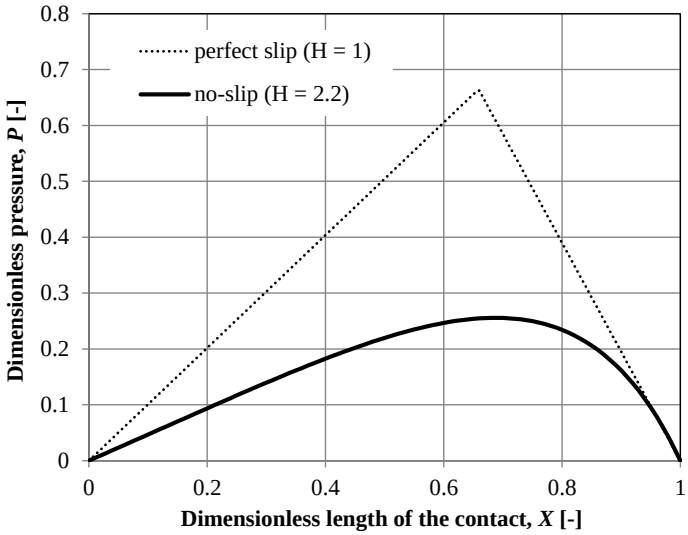

FIGURE 4.5: *Dimensionless hydrodynamic pressure distribution, P, of a perfect slip surface generated by an artificial complex slip surface (L_s = 0.65) for two parallel moving surfaces, and of a no-slip surface for optimized slope incline ratio, H = 2.2.*

In the two-dimensional case, varying the slip zone in *y*-direction (perpendicular to the sliding direction) by optimization with varying the slip zone in the *x*-direction gives a better hydrodynamic pressure generation. This is understandable, because with the CSS pattern, the side leakage is inhibited utilizing the no-slip boundary condition. This analysis is presented in more detail in the appending Paper A. These results lead to the conclusion that a complex slip surface is superior to a homogeneous slip surface with respect to the load.

4.2.2. Effect of critical shear stress

The focus of this section is to show the importance of the critical shear stress for lubricated sliding contacts with slip. The complete results are presented in appended Paper A (in the two-dimensional case) and Paper B (in the one-dimensional case).

A change in critical shear stress of a contact with a homogeneous slip surface has a significant effect on the predicted load support, as can be concluded from Fig. 4.6 (one-dimensional case), and the appending Paper A (two-dimensional case). It is interesting to note that for a modest value of slope incline ratio, H, for example, $H = 2.2$, when the dimensionless critical shear stress, T_c, increases, the value of the dimensionless load support, W, first decreases, reaches a minimum value when $T_c \approx 0.42$ and then starts to increase, finally reaching the no-slip limit (the Reynolds load support). For other values of H, a similar variation of W with T_c is found. However, for increasing H the minimum in W shifts to lower values of T_c and higher values for W. When $T_c = 0$, for all slope incline ratios, fluid load support is half the Reynolds load support. In the two-dimensional case, using a different slip model, i.e. the two-component slip model, a similar trend is obtained in predicting load support with varying slope incline ratio (see Paper A).

Figure 4.7 shows the hydrodynamic load support of an artificial complex slip surface versus the surface critical shear stress for several slope incline ratios. It can be noted that at a large slope incline ratio, the surface critical shear stress has little effect on the hydrodynamic load support. At a small slope incline ratio, for example, $H = 1$, the load support capacity decreases with an increase in the surface critical shear stress. It is also shown that in the case of parallel sliding surfaces, when the dimensionless critical shear stress rises to 1 or larger, the benefit of employing the engineered complex slip surface will vanish. Therefore, the configuration of a surface with a high critical shear stress ($T_c \geq 1$ in this case) is not advisable for improving the load support. In other words, in lubricated-MEMS devices which frequently exhibit parallel sliding surfaces, the benefit of an artificial complex slip surface is maximal if the critical shear stress on the slip surface is designed as low as possible. For a low critical shear stress, more lubricant can be entrained into the lubricated contact gap inducing higher hydrodynamic pressure. In real applications, the artificial slip surface can be obtained with a super-hydrophobic surface. Therefore, for maximum load support, it is very beneficial to engineer the critical shear stress to zero (i.e. perfect slip).

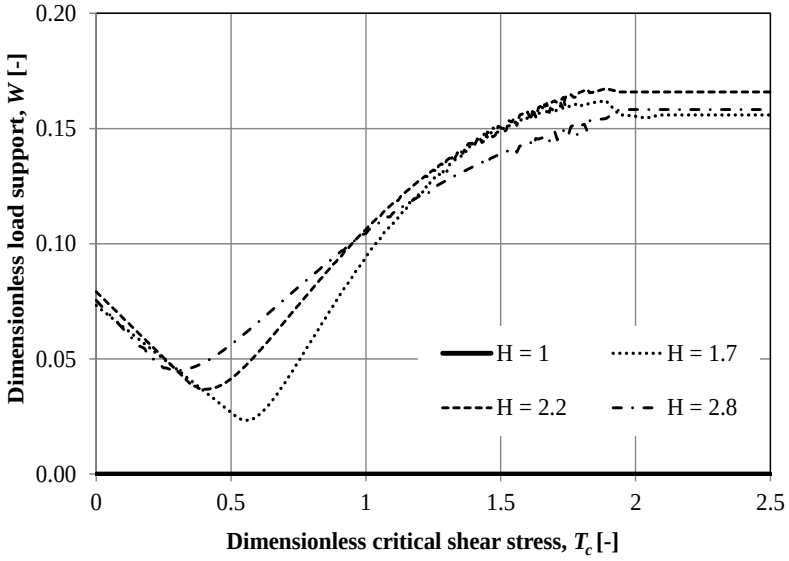

FIGURE 4.6: *Effect of the critical shear stress on the load support of an artificial homogeneous slip surface (L_s = 1) in the lubricated sliding contact with different values of the slope incline ratio, H.*

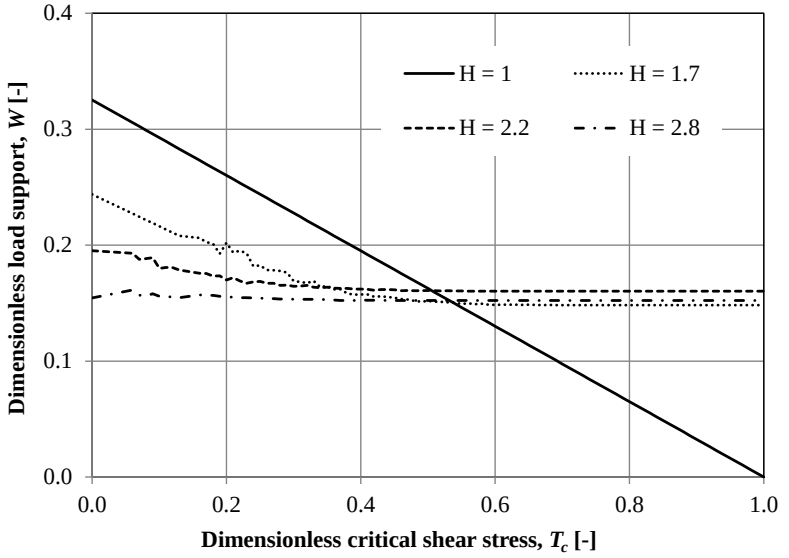

FIGURE 4.7: *Effect of the critical shear stress on the load support of an artificial complex slip surface (L_s = 0.65) in the lubricated sliding contact with different values of the slope incline ratio, H.*

4.2.3. Effect of slip length

Now, the effect of slip length on lubrication behavior is studied. Firstly, the case of the lubricated parallel sliding contact with the artificial complex slip surface is studied. For more details, the reader is referred to appending Papers A, D, E and G. In the following simulations, the dimensionless slip length, B, is varied from 1 to 50 [7, 8, 25, 30, 72]. A perfect slip surface (i.e. $\tau_c = 0$) is assumed for a maximum load support, as discussed in the previous section.

As can be seen in Fig. 4.8, for a lubricated parallel sliding contact (i.e. the wedge effect is absent), the increase of the dimensionless slip length leads to a large improvement in the dimensionless load support. However, for B greater than, say 20, the variation in B has an insignificant effect on the performance.

With respect to the friction force, the increase in the dimensionless slip length leads to a decrease in the predicted dimensionless friction force, F. It can also be observed that the friction force estimated by the optimized CSS pattern is smaller than the no-slip prediction. If B decreases to zero, then F increases to its no-slip value, which means that the lubricated contact with slip pattern surface behaves like a traditional one. In conclusion, a high slip length designed for lubricated-MEMS leads to greater improvement in load support and also to a reduction in friction force.

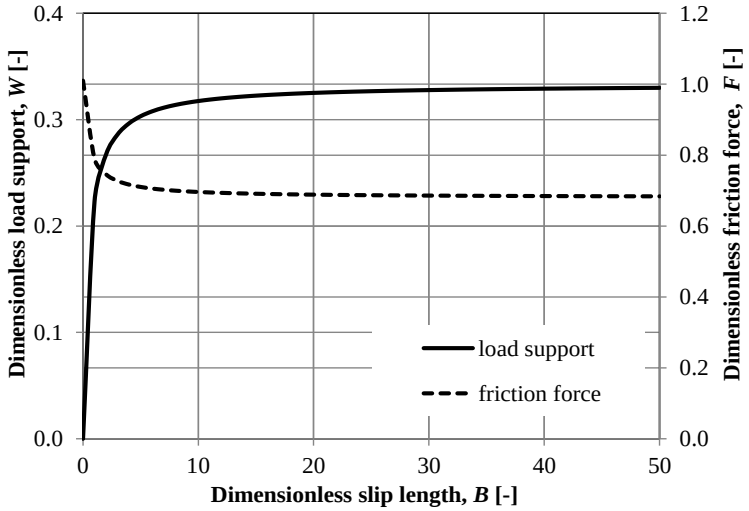

FIGURE 4.8: *Effect of the slip length on the hydrodynamic performance of an artificial complex slip surface ($L_s = 0.65$) in the lubricated parallel sliding contact.*

Secondly, the case in which the wedge effect is present (i.e. $H \neq 1$), either with a complex slip condition or homogeneous slip, is investigated. As can be concluded from Figs. 4.9 and 4.10 (one-dimensional case) and the appending Paper A (two-dimensional case), in the case of a complex slip surface, compared to the contact without the wedge effect, the trend of the slip length is quite similar to that with the wedge effect. However,

from the simulation results, it is found that there is a threshold value of the slip length which is unique for each slope incline ratio. For a high slope incline ratio (H = 2.8 in this case), adding the slip property to the surface does not affect the load support and the friction force. One can remark that the wedge effect reduces the beneficial effect of the existence of the (complex) slip with respect to the load support and the friction force.

In the case of the homogeneous slip, with respect to load support, different results are obtained, see Fig. 4.11. With the increase in slip length, the predicted load support decreases. However, the decrease in load support is not large. This trend prevails for all the slope incline ratios considered here as well as for the trend of the friction force, see Fig. 4.12. When B = 5 and larger, the artificial homogeneous slip boundary can reduce the load support by half of what Reynolds theory predicts (no-slip condition). It indicates that there is no-unique value of B for each of the slope incline ratios. It can be noted that when H = 1, there is no load support for the homogeneous slip for all slip lengths and thus the lubrication can break down. This, of course, is an unwanted situation in lubricated-MEMS. For more details regarding this issue, the reader is referred to appending Papers A and H.

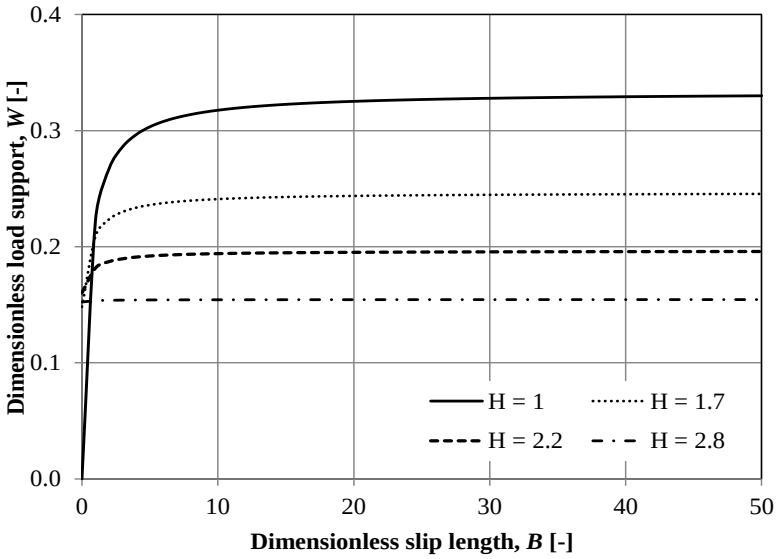

FIGURE 4.9: *Effect of the slip length on the load support of an artificial complex slip surface (L_s = 0.65) in the lubricated sliding contact with different values of the slope incline ratio, H.*

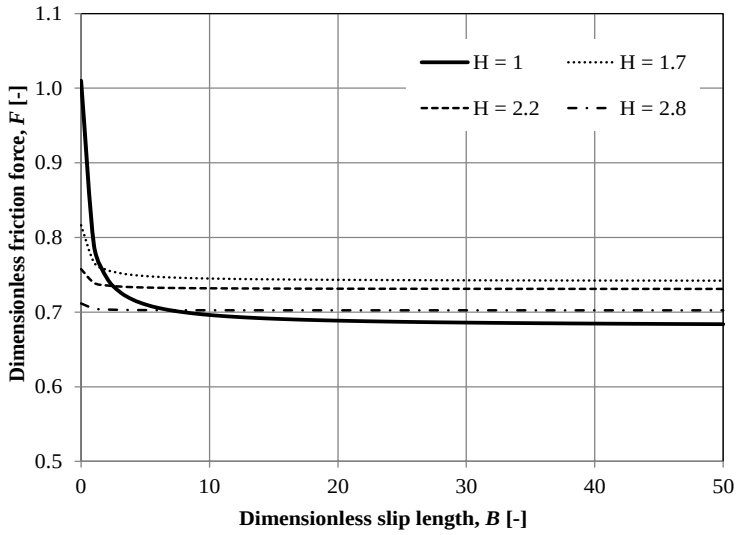

FIGURE 4.10: *Effect of the slip length on the friction force of an artificial complex slip surface (L_s = 0.65) in the lubricated sliding contact with different values of the slope incline ratio, H.*

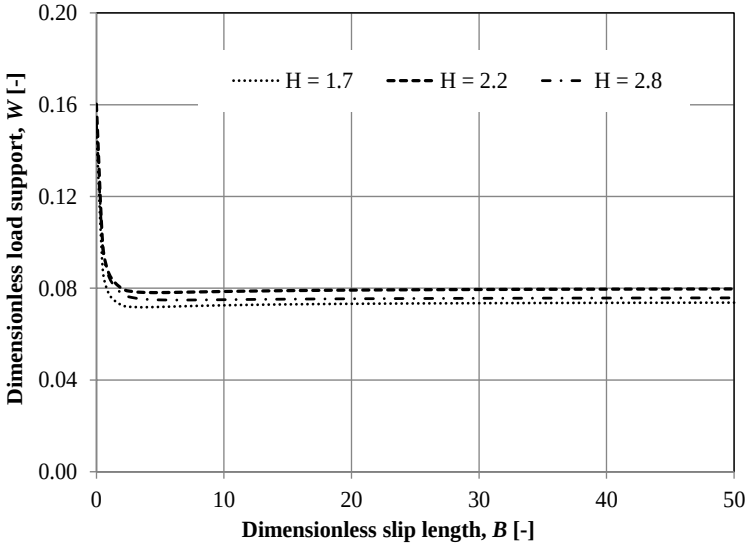

FIGURE 4.11: *Effect of the slip length on the load support of an artificial homogeneous slip surface (L_s = 1) in the lubricated sliding contact with different values of the slope incline ratio, H.*

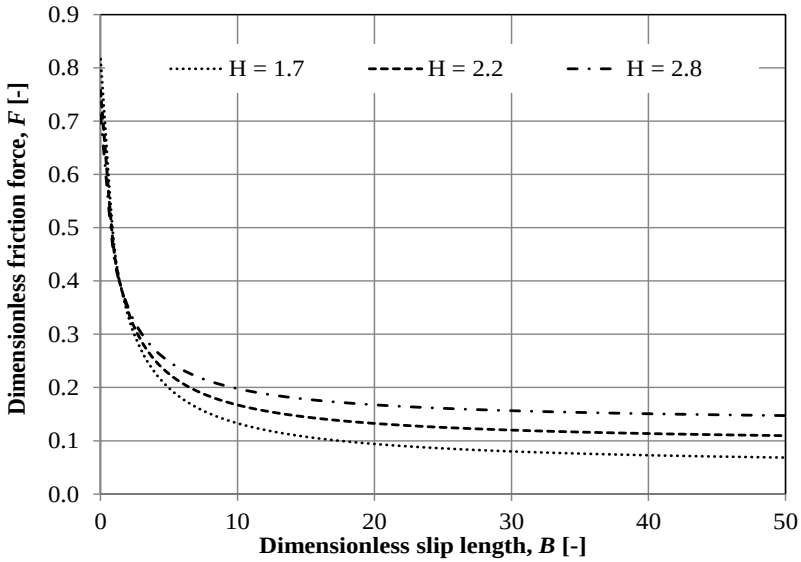

FIGURE 4.12: *Effect of the slip length on the friction force of an artificial homogeneous slip surface (L_s = 1) in the lubricated sliding contact with different values of the slope incline ratio, H.*

4.3. Interaction of boundary slip with surface texture

Surface texturing ("artificial physical roughness") is well known and seems to be a promising way of improving the performance of lubricated sliding contacts. In the case of parallel sliding surfaces, like in most MEMS devices, it is of importance that surface texturing maximizes the pressure and thus the load support. In a traditional (smooth, no-slip) parallel sliding contact, no hydrodynamic load support takes place.

Figure 4.13 shows a schematic representation of a lubricated sliding contact with combined surface texturing and slip (called textured slip pattern) used in this research. The analysis of the combined textured slip contact with uniform film thickness (two parallel sliding surfaces) is of particular interest. The parameter L_{ts} for the dimensionless textured slip zone is introduced and categorized into three kinds of texturing, i.e. flat (L_{ts} = 0), partial texturing (L_{ts} < 1) and full texturing (L_{ts} = 1). The texture cell can be described by three dimensionless parameters: the texture density ρ_T, relative dimple depth ε, and the texture cell aspect ratio λ. The texturing zone L_{ts} may consist of a number of texture cells depending on the chosen texture cell aspect ratio. In this research, the slip boundary is employed on all sides of the texture cell (see Fig. 4.13). For all following simulations considered here, it is assumed that the texture density, ρ_T, is constant and equal to 0.5, and the relative texture cell depth, ε, is fixed at a value of 1. Thus, the variation of λ is achieved by modifying the dimple length, d_c, while keeping a constant land film thickness, h_F, and dimple depth, d_h.

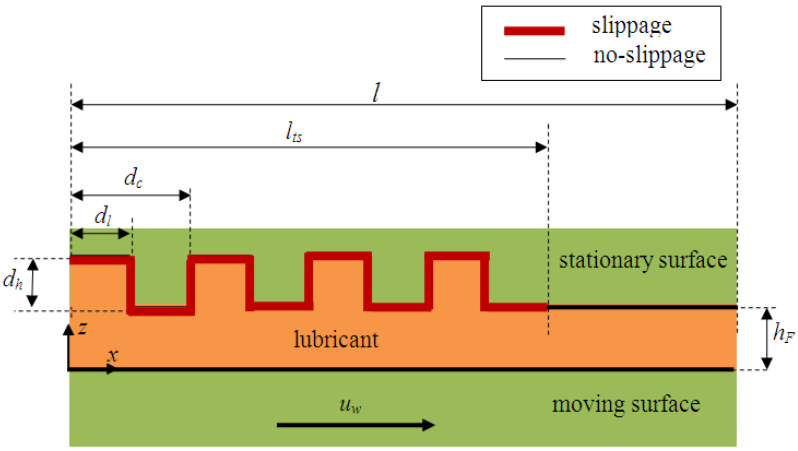

FIGURE 4.13: *Schematic of a lubricated parallel sliding contact with partially textured stationary surface combined with slippage on all sides of the texture cell.*

An assumption is made that at the inlet and outlet of the domain, the pressure is set to be ambient and the cavitation boundary condition is not used. In this study, a rectangular geometry for the texture cell shape is used.

In the combined textured slip pattern, there are two main parameters, i.e. slip parameter (i.e. slip length and critical shear stress) and the texture parameter (i.e. texture cell aspect ratio λ and textured region L_{ts}). Using a parametric analysis, the optimum value of the texture parameter, as well as the slippage parameter, is computed. Results suggest the feasibility of controlling friction by achieving slippage on the textured surface in lubricated contact.

In the literature, there are two main theories dealing with the relation between surface roughness and boundary slip. The first is that surface roughness inhibits boundary slip or increases the critical shear stress [14, 18, 49]. The second one is, however, the opposite. This theory states that the surface roughness increases boundary slip [50].

This thesis explores the possibility of employing a boundary slippage combined with artificial surface roughness (texturing) in MEMS sliding applications in order to improve performance characteristics (load carrying capacity and coefficient of friction). The results of these simulations are presented in the appending Papers B, C, G and H. In addition, the critical shear stress as main parameter for boundary slip at the textured surface with slip is also investigated in order to obtain an answer to the question "does texturing as an artificial roughness inhibit or even accelerate the occurrence of boundary slip?". A detailed discussion about this issue is presented in more detail in the appending Paper C.

Figure 4.14 shows the effect of the dimensionless length of the textured slip zone, L_{ts} (simulating partial texturing or full texturing) on the dimensionless load support, W, and varying the dimensionless slip length, B. It can be observed that there is a significant increase in load support when boundary slippage is combined with texturing both for low and high texture cell aspect ratio λ. When $B = 0$ (i.e. the no-slip textured surface), the optimal textured zone, L_{ts}, is around 0.55. This result corresponds to the one obtained by

Etsion and Halperin [74] based on a numerical solution of the two-dimensional Reynolds equation for textured parallel thrust bearings, and later by Pascovici *et al.* [83] based on an analytical solution of the one-dimensional Reynolds equation for partially textured parallel sliding contacts.

It can also be seen from Fig. 4.14 that there is a shift of the maximum of the dimensionless load support if the slip condition exists on the textured surface. It means that for improving the load support significantly, in addition to applying slip on the texture cells, the texturing zone needs to be sufficiently extended. The optimal textured slip zone occurs when L_{ts} = 0.75. With respect to the effect of the texture cell aspect ratio, λ, increasing λ leads to a reduction in the predicted load support, and this effect only becomes very significant in the case of purely textured contact (i.e. B = 0). It indicates that the presence of boundary slip on the texture cells creates a more dominant effect and results in an increase in load support of textured parallel sliding surfaces. For more details, see appending Papers B and H.

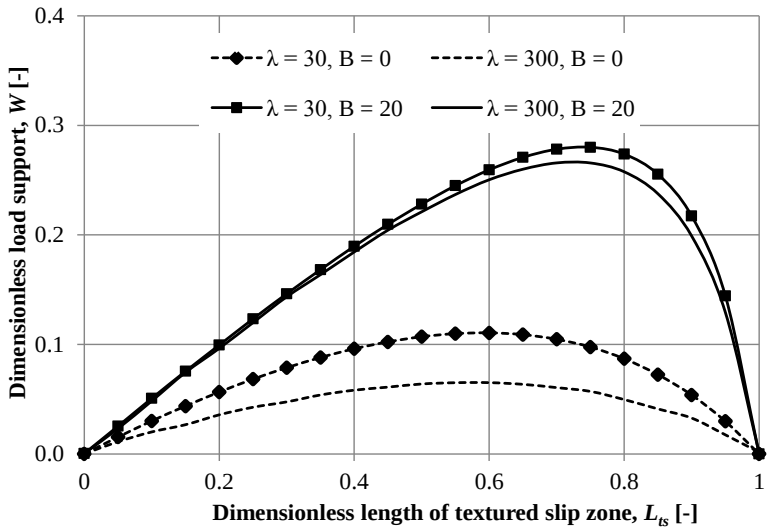

FIGURE 4.14: *Effect of the dimensionless length of textured slip zone, L_{ts}, texture aspect ratio, λ, and dimensionless slip length, B, on the dimensionless load support of a combined textured slip surface*.

Figure 4.15 shows the effect of the dimensionless length of the textured slip zone, L_{ts}, (simulating partial texturing or full texturing) on the dimensionless load support, W, and varying the critical shear stress, T_c. It shows that the load support increases rapidly and then decreases with the increase of the texturing zone. It means that the superiority of partially textured sliders against fully textured sliders is noted. Full texturing, as well as flat contact, is unable to generate hydrodynamic lift in parallel sliders. Obviously, as can be seen from Fig. 4.15, increasing the dimensionless critical shear stress, T_c, is not recommended whatever the value of the texture cell aspect ratio, λ. A perfect slip surface (i.e. T_c = 0) is

recommended. One can remark that there is an optimum value for the dimensionless texturing slip zone for each value of T_c, which decreases with increasing T_c. It is therefore evident that increasing the T_c would make a shift of the optimum texturing zone towards the leading edge of the contact (left-hand side of the curve). However, when the texture cell aspect ratio, λ, is increased by a factor of 10, no shift of the optimum value for L_{ts} is found. In other words, the optimum value of W is practically independent of the texture cell aspect ratio λ. More simulation results concerning the texture parameter effect on the load support in the case of a textured pattern, either with slip or no-slip conditions, are presented in the appending Paper B.

With respect to the effect of the texture cell aspect ratio, it is noted that when the dimensionless critical shear stress T_c is set to be very high, λ has a strong effect on the load support. This is as expected because when T_c is very high, the combined textured slip surface may behave like the traditional textured surface situation. For a perfect slip surface (T_c = 0), the load support profile shows a different trend, i.e. lowering or increasing the λ does not affect the load support significantly. This result leads to two conclusions: (1) as explained earlier (see Fig. 4.14), the boundary slip effect has a much higher contribution in generating hydrodynamic pressure than the texturing effect (i.e. texture aspect ratio), and thus results in an increase in the load support of textured parallel sliding surfaces, (2) there are unique thresholds of T_c for every λ. This result also explains why the (artificial) surface roughness could affect the boundary slippage as discussed by [14, 18, 49, 50]. For details, the reader is referred to appending Paper C.

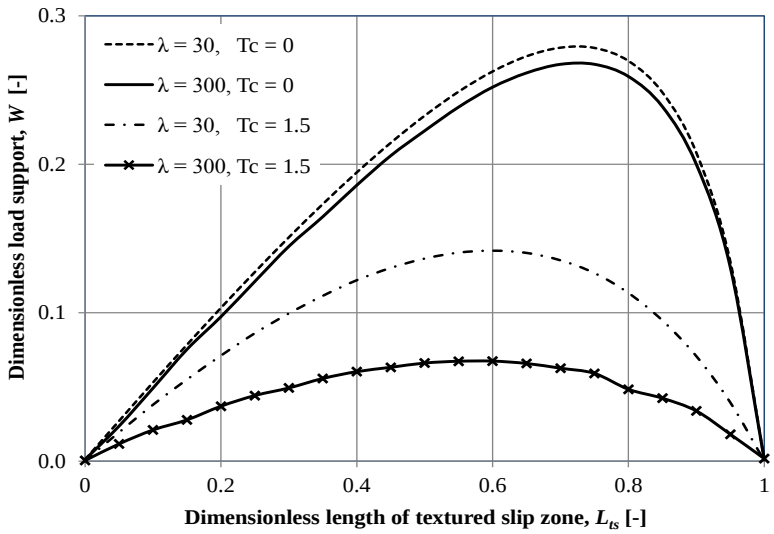

FIGURE 4.15: *Effect of the length of textured slip zone, L_{ts}, texture aspect ratio, λ, and dimensionless critical shear stress, T_c, on the dimensionless load support of a combined textured slip surface.*

In Figure 4.16, the effect of a textured slip zone for several texture cell aspect ratios on the dimensionless friction force is presented. As is known, the ability to control and manipulate the friction force during sliding is an extremely important key to prolonging the lifetime of lubricated-MEMS. Better understanding of the friction force phenomena on microscopic level is needed to provide designers and engineers with the required tools and capabilities to control friction and predict the failure of lubrication in MEMS due to stiction.

Figure 4.16 also reveals that the friction force of the combined textured slip surface (with $B = 20$) becomes smaller than that of a traditional textured contact ($B = 0$) for the texture cell aspect ratio considered here. The friction force decreases with increasing the textured slip zone, L_{ts}. It can be seen that when the textured slip zone covers the whole surface, i.e. full texturing, the friction force has a minimum value. If the reduction in friction force is only of particular interest, the fully textured slip surface ($L_{ts} = 1$) is very beneficial. But if performance is also related to load support, a fully textured slip surface is not recommended because when $L_{ts} = 1$, the predicted load support is very small for all λ (see Fig. 4.15). With respect to the influence of the texture cell aspect ratio, the dimensionless friction force does not vary significantly either for the purely textured contact or for the combined textured slip contact. Consequently, in terms of the dimensionless coefficient of friction, see Fig. 4.17, the load support has a more dominant effect than the friction force to vary the coefficient of friction.

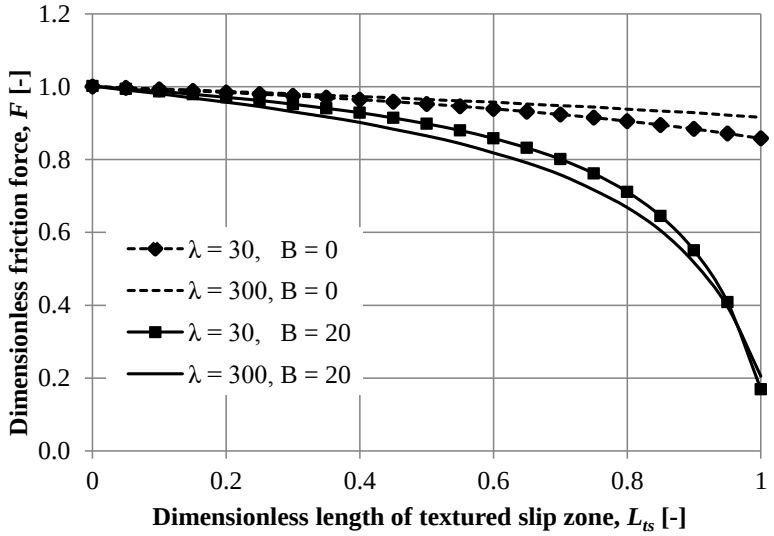

FIGURE 4.16: *Effect of the length of textured slip zone, L_{ts}, texture aspect ratio, λ, and dimensionless slip length, B, on the dimensionless friction force, F, of a combined textured slip surface.*

Based on Fig. 4.17, it is shown that extending the length of the textured region, L_{ts} results in the decrease-then-increase behavior of the coefficient of friction. This trend seems to be very clear in the case of a purely textured pattern. The optimum texturing zone with respect to the minimum coefficient of friction is very close to the optimum for the maximum load carrying capacity criteria. As a concluding remark for lubricated-MEMS, it is very beneficial to implement an optimized textured slip surface for achieving ideal lubrication performance, i.e. a reduced coefficient of friction and an increased load support. For more details, see Paper H.

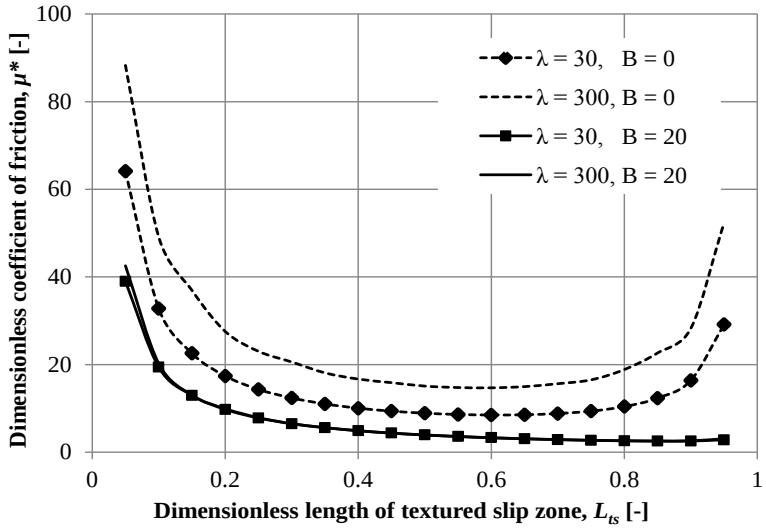

FIGURE 4.17: *Effect of the length of textured slip zone, L_{ts}, texture aspect ratio, λ, and dimensionless slip length, B, on the dimensionless coefficient of friction, μ^*, of a combined textured slip surface.*

"Which pattern is better for obtaining maximum lubrication performance: the combined textured slip surface or the artificial complex slip smooth surface?" To answer this question, a comparison is made on the basis of the hydrodynamic performance for various possible surface boundary conditions, i.e. traditional (smooth, no-slip) contact, artificial complex slip surface, purely textured surface and combined textured slip pattern. In this comparison, all parameters including the length of the slip region, L_s, the length of the texturing zone, L_{ts} and the texture cell aspect ratio, λ have been initially optimized (with respect to maximum load support). From the simulation results, see Table 4.1, Fig. 4.18 and appending Paper B (using the Reynolds approach) and Paper G (using the CFD approach), it is concluded that compared with other patterns, an artificial complex slip smooth surface generates the best lubrication performance (i.e. highest load support and lowest coefficient of friction). Additionally, it can be utilized as a guideline for the fabrication of modified sliding surfaces, for instance, in lubricated-MEMS.

Table 4.1: *Optimized lubricated contact characteristics.*

Contact type	H	L_s	L_{ts}	λ	B	W	F	μ^*
no-slip smooth surface	2.2	-	-	-	-	0.1602	0.7533	4.7011
complex slip smooth surface	1	0.65	-	-	50	0.3297	0.6859	2.0804
purely textured surface	1	-	0.55	20	-	0.1121	0.9567	8.5320
combined textured slip surface	1	0.75	0.75	20	50	0.2964	0.7838	2.6448

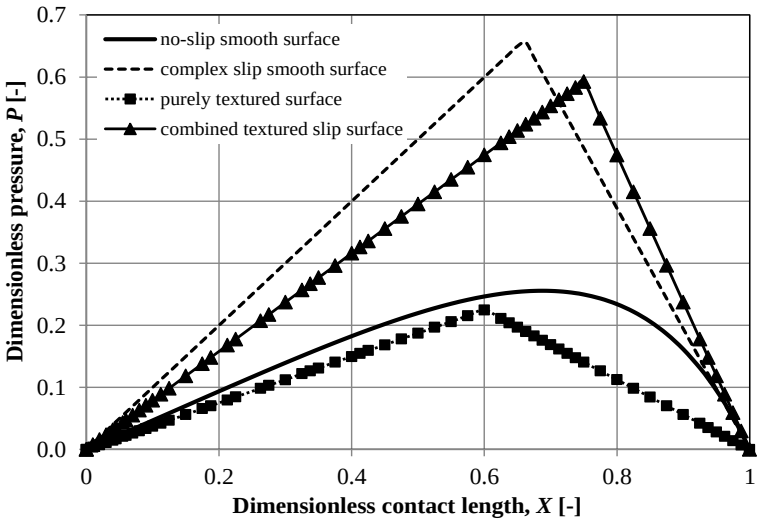

FIGURE 4.18: *Dimensionless pressure distribution for several conditions. All configurations are calculated based on the optimized values of characteristics as indicated in Table 4.1.*

4.4. Validation

The modified Reynolds equation with slip was proposed and presented in Chapter 3. In order to validate the model, comparisons with the experimental study by Choo *et al.* [7] were made.

As described in [7], the experiment was conducted using a tribometer to show the effect of hydrophobicity on the coefficient of friction between two shearing surfaces lubricated by a 72% aqueous glycerol solution. The tribometer was constructed for measuring friction at low loads, to investigate the feasibility of using the liquid-slip

phenomenon for the lubrication of high sliding MEMS. In this way, a low-load lubricated sliding contact was constructed and the hydrodynamic lubrication condition in ball-on-flat contact was investigated over a wide range of sliding velocities. A schematic diagram of the tester is shown in Fig. 4.19. An upper stationary flat is held on a cantilever arm assembly and loaded against the curved surface of a rotating ball. The lower specimen was a steel ball (AISI52100), while the upper specimen was a hydrophobic mica surface. The sliding velocity is varied and controlled in the range 1-2.5 m/s and loads below 0.2 N. For the experimental setup and procedure and test lubricant and specimens, the reader is referred to reference [7] for more details.

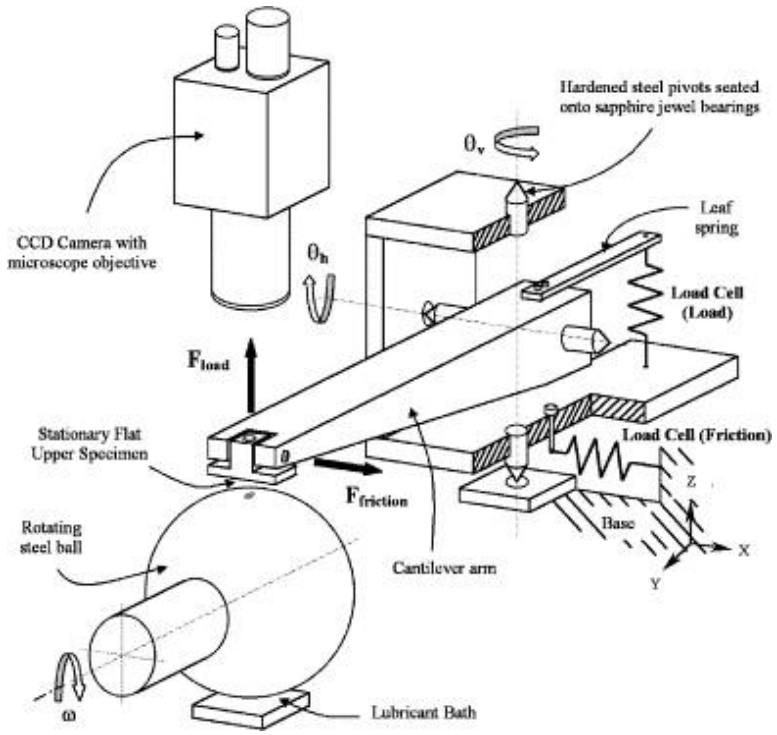

FIGURE 4.19: *Schematic of tribometer* [7].

The solid surfaces are assumed to be rigid, no elastic deformation is considered (see Fig. 4.20).

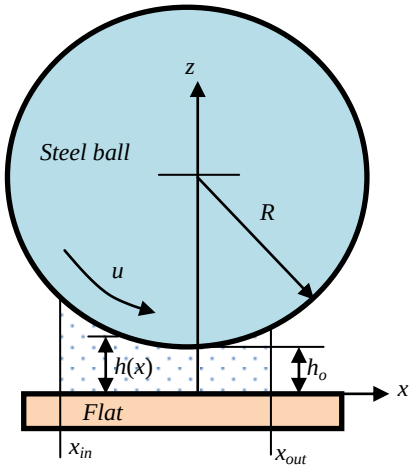

FIGURE 4.20: Schematic of fluid flow in a thin gap between roller and flat.

As shown in Fig. 4.20, the gap can be written approximately as [87]

$$h(x) = h_o + x^2 / 2R \tag{3.5}$$

where h_o is the minimum film thickness at $x = 0$ and R is the radius of the steel ball. In the numerical simulations the following parameters are used: $x_{in}/R = -0.2$, and $x_{out}/R = 0.1$. The pressure boundary condition at the inlet is $p = 0$ at $x_{in}/R = -0.2$. At the outlet, the free boundary pressure condition of Reynolds is applied, i.e. $p = 0$ and $\partial p / \partial x = 0$. Finite volume method and tri-diagonal-matrix-algorithm [70, 71] are used in the numerical solution. The input data used for the analysis are presented in Table 4.2. The coefficient of friction is obtained by dividing friction by load.

Table 4.2: *Main parameters.*

Lubricant viscosity	η	0.0028 Pa.s (at 25^{o}C)
Critical shear stress	τ_c	0
Slip length	b	20 μm
Sliding velocity	u	1 to 2.5 m/s
Radius of the steel ball	R	25.4 mm
Normal load	w	0.05, 0.1 and 0.2 N

Figure 4.21 shows a comparison between the measured values and the predicted values of the coefficient of friction for three different normal loads (0.05, 0.1, 0.2 N). It is shown that the measured coefficient of friction decreases with load but increases with velocity, having values between 0.15 and 0.25 for 0.05 N load, between 0.09 and 0.15 for 0.1 N and between 0.06 and 0.10 for 0.2 N load, and these compare well with the simulation results, especially for the load of 0.2 N. For other loads (i.e. 0.1 and 0.05 N), the predicted values are approximately 10% higher than the measured values. A possible reason for the friction being lower than predicted in Fig. 4.21 might be due to shear heating in the contact during the experiment resulting in a reduced viscosity. In order to show the beneficial effect of slip on the friction reduction, the corresponding case of no-slip is also presented. It is clear that the predicted values for the slip surface are lower than those predicted for a no-slip surface. The average reduction in friction coefficient was calculated to be 22.3% at 0.05 N, 21.7% at 0.1 N and 19.6% at 0.2 N, indicating an increasing reduction at lower loads. These findings match well with the results of Spikes [6], which stated that the difference in coefficient of friction between a no-slip and a slip situation increases at very low bearing pressures.

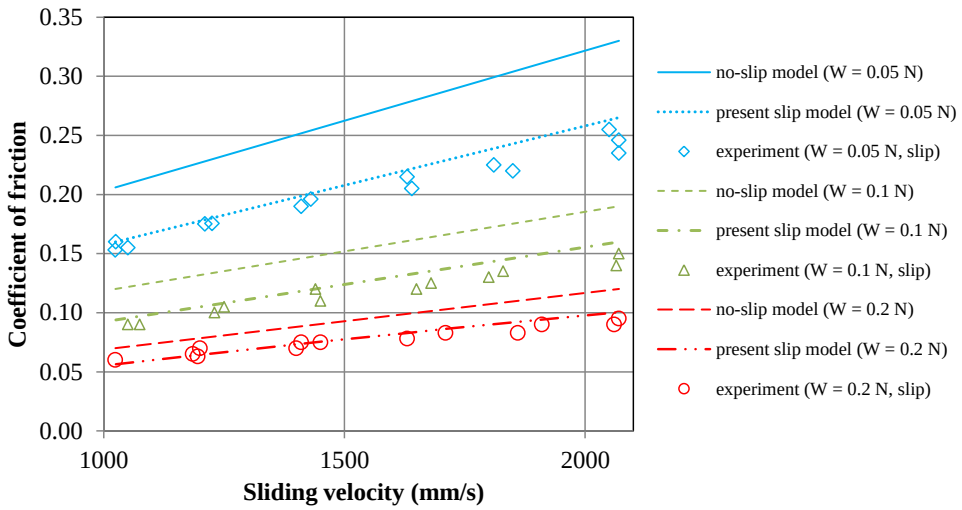

FIGURE 4.21: *Comparison of measured* [7] *and calculated hydrodynamic coefficient of friction for a lubricated sliding contact with slip as a function of velocity for different loads: (1) 0.05 N, (b) 0.1 N and (c) 0.2 N. (Note: no-slip situation is presented to show the beneficial effect of slip on the friction reduction).*

It should be noted that the calculated results are obtained using the same slip parameters at all three loads. In general, it can be said that there is reasonably good agreement between the modified Reynolds theory developed here and the experiment.

Chapter 5

Conclusion and future work

5.1. Conclusion

The main objective of the work presented here is to implement boundary slip in the lubrication of MEMS devices such that high load support and low friction are obtained. The critical shear stress for boundary slip is adopted in modeling lubrication with slip. The modified Reynolds equation developed allows simulation of cases in which (1) the zero or non-zero critical shear stress is present and/or (2) slip occurs either at one or both surfaces (stationary and sliding surface).

The artificial slip surface is introduced in reducing the failure of lubricated-MEMS due to the stiction. Within the current research, attempts are made to obtain an optimized artificial slip surface. Two approaches are used, i.e. parametric analysis and genetic algorithm. In order to validate the proposed model, experimental validation of published work has been completed. A good agreement exists between the present model and some experimental observations of ball-on-flat tests at low loads, as well as in lubricated-MEMS. In addition, validation through general results found in the literature has also been conducted.

In conclusion, it is shown that a surface with an optimized complex slip surface (CSS) pattern in a lubricated contact has many advantages compared to a surface without slip. The effect of an optimized CSS pattern on the hydrodynamic performance is most effective with respect to the maximum load support for parallel sliding surfaces when (1) the critical shear stress is zero, and (2) slip is applied only on the stationary surface. In the case of combined textured slip pattern, it is found that slip contributes more in generating hydrodynamic pressure than texturing. It is also demonstrated that for parallel sliding surfaces, the (partially) textured surface with boundary slip is superior to the textured surface but it is not as effective as the smooth configuration with a complex slip surface for the best hydrodynamic performance (i.e. high load support and low friction).

5.2. Future work

The long-term goal is to develop engineering tools to prolong the lifetime of lubricated MEMS devices. Therefore, two main research directions are suggested:

(1) For texturing, it is advised to put some effort into investigating texture shapes,
(2) It is suggested that research be carried out on rough surfaces, texturing on roughness scale at the slip surface.

References

1. Henck, S.A., 1997, "Lubrication of digital micromirror devices," *Tribology Letters* **3**, pp. 239 – 247.
2. de Boer, M.P. and Mayer, T.M., 2001, "Tribology of MEMS," *MRS Bulletin* **26**(4), pp. 302 – 304.
3. Israelachvili J., 1995, *Intermolecular and Surface Force. vol. 1. 2nd edition*, Academic Press, London.
4. van Spengen, W.M., Puers, R. and De Wolf, 2003, "On the physics of stiction and its impact on the reliability of microstructures," *Journal of Adhesion Science and Technology* **17,** pp. 563 – 582.
5. Spikes, H.A., 2003, "The half-wetted bearing. Part 1: extended Reynolds equation," *Proceedings of the Institution of Mechanical Engineers, Part J: Journal of Engineering Tribology* **217**, pp. 1 – 14.
6. Spikes, H.A., 2003, "The half-wetted bearing. Part 2: Potential application in low load contacts," *Proceedings of the Institution of Mechanical Engineers, Part J: Journal of Engineering Tribology* **217**, pp. 15 – 26.
7. Choo, J.H., Spikes, H.A., Ratoi, M., Glovnea, R. and Forrest, A., 2007, "Friction reduction in low-load hydrodynamic lubrication with a hydrophobic surface," *Tribology International* **40**, pp. 154 – 159.
8. Choo, J.H., Glovnea, R.P., Forrest, A.K. and Spikes, H.A., 2007, "A low friction bearing based on liquid slip at the wall," *ASME Journal of Tribology* **129**, pp. 611 – 20.
9. Ku, I.S.Y., Reddyhoff, T., Wayte, R., Choo, J.H., Holmes, A.S. and Spikes, H.A., 2012, "Lubrication of microelectromechanical devices using liquids of different viscosities," *ASME Journal of Tribology* **134** pp. 012002-1 – 7.
10. Reynolds, O., 1886, "On the theory of lubrication and its application to Mr. Beauchamp Tower's experiments, including an experimental determination of the viscosity of olive oil," *Philosophical Transactions of the Royal Society of London, Part I* **177**, pp. 157 – 234.
11. Hamrock, B.J., 1994, *Fundamentals of Fluid Film Lubrication*, McGraw-Hill, In., New York.
12. Spearing, S.M., 2000, "Materials issues in microelectroctromechanical systems (MEMS)," *Acta Materialia* **48**, pp. 179 – 196.
13. Navier, C.L.M.H., 1823, "Mémoire sur les lois du mouvement des fluides," *Mémoires de l'Académie Royale des Sciences de l'Institut de France* **6**, pp. 389 – 440.
14. Pit, R., Hervet, H. and Leger, L., 2000, "Direct experimental evidence of slip in hexadecane: solid interfaces," *Physical Review Letters* **85**, pp. 980 – 983.
15. Craig, V.S.J., Neto, C. and Williams, D.R.M., 2001, "Shear-dependent boundary slip in an aqueous Newtonian liquid," *Physical Review Letters* **87**, 054504.
16. Zhu, Y. and Granick, S., 2001, "Rate-dependent slip of Newtonian liquid at smooth surface," *Physical Review Letters* **87**, 096105.
17. Zhu, Y. and Granick, S., 2002, "No-slip boundary condition switches to partial slip when fluid contains surfactant," *Langmuir* **18** (26), pp. 10058－10063.
18. Zhu, Y. and Granick, S., 2002, "Limits of the hydrodynamic no-slip boundary condition," *Physical Review Letters* **88**, 106102.
19. Spikes, H.A. and Granick, S., 2003, "Equation for slip of simple liquid at smooth solid surfaces," *Langmuir* **19**, pp. 5065 – 5071.
20. Patankar, N.A, 2003, "On the modeling of hydrophobic contact angles on rough surfaces," *Langmuir* **19**, pp. 1249 **–** 1253.
21. Jung, Y.C. and Bhushan, B., 2006, "Contact angle, adhesion and friction properties of micro and nanopatterned polymers for superhydrophobicity," *Nanotechnology* **17**, pp. 4970 – 4980.

22. Zou, M., Cai, L. and Wang, H., 2006, "Adhesion and friction studies of a nanotextured surface produced by spin coating of colloidal silica nanoparticle solution," *Tribology Letters* **21**, pp. 25 – 30.
23. Khonsari, M.M. and Booser, E.R., 2001, *Applied Tribology*, John Wiley & Sons, New York.
24. Leong, J.Y., Reddyhoff, T., Sinha, S.K, Holmes, A.S. and Spikes, H.A., 2013, "Hydrodynamic friction reduction in a MAC–hexadecane lubricated MEMS contact," *Tribology Letters* **49**, pp. 217 – 225.
25. Wu, C.W., Ma, G.J. and Zhou, P., 2006, "Low friction and high load support capacity of slider bearing with a mixed slip surface," *ASME Journal of Tribology* **128**, pp. 904 – 907.
26. Salant, R.F. and Fortier, A.E., 2004, "Numerical analysis of a slider bearing with a heterogeneous slip/no-slip surface," *Tribology Transaction* **47**, pp. 328 – 334.
27. Fortier, A.E. and Salant, R.F., 2005, "Numerical analysis of a journal bearing with a heterogeneous slip/no-slip surface," *ASME Journal of Tribology* **127**, pp. 820 – 825.
28. Guo, F. and Wong, P.L., 2006, "Theoretical prediction of hydrodynamic effect by tailored boundary slippage," *Proceedings of the Institution of Mechanical Engineers, Part J: Journal of Engineering Tribology* **220**, pp. 43 – 48.
29. Bayada, G. and Meurisse, M.H., 2009, "Impact of the cavitation model on the theoretical performance of heterogeneous slip/no-slip engineered contacts in hydrodynamic conditions," *Proceedings of the Institution of Mechanical Engineers, Part J: Journal of Engineering Tribology* **223**, pp. 371 – 81.
30. Rao, T.V.V.L.N., 2010, "Analysis of single-grooved slider and journal bearing with partial slip surface," *ASME Journal of Tribology* **132**, pp. 014501-1 –014501-7.
31. Rao, T.V.V.L.N., Rani, A.M.A., Nagarajan, T. and Hashim, F.M., 2012, "Analysis of slider and journal bearing using partially textured slip surface," *Tribology International* **56**, pp. 121 – 128.
32. Aurelian, F., Patrick, M. and Mohamed, H., 2011, "Wall slip effects in (elasto) hydrodynamic journal bearing," *Tribology International* **44**, pp. 868 – 877.
33. Schnell, E., 1956, "Slippage of water over non-wettable surfaces," *Journal of Applied Physics* **27**, pp 1149 – 1152.
34. Churaev, N.V., Sobolev, V.D. and Somov, A.N., 1984, "Slippage of liquid over lyophobic solid surfaces," *Journal of Colloid and Interface Science* **97**, pp 574 – 581.
35. Baudry, J. and Charlaix, E., 2001, "Experimental evidence for a large slip effect at a Non-wetting fluid-solid interface," *Langmuir* **17**, pp. 5232 – 5236.
36. Tretheway, D.C. and Meinhart, C.D., 2002, "Apparent fluid slip at hydrophobic microchannel walls," *Physics of Fluids* **14** (3), L9.
37. Cottin-Bizonne, C., Cross, B., Steinberger, A. and Charlaix, E., 2005, "Boundary slip on smooth hydrophobic surfaces: Intrinsic effects and possible artefacts," *Physical Review Letters* **94**, 056102.
38. Choi, C.H., Westin, K.J.A. and Breuer, K.S., 2003, "Apparent slip flows in hydrophilic and hydrophobic micro-channels," *Physics of Fluids* **15**, pp. 2897 – 2902.
39. Bonaccurso, E., Kappl, M. and Butt, H.J., 2002, "Hydrodynamic force measurements: boundary slip of hydrophilic surfaces and electrokinetic effects," *Physical Review Letters* **88**, 076103.
40. Hervet, H. and Léger, L., 2003, "Flow with slip at the wall: from simple to complex fluids," *C. R. Physique* **4**(2), pp. 241 – 249.
41. Thompson, P.A. and Troian, S.M., 1997, "A general boundary condition for liquid flow at solid surfaces," *Nature* **389**, pp. 360 – 362.
42. Priezjev, N.V. and Troian, S.M., 2004, "Molecular origin and dynamic behavior of slip in sheared polymer films," *Physical Review Letters* **92**(1), 018302.
43. Nagayama, G. and Cheng, P., 2004, "Effects of interface wettability on microscale flow by molecular dynamic simulation," *International Journal of Heat and Mass Transfer* **47**, pp. 501 – 513.
44. Smith, F.W., 1959, "Lubricant behavior in concentrated contact systems—the castor oil–steel system, " *Wear* **2**, pp. 250 – 63.

45. Smith, F.W., 1960, "Lubricant behavior in concentrated contact—some rheological problems," *ASLE Transactions* **3**, pp. 18 – 25.
46. Bair, S. and Winer, W.O., 1979, "Shear strength measurements of lubricants at high pressure," *ASME Journal of Lubrication Technology* **101**, pp. 251 – 256.
47. Bair, S. and Winer, W.O., 1990, "The high shear stress rheology of liquid lubricants at pressures of 2 to 200MPa," *ASME Journal of Tribology* **112**, pp. 246 – 252.
48. Bair, S. and Winer, W.O., 1992, "The high pressure high shear stress rheology of shear stress rheology of liquid lubricants," *ASME Journal of Tribology* **114**, pp. 1 – 13.
49. Granick, S., Zhu, Y. and Lee, H., 2003, "Slippery questions about complex fluids flowing past solids," *Nature Materials* **2**, pp. 221－227.
50. Bonaccurso, E., Butt, H.J. and Craig, V.S.J., 2002, "Surface roughness and hydrodynamic boundary slip of a Newtonian fluid in a completely wetting system," *Physical Review Letters* **90**(14), 144501.
51. Wu, C.W. and Ma, G.J., 2005, "On the boundary slip of fluid flow," *Science in China Ser. G Physics, Mechanics & Astronomy* **48**, pp. 178－87.
52. Wu, C.W., Ma, G.J. and Sun, H.S., 2005, "Viscoplastic lubrication analysis in a metal-rolling inlet zone using parametric quadratic programming," *ASME Journal of Tribology* **127**, pp. 605－610.
53. Hoglund, E., 1989, "The relation between lubricant shear stress strength analyzer and chemical composition of the base oil," *Wear* **130**, pp. 213 – 224.
54. Ostensen, J.O., Wikstrom, V. and Hoglund E., 1993, "Interaction effects between temperature, pressure and type of base oil on lubricant shear strength coefficient," *Tribologia Finnish Journal of Tribology* **11**, pp. 123 – 132.
55. Kato, K., Iwasaki, T., Kato, M. and Inoue, K., 1993, "Evaluation of limiting shear stress of lubricants by roller test," *JSME International Journal Series C* **36**, pp. 512 – 522.
56. Wikstrom, V. and Hoglund E., 1994, "Investigation of parameter affecting the limiting shear stress-pressure coefficient: a new model incorporating temperature," *ASME Journal of Tribology* **116**, pp. 612 – 620.
57. Wilson, W.R.D. and Huang, X.B., 1989, "Viscoplastic behavior of a silicone oil in a metalforming inlet zone," *ASME Journal of Tribology* **111**, pp. 585 – 590.
58. Stahl, J. and Jacobson, B.O., 2003, "A non-Newtonian model based on limiting shear stress and slip planes-parametric studies," *Tribology International* **36**, pp. 801 – 806.
59. Wu, C.W. and Ma, G.J., 2005, "Abnormal behavior of a hydrodynamic lubrication journal bearing caused by wall slip," *Tribology International* **38**, pp. 492 – 499.
60. Wu, C.W, 2008, "Performance of hydrodynamic lubrication journal bearing with a slippage surface," *Industrial Lubrication and Tribology* **60**, pp. 293 – 298.
61. Wu, C.W. and Sun, H.X., 2006, "Quadratic programming algorithm for wall slip and free boundary pressure condition," *International Journal for Numerical Methods in Fluids* **50**, pp. 131 – 145.
62. Ma, G.J., Wu, C.W. and Zhou, P., 2007, "Influence of wall slip on the hydrodynamic behavior of a two-dimensional slider bearing," *Acta Mechanica Sinica* **23**, pp. 655 – 661.
63. Ma, G.J., Wu, C.W. and Zhou, P., 2007, "Wall slip and hydrodynamics of two-dimensional journal bearing," *Tribology International* **40**, pp. 1056 –1066.
64. Ma, G.J., Wu, C.W. and Zhou, P., 2007, "Hydrodynamics of slip wedge and optimization of surface slip property," *Science in China Series G: Physics, Mechanics & Astronomy* **50**, pp. 321 – 330.
65. Ma, G.J., Wu, C.W. and Zhou, P., 2007, "Multi linearity algorithm for wall slip in two dimensional gap flow," *International Journal for Numerical Methods in Engineering* **69**, pp. 2469 – 2484.
66. Guo, F. and Wong, P.L., 2010, "Full and partial boundary slippage effect on squeeze film bearings, " *Tribology International* **43**, pp. 997 – 1004.

67. Lin, Q., Wei, Z. and Tang, Y., 2012, "Numerical study on shear flow in sliding bearing with partial slip surface," *Procedia CIRP* **3**, pp. 197 – 202.
68. Wang, L.L., Lu, C.H., Wang, M. and Fu, W.X., 2012, "The numerical analysis of the radial sleeve bearing with combined surface slip," *Tribology International* **47**, pp. 100 – 104.
69. Cameron, A, 1966, *The Principles of Lubrication*, Longman Green and Co., ltd.
70. Patankar, S.V., 1980, *Numerical Heat Transfer and Fluid flow*, Taylor & Francis, Levittown.
71. Versteeg, H.K. and Malalasekera, W., 1995, *An Introduction to Computational Fluid Dynamics – The Finite Volume Method*, John Wiley & Sons Inc., New York.
72. Watanabe, K., Yanuar and Udagawa, H., 1999, "Drag reduction of Newtonian fluid in a circular pipe with a highly water-repellant wall," *Journal of Fluid Mechanics* **381**, pp. 225 – 228.
73. Ou, J., Perot, B. and Rothstein, J.P., 2004, "Laminar drag reduction in microchannels using ultrahydrophobic surfaces," *Physics of Fluids* **16** (12), 4635.
74. Etsion, I., Halperin, G., Brizmer, V. and Kligerman, Y., 2004, "Experimental investigation of laser surface textured parallel thrust bearing," *Tribology Letters* **17**, pp. 295 – 300.
75. Kovalchenko, A., Ajayi, O., Erdemir, A., Fenske, G. and Etsion, I., 2005, "The effect of laser surface texturing on transitions in lubrication regimes during unidirectional sliding contact," *Tribology International* **38**, pp. 219 – 225.
76. Etsion, I. and Halperin, G., 2002, "A laser surface textured hydrostatic mechanical seal," *Tribology Transactions* **45**, pp. 430 – 434.
77. Ryk, G., Kligerman, Y. and Etsion, I., 2002, "Experimental investigation of laser surface texturing for reciprocating automotive components," *Tribology Transactions* **45**, pp. 444 – 449.
78. Podgornik, B. and M. Sedlacek, M., 2012, "Performance, characterization and design of textured surfaces," *ASME Journal of Tribology* **134**, pp. 041701-1－7.
79. Tønder, K., 2001, "Inlet roughness tribodevices: dynamic coefficients and leakage," *Tribology International* **34**, pp. 847 – 852.
80. Brizmer, V., Kligerman, T. and Etsion, I., 2003, "A laser surface textured parallel thrust bearing," *Tribology Transactions* **46**, pp. 397 – 403.
81. Rahmani, R., Shirvani, A. and Shirvani, H., 2007, "Optimization of partially textured parallel thrust bearings with square-shaped micro dimple," *Tribology Transactions* **50**, pp. 401 – 406.
82. Rahmani, R., Mirzaee, I., Shirvani, A. and Shirvani, H., 2010, "An analytical approach for anlysis and optimization of slider bearings with infinite width parallel textures," *Tribology International* **43**, pp. 1551 – 1565.
83. Pascovici, M.D., Cicone, T., Fillon, M. and Dobrica, M.B., 2009, "Analytical investigation of a partially textured parallel slider," *Proceedings of the Institution of Mechanical Engineers, Part J: Journal of Engineering Tribology* **223**, pp. 151 – 158.
84. Dobrica, M.B., Fillon, M., Pascovici, M.D. and Cicone, T., 2010, "Optimizing surface texture for hydrodynamic lubricated-contacts using a mass-conserving numerical approach," *Proceedings of the Institution of Mechanical Engineers, Part J: Journal of Engineering Tribology* **224**, pp. 737 – 750.
85. Tala-Ighil, N., Fillon, M. and Maspeyrot, P., 2011, "Effect of texture area on the performances of a hydrodynamic journal bearing," *Tribology International* **44**, pp. 211 – 219.
86. Sivanandam, S.N. and Deepa, S.N., 2008, *Introduction to Genetic Algorithm*, Springer-Verlag, Berlin Heidelberg.
87. Cameron, A., 1981, *Basic Lubrication Theory* (3rd edt.), Ellis Horwood Ltd.: Chichester, U.K.

Part II

Part II

Paper A:

M. Tauviqirrahman, R. Ismail, Jamari, D.J. Schipper, 2013, "Optimization of the complex slip surface and its effect on the hydrodynamic performance of two-dimensional lubricated contacts", Computers and Fluids, Volume 79, pp. 27 – 43.
doi: 10.1016/j.compfluid.2013.02.021.

Paper B:
M. Tauviqirrahman, R. Ismail, Jamari, D.J. Schipper, 2013, "Study of surface texturing and boundary slip on improving the load support of lubricated parallel sliding contacts", Acta Mechanica, Volume 224, Issue 2, pp. 365 – 381. doi: 10.1007/s00707-012-0752-7.

Paper C:
M. Tauviqirrahman, Muchammad, Jamari, D.J. Schipper, 2013, "Numerical study of the load carrying capacity of lubricated parallel sliding textured surfaces including wall slip", accepted for publication in STLE Tribology Transactions.

Paper D:
M. Tauviqirrahman, R. Ismail, Jamari, D.J. Schipper, 2013, "Computational analysis of the lubricated-sliding contact with artificial slip boundary", International Journal of Applied Mathematics and Statistics, Volume 35, Issue 5, pp. 67 – 80.

Paper E:
M. Tauviqirrahman, R. Ismail, Jamari, D.J. Schipper, 2011, "Optimization of partial slip surface at lubricated-MEMS", Proceedings of 2nd International Conference on Instrumentation, Control and Automation, Issue date: 15-17 Nov., pp. 375 – 379, ISBN: 978-1-4577-1460-3, IEEE Catalog Number: CFP1179P-DVD.
doi: 10.1109/ICA.2011.6130190.

Paper F:
M. Tauviqirrahman, R. Ismail, Jamari, D.J. Schipper, 2011, "Effect of boundary slip on the load support in a lubricated sliding contact", AIP (American Institute of Physics) Conference Proceedings, Volume 1415, Issue 51, pp. 51 – 54, ISBN: 978-0-7354-0992-7. doi:10.1063/1.3667218.

Paper G:
M. Tauviqirrahman, Muchammad, Jamari, D.J. Schipper, 2013, "CFD analysis of artificial slippage and surface texturing in lubricated sliding contact", accepted for publication in Tribology International.

Paper H:
M. Tauviqirrahman, R. Ismail, Jamari, D.J. Schipper, 2013, "Combined effects of texturing and slippage in lubricated parallel sliding contact", Tribology International, Volume 66, pp. 274 – 281. doi: 10.1016/j.triboint.2013.05.014.

M. Tauviqirrahman, R. Ismail, Jamari, D.J. Schipper, 2013

Optimization of the complex slip surface and its effect on the hydrodynamic performance of two-dimensional lubricated contacts

Computers and Fluids, Volume 79, pp. 27 – 43.

Paper A

Optimization of the Complex Slip Surface and Its Effect on the Hydrodynamic Performance of Two-Dimensional Lubricated Contacts

M. Tauviqirrahman,[1,*)] R. Ismail,[1)] Jamari,[2)] and D.J. Schipper[1)]

[1]Laboratory for Surface Technology and Tribology,
Faculty of Engineering Technology, University of Twente, The Netherlands
*Email: mtauviq99@gmail.com

[2]Laboratory for Engineering Design and Tribology,
Department of Mechanical Engineering, University of Diponegoro, Indonesia

Published in: Computers and Fluids, 2013, Volume 79, pp. 27 – 43

Abstract **In micro-electro-mechanical-system (MEMS) containing moving components, there is a need to achieve low friction and high load carrying capacity by lubrication. The aim of this paper is to study the hydrodynamic performance of a two-dimensional lubricated sliding contact in which one of the solid surfaces is designed such that partly slip boundary takes place, i.e. the complex slip surface (CSS). The approach is to use the genetic algorithm for determining the optimized complex slip surface (CSS) pattern as well as an optimized slope incline ratio simultaneously. A surface with an optimized complex slip surface (CSS) pattern in a lubricated contact generates many advantages compared to a surface without slip. The sliding surfaces considered show that the maximum load carrying capacity can be increased by approximately three times when compared to what the traditional hydrodynamics (no-slip) predict for a lubricated slider with an optimal slope incline ratio. The friction force can also be decreased significantly. The effect of an optimized complex slip surface on the hydrodynamic performance is much larger at a low initial critical shear stress than at a high initial critical shear stress. Numerical analyses indicate that varying the location and size area of the CSS pattern by taking into account the transverse direction (perpendicular to the sliding direction) in the optimization process, significantly affects the hydrodynamic performance.**

Keywords: critical shear stress, genetic algorithm, slip boundary

1. Introduction

Micro-electro-mechanical-system (MEMS) devices are widely used, and nowadays, MEMS devices are becoming prevalent in commercial applications. MEMS devices may contain rotating and/or sliding elements. Hence, the requirements for protection of moving surfaces in MEMS become of interest. The insertion of a lubricant into the region around the interacting devices could avoid direct contact between the surfaces, so the wear can be minimized. However, as the overall size of the machine is reduced, the capillary and surface tension force of liquid become large, which induce stiction, rendering the devices to fail or malfunction. Consequently, the reliability of MEMS with moving parts will be poor and have a limited lifetime. A challenge associated with MEMS is the provision of adequate lubrication for moving parts.

In traditional liquid lubrication, it has generally been accepted that the correct boundary condition between a fluid and a solid surface is the no-slip boundary condition, i.e. fully wetted. In MEMS, this wetting is actually an unwanted process because it can lead to the occurrence of stiction and as a result micro-parts cannot be moved [1]. Currently, many workers attempted to solve the stiction problem by introducing a slip boundary on the opposing surfaces when liquid lubrication is considered in MEMS [2-7]. When one or both surfaces are non-wetted by the fluid, a slip boundary can occur due to weak bonding between the fluid and the solid surface, which reduces the shear stress in the fluid adjacent to the non-wetted surface.

In the application on lubrication problems, Spikes [2-3] proposed a possible means of reducing the friction force in liquid-lubricated bearings by making one surface non-wetted or partially wetted and very smooth while the other is fully wetted, so that the liquid slips against the former under shear but adheres to the latter. The results show that the 'half-wetted" bearing is able to combine good load carrying capacity resulting from fluid entrainment with very low friction due to very low or zero Couette friction. Hild *et al*. [4] investigated the effect of slip on the friction force. It was found that the friction force in a hydrophilic-hydrophobic contact becomes significantly smaller than that of a hydrophilic-hydrophilic surface pair. An identical result was shown by Choo *et al*. [5-6]. Experimentally the effect of wettability on the friction coefficient between two shearing surfaces was studied. The results obtained with two hydrophilic contacting surfaces were found to be consistent with the hydrodynamic theory. It means that no-slip occurs at these surfaces. They found that a reduction in the friction force occurs when one surface was made hydrophobic and the other hydrophilic.

Most of the published works mentioned focused on the homogeneous slip surface and did not concern about the possibilities of different non-homogeneous surface patterns for improving the hydrodynamic lubrication performance. These studies mainly focused on only one parameter, i.e. the friction force. In an engineering application, there is a very high possibility that a slip boundary causes a friction force reduction; although at the same time the slip boundary on a hydrophobic surface may reduce the hydrodynamic pressure and thus the load carrying capacity. In MEMS, by lubrication, a low friction force and a high load carrying capacity is wanted.

The study of the slip boundary containing non-homogeneous slip/no-slip surface patterns of lubricated sliding contact was investigated by Salant and Fortier [8], Wu *et al*. [9], Ma *et al*. [10] and recently by Bayada and Meurisse [11]. Salant and Fortier [8] conducted a numerical analysis of a finite slider bearing with a non-homogeneous engineered slip/no-slip pattern surface by means of the modified slip length. However, if the critical shear stress is non-zero and slip occurs in the slip area, they could not find a steady-state numerical solution and thus concluded that the bearing operates in an unstable state. In the present paper, such a numerical instability is not found if the critical shear stress is varied. Wu *et al*. [9] analyzed the effect of the non-homogeneous engineered slip/no-slip pattern on the hydrodynamic performance. It was shown that surface optimization of a parallel sliding gap with a slip surface can double the hydrodynamic load carrying capacity and reduce the friction force by a half of what the Reynolds theory predicts for an optimal slope of inclination of a traditional slider contact. However, the analysis dealt with is a one-dimensional gap flow and the result may not be used to address an engineering application, especially on micro-scale in which the ratio of length to width of the opposing surfaces in contact cannot be considered as infinite. For a two-dimensional (finite length) journal bearing, Ma *et al*. [10] showed that the optimization of the shape and the size of the surface may give advanced properties. However, the optimization was only carried out for one parameter, i.e. the shape and size of the slip area for one value. Bayada and Meurisse [11] investigated the importance of the choice of the cavitation model in the analysis of the slip/no-slip hydrodynamic contacts. Results of several non-homogeneous slip/no-slip patterns were presented by alternating slip and no-slip areas manually, applied to one-dimensional plane slider bearings. A two-dimensional slider bearing analysis was conducted on a gap in which a convergent slope incline ratio is present.

In the present work, the term "complex slip surface pattern (CSS pattern)" is used to address a non-homogeneous engineered slip/no-slip pattern, i.e. a surface consisting of a slip area and a no-slip area. Using the two component slip model together with the genetic algorithm for optimization of the complex slip surface (CSS) pattern, the hydrodynamic performance in terms of load carrying capacity and friction force are studied. The purpose of this work is to determine the effect of an optimized CSS pattern of a two-dimensional lubricated sliding contact on the hydrodynamic performance using genetic algorithm (see Appendix A for a short explanation of the genetic algorithm and Ref. [12] for details). It will be shown that even

though based on the finite difference method, similar as Salant and Fortier did [8], our numerical technique can get a stable solution at any value of the critical shear stress without any difficulty. In this paper, the optimization, by employing a genetic algorithm, is carried out for determining an optimum for both the CSS pattern and the slope incline ratio simultaneously, not separately as conducted by Wu *et al*. [9] and Ma *et al*. [10].

2. Mathematical model

2.1. Modified Reynolds equation with slip boundary

Suppose a lubricated contact equivalent to a bottom plane moving in the x-direction, and an upper stationary surface (Fig. 1). The gap between the two surfaces is denoted by $z = h(x,y)$. The critical shear stress model is adopted, i.e. slip occurs when the surface shear stress reaches the critical value. In the complex slip surface (CSS) pattern, a surface can be divided into two regions having different properties. One region with a specific geometry with a very high critical shear stress, and thus the no-slip condition can be assumed, and the remaining region has a low critical shear stress, so slip may occur.

In this work, on a part of the upper stationary surface, the CSS pattern is located and on the remaining part of the upper surface as well as the bottom surface, a no-slip condition is imposed.

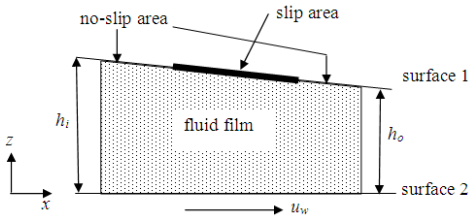

(a)

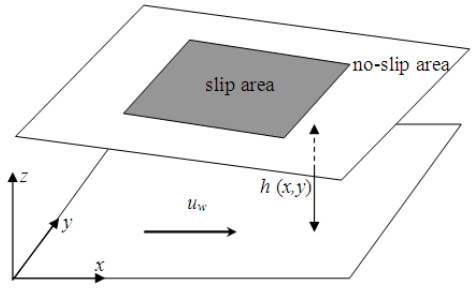

(b)

FIGURE 1: *Schematic representation of a lubricated sliding contact with the complex slip surface (CSS) pattern located at the upper surface: (a) longitudinal view, (b) isometric view.*

Following the usual approach to derive the Reynolds equation from the Navier-Stokes equation by assuming the classical assumption except that now slip is allowed, one obtains the following modified Reynolds equation.

$$\frac{\partial}{\partial x}\left(h^3\frac{\partial p}{\partial x}\right)+\frac{\partial}{\partial y}\left(h^3\frac{\partial p}{\partial y}\right)=6u_w\eta\frac{\partial h}{\partial x} +6\eta\frac{\partial(u_s h)}{\partial x}+6\eta\frac{\partial(v_s h)}{\partial y} \tag{1}$$

where u_w is the sliding velocity of the bottom surface; and u_s and v_s the slip velocities along and perpendicular to the sliding direction of the slip area on the upper surface respectively. The methodology used in the derivation of the modified Reynolds equation considering a slip boundary is similar to that employed in Choo *et al*. [5-6]. In two-dimensional flow of fluid film, the surface shear stress are given by

$$\vec{\tau}_a=\vec{\tau}_{xa}+\vec{\tau}_{ya} \tag{2}$$

where subscript *x* and *y* denote the shear stress components in *x*- and *y*-direction respectively, and the subscript a denotes surface 1 and 2 (see Fig. 1). Based on the boundary condition applied, the surface shear stress can be derived as:

$$\tau_{x1}=\frac{h}{2}\frac{\partial p}{\partial x}+\frac{u_s-u_w}{h}\eta \tag{3a}$$

$$\tau_{y1} = \frac{h}{2}\frac{\partial p}{\partial y} + \frac{v_s}{h}\eta \quad (3b)$$

$$\tau_{x2} = -\frac{h}{2}\frac{\partial p}{\partial x} + \frac{u_s - u_w}{h}\eta \quad (3c)$$

$$\tau_{y2} = -\frac{h}{2}\frac{\partial p}{\partial y} + \frac{v_s}{h}\eta \quad (3d)$$

For Eq. (1), the satisfied condition is as follows

$$\tau_1 \geq \tau_{c1} \quad \text{(for slip regions)} \quad (4a)$$

$$\tau_1 < \tau_{c1} \quad \text{(for no-slip regions)} \quad (4b)$$

$$\tau_2 < \tau_{c2} \quad (4c)$$

where τ_{c1} and τ_{c2} are the shear stress when slip takes place at solid surface 1 and 2, respectively, and can be expressed as follows

$$\overrightarrow{\tau_c} = \overrightarrow{\tau_{cx}} + \overrightarrow{\tau_{cy}} \quad \text{and} \quad |\tau_c| = \sqrt{\tau_{cx}^2 + \tau_{cy}^2} \quad (5)$$

while τ_1 and τ_2 denote the local shear stress at surface 1 and 2, respectively. Slip boundary occurs when shear stress of solid surface $\tau_{1,2}$ exceeds the critical shear stress, then shear stress and slip velocities in the *x*- and *y*- directions can be expressed as $\tau_x = \tau_{cx}$, $u = u_s$ and $\tau_y = \tau_{cy}$, $v = v_s$.

In a two-dimensional wall slip problem, both the magnitude and the direction of the possible slip velocity are not known a priori which brings some difficulties in mathematical analysis for the hydrodynamic fluid flow. For Eq. (1), the slip velocities u_s and v_s are unknown terms. Therefore, to solve Eq. (1), an equation relating the slip velocity to the surface shear stress is needed. In this paper, the two component slip model given by Spikes and Granick [13] is adopted. Slip is envisaged to occur when the shear stress at the surface reaches a critical threshold value, τ_{oc} . And once slip begins, it takes place at a constant slip length. Basically, the model used is a combination of the critical shear stress model [2] and the slip length model [14]. Based on the two component slip model, the surface shear stress when slip takes place (in *x*-direction) can be expressed by [5-6].

$$\tau_{cx} = \tau_{oc} + (\eta / \beta)u_s \quad (6)$$

where τ_{oc} is the critical shear stress for the onset of slip (often quoted as initial critical shear stress), β is the slip length and u_s is the corresponding slip velocity. The similar expression can be stated for the shear stress in the *y*-direction, i.e. τ_{cy}. In the present work, the assumption of the uniform initial critical shear stress and the uniform slip length are employed [5-6, 8]. It should be pointed out that if the initial critical shear stress is set to zero, this equation reduces to the constant slip length model and if the slip length is set to infinite, it reduces to the critical shear stress model [5-6].

In Ref. [2], an approach in solving the case when slip occurs was demonstrated, i.e. using a shear stress boundary condition. It was shown that if slip occurs at a critical shear stress, the velocity profile (in *x*-direction) can be expressed as:

$$u = u_w + \frac{1}{\eta}\frac{\partial p}{\partial x}\left(\frac{z^2}{2} - hz\right) + \frac{\tau_{cx}}{\eta}z \quad (7)$$

If it is assumed that the surface shear stress at the slip area acts to resist slip, at the stationary surface ($z = h$), the slip velocity in *x*-direction reads:

$$u_s = u_w - \frac{1}{\eta}\frac{\partial p}{\partial x}\frac{h^2}{2} - \Lambda_x \frac{\tau_{cx}}{\eta}h \quad (8)$$

where Λ_x is a sign function of slip direction. Combining Eqs. (6) and (8) gives an expression for the slip velocity in *x*-direction [5-6]:

$$u_s = \frac{\left(u_w - \frac{1}{\eta}\frac{\partial p}{\partial x}\frac{h^2}{2} - \Lambda_x \frac{|\tau_{oc}|}{\eta}h\right)}{\left(1 + \frac{h}{\beta}\right)} \quad (9)$$

The similar expression can be derived for the slip velocity in the *y*-direction, i.e. v_s. Slip only takes place when u_s and v_s are not equal to zero. Since the slip velocity direction cannot be known in advance, the corresponding sign functions (i.e. Λ_x and Λ_y) are introduced when

the formula is derived. It should be noted that the application of the two-component slip model used in the present study is an extension of the modified slip length model presented by Salant and Fortier [8] and Wang *et al.* [15] in which the slip is assumed in the direction of motion, i.e. in the positive *x*-direction. However, the model presented here may incorporate some possible slip directions. Based on Eq. (9), slip occurs if [5-6]

$$\frac{\partial p}{\partial x} < \frac{2}{h^2}\left(u_w \eta - |\tau_{oc}| h\right) \tag{10}$$

(for $u_s > 0$, i.e. slip takes place in the positive *x*-direction) or

$$\frac{\partial p}{\partial x} > \frac{2}{h^2}\left(u_w \eta + |\tau_{oc}| h\right) \tag{11}$$

(for $u_s < 0$, i.e. slip takes place in the negative x-direction)

A similar expression can be derived to determine the slip criteria in terms of $\partial p / \partial y$ for the *y*-direction to obtain the slip velocity v_s. It can be observed that Eqs. (10) and (11) and their equivalent in the *y*-direction convert the critical shear stress criterion of slip boundary as presented by Eq. (4) into the local value of the pressure gradients. It should be noted that in the present study, because the critical shear stress criterion of slip boundary is not applied in a vector form, the slip computation becomes independent in both *x*- and *y*-directions.

2.2. Solution Method

In the present numerical analysis, the shear stress is related with slip velocity and varies over the calculation region and so cannot be extracted from the differential term in Eq. (1). Even so, solution of modified Reynolds equation is quite straightforward using numerical method, which is consistent with references [2, 8-9]. In this work, the modified Reynolds equation (Eq. (1)) is solved numerically using finite difference equations obtained by means of the micro control volume approach [16]. Those equations are solved iteratively for pressure at each grid point using the alternating-direction-implicit (ADI) method with the tri-diagonal-matrix-algorithm (TDMA). Initially, the slip velocities u_s and v_s are set equal to zero everywhere, and the equations are solved. In each iteration step, in order to adjust whether slip occurred at each grid position, Eqs. (10) and (11) and their equivalent in the *y*-direction are employed. If slip occurs then Eq. (9) and its *y*-direction equivalent are used to determine the slip velocities, u_s and v_s, and the equations are again solved. Iteration continues until the solution converges. For more details, see Appendix B.

It can be noted that the following simulation results are obtained with an accuracy of tolerance (Tol) of 10^{-6} :

$$\max\left(\frac{\left|\Phi_{i,j}^{new} - \Phi_{i,j}^{old}\right|}{\left|\Phi_{i,j}^{new}\right|}\right) \le \text{Tol},$$

$\Phi_{i,j}$ is the field variable. The iteration is conducted for Tol = 10^{-5}, Tol = 10^{-6}, and Tol = 10^{-7}, and no difference in the calculated values is found.

By employing a discretization scheme, the computed domain is divided into a number of control volumes using a grid with uniform mesh size of 50 x 50 nodes (obtained from a mesh refinement study; see Appendix C for details). At the inlet and outlet of the domain, the pressure is set to be zero. The Reynolds cavitation model is applied, i.e. at each step of the iterative algorithm computing the pressure in the linearly discretized equation, negative values for the pressure are set to zero [11]. The load carrying capacity is determined by integrating the calculated hydrodynamic pressure, while the shear stress at the stationary surface is integrated to determine the friction force.

In order to maximize the load carrying capacity, the boundary conditions of the model are optimized. In the present study, the optimization procedure is conducted using the genetic algorithm. The object of optimization is to maximize the hydrodynamic load carrying capacity. The load carrying capacity satisfies two main functional purposes: (1) carry the load, and (2) minimize the contact between the solids, and thus reducing wear. The optimization

analysis attempts to satisfy both functional requirements with various design parameters, i.e. slip zones (CSS pattern) and film height of the lubricated sliding contact. The CSS geometry shape is a function of the location coordinate. The computer code contains the finite difference method used to solve the hydrodynamic pressure, in combination with a numerical optimization library based on the genetic algorithm.

3. Numerical results and analysis

3.1. Sliding lubricated contact with homogeneous slip surface

A previous study [2, 3, 5, 6] demonstrated that slip was able to reduce the friction force if at one of the contacting surfaces slip is applied over the whole surface (homogenous slip surface). Consequently, it is interesting to compare the classical (no-slip) surface with such slip surface of a lubricated sliding contact. The focus of this section is to investigate the effect of the homogeneous slip surface not only on the friction force as discussed in Ref. [5, 6], but more on the pressure distribution (and thus the load carrying capacity).

Let us consider a particular case of a two-dimensional contact with a certain slope incline ratio h^* as depicted in Fig. 1. In a real hydrodynamic lubricated contact, the slip condition can occur on two contacting surfaces, i.e. the stationary surface and the moving surface. However, in this section, the surface where slip is allowed to occur is assumed on the (top) stationary surface. The slip boundary is considered as homogenous slip, i.e. slip is applied everywhere. In the numerical process, the (bottom) moving surface has a high critical shear stress so that no-slip occurs. Computations have been made for such contact with the following base values: $L_x^* = L_y^* = 1$. For slip analysis, the dimensionless slip length B varies from 1 to 50, which are reasonable values of the slip length based on the results published in literature [5, 6, 8, 17]. In the present study, the dimensionless slip length B is determined by normalizing the slip length β with the outlet film thickness h_o. The variation of the dimensionless initial critical shear stress τ_{oc}^* is also discussed.

Figure 2 shows the comparison of the pressure distribution obtained with the no-slip boundary and the (homogeneous) slip boundary respectively for a slope incline ratio $h^* = 2.3$, i.e. the convergent wedge effect is present. It is assumed that $\tau_{oc}^* = 0$, and $B = 50$. The results clearly show that in case of a homogeneous slip surface the hydrodynamic pressure decreases. The maximum pressure for homogeneous slip situation is half that of the corresponding traditional (i.e. no-slip) lubricated contact. The homogeneous slip boundary will reduce the pressure through the reduction of the velocity gradients at the surface. The hydrodynamic pressure gradient of the homogeneous slip case is continuous as well as in the no-slip case.

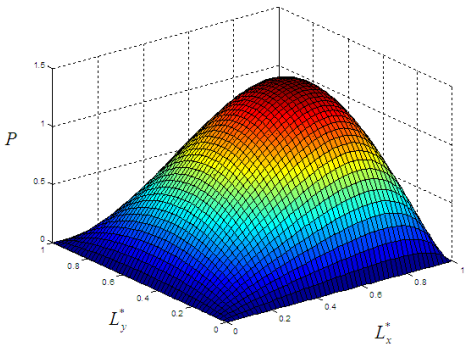

(a)

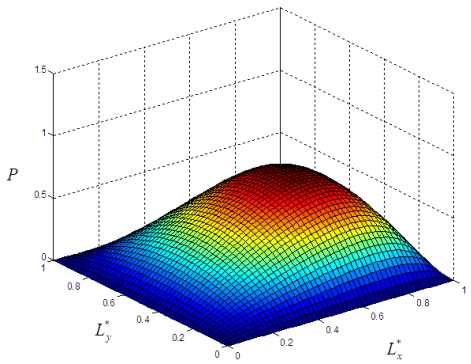

(b)

FIGURE 2: *Three dimensional pressure distribution for (a) no-slip analysis (B = 0), (b) slip boundary analysis (B = 50). The profiles are calculated for $h^* = 2.3$ and $\tau_{oc}^* = 0$.*

Figures 3 and 4 show the distributions of the dimensionless hydrodynamic pressure for different slip lengths B at the center of the lubricated contact (L_y^* = 0.5) for a convergent slope incline ratio (h^* = 2.3). It is found that the height of the pressure peaks is affected by the slip length, which is clearly visible in Figs. 3 and 4. Two observations can be made based on Figs. 3 and 4. At first, the pressure peaks decrease with the increase of the slip length. Especially, the decrease of the pressure is more obvious for high slip length, which is consistent with the trend of load carrying capacity with change of slope incline ratio (see Fig. 5). However, when the dimensionless slip length is equal to 10 and above, the decrease of pressure peaks is insensitive to the further increase of slip length. Secondly, in the transversal direction, the pressure peaks are all at the center-line of the lubricated contact (L_x^* =0.5).

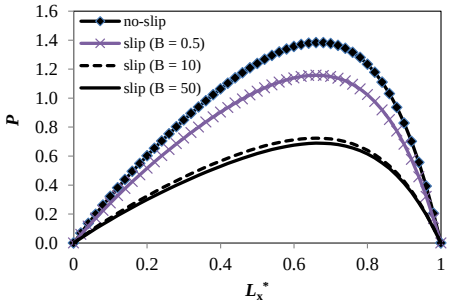

FIGURE 3: *Longitudinal pressure distribution for different homogeneous slip conditions,* $L_y^* = 0.5$. *The profiles are calculated for* h^* = 2.3 *and* τ_{oc}^* = 0.

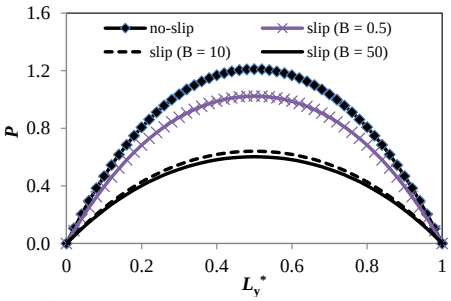

FIGURE 4: *Transversal pressure distribution for different homogeneous slip conditions,* $L_x^* = 0.5$. *The profiles are calculated for* h^* = 2.3 *and* τ_{oc}^* = 0.

Figure 5 shows the effect of slope incline ratio on the load carrying capacity for different slip conditions. It can be found that for the classical no-slip contact as h^* increases from 1, the load carrying capacity increases from zero, reaches a maximum at a value of h^* close to 2.3, and then decreases, as would be expected. The behavior of the homogeneous slip surface is similar for all B values, i.e. the maximum load carrying capacity for all slip conditions also occurs when h^* is about 2.3. It can also be observed that the load carrying capacity estimated by homogeneous slip is smaller for all h^* than the no-slip prediction, and will be much smaller for higher B. However, the decrease of the load carrying capacity is not infinitely large. This is because when the dimensionless slip length B is greater than, say 5 as shown in Fig. 6, the load carrying capacity is not influenced with further increase of the slip length. If B is smaller than that value, the load carrying capacity increases to its no-slip value, which means that the lubricated contact with homogeneous slip surface behaves like a traditional one. In the case of slip, considering a high B and τ_{oc}^* = 0, the dimensionless load carrying capacity W_{slip} decreases to about one half compared to that of the no-slip surface as shown in the insert of Fig. 6. It is interesting to note that the value of $W_{slip}/W_{no\text{-}slip}$ is similar with those given in Ref. [9] although the slip model used is different. Therefore, when B is greater than 5 and τ_{oc}^* = 0, the slip can be considered as perfect slip. For such values, the critical shear stress τ_c can be very low. Based on Fig. 5 it can be observed that for parallel sliding surfaces (h^* = 1) the generated load carrying capacity is not affected with the change of slip length. In other words, although slip is applied (homogeneously), the lubrication performance does not change, i.e. no load carrying capacity as well as in the classical no-slip contact. It indicates that the convergent slope incline ratio in the homogeneous slip case has a prominent role in determining the hydrodynamic behavior.

It should be noted that the simulation results presented in Figs. 4-6 were calculated using a zero initial critical shear stress. It means that the shear stress of the interface when slip occurs is assumed to be only influenced by the slip length.

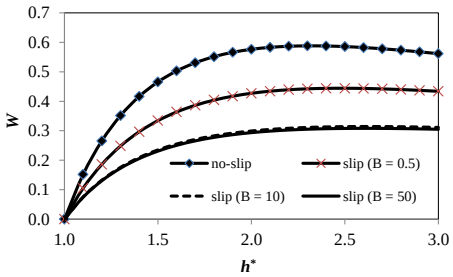

FIGURE 5: *Dimensionless load carrying capacity W versus slope incline ratio h^* for different slip conditions. The profiles are calculated for $\tau_{oc}^* = 0$.*

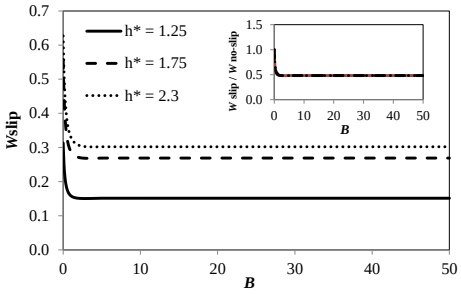

FIGURE 6: *Dimensionless load carrying capacity of the homogeneous slip W_{slip} versus dimensionless slip length B for different slope incline ratios h^*. The insert shows the corresponding ratio of dimensionless load carrying capacity for homogeneous slip W_{slip} to that of the no-slip surface $W_{no\text{-}slip}$ calculated for the same h^* values. For all profiles $\tau_{oc}^* = 0$ is used.*

According to the two slip component model adopted here (Eq. 4), the initial critical shear stress may have a role in affecting the fluid behavior. Therefore, the issue of how does the initial critical shear stress as well as the slip length affect the load carrying capacity for the homogeneous slip surface contact will be explored here. To answer this question, the comparison of the dimensionless load carrying capacity W of the homogeneous slip for several slope incline ratios h^* and the other slip parameters (i.e. B and τ_{oc}^*) will be presented. It can be noted that in Eq. (6), there are two terms on the right-hand side of the equation, i.e. the initial critical shear stress and the corresponding slip velocity. For the case of $\tau_{oc} \neq 0$, if β is set to close to zero, the generated τ_c will be very large, and vice versa if β is set to very large, the τ_c will be very low. In this section, the variation of τ_{oc} for such conditions (high β and low β) will be investigated.

Figure 7 shows that the effect of the dimensionless initial critical shear stress τ_{oc}^* on the ratio of dimensionless load carrying capacity of the homogeneous slip surface W_{slip} over the no-slip surface $W_{\text{no-slip}}$ for different slope incline ratios in the case of high B. In this simulation the B chosen is 50 with the reason that if B varies from about 5 to infinite, the load carrying capacity generation has exactly the same value as shown in Fig. 6. From Fig. 7, it can be found that for a very low value of τ_{oc}^*, for example $\tau_{oc}^* = 0$, the load carrying capacity is half that of the classical (no-slip) lubricated contact. However, as τ_{oc}^* increases, load carrying capacity first decreases, reaches a minimum and then rises again, eventually to level out at the classical Reynolds load carrying capacity value when the situation of no-slip over the whole surface is present. These trends are similar to what is described by Spikes [2] using the critical shear stress model. As shown in Fig. 8, over the entire slope incline ratio range, the surface with homogeneous slip boundary, for very low τ_{oc}^*, produces lower values of load carrying capacity than the conventional (no-slip) surface. Only for very high τ_{oc}^*, the load carrying capacity approaches the Reynolds, no-slip case. It can be concluded that for very high B, the calculated W become sensitive to the variation of τ_{oc}^*. Generally, with respect to the load carrying capacity, no improvement can be obtained by applying a homogenous slip boundary both using low τ_{oc}^* or high τ_{oc}^*. At parallel sliding surfaces in the case of such homogeneous slip boundaries, no hydrodynamic pressure and thus no load carrying capacity can be generated.

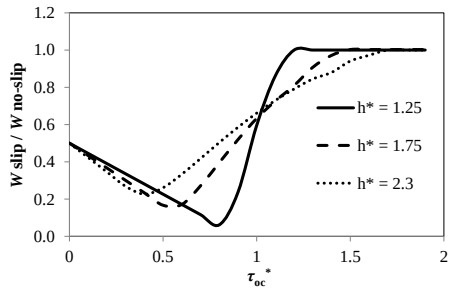

FIGURE 7: *Effect of the dimensionless critical shear stress τ_{oc}^* on the ratio of the dimensionless load carrying capacity of the homogeneous slip surface W_{slip} over the no-slip surface $W_{no\text{-}slip}$. The slip profiles are calculated for B = 50.*

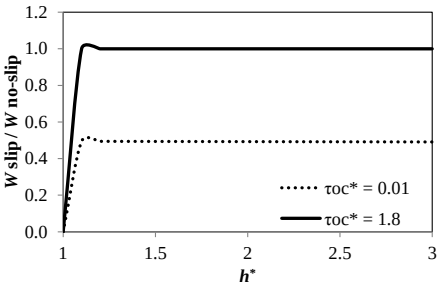

FIGURE 8: *Effect of slope incline on the ratio h^* on the ratio of the dimensionless carrying capacity of the homogeneous slip surface W_{slip} over the no-slip surface $W_{no\text{-}slip}$ for two different initial critical shear stress τ_{oc}^* values (i.e. very low τ_{oc}^* and very high τ_{oc}^*). The slip profiles are calculated for B = 50.*

Figure 9 shows the effect of the dimensionless critical shear stress τ_{oc}^* on the dimensionless load carrying capacity W for different slope incline ratios h^* for a very low slip length which is close to zero ($B \approx 0$, in this case the B chosen for the simulations is 0.01). It is found that very little reduction in W is obtained when the τ_{oc}^* is increased. For example, for the lubricated contact geometry subject to a high dimensionless initial critical shear stress τ_{oc}^* of 0.8 and slope incline ratio h^* of 2.3, the load carrying capacity W differs from the zero τ_{oc}^* situation by only 8% (lower). As shown in the insert of Fig. 9, hydrodynamic load carrying capacity using a homogeneous slip boundary for very low B is almost the same as that of the traditional lubricated contact. The very small decrease in the load carrying capacity can be understood because according to the theory, setting the slip length close to zero results in a value of τ_c that is dominated by the second term on the right hand side of Eq. (4). This makes the τ_c not too sensitive to the initial critical shear stress. This result contradicts with the previous results in the case of very high B (Figs. 7 and 8). It means that the effect of slip length on the slip property of the interface is more dominant than the initial critical shear stress as mentioned earlier. The same trend (very small decrease in W) can be found in Fig. 10. If the slope incline ratio is researched, for the whole range of h^*, the dimensionless load carrying capacity W is not sensitive to the increase of τ_{oc}^*.

The overall conclusion that can be drawn from these results is that the initial critical shear stress affects the homogeneous slip flow hydrodynamics in two different ways: It decreases the hydrodynamic load carrying capacity at high slip lengths, but has very little effect at low slip lengths. In general, it indicates that the calculated results are only weakly dependent on the initial critical shear stress but moderately sensitive to the slip length, which is consistent with the experimental work of Choo *et al.* [6]. It is also found that the load carrying capacity using a homogeneous slip surface when perfect slip is assumed, i.e. zero τ_{oc}^* and very high B, is only 50% of that of the corresponding no-slip contact. Controlling the initial critical shear stress and slip length of the interface property using homogeneous slip boundary still cannot help improving the lubrication performance.

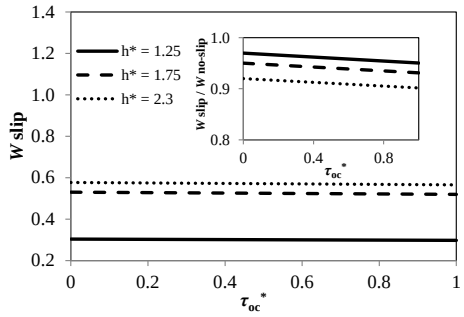

FIGURE 9: *Dimensionless load carrying capacity of the homogeneous slip surface W_{slip} versus dimensionless initial critical shear stress τ_{oc}^* for different values of the slope incline ratio. The insert shows the corresponding ratio of dimensionless load carrying capacity with slip W_{slip} over the no-slip surface $W_{no\text{-}slip}$ calculated at the same h^*. The slip profiles are calculated for B = 0.01.*

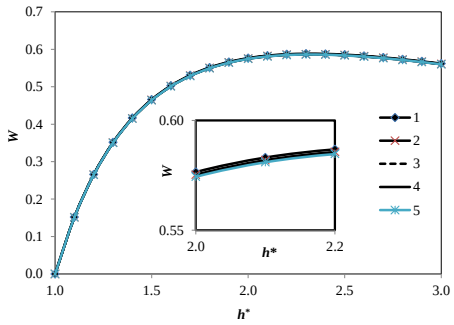

FIGURE 10: *Dimensionless load carrying capacity W versus slope incline ratio h^* for different slip conditions: 1) no-slip; (2) $\tau_{oc}^* = 0.01$; (3) $\tau_{oc}^* = 0.2$; (4) $\tau_{oc}^* = 0.4$; (5) $\tau_{oc}^* = 0.8$. The profiles are calculated for B = 0.01. The insert shows how close the predicted results with slip are to the classical no-slip situation.*

In Fig. 11 the friction force ratio of a lubricated contact with a homogeneously distributed slip boundary over the classical no-slip surface versus the slope incline ratio is presented. The results are evaluated for two different homogeneous slip conditions, i.e. perfect slip ($\tau_{oc}^* = 0$ and $B = 50$) and non-perfect slip ($\tau_{oc}^* = 0.3$ and $B = 50$). Figure 11 shows that as the slope incline ratio is reduced, the friction force decreases. For the same value of h^*, the lubricated contact with the perfect slip has a lower friction force. Compared with the traditional surfaces, the friction force is decreased significantly especially when decreasing the slope incline ratio and using homogeneous slip. The point that wants to be emphasized here is that for lubricated MEMS slightly or full parallel sliding surfaces are often employed. If the reduction of friction is only of particular interest, the homogeneous slip is very beneficial. However if the performance is related to the load carrying capacity, homogeneous slip is not recommended because of the deterioration of the load carrying capacity.

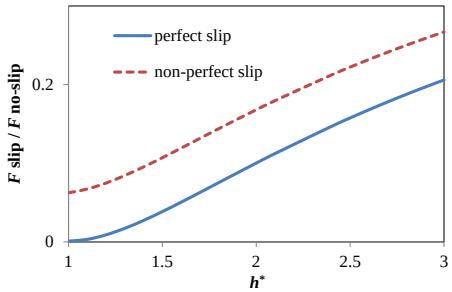

FIGURE 11: *Effect of slope incline ratio h^* on the ratio of the dimensionless friction force for homogeneous slip F_{slip} over the no-slip surface $F_{no\text{-}slip}$ for two different slip conditions: (1) perfect slip ($\tau_{oc}^* = 0$ and $B = 50$); (2) non-perfect slip ($\tau_{oc}^* = 0.3$ and $B = 50$).*

Generally, at lubricated MEMS the reduction in pressure generation and as a result a lower load carrying capacity is often unwanted. For this reason, various geometries of the slip area (which is addressed to as complex slip surface – CSS pattern) as well as the slope incline ratio are investigated, by the optimization, on their effect on the hydrodynamic performance. In this way, a high load carrying capacity combined with a low friction force can be obtained.

3.2. Lubricated sliding contact with complex slip surface (CSS) pattern surface

In the present study, the concept of a complex slip surface (CSS) is introduced. It means that a surface is engineered such that slip occurs in

certain regions and is absent in the other parts. It is believed that a judicious choice of a CSS pattern can alter the flow pattern in the liquid lubricating film so as it will lead to enhanced MEMS caharacteristics and improved operation stability. Therefore, the CSS pattern area as well as the slope incline ratio will be examined by optimization.

In real lubricated contact problems, the number of lubrication contact parameters can be very large and their influence on the lubrication performance can be very complicated. By applying the Genetic Algorithm (GA) to optimize the lubrication contact parameters, an optimal or a group of sub-optimal solutions can be obtained.

For a two-dimensional sliding lubricated contact (for example L_x/L_y = 1), there are at least two main parameters that can be used as design variables. They are the CSS pattern area and the slope incline ratio. For the stationary surface consisting of two zones with slip and no-slip, the CSS pattern parameter can be described with four design variables. Therefore, the total of design variables are five for the optimization problem, i.e. c_1, c_2, c_3, c_4 that shape the width and the length of the rectangular slip region for the CSS pattern (Fig. 12), and h^* that influences the wedge effect. It should be noted that c_1, c_2, c_3, and c_4 are measured to the center of the coordinate system located at the bottom left corner of the surface (see Fig. 12).

The two-dimensional lubricated sliding contact optimization problem is defined as: finding the geometry of a specific CSS pattern area and the slope incline ratio, so that the load carrying capacity is maximized. For the five design variables defined previously, the optimization procedure can be conducted using two approaches. At first, the optimization of the CSS pattern (the size of the slip area) at a certain fixed slope incline ratio. Secondly, the optimization of the combination between the geometry of CSS pattern and the slope incline ratio. The latest can give the area of CSS pattern and the slope incline ratio simultaneously, which maximize the load carrying capacity. A GA program is written to be able to solve the two approaches mentioned.

3.2.1. *Case 1*: Optimization of CSS pattern

Figure 12 shows a CSS pattern at the surface whose shape is rectangular, and the design variables are c_1, c_2, c_3, and c_4. In the numerical simulation, no-slip occurs at the moving surface and the part of the stationary surface by assuming a high critical shear stress. In the slip area of the stationary surface, the dimensionless initial critical shear stress of zero and the dimensionless slip length of 50 are assumed, i.e. perfect slip.

The optimization for *case 1* can be stated as follows:
find c_1, c_2, c_3, and c_4, given a slope incline ratio which maximize the load carrying capacity with the constrains:

$0<c_1<L_x^*$; $0<c_2<L_x^*$; $0<c_3<L_y^*$; $0<c_4<L_y^*$; $c_2>c_1$ and $c_4>c_3$.

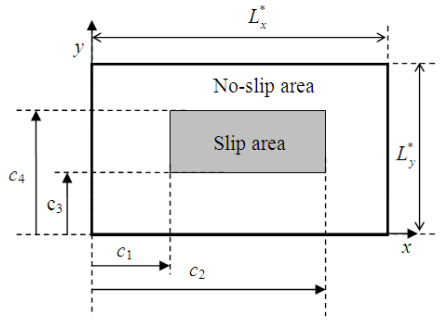

FIGURE 12. *Geometry of the complex slip surface pattern on the stationary surface for a two-dimensional lubricated contact, see also Fig. 1.*

Figure 13 gives the results of the ratio of the dimensionless maximum load carrying capacities $W_{CSS}/W_{no\text{-}slip}$ and the ratio of the dimensionless friction forces $F_{CSS}/F_{no\text{-}slip}$ as a function of the slope incline ratio for the no-slip and CSS patterned situation. The dimensionless maximum load carrying capacity was obtained by optimizing the slip pattern area. Table 1 gives the optimized parameters (CSS pattern) corresponding to the maximum load carrying capacity for the different values of the slope incline ratio. When the slope incline ratio, h^*, is changed from 1.05 to 3.0, the ratio of the maximum load carrying capacity with the CSS

pattern, $W_{\text{CSS-pattern}}$, to that with the no-slip situation (traditional lubricated contact), $W_{\text{no-slip}}$ ranges from about 14 to 1.2 (Fig. 13a). This means that the enhancement on the load carrying capacity with the optimized CSS pattern on the stationary upper surface decreases with increasing the slope incline ratio. Once the slope incline ratio reaches a value above 3.0, the two types of lubricated contacts are almost equivalent (see insert of Fig. 13a). From the insert of Fig. 13a, it can also be found that the dimensionless load carrying capacity with the no-slip situation obtains a maximum value when slope incline ratio $h^* = 2.3$. However, when the slope incline ratio equals 1 (parallel sliding surfaces) the contact without slip gives no load carrying capacity whilst for the optimized CSS pattern the maximum load carrying capacity is achieved. This result is analogous to that found for a journal bearing with zero eccentricity, one of which is a complex slip surface [15, 18]. At $h^* = 1$, the W_{CSS} equals 1.53, which is 2.6 times the value of $W_{\text{no-lip}}$ at the optimal h^* (i.e. $h^* = 2.3$). From the Table 1, it is interesting to note that for all determined optimized CSS patterns for each slope show that $c_1 = 0$ which means that for maximizing the load carrying capacity the slip area must be located at leading edge of the contact. In addition, the optimized CSS pattern area is obviously symmetric perpendicular to the sliding direction. In Fig. 13b, it is shown that the lubricated contact with the optimized slip zone gives lower values for the friction force than the traditional contact for the same value of the slope incline ratio. The lower the slope incline ratio, the higher the friction force. It is also found that contrary to the trend of the load carrying capacity, close to the slope incline ratio of 3 and above of this value, the friction force is still much lower than the traditional lubricated contact. It can be concluded that when $h^* = 1$ (parallel moving surfaces) and a surface containing a specific optimized CSS pattern, the lubricated contact gives a low friction force in combination with a rather high load carrying capacity. This situation is very beneficial in designing lubricated-MEMS which frequently exhibits parallel gaps.

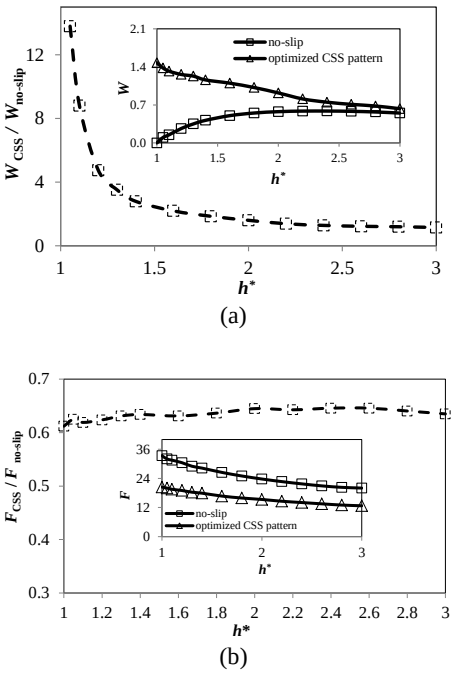

FIGURE 13: *Optimization results versus the slope incline ratio: (a) dimensionless load carrying capacity ratio of the load carrying capacity of lubricated contact with a CSS pattern over the traditional no-slip contact, and (b) the corresponding friction force.*

TABLE 1: *Optimized geometry of CSS pattern with respect to the dimensionless load carrying capacity, $L_x/L_y=1$.*

h^*	1.0	1.05	1.1	1.2	1.3	1.4	1.6	1.8	2.0	2.2	2.4	2.6	2.8	3.0
c_1	0	0	0	0	0	0	0	0	0	0	0	0	0	0
c_2	0.60	0.63	0.61	0.67	0.69	0.71	0.74	0.76	0.80	0.79	0.78	0.83	0.83	0.78
c_3	0.12	0.10	0.11	0.12	0.11	0.11	0.13	0.23	0.14	0.12	0.22	0.17	0.14	0.13
c_4	0.88	0.90	0.89	0.88	0.89	0.89	0.87	0.77	0.86	0.88	0.78	0.83	0.86	0.87

3.2.2. *Case 2*: Optimization of CSS pattern and slope incline ratio simultaneously

In this section the optimization is performed such that the slope incline ratio and CSS pattern geometry are allowed to vary simultaneously. In the slip area of the stationary surface, the dimensionless initial critical shear stress of zero and the dimensionless slip length of 50 are assumed, i.e. perfect slip.

The optimization for *case 2* can be stated as follows:

find c_1, c_2, c_3, c_4, and h^*
maximizing the load carrying capacity with the constrains:
$0<c_1< L_x^*$; $0<c_2< L_x^*$; $0<c_3< L_y^*$; $0<c_4< L_y^*$;
$c_2>c1$; $c_4>c_3$ and $0<h^*<3.5$

Table 2 shows the optimized slope incline ratio and the dimensions of the CSS pattern for maximum load carrying capacity. For comparison, the optimization is also conducted for the traditional (no-slip) lubricated contact situation.

TABLE 2: *Optimized parameters of two-dimensional lubricated contact, $L_x/L_y=1$.*

Type of lubricated contact	c_1	c_2	c_3	c_4	h^*
CSS pattern	0	0.70	0.15	0.85	0.95
No-slip	-	-	-	-	2.3

For the traditional (no-slip) lubricated contact, the classical Reynolds theory predicts that, only when $h^* > 1$, a hydrodynamic pressure is generated, and as a result the maximum load carrying capacity W_{max} determined, occurs when $h^* = 2.3$. However, for the CSS pattern, the W_{max} occurs at $h^* = 0.95$ (slightly diverging). One would expect this slope incline ratio to introduce cavitation, but apparently the combination of the slip zone configuration on the stationary surface and the slope incline ratio ensures positive hydrodynamic pressures and thus the load carrying capacity as discussed in the next section. With the CSS pattern, and $h^* = 0.95$, the lubricated contact gives the maximum dimensionless load carrying capacity and the minimum dimensionless friction force of 1.58 and 20.4 respectively while the traditional lubricated contact gives its maximum dimensionless load carrying capacity and minimum dimensionless friction force of 0.58 and 22.6 respectively at $h^* = 2.3$. So, with an optimal slope incline ratio of $h^* \approx 1$, the maximum load carrying capacity increased by about 2.7 times and the surface friction force reduced clearly when compared to what Reynolds equation predicts for an optimal slope incline ratio of a no-slip lubricated contact. These results are comparable to either the infinite length lubricated contact in terms of slope incline ratio [9] or the finite length lubricated contact in terms of location of the slip zone [8]. This indicates that the optimal lubricated sliding contact depends on the combination of the slope incline ratio, and the location and the size of the slip area (CSS pattern). Using the genetic algorithm adopted in the present work, all parameters can be optimized simultaneously.

The question arises "why does the optimized CSS pattern exhibit the increased hydrodynamic performance?". The slip velocity field, as shown in Fig. 14 may give us a further understanding for these phenomena. At the leading edge of the lubricated contact where the slip area is present, the slip direction is the same as that of the lubricant flow. The lubricant at the interface of the stationary upper surface moves with a specific value. This will be different if the no-slip situation is imposed. In addition, the no-slip condition at either the outlet or two-sides of the lubricated contact will slow down the lubricant flow out of the contact. The coupling action of what is mentioned earlier, the lubricant flow generates a higher hydrodynamic pressure, and thus an increased load carrying capacity even when the wedge effect is not present.

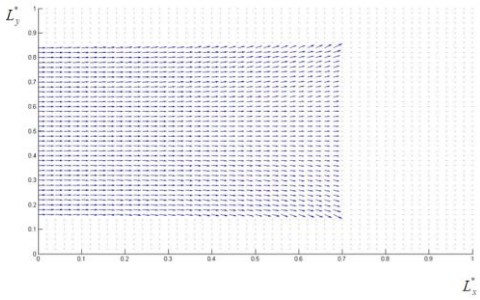

FIGURE 14: *Velocity field at the CSS patterned surface (Table 2) of a lubricated sliding contact ($L_x/L_y = 1$).*

To strengthen the possible reasons why a surface containing an optimized complex slip surface (CSS) pattern leads to better hydrodynamic lubrication performance, it is necessary to investigate the importance of varying the slip area in the *y*-direction (transverse to the sliding direction) for achieving hydrodynamic

performance. Figure 15 gives a comparison of the dimensionless pressure distributions of lubricated contacts for three types of surfaces which are applied to the stationary surface as indicated in Table 3. At first, the surface with homogeneous slip, i.e. slip is applied everywhere. Secondly, the surface with a mixed slip pattern (a term that is addressed by Wu *et al*. [9] if slip takes place over 65 percent of the stationary surface at the inlet), and thirdly, the surface with optimized CSS pattern. In this investigation, the surfaces are evaluated for the slope incline ratio of $h^* = 1.0$ (parallel sliding surfaces). The choose of $h^* = 1$ is considered in the present work such that the results can directly comparable with other studies, for example [9-11, 15, 18] discussing the lubricated contact with the parallel gap as of main interest. It can be seen from Fig. 15 that when slip is applied over the whole surface, no hydrodynamic pressure generation is obtained. The pressure distribution behavior is interesting when comparing the result obtained from the mixed slip surface and the CSS pattern. It can be observed that both of them give similar pressure distributions as the Rayleigh step bearing. The pressure gradient is not continuous at the boundary of the slip area and the no-slip area, where the maximum pressure occurs. However, the mixed slip surface optimized only in the *x*-direction (along the sliding direction) gives a lower (average) pressure than the CSS patterned surface. It indicates that varying the slip zone in the *y*-direction (transverse to the sliding direction) by optimization next to varying the slip zone in the *x*-direction gives a better hydrodynamic pressure generation. This can be understood because at the CSS pattern the side leakage is inhibited utilizing the no-slip boundary condition as discussed earlier. This explains why the optimized CSS pattern gives a higher fluid load carrying capacity than the mixed slip surface. For the analysis evaluated at the same parameters ($h^* = 1$, $\tau_{oc}^* = 0$ and $B = 50$) the load carrying capacity corresponding to the CSS pattern case is 1.53, while the corresponding mixed slip surface is 0.99. The load carrying capacity of the CSS pattern can be increased by 1.5 times, a significant advantage over the the mixed slip surface.

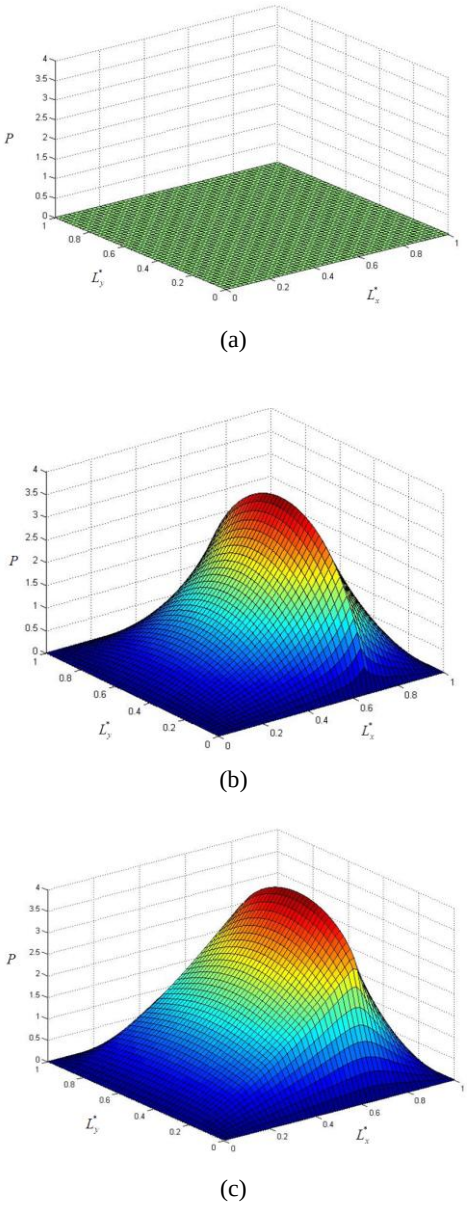

FIGURE 15: *Three dimensional pressure distribution of lubricated contacts for three types of surfaces, i.e. surface containing: (a) homogenous slip; (b) mixed slip surface; and (c) CSS pattern. The profiles are predicted for* $h^* = 1$.

TABLE 3: *Possible geometry of the slip area of a two-dimensional lubricated contact, $h^* = 1$ and $L_x/L_y=1$.*

Type of surface	c_1	c_2	c_3	c_4
Homogeneous slip	0	1	0	1
Mixed slip surface [9]	0	0.65	0	1
CSS pattern [present]	0	0.70	0.15	0.85

Figures 16 and 17 show the distributions of the dimensionless hydrodynamic film pressure at the center of the sliding contact for different conditions. The optimized slope incline ratio is considered for each corresponding conditions, i.e. $h^* = 0.95$ for the CSS pattern and the mixed slip surface, and $h^* = 2.3$ for the homogeneous slip and no-slip contact. Based on Fig. 16, it can be concluded that the trend of variation of the pressure distributions is significantly higher for the mixed slip and CSS patterned surface. Figure 17 shows the pressure distribution perpendicular to the sliding direction. The increase of pressure is more obvious as the position and the length of slip zone is optimized. Again, the optimization procedure of the construction of the slip zone in the *x* and *y*-direction proves more beneficial than homogeneous slip, mixed slip and traditional no-slip pattern although such configurations are generated using the corresponding optimal slope incline ratio.

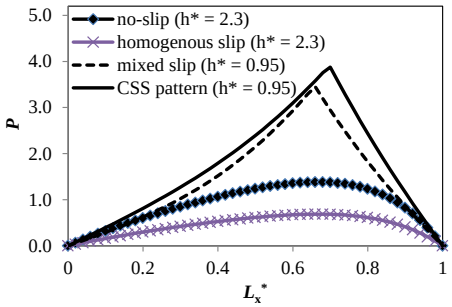

FIGURE 16: *Longitudinal pressure distribution for different conditions. The profiles are evaluated for B = 50, $\tau_{oc}^* = 0$ and the corresponding optimal h*.*

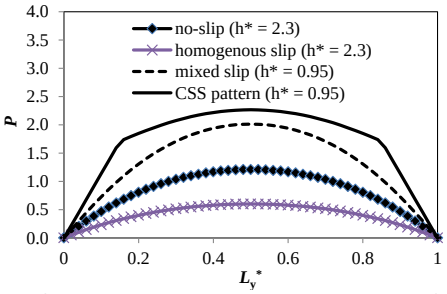

FIGURE 17: *Transversal pressure distribution for different conditions. The profiles are evaluated for B = 50, $\tau_{oc}^* = 0$ and the corresponding optimal slope incline ratio h*.*

3.3. Effect of the initial critical shear stress on hydrodynamics of lubricated contacts with CSS pattern

In order to study the influence of the initial critical shear stress on the hydrodynamic performance of the two-dimensional lubricated contact with the optimized CSS pattern on the stationary surface calculations were performed. It will be shown that particular care must be taken in choosing the slip property, i.e. the critical shear stress on the CSS pattern because an inappropriate choice can lead to a decrease in the load carrying capacity. In the present work, computations have been made by comparing the performance of the CSS pattern over the classical no-slip contact for two different conditions of h^*, i.e. with and without the presence of the wedge effect. The dimensionless slip length *B* of 50 is used. Figure 18 gives the effect of the dimensionless initial critical shear stress τ_{oc}^* on the performance parameter ratios (which are the ratios as used in the previous section) of the lubricated contact with the optimized CSS slip area (see Table 3 for the optimized parameters of the slip zone) to that of the traditional lubricated contact for $h^*_{\text{optimal}} = 2.3$. These results show that in the case of $h^*_{\text{optimal}} = 0.95$, in relation to the load carrying capacity, it is observed that for the τ_{oc}^* of zero, the dimensionless load carrying capacity with CSS pattern is over 2.75 times that of the traditional lubricated contact. However, the load carrying capacity decreases with increasing initial critical shear stress. For a high value of

the dimensionless initial critical shear stress τ_{oc}^*, the fluid load carrying capacity goes down and finally the film collapse occurs when the τ_{oc}^* reaches 1.65 and above. It means that CSS pattern behaves, from that value and on, similarly as the no-slip contact. In relation to the friction force, the reductions using the optimized CSS pattern can be achieved (12% lower) when τ_{oc}^* = 0. The friction force ratio, F_{slip} / $F_{\text{no-slip}}$ rises with the increase of τ_{oc}^*, reaches to a maximum value at τ_{oc}^* = 1.25, then decreases slightly, and finally reaching a value when no slip occurs over the entire upper surface at the corresponding slope incline ratio.

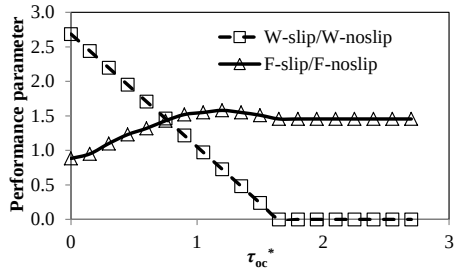

(a)

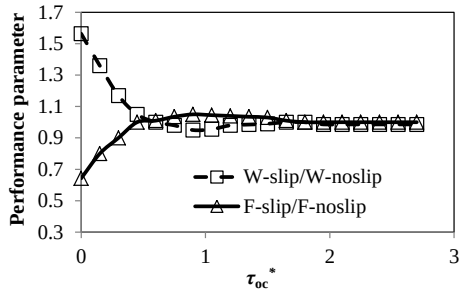

(b)

FIGURE 18: *Effect of the initial critical shear stress on the hydrodynamic performance parameters of lubricated sliding contacts evaluated for two different conditions of CSS pattern: (a) h^* = 0.95; and (b) h^* = 2.3. All no-slip profiles are calculated for the optimized slope incline ratio (h^* = 2.3).*

For the case in which the wedge effect is dominant, as shown in Fig. 18b, the CSS pattern with h^* = 2.3 produces a lower value for the load carrying capacity than that for the CSS pattern with the h^*_{optimal} = 0.95. For h^* = 2.3, a maximum improvement of 56% (or 1.56 times compared with the classical case) is observed for τ_{oc}^* = 0 in relation to the load carrying capacity. In addition, as τ_{oc}^* increases, the load carrying capacity ratio, W_{slip} / $W_{\text{no-slip}}$ decreases, reaches a minimum value and then increases slightly, and finally approaches the level of the load carrying capacity value for the no-slip situation. It is interesting to note that these trends are similar to what was described by Ma *et al*. [10] in the case of a journal bearing when the wedge effect is present. It can also be observed that F_{slip} / $F_{\text{no-slip}}$ for h^* of 2.3 behaves similar with the trend for h^* of 0.95. However, F_{slip} / $F_{\text{no-slip}}$ for h^* = 2.3, when τ_{oc}^* reaches 1.35 and above, is equal to 1, which is smaller than that for h^* = 0.95. Generally, for a maximum load carrying capacity in combination with a minimum friction force, a very low initial critical shear stress should be employed in the design of the lubricated-MEMS.

3.4. Effect of the slip length on hydrodynamics of lubricated contacts with CSS pattern

In this section, the effect of slip length on the lubrication behavior is studied. The dimensionless slip length is varied from 1 to 50 [5, 6, 8, 17]. A zero initial critical shear stress is used for a maximum load carrying capacity as discussed in the previous section.

As can be seen in Fig. 19, for an optimized h^*, i.e. h^* = 0.95, the increase of the dimensionless slip length *B* leads to a large improvement in the dimensionless load carrying capacity of the lubricated sliding contact compared with what Reynolds theory predicts for an optimal h^* for classical no-slip case. However, for *B* greater than say 20, the variation in *B* has an insignificant effect on the performance. In the case of h^* = 0.95, a value for *B* of 20 can be considered as an optimum value for generating a high *W*. For a higher value of h^*, i.e. h^* = 2.3, there is a shift of the optimum dimensionless slip length towards the *B* value which is smaller than the optimum of *B* for the case of h^* = 0.95, i.e somewhere between *B* = 10 and *B* = 15. It indicates that there is a threshold value of the

dimensionless slip length which is unique for each h^*.

In addition, in the case of high B, the increase of W by optimized CSS pattern for $h^* = 0.95$ is observed to be more spectacular (up to 175%) than that for $h^* = 2.3$ (only up to 56%). It means that the wedge effect of a CSS structured surface in a lubricated sliding contact has a disadvantage with respect to the W^*. Therefore, better results can be achieved when a CSS pattern in lubricated contact is evaluated for a low h^* value ($h^* \approx 1$). This is consistent with the optimization result for the slope incline ratio as discussed in the previous section.

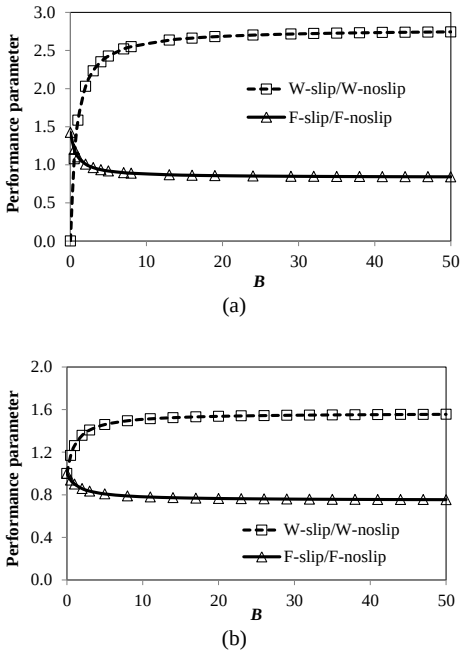

FIGURE 19: *Effect of the dimensionless slip length B on the hydrodynamic performance parameters of CSS patterned surface in a lubricated sliding contact for two different conditions: (a) $h^* = 0.95$; and (b) $h^* = 2.3$. All no-slip profiles are calculated for the optimized slope incline ratio ($h^* = 2.3$).*

With respect to the dimensionless friction force, the increase of the dimensionless slip length leads to a decrease in the predicted friction force. As indicated in Fig. 19, the optimum dimensionless slip length reveals a high load carrying capacity and on the other side reduces the friction force. It can also be observed that the friction force estimated by the optimized CSS pattern is smaller than the no-slip prediction. For higher B, the optimized CSS pattern gives a significantly reduction in the friction force. However, the decrease of F is limited. This is because when the dimensionless slip length B is greater than, say 20 and 15, respectively, in the case of $h^* = 0.95$ and $h^* = 2.3$ as shown in Fig. 19, the friction force performance is not influenced with further increase of the dimensionless slip length. If B decreases at those values, F increases to its no-slip value, which means that the lubricated contact with CSS pattern surface behaves like a traditional one. In conclusion, the high slip length designed for the CSS pattern leads to a greater improvement in load carrying capacity and reduction in friction force.

4. Discussion

According to the classical Reynolds theory, a convergent geometrical wedge is one of the most important conditions to generate hydrodynamic pressure. In this paper, it is shown that (slightly) parallel moving surfaces with an optimized complex slip surface, can also provide a fluid load carrying capacity. This finding is similar to the result of lubricated sliding contact analysis by Wu *et al*. [9]. However, in the two-dimensional analysis discussed, an optimization of the slip area in the y-direction (perpendicular to the sliding direction) becomes possible and its effect on the hydrodynamic pressure can be investigated. Optimizing the slip area in the x- and y-direction has proven to have advantages above optimizing in the x-direction only. A numerical analysis is conducted for the two dimensional problem. The particular case where the slip area equals 0.65 the length of contact is considered. It means that c_1=0, c_2=0.65, c_3=0, and c_4=1. Wu *et al.* [9] found that for such slip pattern (except that $c_4 = \infty$ due to $L_y/L_x = \infty$), the surface optimization of a parallel sliding gap with a mixed slip surface can double the hydrodynamic load carrying capacity and reduce the friction force significantly compared to the predicted values for an optimal wedge assuming no slip boundary in the contact. In our cases, based on two-dimensional analysis, by optimizing the slope incline ratio together with

the CSS pattern both along and transverse to the sliding direction, the improvement of load carrying capacity can be approximately three times larger than the Reynolds theory predicts for an optimal slope incline ratio for a traditional sliding contact. Besides that, the optimized CSS pattern at the optimized slope incline ratio generates low friction. The reduction of friction force is up to 12% compared with what the Reynolds theory predicts for an optimal slope incline ratio for a traditional sliding contact.

In the present paper, the modified Reynolds equation with slip boundary is presented to find the pressure distribution for hydrodynamically lubricated sliding contacts. The two component slip model is adopted for modeling slip boundary. A finite difference code has been developed to solve such equation. As mentioned in the previous section, when the initial critical shear stress is zero, the two component slip model presented here is comparable with the slip length model demonstrated by Salant and Fortier [8]. Computations have been made to simulate this situation for validating the numerical algorithm. From Fig. D.1 (see Appendix D), it is shown that the results obtained are in a good agreement with the work of Salant and Fortier [8] for CSS pattern with zero initial critical shear stress. Salant and Fortier [8], however, met an instability problem for any critical shear stress. In the present work, no instability problem due to the used numerical algorithm took place when the initial critical shear stress is not zero. Surface optimization of a parallel sliding gap with a slip surface was investigated by Wu *et al.* [9] using a quadratic programming algorithm. However, in their work an infinite wide slider was employed. It means that the gradient pressure in *y*-direction (transverse to the sliding direction) was not taken into account in the analysis. In the present paper, a comparison between the CSS pattern (i.e. the variation in *x*-and *y*- direction) and the mixed slip pattern (i.e. the variation in only *x*-direction) has been made suitable for two-dimensional analysis (see Figs. 15-17). It can be noted that an improvement of the hydrodynamic performance is achieved using the CSS pattern, i.e. over 1.5 times larger than the result by optimizing the slip zone in *x*-direction only. Therefore, for "optimal" results of the optimization, one can not neglect the possibility in alternating the slip area in the *y*-direction (perpendicular to the sliding velocity). In lubricated MEMS, it may be impossible to consider the sliding contacts as infinite wide, because on micro-scale the ratio of length to width dimension is finite, and the effect of the pressure gradient both in the-*x* and *y*- direction are significant.

The CSS patterned surface is also compared with the pocket bearing and step bearing (see Appendix E). Again, it is shown that a CSS pattern performs better than these bearings with respect to the load carrying capacity and friction force.

In a real system, for example in lubricated-MEMS containing moving surfaces, the complex slip surface (CSS) pattern can be a promising way for increasing the load carrying capacity and reducing the friction force. MEMS technology frequently exhibits parallel surfaces in near contact. In such contact, using a homogeneous slip and/or no-slip condition, no-load carrying capacity takes place. Based on the numerical simulations, an optimized complex slip surface (CSS) pattern leads to better performance in terms of hydrodynamic lubrication performance.

In hard disk drives and micro-machines such as MEMS, where the loads are very low and the surfaces are very smooth, CSS pattern appears to be very promising for designing low-friction lubricated mechanisms because they are relatively easy to obtain. If compared to the application of "physical roughness" which needs the technology of texturing of the opposing surfaces on micro-scale, the CSS pattern for increased-MEMS performance by lubrication may be more applicable. The CSS pattern may consist of the combination of two surface types, i.e. hydrophobic and hydrophilic. They can lead to a method to control slip boundary. A (super) hydrophobic surfaces show slip boundary compared to hydrophilic surfaces. For most hydrophilic surfaces, no-slip occurs.

In particular, the amount of hydrophobicity and the ratio of hydrophilic to hydrophobic area as well as in the case of complex slip surface presented here using genetic algorithm is of interest for generating a maximum load carrying capacity in systems in which the wedge effect is

not present. Usually, the better the surface hydrophobicity, the lower the critical shear stress. The critical shear stress of the superhydrophobic surface is as low as 0.33 Pa [19-22], which can be considered as a perfect slip surface. This value is much lower than the reported critical shear stress of the interface for oil and steel, ranging from 0.16 to 8 MPa [23]. The perfect slip surface (also called as the ideal slip surface) is a term that used to address the surface of which $\tau_{oc} = 0$ and $\beta = \infty$ (based on the two-component slip model). Such surface results in the critical shear stress to be close to zero (i.e. very low). From Figs. 6 and 19, it can be observed that there is an optimal value of dimensionless slip length B which is unique for different cases depending on the slope incline ratio and the area of slip. Above that value, the variation in B has an insignificant effect of the load carrying capacity. So, surfaces with $\tau_{oc} = 0$ and $\beta > \beta_{\text{optimal}}$ can be considered as perfect slip surfaces. The perfect slip surface can be engineered by modifying the geometrical micro- or nanostructure of the surface and controlling in this way the surface energy. Micro-structured pattern can be made using lithographic techniques, plasma etching or metal assisted etching. This method is then followed by hydrophobic treatment which can be accomplished by techniques such as film or molecule deposition, solution coating or self-assembly of hydrophobic layers [24].

Based on the analysis discussed in the previous section, for a two-dimensional lubricated contact with complex slip surface pattern containing two areas with and without slip, the maximum load carrying capacity can always be achieved by designing geometrical parameters of the slip zone and the slope incline ratio either separately or simultaneously. The numerical analysis used (genetic algorithm) makes it possible to conduct that procedure, and therefore the computation time will be effective. The lubricated contact with a CSS pattern and a low value of the critical shear stress in the slip area is expected to give a maximum hydrodynamic performance. Moreover, the fact that the load carrying capacity can be obtained by an optimized CSS pattern on perfectly flat surfaces seems to be a very promising way for designing very low-friction lubricated mechanisms.

5. Conclusions

As a conclusion, this paper focuses numerically on the mechanism to generate a high hydrodynamic pressure and a low friction force in two-dimensional lubricated contacts by optimizing the complex slip surface (CSS) pattern on a solid surface and slope incline ratio. Using an optimization technique based on a genetic algorithm, hydrodynamic lubricated contact can be designed with a high hydrodynamic performance.

In two-dimensional lubricated sliding contacts, if slip occurs at the entire stationary surface, the hydrodynamic load carrying capacity is only half of that without a slip boundary. It is also demonstrated that a surface containing a CSS pattern raises the hydrodynamic performance over the traditional (no-slip) lubricated contact. It is found that a combined optimization for slope incline ratio and CSS pattern (both along and transverse to the sliding direction) seems to be a powerful approach for obtaining a high hydrodynamic performance (high load carrying capacity and low friction force). Surface optimization of a CSS pattern with a slightly parallel moving surface can increase the maximum load carrying capacity by approximately three times when compared to what a classical Reynolds equation predicts for an optimal slope incline ratio. The friction force can also be decreased significantly. However, particular care must be taken in choosing such optimized pattern with respect to the slip property (slip length and initial critical shear stress) due to the possible deterioration of the hydrodynamic performance. In order to obtain an improvement of the performance, the lubricated contact with the optimized CSS pattern should be designed with a low initial critical shear stress and very high slip length.

Nomenclatures

f = friction force
h_i = inlet film thickness
h_o = outlet film thickness
L_x = length of lubricated surface in the x-direction
L_y = length of lubricated surface in the y-direction

p = fluid film pressure
u_w = wall velocity
u_s = slip velocity at the surface in the x-direction (along the sliding direction)
v_s = slip velocity at the surface in the y-direction (perpendicular to the sliding direction)
w = load carrying capacity, $\int_0^{L_y}\int_0^{L_x} p(x,y)dxdy$
β = slip length
τ_x = shear stress in the x-direction
τ_y = shear stress in the y-direction
τ_c = the surface shear stress when slip occurs
τ_{oc} = initial critical shear stress (or critical shear stress for the onset of slip)
η = dynamic viscosity

Dimensionless parameters

$$B = \beta / h_o$$
$$F = fh_o / (u_w \eta L_x L_y)$$
$$h^* = h_i / h_o$$
$$L_x^* = x / L_x$$
$$L_y^* = y / L_y$$
$$P = ph_o^2 / (u_w \eta L_x)$$
$$W = wh_o^2 / (u_w \eta L_x^2 L_y)$$
$$\tau_{oc}^* = \tau_{oc} h_o / (u_w \eta)$$

References

1. Israelachvili, J., 1995, *Intermolecular and Surface Force. vol. 1. 2nd edition*, Academic Press, London.
2. Spikes, H.A., 2003, "The half-wetted bearing. Part 1: extended Reynolds equation," *Proceedings of the Institution of Mechanical Engineers, Part J: Journal of Engineering Tribology* **217**, pp. 1 – 14.
3. Spikes, H.A., 2003, "The half-wetted bearing. Part 2: Potential application in low load contacts," *Proceedings of the Institution of Mechanical Engineers, Part J: Journal of Engineering Tribology* **217**, pp. 15 – 26.
4. Hild, W., Opitz, A., Schaefer, J.A. and Scherge, M, 2003, "The effect of wetting on the microhydrodynamics of surfaces lubricated with water and oil, " *Wear* **254**, pp. 871 – 875.
5. Choo, J.H., Spikes, H.A., Ratoi, M., Glovnea, R. and Forrest, A., 2007, "Friction reduction in low-load hydrodynamic lubrication with a hydrophobic surface," *Tribology International* **40**, pp. 154 – 159.
6. Choo, J.H., Glovnea, R.P., Forrest, A.K. and Spikes, H.A., 2007, "A low friction bearing based on liquid slip at the wall," *ASME Journal of Tribology* **129**, pp. 611 – 620.
7. Yang, J. and Kwok, D.Y., 2003, "Effect of liquid slip in electrokinetic parallel-plate microchannel flow," *Journal of Colloid and Interface Science* **260**, pp. 225 – 233.
8. Salant, R.F. and Fortier, A.E., 2004, "Numerical analysis of a slider bearing with a heterogeneous slip/no-slip surface," *Tribology Transaction* **47**, pp. 328 – 334
9. Wu, C.W., Ma, G.J. and Zhou, P., 2006, "Low friction and high load support capacity of slider bearing with a mixed slip surface," *ASME Journal of Tribology* **128**, pp. 904 – 907.
10. Ma, G.J., Wu, C.W. and Zhou, P., 2007, "Wall slip and hydrodynamics of two-dimensional journal bearing," *Tribology International* **40**, pp. 1056 –1066.
11. Bayada, G. and Meurisse, M.H., 2009, "Impact of the cavitation model on the theoretical performance of heterogeneous slip/no-slip engineered contacts in hydrodynamic conditions," *Proceedings of the Institution of Mechanical Engineers, Part J: Journal of Engineering Tribology* **223**, pp. 371 – 81.
12. Sivanandam, S.N. and Deepa, S.N., 2008, *Introduction to Genetic Algorithm*, Springer-Verlag, Berlin Heidelberg.
13. Spikes, H.A. and Granick, S., 2003, "Equation for slip of simple liquid at smooth solid surfaces," *Langmuir* **19**, pp. 5065 – 5071.
14. Vinogadrova, O.I., 1999, "Slippage of water over hydrophilic surfaces," *International Journal of Mineral Processing* **56**, pp.31 – 60.
15. Wang, L.L., Lu, C.H., Wang, M. and Fu, W.X., 2012, "The numerical analysis of the radial sleeve bearing with combined surface slip," *Tribology International* **47**, pp. 100 – 104.

16. Patankar, SV., 1980, *Numerical Heat Transfer and Fluid Flow*, Taylor & Francis, Levittown.
17. Watanabe, K., Yanuar and Udagawa, H., 1999, "Drag reduction of Newtonian fluid in a circular pipe with a highly water-repellant wall," *Journal of Fluid Mechanics* **381**, pp. 225 – 228.
18. Fortier, A.E. and Salant, R.F., 2005, "Numerical analysis of a journal bearing with a heterogeneous slip/no-slip surfaces," *ASME Journal of Tribology* **127**, pp. 820 – 825.
19. Zhu, Y. and Granick, S., 2002, "Limits of the hydrodynamic no-slip boundary condition," *Physical Review Letters* **88**, 106102.
20. Zhu, Y. and Granick, S., 2002, "No-slip boundary condition switches to partial slip when fluid contains surfactant," *Langmuir* **18** (26), pp. 10058－10063.
21. Granick, S., Zhu, Y. and Lee, H., 2003, "Slippery questions about complex fluids flowing past solids," *Nature Materials* **2**, pp. 221－227.
22. Wu, C.W. and Ma, G.J., 2005, "On the boundary slip of fluid flow," *Science in China Ser. G Physics, Mechanics & Astronomy* **48**, pp. 178－87.
23. Wu, C.W., Ma, G.J. and Sun, H.S., 2005, "Viscoplastic lubrication analysis in a metal-rolling inlet zone using parametric quadratic programming," *ASME Journal of Tribology* **127**, pp. 605－610.
24. Xiu, Y., 2008, *Fabrication of Surface Micro-and Nanostructures for Superhydrophobic Surfaces in Electric and Electronic Applications*, PhD thesis, Georgia Institute of Technology, Atlanta.

Appendix A: Genetic Algorithm Concepts at a Glance

Genetic algorithm was first developed by John Holland [12]. A genetic algorithm is basically algorithm based on natural biological evolution. It is a search technique to find approximate solutions for optimization and search problems. The algorithm works on a designs population. The population evolves from generation to generation, gradually improving its adaption to the environment through natural selection; fitter individuals have better chances of transmitting their characteristics to later generations [12].

The basic genetic algorithm is given as follows [12]:

1. *Initial population*: Generate random population of chromosomes.
2. *Fitness*: Evaluate the fitness of each chromosome in the population.
3. *Test*: If the end condition is satisfied, stop, and return to the best solution in current population.
4. *New population:* Create a new population by repeating the following steps until the new population is complete. *Reproduction*: Select two parent chromosomes from the population according to their fitness. *Crossover*: With a crossover probability, crossover the parents to form new children. If no crossover was performed, children are an exact copy of the parents. *Mutation*: With a mutation probability, mutate new children at each locus (position in chromosome). *Accepting*: Place new children in the new population.
5. *Replace*: Use new generated population for further run of the algorithm.
6. *Loop*: Go to step 2.

Appendix B: Flow Diagram of Numerical Calculation

Figure B.1 shows the flow diagram of numerical analysis used in solving the modified Reynolds equation for hydrodynamic pressure (Eq. (1)).

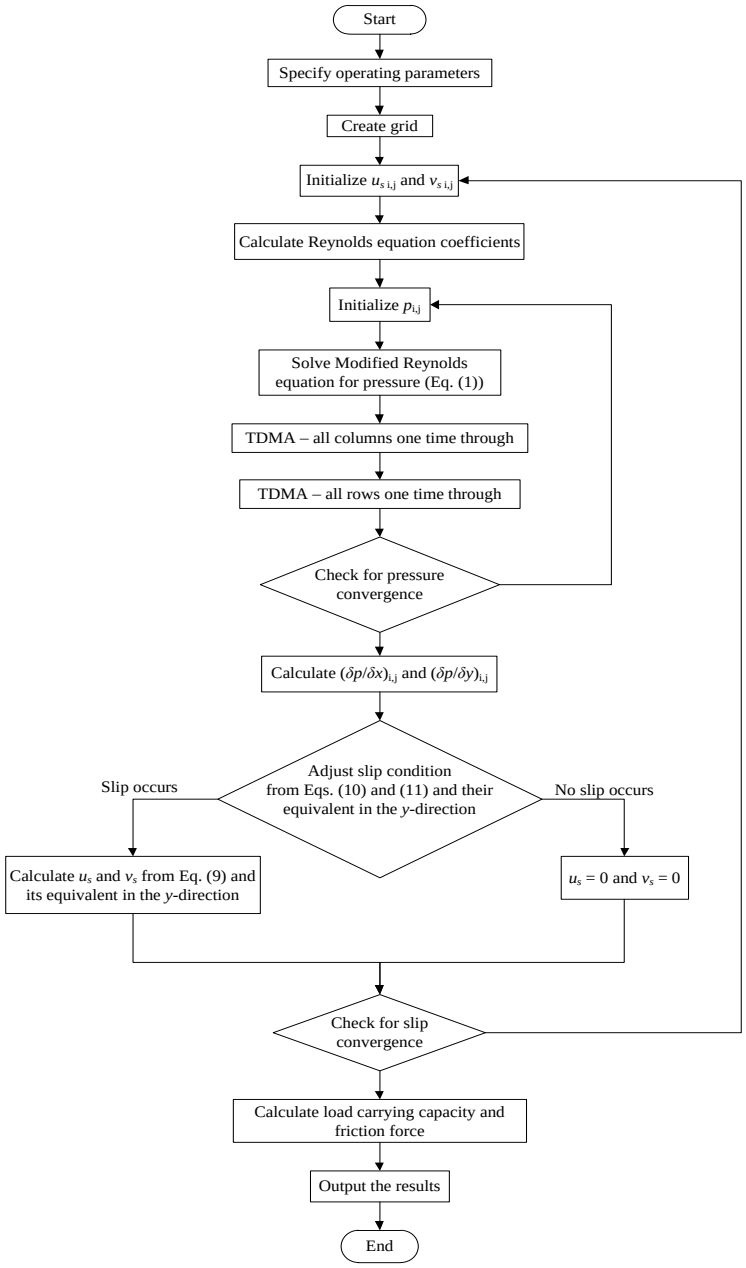

FIGURE B.1: *Flow chart.*

Appendix C: Grid Refinement Study

The numerical simulations to ensure grid independent results are conducted using different mesh sizes, i.e. 30 X 30, 50 X 50, 100 x 100, and 200 x 200 grid points. The load carrying capacities for these different meshes are compared and presented in Fig. C.1 for several slope incline ratio h^* values. There are two conditions investigated, at first, for the case of the contact with traditional no-slip boundary condition, and secondly, the contact with homogeneous slip condition. The results in the case of slip analysis are evaluated for a dimensionless slip length B = 50, a reasonable value of the slip length based on literature [5, 6, 8, 17]. From the figure, it can be seen that if the mesh number is above 50 x 50, the simulation results do not differ anymore. But obviously the computational cost increases. Therefore, a 50 x 50 grid system is adopted for all simulation cases.

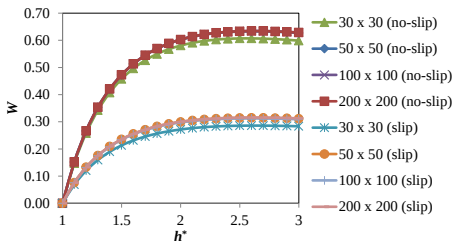

FIGURE C.1: *Dimensionless load carrying capacity W versus slope incline ratio h^* for different grid nodes. The slip analysis is evaluated for $\tau_{oc}^* = 0$ and B = 50.*

Appendix D: Comparison with other model

In this section, the prediction of the lubrication performance between the two-component slip model presented here and the constant slip length model proposed by Salant and Fortier [8] is demonstrated. As discussed in Section 2.1, if the initial critical shear stress is set to zero, the two-component slip model reduces to the constant slip length model.

Salant and Fortier [8] analyzed a non-homogeneous slip surface of a two-dimensional slider bearing with zero initial critical shear stress, similar to that as shown in Fig. 12. In this way, the numerical procedure, when the initial critical shear stress is zero, can be compared with what is proposed by Salant and Fortier [8]. The following base values c_1 = 0, c_2 = 0.725, c_3 = 0.125, c_4 = 0.875 are used. Figure D.1 shows that the numerical results are in agreement with those given by Salant and Fortier [8]. The load carrying capacity decreases with h^* over the entire range as well as the friction force (see insert in Fig. D.1).

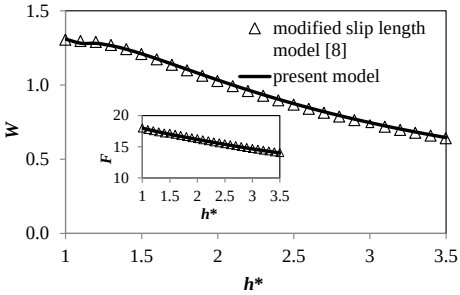

FIGURE D.1: *Comparison of the two-component slip model with the numerical solutions of the modified slip length [8] in predicting hydrodynamic load carrying capacity W and friction force F (see the insert). The solid curves are the theoretical predictions of the present model; the open symbols are those predicted by Salant and Fortier* [8].

Appendix E: Comparison with other bearing configurations

Numerical simulations presented here are performed to compare between the CSS pattern, the pocket bearing, and the step bearing. The dimensions of the pocket region in the X-Y plane are identical to the dimensions of the optimized CSS pattern, i.e. c_1 = 0, c_2 = 0.7, c_3 = 0.15, c_4 = 0.85 with the dimensionless depth of the pocket D varying from 0 to 2. The parameter D is defined as the ratio of the depth of the recess d over the output film thickness h_o. For step bearing, the geometry in the X-Y plane is identical to the geometry of the mixed slip surface as mentioned in the previous section, i.e. c_1 = 0, c_2 = 0.65, c_3 = 0, c_4 = 1 with the depth of the step varying from 0 to 2 h_o. Two parameters are studied to evaluate the performance of the sliding contact: load carrying capacity and friction force. Investigations are made for the

recess depth D of the pocket and the step bearing. The parallel sliding surface is of primary concern. The results are compared with those of the optimized CSS pattern.

With respect to the load carrying capacity, for the bearings considered, the load carrying capacity increases with recess depth, reaches a maximum, and then decreases as indicated in Fig. E.1. However, the optimum depth for the step bearing is smaller than that for the pocket bearing. The corresponding load carrying capacity for the step bearing is also smaller than that for the pocket bearing for depths which are larger than 0.4 h_o. For a low depth ($D < 0.4$), the W prediction of the pocket and the step bearing are nearly the same.

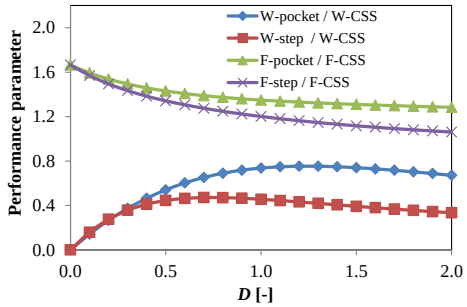

FIGURE E.1: *Effect of the dimensionless recess depth D on the hydrodynamic performance parameters of a lubricated sliding contact, $h^* = 1$.*

It can also be seen from Fig. E.1 that the load carrying capacitiy generated by the pocket and step bearing for the optimized depth is still less efficient when compared with the optimized CSS pattern. The difference in performance is quite large. For example, for the optimized depth the load carrying capacity differs from the optimized CSS pattern prediction by 42% (lower) and 53% (lower), respectively for the pocket and step bearing. In general, the results of this study indicate that the optimized CSS pattern gives an improved load carrying capacity, substantially larger than the pocket bearing and the step bearing even if the optimal depth is used.

In relation to the friction force, the effect of the depth shows a same trend for the two bearing configurations compared with the CSS patterned surface. The friction force for the two configurations is maximal at a zero depth and decreases with increasing depth. The behavior of the friction of the pocket bearing is similar to that of the step bearing. The difference is that the pocket bearing produces smaller friction force than step bearing. However, the friction force predicted by these bearings is still larger than the optimized CSS pattern. Generally, the lubricated contact with the optimized CSS pattern gives a lower friction force and a higher load carrying capacity.

Paper B

M. Tauviqirrahman, R. Ismail, Jamari, D.J. Schipper, 2013

Study of surface texturing and boundary slip on improving the load support of lubricated parallel sliding contacts

Acta Mechanica, Volume 224, Issue 2, pp. 365 – 381.

A Study of Surface Texturing and Boundary Slip on Improving the Load Support of Lubricated Parallel Sliding Contacts

M. Tauviqirrahman,[1,*)] R. Ismail,[1)] Jamari,[2)] and D.J. Schipper[1)]

[1]Laboratory for Surface Technology and Tribology,
Faculty of Engineering Technology, University of Twente, The Netherlands
*Email: mtauviq99@gmail.com

[2]Laboratory for Engineering Design and Tribology,
Department of Mechanical Engineering, University of Diponegoro, Indonesia

Published in: Acta Mechanica, 2013, Volume 224, Issue 2

Abstract **Currently, there is a great interest in the use of engineered complex slip surfaces as well as the surface texturing because these surfaces are able to improve the tribological performance of lubricated contacts. In this paper, based on the modified Reynolds equation, a systematic comparison is made with various surface conditions, i.e. texturing, slip and the combination of those configurations with respect to the performance of flat classical (no-slip) contact. Optimum values of design parameters (slip length, slip zone, texture cell aspect ratio and texturing zone), allowing for maximum load support, are presented. In the case of combined texture/slip pattern, it is shown that the load support do not practically depend on the texture cell aspect ratio. The slip effect has a much more contribution in inducing the pressured distribution than the texturing effect. It is also demonstrated that partial texturing gives a better improvement than full texturing. However, compared to a flat complex slip surface, a partially textured surface is still less efficient to enhance the load support, even if this textured configuration is combined with a slip condition.**

Keywords: complex slip, critical shear stress, hydrodynamic lubrication, surface texture

1. Introduction

The purpose of lubrication is to separate surfaces in relative motion in order to reduce friction and wear and to support the load. The performance and efficiency in hydrodynamic lubrication by surface texturing has been subject to both analytical and experimental research over the last decade. Experimentally, texturing surfaces are most often revealed in mechanical seals [1], reciprocating (cylinder-liner) contacts [2] and two parallel sliding surfaces [3,4] and it was found that texturing enhances load support and reduces hydrodynamic friction. Numerically, the approaches about the analysis of surface texturing with respect to the effect on the tribological performance fall into two classes, using computational fluid dynamics (CFD) models based on Navier-Stokes [5–10], or using Reynolds [11–21]. These models were mainly applied either for macro-texture mode (single cell texture configuration) [5–7,9,10,14,21] or for micro-texture (multiple cells mode) based on a so-called collective effect of the dimples [8,11–13,15–20].

Sahlin *et al*. [6] applied the CFD analysis of a single macro-texture to study the effect of textures on the hydrodynamic lubrication and claimed that the load support gains with the increase in texture width and depth, as well as Reynolds number. Similarly, following a three-dimensional CFD study, Han *et al*. [9] also presented a study on the geometry optimization. Optimum values for maximum load support were found. A key issue in the treatment of cavitation phenomena on textured surfaces has also been the focus of a great deal of research

effort. Brajdic-Mitidieri *et al.* [7] used the Navier-Stokes equation combined with a cavitation model to analyze the lubricant behavior in plain pad bearings having a closed pocket. Such texture could produce reduction in the friction coefficient, especially at very low slope incline ratio (inlet over outlet film thickness) which originates both from an increase in load support as well as a reduction in shear stress in the pockets. Analytically, based on the first-order Reynolds equation and the continuity of flow, the effect of cavitation ('inlet suction') was proposed by Fowell *et al*. [14] on a particular single dimple ('pocket') configuration, in which the textured zone starts with a dam. Recently, Shi and Ni [10], using CFD approach, investigated the effects of periodical macro-groove texture on the sliding lubrication under the cavitation condition. They concluded that with the increase in cavitation pressure, the hydrodynamic pressure effect becomes more pronounced, while the friction force does not change very much.

Additionally, the study of tribological effects obtained by introducing surface micro-texture (multiple cell configurations) of the textured surface without periodic boundary condition was brought to the center of attention by various researchers. Different surface texture models (random texture model, dimple model, sinusoidal model, cylindrical model, elliptical model, etc.) were adopted by different researchers to conclude that the surface texture enhances the hydrodynamic performance. Efforts were made in several works to determine the optimal texturing parameters that would maximize the fluid film thickness (equivalent to maximizing the load support) or minimize friction. Parallel and full texturing were two extreme cases of texture arrangement. The first study to mention "partial texturing" was dedicated by Tonder [11] by theoretical studies to the positive effect of variable roughness profiles on load support. The author pointed out that by introducing a series of dimples or roughness at inlet of a sliding surface, an extra pressure and thus support higher load can be obtained. Brizmer *et al*. [12] demonstrated the potential of laser surface surface texturing in the form of regular micro-dimples for providing load support with parallel sliding contact. A model of a textured parallel slider was developed, and the effect of surface texturing on load support was analyzed through employing a numerical approach. After a relatively large number of numerical simulations, they found that the textured portion, the area density of pores, the pores height ratio, and the bearing length-to-width ratio are the most affecting parameters in predicting hydrodynamic load support. It was also shown that the micro-dimple effect, which corresponds to full width texturing, is not useful for developing the large load support expected from a hydrodynamically lubricated contact. Subsequently, several studies were published in the literatures [16–20], confirming the findings of reference [12]. One emerging conclusion of these studies is that partial texturing leads to better performance than full texturing. The previously mentioned models and simulation results also provide excellent set of guidelines for the optimum design of surface texture in some fields.

Recently, in addition to the surface texturing, the use of deterministic (artificial) slip surface has become popular with respect to lubrication, since this type of surface enhancement would give a better tribological performance. Two deterministic slip surface modes are used currently: homogeneous slip surface (i.e. slip applied over the whole surface) and complex slip surface (i.e. surface consisting of slip area and no-slip area). Such modes will be further discussed herein. The deterministic slip surface can be obtained by modifying geometrical micro- or nanostructure of the surface and controlling in this way the surface energy. Micro-structured pattern can be made using lithographic techniques, plasma etching, or metal-assisted etching. The hydrophobic treatment can be accomplished by techniques such as film or molecule deposition, solution coating, or self-assembly of hydrophobic layers. The developments of (super) hydrophobic surfaces were described in detail in Ref. [22].

The great challenge for a hydrophobic surface from the perspective of a numerical simulation is choosing a model for the slip boundary. This is because the hydrodynamic behavior of lubricated contacts is mainly governed by the boundary conditions of the lubricant that provide lubrication. From the numerical point of view, there are two main wall slip models which have

been adopted to describe the slip boundary, that is, the slip length model [23–26] and the critical shear stress model [27–31].

Spikes [27] based on the critical shear stress model investigated the influence of homogeneous slip on the hydrodynamic properties of a half-wetted bearing. In the half-wetted bearing, the stationary surface is made very smooth to promote wall slip. The moving surface is conventional, so that the lubricant does not slip along it. In this configuration, the bearing can generate a high load support resulting from fluid entrainment and a low friction due to a reduced Couette friction. Later, a new equation based on the critical shear stress concept for Newtonian slip flow was developed by Spikes and Granick [28]. In this model, slip is envisaged to occur only when a critical surface shear stress is reached, and once slip begins, it takes place at a constant slip length. It was also shown that this slip model was able to reconcile results from different experimental investigations [31]. Salant and Fortier [29] conducted a numerical analysis of a finite slider bearing with an engineered complex slip surface and found that such a bearing can provide a high load support in combination with low friction. Unfortunately, if the critical shear stress was nonzero, they could not find a steady-state numerical solution. In the present paper, such a numerical instability is not found if the critical shear stress is varied. Wu *et al*. [30] studied the behavior of a slider bearing with a complex slip surface, and their results indicated that convergent, parallel, and divergent wedge can provide hydrodynamic load support. The analysis of engineered complex slip contacts in the case of parallel sliding contact with an approach of alternating slip/no-slip areas was also carried out by Bayada and Meurisse [24]. The influence of the cavitation model and boundary conditions was studied in more detail. It was found that if complex slip areas are introduced, then a nonzero load support can be obtained whose theoretical value strongly depends on the cavitation model.

When performing the literature survey, one will find that the number of researches about the interplay of surface texture and slip boundary effect interaction with respect to lubrication is still very limited. Bayada and Meurisse [24] compared the slip/no-slip heterogeneity with roughness. They concluded that film rupture in diverging zones can be provoked by a certain complex slip boundary configuration which is similar to that caused by geometrical roughness. In a recent publication, Rao [25] employed a deterministic slip on a stationary surface having a single-groove at slider and journal bearing to obtain pressure and shear stress distribution. The modified Reynolds equation with Navier-slip boundary condition was solved numerically with regard to wall slip effect and texture simultaneously.

Very interesting numerical works regarding the combination of textured and engineered complex slip effect are obtained in Ref. [26]. Aurelian *et al*. [26] investigated the influence of wall slip over the load support and power loss in hydrodynamic fluid bearings. A simple textured/wall slip combination pattern was investigated. The main conclusion of their study was that choosing the texture/slip zone geometry should be taken carefully because inappropriate choice can lead to a drastic deterioration of the bearing performance, especially in relation to the load support. However, in their study, the constant slip length model was used, and wall slip by exceeding a critical shear stress was neglected.

In the present work, the artificial slip boundary is used to study the influence of slip (location and parameter) on the lubricated parallel sliding contact. The effect of micro-texturing in the form of the rectangular-shape texture with various texture aspect ratios (dimple length over dimple depth) and different conditions (slip and no-slip assumptions) will also be examined. To get results, first, it is intended to propose a new modified Reynolds equation with slip based on the critical shear stress model, which is suitable to impose on the cases in which there might be some slip configuration possibilities. Then, the results are presented for the case of flat surface. The effect of the variation of slip parameters is studied, including the critical shear stress and the slip length. Finally, the combined effect of texturing and slip boundary for different texture aspect ratios is studied. Situations where surface texturing occurs either over the whole stationary surface (full texturing) or on some sections only (partial texturing) will be investigated. In the

following computations, the predicted load support with uniform film thickness will be compared with that generated by a classical no-slip contact which is calculated for optimized slope incline ratio.

2. Mathematical model

In a classical hydrodynamic lubrication problem, the governing equations in a full fluid region can be described by the well-known Reynolds equation. The isoviscous Newtonian one-dimensional Reynolds equation is derived from a simple form of the *x*-component of the Navier-Stokes equation that assumes an incompressible flow and neglecting the convective effects in the film:

$$\frac{\partial^2 u}{\partial z^2} = \frac{1}{\eta}\frac{\partial p}{\partial x} \tag{1}$$

In order to obtain the velocity distribution by integration of Eq. (1), it is necessary to define the surface boundary conditions. Let us consider a lubricated contact equivalent to a lower plane moving in the *x*-direction with surface velocity *U*, and an upper stationary surface. In this study, the occurrence of slip in the lubricated sliding contact is determined by two criteria. First, slip may only occur in those areas where both stationary and moving surface have been treated to allow it. Second, the shear stress on both surfaces must exceed a critical shear stress value, referred to as τ_{ca} for stationary surface and τ_{cb} for the moving surface. When both criteria are met, the resulting slip velocity is proportional to the difference between the shear stress and the critical value, with proportionality factors referred to as α_a for the stationary surface and α_b for the sliding surface. It means that each of the sliding surfaces has a unique slip property. The product of the slip coefficient with the viscosity, $\alpha\eta$, is commonly named 'slip length'. The surface boundary conditions are proposed as follows:

$$\text{at } z = h \quad \begin{cases} u = \alpha_a\left(-\eta\dfrac{\partial u}{\partial z} - \tau_{ca}\right) & \text{for } \tau_a \geq \tau_{ca} \\ u = 0 & \text{for } \tau_a < \tau_{ca} \end{cases} \tag{2a}$$

$$\text{at } z = 0 \quad \begin{cases} u = U + \alpha_b\left(\eta\dfrac{\partial u}{\partial z} + \tau_{cb}\right) & \text{for } \tau_b \geq \tau_{cb} \\ u = U & \text{for } \tau_b < \tau_{cb} \end{cases} \tag{2b}$$

The solution of Eq. (1) yields the distribution of the fluid velocity, subject to the boundary equations, Eq. (2). It reads:

$$\begin{aligned} u = {} & \frac{1}{2\eta}\frac{\partial p}{\partial x}z^2 \\ & -\left(\frac{h}{2\eta}\frac{\partial p}{\partial x}\frac{h+2\alpha_a\eta}{h+\eta(\alpha_a+\alpha_b)} + \frac{U}{h+\eta(\alpha_a+\alpha_b)} + \frac{\alpha_a\tau_{ca}+\alpha_b\tau_{cb}}{h+\eta(\alpha_a+\alpha_b)}\right)z \\ & + U\frac{h+\alpha_a\eta}{h+\eta(\alpha_a+\alpha_b)} - \frac{h}{2\eta}\frac{\partial p}{\partial x}\frac{\alpha_b\eta(h+2\alpha_a\eta)}{h+\eta(\alpha_a+\alpha_a)} \\ & + \frac{\alpha_b\tau_{cb}(h+\alpha_a\eta) - \alpha_b\alpha_a\eta\tau_{ca}}{h+\eta(\alpha_a+\alpha_b)} \end{aligned} \tag{3}$$

The modified Reynolds equation is derived by expressing the integrated continuity equations. If the fluid density is assumed to be mean density across the film, it is convenient to express the continuity equation in integral form as follows:

$$\int_0^h \frac{\partial}{\partial x}u\,dz = -(u)_{z=h}\frac{\partial h}{\partial x} + \frac{\partial}{\partial x}\left(\int_0^h u\,dz\right) = 0 \tag{4}$$

Therefore, the modified form of the one-dimensional Reynolds equation with slip reads:

$$\begin{aligned} & \frac{\partial}{\partial x}\left(h^3\frac{h^2+4h\eta(\alpha_a+\alpha_b)+12\eta^2\alpha_a\alpha_b}{h(h+\eta(\alpha_a+\alpha_b))}\frac{\partial p}{\partial x}\right) \\ & = 6\eta U\frac{\partial}{\partial x}\left(\frac{h^2+2h\alpha_a\eta}{h+\eta(\alpha_a+\alpha_b)}\right) - 6\eta\tau_{ca}\frac{\partial}{\partial x}\left(\frac{\alpha_a h(h+2\alpha_b\eta)}{h+\eta(\alpha_a+\alpha_b)}\right) \\ & + 6\eta\tau_{cb}\frac{\partial}{\partial x}\left(\frac{\alpha_b h(h+2\alpha_a\eta)}{h+\eta(\alpha_a+\alpha_b)}\right) - 12\eta U\frac{\alpha_a\eta}{h+\eta(\alpha_a+\alpha_b)}\frac{\partial h}{\partial x} \\ & + 6h\frac{\partial p}{\partial x}\frac{\partial h}{\partial x}\frac{h\alpha_a\eta+2\alpha_a\alpha_b\eta^2}{h+\eta(\alpha_a+\alpha_b)} + 12\eta\tau_{ca}\left(\frac{\alpha_a(h+\alpha_b\eta)}{h+\eta(\alpha_a+\alpha_b)}\frac{\partial h}{\partial x}\right) \\ & - 12\eta\tau_{cb}\left(\frac{\alpha_a\alpha_b\eta}{h+\eta(\alpha_a+\alpha_b)}\frac{\partial h}{\partial x}\right) \end{aligned} \tag{5}$$

It can be clearly seen that the modified form of the Reynolds equation presented in Eq. (5) is different from that used in the studies presented previously [23–31]. The modified Reynolds equation includes the critical shear stress terms and the possibility of slip that may occur on both sliding surfaces. It must be pointed out that the

present model (Eq. (5)) can be used to solve the cases in which (1) the zero or nonzero critical shear stress is present and/or (2) slip occurs either at both surfaces (stationary and sliding surfaces) or at one of the surfaces, by setting $\alpha_a, \alpha_b, \tau_{ca}, \tau_{cb}$ to its specified value according to the appropriate boundary condition of the lubricated sliding contact.

Besides the analysis of the effect of boundary slip, the present study will also investigate the significance of the texture on lubrication. The behavior of hydrodynamic lubrication between a stationary textured surface and a moving surface can be estimated by a classical form of the Reynolds equations which is obtained by putting $\alpha_a, \alpha_b, \tau_{ca}, \tau_{cb}$ in Eq. (5) to zero.

In the case of the present study, the lubricated sliding contact is operating under steady-state conditions. The load support is determined by integrating the calculated hydrodynamic pressure field along the surface contact.

3. Solution method

In this work, the modified Reynolds equation is solved numerically using a finite difference equations obtained by means of the micro-control volume approach [32]. The entire computed domain is assumed as a full fluid lubrication. By employing the discretization scheme, the computed domain is divided into a number of control volumes. The mesh number for all the situations obtained from a mesh refinement study is approximately 2,000 and 4,000 nodes, respectively, for the case of flat and textured surface. For all derivatives, the central difference is used except at the boundaries. Appropriate one-sided difference is used at the boundaries.

Once Eq. (5) is solved for the hydrodynamic pressure distribution, the load support can be calculated. The modified Reynolds equation is solved using TDMA (tri-diagonal matrix algorithm), [32]. For the case of nonzero critical shear stress, an iterative procedure is used. Initially, the proportionality factor α_a is set equal to zero everywhere, and the equations are solved. In the regions where slip is possible, at locations where the critical shear stress is exceeded, the value of α is changed to its specified nonzero value according to the property of the surfaces, while in regions where the shear stress is below the critical shear stress, α is set equal to zero, and the equations are again solved. Iteration continues until the solution converges. For the case of zero critical shear stress, the equations are solved directly, with α equal to zero in no-slip regions and α equal to a specified value in slip regions.

It can be noted that the following simulation results are obtained to an accuracy of tolerance Tol = 10^{-6} where

$$\max\left(\frac{\left|\Phi_{i,j}^{new}-\Phi_{i,j}^{old}\right|}{\left|\Phi_{i,j}^{new}\right|}\right)\le \text{Tol},$$

is the field variable. The iteration is also conducted for Tol = 10^{-5} and Tol = 10^{-7}, and there is no difference in the values.

The boundary conditions, known as Reynolds boundary conditions, are used to determine the rupture zone of the film. They consist in ensuring that $p = 0$ and $\partial p / \partial x = 0$ at the rupture limits of the film lubricant. Numerically, Reynolds cavitation model is done by setting the sub-cavitation values of the pressure obtained during each step of the iterative algorithm to cavitation pressure [24]. For the present study, a zero cavitation pressure (gauge) has been assumed for convenience. Since the Reynolds boundary conditions are employed, using either the partial surface texturing or the full surface texturing enable us to obtain the performance where the total produced pressure becomes positive for any variations in the geometry of the dimple for the given velocity direction. The appropriate treating of the cavitation in the lubricated sliding contact can be done by applying mass-flow conserving model such as the so-called Floberg-Elrod-Adams (FEA) model. The real interaction of the cavitation in the results may be considered as another research topic including appropriate boundary conditions. However, as discussed in Ref. [24], Reynolds cavitation model can be considered as a conservative one if the artificial slip that is comparable to surface texturing is used at the

lubricated contact in which of the leading edge is slip (or textured) zone.

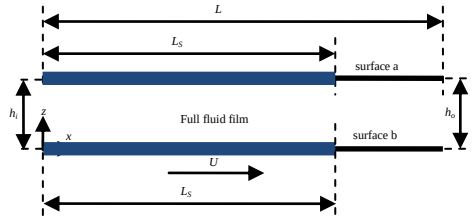

FIGURE 1: *The schematic of a lubricated flat sliding contact with boundary slip applied both on the stationary and moving surface. L_S (slip zone) is the zone on both surfaces treated to allow slip and the other parts are not.*

The boundary slip effects are first investigated for flat surfaces in the case of lubricated sliding contact. A parameter is introduced in order to define the slip zone L_S as presented in Fig. 1. For the slip zone L_S which is set equal to the contact length L, the boundary slip is termed as homogenous slip ($L_S = L$) which means the slip is applied everywhere along the contact length. For the slip zone which covers only a specific zone of the surface, the term of complex slip is used. On the other words, in the present study, complex slip condition is referred when the ratio of the slip zone L_S to the contact length L is < 1. Next, the study is extended to the influence of surface texturing with no-slip (Fig. 2). Finally, surface texturing is combined with slip (texture/slip combination) as indicated in Fig. 3. In this study, the shape of the texture cell is chosen to be rectangular as this would be relatively easy to. As noted, most of the results from the literature review show that there is a little effect of the texture shape on the tribological performances of the LST (laser surface textured) surfaces.

A texture cell is characterized by three non-dimensional parameters: the texture density ρ_T (defined as the ratio between the dimple length l_D and the texture cell length l_C), relative dimple depth K (defined as the ratio between the dimple depth h_D and the land film thickness h_F), and the texture aspect ratio λ (defined as the ratio between the dimple length l_D and the dimple depth h_D) as shown in Fig. 2. In the analysis of textured parallel sliding surface, h_F are set equal to h_o (output film thickness).

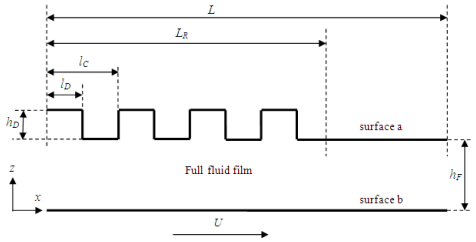

FIGURE 2: *The schematic of lubricated parallel sliding contacts with texturing on the stationary surface. L_R is the texturing zone applied partly on stationary surface.*

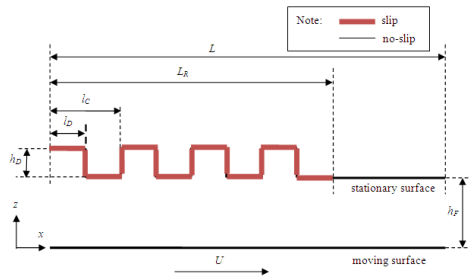

FIGURE 3: *The schematic of lubricated parallel sliding contacts with textured configuration combined with a boundary slip on the whole edges of the texture cell.*

The parameter of texturing zone, L_R is introduced and categorized into two kinds of texturing, that is, partial texturing (L_R/L is < 1) and full texturing ($L_R = L$). As presented in Fig. 3, the texturing zone L_R may consist of a number of texture cells depending on the chosen texture cell aspect ratio.

4. Results

To investigate the effect of the slip parameters and texturing characteristics on the lubrication performance of sliding surfaces with respect to the enhancement of the load support, various parameters are set up. The primary parameters of the lubricated sliding contact are given as follows: sliding velocity U is 1 m/s (the corresponding Reynolds number R_e is 1

assuming fluid density ρ is 1,000 kg/m^3 and dynamic viscosity η is 0.001 Pa.s), total length of lubricated contact L is 20x10^{-3} m and outlet film thickness h_o is 1x10^{-6} m. In the following simulations, slip coefficient α varies from 0 to 0.1 m^{2}s/kg (the corresponding slip length is 1x10^{-4} m) based on the results published in the literature [23,25,29,31,33], and the critical shear stresses range from 0 to 1,000 Pa, reasonable values based on literature [34–38]. All parameters and the range in which they are varied for all cases investigated in the present study are summarized in Table 1. The whole analysis has been based on Reynolds cavitation model which may, of course, be questioned. However, that model is rather generally accepted, and the effects may essentially modify the quantitative results but not the general phenomena.

TABLE 1: *Simulated parameters.*

Parameter	Data setting	Unit
Slip coefficient α	0 – 0.1	m^{2}s/kg
Critical shear stress τ_c	0 – 1000	Pa
Texture density ρ_T	0.5	[-]
Relative dimple depth K	1	[-]
Dimple aspect ratio λ	20 – 300	[-]

For the analysis of a lubricated contact with combined texture/slip condition, the boundary slip is employed to all edges of the texture cell (see Fig. 3). The simulation results will be presented in dimensionless form, i.e. $P = ph_o^2 / \eta LU$ for dimensionless pressure, $W^* = Wh_o^2 / (U\eta L^2)$ for dimensionless load support in which W is the load per unit length, $\tau_c^* = \tau_c h_o / \eta U$ for dimensionless critical shear stress. It must be noted that in the present study, the dimensionless load support W^* is proportional to η U. Keeping the η and ρ as constant and thus the Reynolds number R_e as constant (where $R_e = \rho U h_o / \eta$), the generated W^* will be independent to the U as well as the calculated P.

In this paper, the simulation has been carried out for various configurations as described in Table 2. For the first configuration, that is, flat classical (no-slip) surface, prediction of load support is conducted when the wedge effect is present ($h^* > 1$). As we know, the converging wedge is considered as the first important condition to produce a hydrodynamic pressure in a classical lubrication film between two solid surfaces with a relative sliding/rolling motion. Emphasis has been given to the last three configurations which are calculated for parallel sliding surface. This is of particular interest because it is believed that the surface modification including surface texturing (called as "physical roughness") and slippage (called as "chemical roughness") will lead to improved sliding contact characteristics. A maximum hydrodynamic load support can be obtained by adjusting some geometrical parameters, such as the slip zone, dimple depth, texturing zone, and texture cell aspect ratio. In the present study, the exploitation of the slip phenomena and the texturing characteristic to improve the performance of sliding contact, with emphasis on increasing load support, are examined by means of numerical analysis. Further, by comparing the results with the classical no-slip lubricated contact at optimal slope incline ratio h^*, the optimized parameters of a pattern containing slip, texturing, or combined texture/slip with respect to the load support can be proposed. It should be pointed out that when h^* equals one, the no-slip contact has a zero load support. Moreover, the fact that the load support can be obtained using parallel sliding surfaces by texturing and utilizing slip seems to be a very promising way for designing lubricated nanotechnology and micro-electro-mechanical-system (MEMS) devices which based on recent technology frequently exhibits parallel gaps.

TABLE 2: *Simulated type of contact.*

	Type of surface	Type of condition
Configuration 1	Flat no-slip	-
Configuration 2	Flat slip	Homogeneous and complex slip
Configuration 3	Pure texturing	Partial and full texturing
Configuration 4	Combined texture and slip	Partial and full texturing

4.1 Flat surface with slip

4.1.1 Effect of critical shear stress

The focus of this section is to show the importance of the critical shear stress for contacts with slip. The influences of wall slip will be investigated for flat surfaces with various

critical shear stress values and compared with a traditional (no-slip) lubricated sliding contact. Parallel sliding surface (uniform film thickness) is of particular interest. The main consideration for this is that for a parallel gap in case of a conventional lubricated contact (no-slip), there is no load support due to the absence of the wedge effect. Besides that, this section also aims to find an optimal slip zone to be applied on a surface to create the complex slip surface for the purpose of the highest load support. This is because of the fact that it is known that a complex slip surface is superior to a homogeneous slip surface with respect to load. In this computation, it is considered that slip does not occur on the moving surface.

From Eq. (5), if α_a, α_b, τ_{ca} and τ_{cb} are set to zero, the modified Reynolds equation developed simplifies to the classical Reynolds equation. Thus, the mechanism to yield the pressure distribution is only based on the wedge effect in which the pressure generation due to the fluid being driven from the thick end to the thin end of the wedge-shaped fluid film by the surface movement. From the analytical solution described in Ref. [39], it was known that at convergence ratio ($h^* = h_i/h_o$) of 2.2, the hydrodynamic pressure gives the highest value. It means that a convergent gap is a main requirement to generate the hydrodynamic pressure based on the classical Reynolds theory.

Figure 4 shows the effect of the length of slip zone, L_S on the ratio of the dimensionless load support, W^* of a complex slip surface to that of a no-slip surface, $W^*_{\text{no-slip}}$ at several dimensionless critical shear stress values. $W^*_{\text{no-slip}}$ is evaluated at $h^* = 2.2$. It is found that dimensionless hydrodynamic load support decreases with increasing the dimensionless critical shear stress, τ_c^*. Setting the critical shear stress value to zero, that is, the perfect slip surface, the highest load support can be achieved for parallel moving surfaces. When the dimensionless critical shear stress is 1, no load support takes place.

Fig. 4 clearly shows that two parallel moving surfaces with an optimized complex slip surface using a perfect slip surface can also provide fluid load support. Based on optimization calculations, the complex slip surface with a slip zone which covers 0.65 times the length of the contact (L_S/L = 0.65) gives the highest load support. It is interesting that this value is similar with those given in Ref. [30] although the slip models and numerical methods used are different. With the critical shear stress of zero (perfect slip surface), the maximum load support for such complex slip surface is over twice that of the corresponding traditional lubricated contact. It must be underlined that for all values of the critical shear stress, if the stationary surface is designed as a homogeneous slip surface (L_S/L = 1), the numerical results show that there is no load support at parallel surfaces.

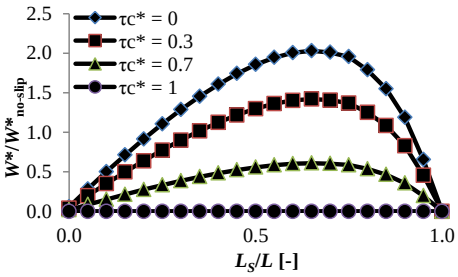

FIGURE 4: *Effect of the slip zone, L_S of parallel sliding surfaces on the ratio of dimensionless load support, W^* of a complex slip surface to that of a no-slip surface, $W^*_{no\text{-}slip}$ at several dimensionless critical shear stress values, τ_c^*. W^* is evaluated at two parallel surfaces, whereas $W^*_{no\text{-}slip}$ is evaluated at optimized convergence ratio ($h^* = 2.2$). The profiles are calculated for dimensionless slip length A = 20.*

Another interesting result is shown in Fig. 5; the maximum pressure distribution for a parallel surfaces with a perfect slip surface using the optimized complex slip surface (L_S/L = 0.65) is approximately three times as large as the maximum pressure obtained from a no-slip wedge when $h^* = 2.2$. Otherwise, with respect to the improvement of the load support with uniform film thickness, such slip zone ratio can be applied not only for a perfect slip surface $\tau_c = 0$ but also for other kinds of surfaces having different critical shear stress values. However, there is a threshold value of the critical shear stress in which the advantage of the load support by the engineered complex slip surface can be break down significantly. From Fig. 6, it is shown that when the dimensionless critical shear stress rises to 0.55 or larger, the

benefit of employing the engineered complex slip surface will vanish. In other words, the configuration of the surface with high critical shear stress ($\tau_c^* \geq$ 0.55 in this case) is not advisable for improving the load support: a classical configuration with optimized slope incline ratio (h^* = 2.2) is recommended (see the inset of Fig. 6). Therefore, for the maximum load support, it is very beneficial to engineer the critical shear stress to zero (perfect slip).

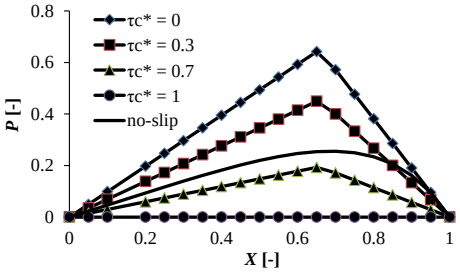

FIGURE 5: *Dimensionless hydrodynamic pressure distribution for several dimensionless critical shear stress values, τ_c^* generated by a complex slip surface (L_S/L = 0.65) for two parallel moving surfaces. The solid curve without markers denotes the pressure generated by a no-slip surface at optimized convergence ratio, h^* = 2.2. The profiles are calculated for dimensionless slip length A = 20.*

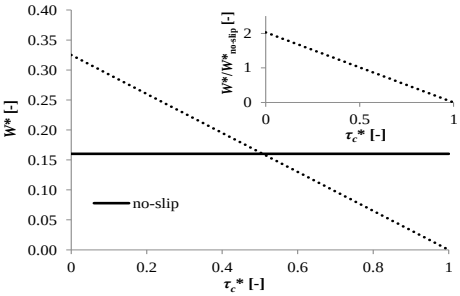

FIGURE 6: *Dimensionless load support versus dimensionless critical shear stress. The dashed line denotes the load support generated by the optimized artificial slip surface (L_S/L = 0.65) for two parallel sliding surfaces. The solid curve denotes the load support generated by a no-slip surface at optimized slope incline ratio h^* = 2.2. The inset shows the corresponding ratio of dimensionless load support by artificial slip, W^* to that no-slip surface, $W^*_{no\text{-}slip}$ versus the critical shear stress. The profiles are calculated for dimensionless slip length A = 20.*

The conclusion in this section is that the critical shear stress has a strong effect on the prediction of the lubrication behavior with slip. This is because the predicted load support is a function of the critical shear stress. The higher the critical shear stress, the smaller the generated load support. Therefore, in constructing the lubricated contact containing an engineering complex slip boundary, a particular care must be taken in choosing the critical shear stress as well as the slip zone length. By designing the slip surface with very low (or close to zero) critical shear stress, a very positive effect with respect to the load support can be achieved.

4.1.2 One-slip versus two-slip surface(s)

The study is extended to investigate the configuration of slip boundaries. In a hydrodynamic lubricated contact, the slip situation can occur on two contacting surfaces, that is, the stationary surface and the moving surface. In this present work, the surface allowing slip to occur on the stationary and the moving surface is termed by “two-slip” surfaces, whereas the term of “one-slip” surface is addressed to the contact in which the slip situation either as a homogeneous slip or as a complex slip can only occur at one surface (the stationary surface or the moving surface).

Computations have been made to simulate this situation, two-slip and one-slip, assuming the critical shear stress is zero for a maximum load support as discussed in the previous section. In the present study, a boundary slip is considered as optimized complex slip surface (L_S/L = 0.65). The main consideration to choose the complex slip surface instead of the homogeneous slip surface is the capability of load support generation for parallel moving surfaces for the "one-slip" boundary as discussed in the previous section, whereas for the case of homogeneous slip and the no-slip contacts, no pressure exists at two parallel moving surfaces. Table 3 lists the three different boundary slip conditions that may exist in hydrodynamic lubricated contacts. Using Eq. (5), all cases as indicated in Table 3 can be analyzed. It should be pointed out that in the case 1, both stationary surface and moving surface have a boundary slip whose area covers 0.65 contact surface length.

TABLE 3: *Slip surfaces with three possibilities of the boundary conditions.*

	Stationary surface (surface a)	Moving surface (surface b)
Case 1	Slip	slip
Case 2	No-slip	slip
Case 3	Slip	no-slip

Figure 7 shows the comparison of the dimensionless pressure distributions with various boundary slip conditions as indicated in Table 3. It can be observed that by applying the complex slip on the stationary surface, while the no-slip situation is present on the moving surface, pressure is generated, and thus, load support can be achieved. The maximum pressure with uniform film thickness is approximately three times as large as the maximum pressure obtained from a no-slip lubricated contact when $h^* = 2.2$. If slip is applied on the moving surface or employed both on the moving and stationary, the load support will be zero as well as in the case of the conventional contact while $h^* = 1$ even when the complex slip boundary is employed.

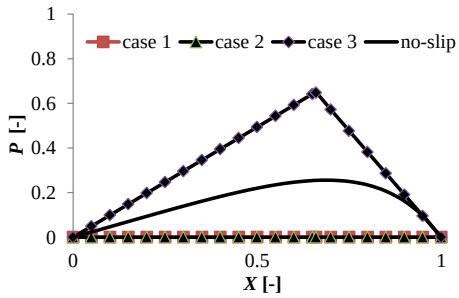

FIGURE 7: *Dimensionless pressure distribution along the contact surface for parallel moving surfaces for several cases as indicated in Table 3. The solid curve without markers denotes the pressure generated by a no-slip surface with $h^* = 2.2$. The slip profiles are calculated for dimensionless slip length A = 20.*

The issue of "how does the slip length affect the load support at the optimized complex slip contact" will be explored. To answer this question, the comparison of the dimensionless pressure distribution at several dimensionless slip length values is given in Fig. 8. In the present study, the dimensionless slip length A is determined by normalizing the "slip length" ($\alpha\eta$) with the outlet film thickness h_o. The comparison is carried out at uniform film thickness using optimized complex slip surface (L_S/L = 0.65). The one-slip, stationary surface (case 3) is employed due to the consideration of the load support improvement as discussed before.

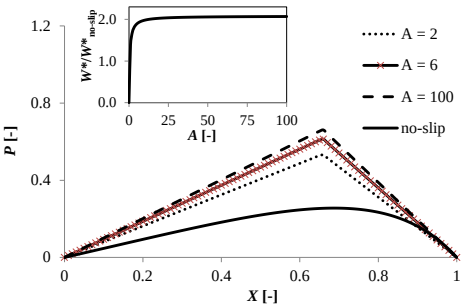

FIGURE 8: *Dimensionless pressure distribution P at several dimensionless slip length values A with uniform film thickness ($h^* = 1$). The solid curve without markers denotes the pressure generated by a no-slip surface at $h^* = 2.2$. The inset shows the ratio of dimensionless load support by complex slip, W^* to that no-slip surface, $W^*_{no\text{-}slip}$ versus the corresponding dimensionless slip length A.*

It is shown that at parallel sliding surfaces, the non-dimensional pressure distribution with complex slip surface is higher when compared with the classical lubricated contact with no-slip condition at optimal slope incline ratio, $h^* = 2.2$. The maximum value of the non-dimensional pressure distribution in the contact with complex slip surface occurs at the region of slip/no-slip interface, that is, at $L_S = 0.65$. Also, the variation in non-dimensional pressure distribution, P is not significant for higher values of the non-dimensional slip length ($A > 100$). This trend is described in-detail by the inset of Fig. 8. The ratio of the load support with optimized complex slip surface, W^* (at h^*=1) to that without the slip boundary, $W^*_{no\text{-}slip}$ (at h^*=2.2) is insensitive to A until A falls below approximately 10. It then falls rapidly to its no-slip value at $A = 0$.

4.2 Textured surface with and without slip

The validity of Reynolds equation in lubricated contacts with surface texturing is of great discussion in the published researches recently.

However, the limits of this equation were well established based on Dobrica and Fillon [8]. They showed the importance of the texture cell aspect ratio λ as well as the Reynolds number R_e when judging the accuracy of Reynolds equation. It was found that the Reynolds equation can be applied in textured contact, as long as λ is sufficiently large, and R_e sufficiently small. In this study, the texture cell aspect ratio λ varies from 20 to 300, and the Reynolds number R_e is 1, values that are in the domain of validity as explained in [8]. Besides that, the variation of λ values (in the range of 20 to 300) are chosen so as to cover a large range of application reported in the literature.

In the present work, the comparison is made for full texturing and partial texturing. The parameter of texturing zone, L_R as indicated in Fig. 2 and 3, is therefore varied. The load support will be investigated as well as the combining effect of texturing and wall slip. It should be pointed out that texturing is only employed on the stationary surface.

4.2.1 Texturing effects over the surface with no-slip situation

Figure 9 shows the effect of the dimensionless texturing zone, L_R over L on the ratio of dimensionless load support, W^* of a textured surface to that of a no-slip surface, $W^*_{\text{no-slip}}$ for different texture cell aspect ratios λ of 20, 50, 100, and 200, respectively. In this discussion, it is assumed that the texture density ρ_T is constant and equal to 0.5, and the relative texture cell depth K (h_D over h_F) is also constant and equal to 1.0. Thus, the variation of λ is conducted by modifying the dimple length l_C while keeping a constant land film thickness h_F and the dimple depth h_D.

Two observations can be made based on Fig. 9. At first, it can be noted that the partial texturing is most effective for $L_R/L = 0.55$ for all values of λ. The full texturing gives the lowest dimensionless load support which is close to zero for all values of λ. Therefore, if load support improvement is of particular interest, the optimized partial texturing is beneficial. However, comparing a flat no-slip surface at optimized slope incline ratio ($h^* = 2.2$), the load support generation with the partial texturing configuration is still not efficient. If comparison is made at the same slope incline ratio, that is, at $h^* = 1$, the (inlet) partially textured is much better than the flat no-slip surface as well as for the fully textured pattern. Second, as investigated by Dobrica and Fillon [8] the texture cell aspect ratio λ is important; however, it needs to be taken with care in the analysis. As can be seen in Fig. 10, in the case of the partial texturing with the optimized texturing zone ($L_R/L = 0.55$), increasing the texture aspect ratio from 20 to 100 gives a significant effect on the dimensionless load support. However, after λ reaches 100 and above, the load support is not influenced with the further increase in the value for the aspect ratio. It can be said that the presence of the texturing zone at the leading edge of the contact produces this positive effect. Experiment and simulation studies [11,12,16–20] are matched well with the present research. A contradictive result is found in case of a fully textured surface. The dimensionless load support increases linearly with the texture cell aspect ratio. However, compared to the partially textured pattern, the generated load support is much lower and close to zero. This is consistent with the result presented in Fig. 10 which shows that for full texturing case, the improvement of load support is not very significant and the contact surface with this kind of texturing behaves like the parallel no-slip moving surface situation.

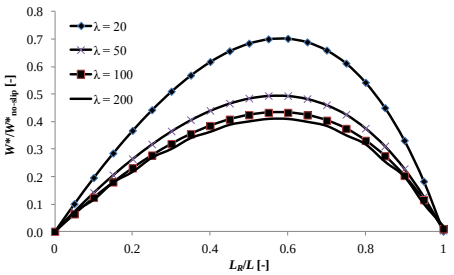

FIGURE 9: *Effect of the texturing zone, L_R on the ratio of dimensionless load support, W^* of a textured surface to that of a no-slip surface, $W^*_{no\text{-}slip}$ for various texture cell aspect ratios λ. W^* is evaluated at two parallel surfaces, whereas $W^*_{no\text{-}slip}$ is evaluated at optimized convergence ratio ($h^* = 2.2$).*

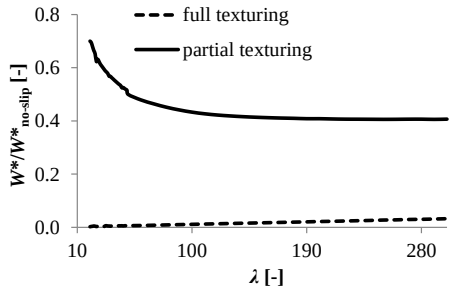

FIGURE 10: *Effect of the texture cell aspect ratio λ on the dimensionless load support, W^*: comparison between optimized partial texturing (L_R/L = 0.55) and full texturing (L_R/L = 1). $W^*_{no\text{-}slip}$ is evaluated at optimized convergence ratio (h^* = 2.2).*

Figure 11 depicts the dimensionless pressure distributions for several textured configurations with different λ. Compared with the classical (no-slip) pattern for optimized slope incline ratio, the partially textured parallel sliding surface with the optimized texturing zone (L_R/L = 0.55) is less effective to produce a high load support both for high λ and for low λ. For example, for the partially textured contact subject to a texture cell aspect ratio of 20, the load support differs from the flat no-slip surface by 30% (lower). As the texturing zone is increased to be full texturing, the discrepancies in load support increases (at a texture cell aspect ratio of 300, it is up 97%). On the other words, full texturing is unable to generate hydrodynamic lift in parallel sliders. This has also been confirmed by recent literatures [18,20].

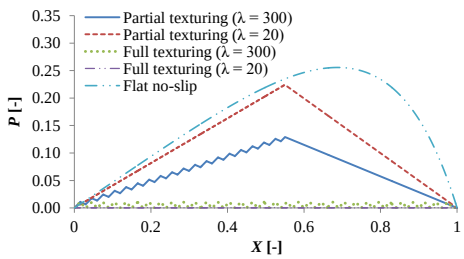

FIGURE 11: *Dimensionless pressure distribution P for several configurations. The textured surfaces are calculated for optimized texturing zone (L_R/L = 0.55).*

4.2.2 Textured/wall slip combination

As explained in the introduction, a slip area can be obtained by treating the surface or applying a coating to obtain a hydrophobic or hydrophilic surface. With these technical approaches, surface energy is controlled. In this section, the combination of the engineered physical roughness (texturing) and slippage with respect to the lubrication is investigated numerically in terms of load support. It is assumed that the boundary slip is employed to all faces of the texture cell (see Fig. 3).

Figure 12 shows the effect of texturing zone L_R and texture aspect ratio λ on the ratio of dimensionless load support W^* of a textured surface to that of a no-slip surface with optimized slope incline ratio (h^* = 2.2), $W^*_{\text{no-slip}}$ for two situations, at first, a solely textured surface and second, a textured surface combined with wall slip condition. For the latter, the dimensionless slip length of 20 is considered. It can be observed that there is a significant increase in load support for the combined textured/slip surface both for low λ and high λ.

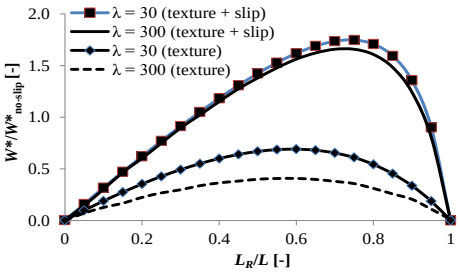

FIGURE 12: *Effect of the texturing zone, L_R and the texture aspect ratio on the dimensionless load support, W^*: of a solely textured surface or of a combined textured/slip surface. $W^*_{no\text{-}slip}$ is evaluated at optimized convergence ratio (h^* = 2.2). For combined textured/slip surface, the A of 20 is assumed.*

From Fig. 12, it can be also seen that there is a shift of the maximum of the dimensionless load support if the slip condition is employed on the textured surface. It means that for improving the load support significantly, besides applying slip on the texture cells, the texturing zone need to be sufficiently extended. The optimal texturing zone combined with slip situation occurs when L_R/L = 0.75. At such texturing zone, the

maximum improvement is 75 % and 66%, respectively for $\lambda = 30$ and $\lambda = 300$. This can be compared with the simple (partially) textured case which is not able to generate more load support for the same texture depth. It indicates that the presence of boundary slip on the texture cells creates a more dominant effect and results in an increase in the load support in textured parallel sliding surfaces.

In order to investigate the effect of the texture cell aspect ratio λ and the dimensionless slip length A for lubricated contacts using texturing combined with slip, computations have been made for this by comparing two cases: partial texturing and full texturing. Figure 13 shows the effect of the texture cell aspect ratio λ and dimensionless slip length A on the ratio of dimensionless load support, W^* of a textured surface to that of a no-slip surface, $W^*_{\text{no-slip}}$. There are three observations which can be made. At first, for all ranges of λ and A, the partially textured configuration is advisable for improving the lubrication performance rather than the full texturing which is similar to the prediction of the no-slip lubrication situation ($W^* = 0$ at parallel sliding surfaces regardless of λ and A). Second, in the absence of the wedge effect, partial texturing produces a mechanism of pressure generation, and thus load support, whose value is higher than the prediction by no-slip surfaces at optimized slope incline ratio ($h^* = 2.2$). Third, from Fig. 13a, in the case of partial texturing pattern with slip, it is found that the increase in texture cell length l_c, and thus λ leads to a decrease in the predicted load support. Also, a reduction is predicted, but for λ greater than 60, the variation on λ has an insignificant effect on the dimensionless load support. If the results are compared with a solely texturing, see Fig. 10, a little reduction in load support is obtained with increasing the λ (only 10%). The opposite trend prevails when the dimensionless slip coefficients are varied. For A lower than 10, the increase in A leads to a large improvement in the load support of the lubricated contact, whereas for A greater than say 10, the variation in A has an insignificant effect on the performance. In conclusion, a well-chosen partially textured configuration with boundary slip leads to a greater improvement in load support, comparing with a simple partially textured surface.

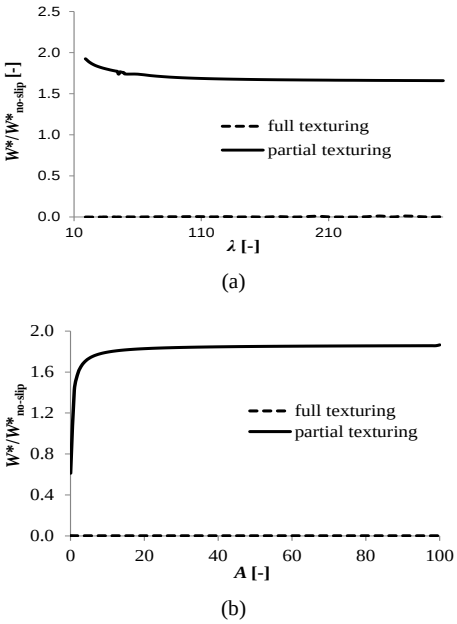

FIGURE 13: *Combined textured /slip surface: (a) Effect of the dimensionless texture cell length λ on the dimensionless load support, $W^*$and (b) Effect of the dimensionless slip length A on the dimensionless load support, W^*. $W^*_{no\text{-}slip}$ is evaluated at optimized convergence ratio ($h^* = 2.2$). W^* for partially textured surface is calculated at optimized texturing zone ($L_R/L = 0.75$).*

Finally, it is necessary to investigate the load support comparison based on the optimization results for various possible surface boundary conditions. In this section, all parameters including the dimensionless slip length A, the texture cell aspect ratio λ, texturing zone L_R and slip zone L_S have been initially optimized based on the previous results as mentioned earlier. Table 4 shows optimized sliding contact configurations of the traditional no-slip contact, the complex slip surface, the solely textured surface, the textured/slip combination pattern.

TABLE 4: *Optimized lubricated contact characteristics.*

Contact type	h^*	L_S	L_R	λ	A	W^*
Flat no-slip	2.2	-	-	-	-	0.1602
Flat slip	1	0.65	-	-	50	0.3297
Texture no-slip	1	-	0.55	20	-	0.1121
Texture + slip	1	0.75	0.75	20	50	0.2964

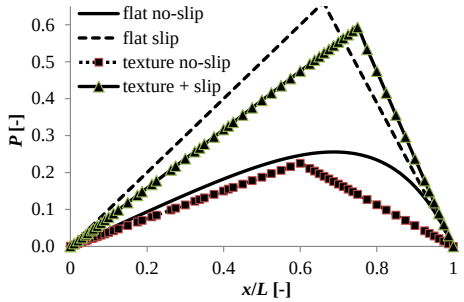

FIGURE 14: *Dimensionless pressure distribution for four conditions: flat traditional (no-slip) surface, flat surface with complex slip, textured no-slip surface, and textured/slip surface. All configurations are calculated based on the optimized values of characteristics as indicated in Table 4.*

As can be seen in Table 4, compared with flat conventional (no-slip) contact for optimized slope incline ratio, the maximum improvement in load support is superior for the flat complex slip surface (100% greater). For the case of partially textured/slip combination pattern, computation predicts a 85% improvement. The partially textured surface (without slip) produces just slightly less load support, $W^* = 0.1121$ which means that the decrease in W^* is present (by 30% lower). On the other words, with respect to the load support, while the (partially) textured surface with boundary slip is superior to the textured surface alone, it is not as effective as the flat configuration with complex slip. It is interesting to note that in a real system, for example, in lubricated-MEMS containing moving surfaces, the fact that the load support can be produced by complex slip surface on perfectly flat surface seems to be a very promising way for designing very high load support lubricated mechanisms. The comparison of the predicted pressure generation is presented in Fig. 14. It is shown that the highest pressure is found for the flat slip surface condition in which the value is approximately three times as large as the maximum pressure obtained from those without slip.

In the point of view of the no-slip case, the prediction shows that the partially textured one is found to have better performance with respect to the load support, and it is comparable with a flat no-slip surface at optimized convergence ratio ($h^* = 2.2$). If parallel sliding surfaces are of particular interest, then it is advisable to partially texturing the inlet of the contact to improve the performance of lubrication in relation to the load support.

5. Conclusion

This paper focused on the possibility of enhancing the hydrodynamic load support of lubricated contacts by engineering a complex slip surface, texturing the surface with and without boundary slip and showing the importance of the critical shear stress. The conclusions based on the analysis presented in this paper are follows:

1. In the case of flat moving surfaces, with the purpose of improvement of the load support, slip at the surfaces in contact must be chosen as a complex slip surface with a slip zone that covers 0.65 of the contact length. The maximum load support with uniform film thickness only can be achieved if the no-slip boundary is applied on the moving surface. Also, particular care must be taken in choosing the surface property, that is, the interface critical shear stress. Reducing the critical shear stress value, to a very low level, that is, close to zero, the complex slip boundary leads to a significant improvement in performance, especially in relation to load support.
2. In the case of textured surfaces, texturing results for both partially and fully textured surfaces give a lower prediction of the load support than the flat surface situation at optimized convergence ratio. However, for the parallel case, texturing, especially with optimized (inlet) partial texturing in which the texturing zone covers 0.55 of the contact length, generates significantly more load support than a flat no-slip surface which cannot generate load support.
3. In the case of a combination of texture and boundary slip, a correct partially textured surface with slip leads to a better improvement in load support, compared to a solely partially textured surface. However, this configuration is still non-advisable for improving the load support: a flat surface with complex slip condition is recommended.

Nomenclatures

h	film thickness
h_i	inlet film thickness
h_o	outlet film thickness
h_D	dimple depth
h_F	land film thickness
h^*	convergence ratio = h_i/h_o
K	relative dimple depth
l_D	dimple length
l_C	texture cell length
L	total length of lubricated surface
L_R	length of textured zone
L_S	length of slip zone
p	fluid film pressure
R_e	Reynolds number
U	sliding velocity
W	load support
z	cross-film coordinate
α_a , α_b	slip coefficient at surface *a* (stationary) and *b* (moving)
ρ	lubricant density
ρ_T	texture density
λ	texture aspect ratio
τ_{ca} , τ_{cb}	critical shear stress at surface *a* and *b*
τ_a , τ_b	shear stress at surface *a* and *b*
η	dynamic viscosity

Dimensionless parameters

$$A = \alpha\eta / h_o$$
$$P = ph_o^2 / \eta LU$$
$$R_e = (\rho U h_o) / \eta$$
$$W^* = Wh_o^2 / (U\eta L^2)$$
$$\tau_c^* = \tau_c h_o / \eta U$$

References

1. Etsion, I. and Halperin, G., 2002, "A laser surface textured hydrostatic mechanical seal," *Tribology Transactions* **45**, pp. 430 – 434.
2. Ryk, G., Kligerman, Y. and Etsion, I., 2002, "Experimental investigation of laser surface texturing for reciprocating automotive components," *Tribology Transactions* **45**, pp. 444 – 449.
3. Etsion, I., Halperin, G., Brizmer, V. and Kligerman, Y., 2004, "Experimental investigation of laser surface textured parallel thrust bearing," *Tribology Letters* **17**, pp. 295 – 300.
4. Kovalchenko, A., Ajayi, O., Erdemir, A., Fenske, G. and Etsion, I., 2005, "The effect of laser surface texturing on transitions in lubrication regimes during unidirectional sliding contact," *Tribology International* **38**, pp. 219 – 225.
5. Arghir, M., Roucou, N., Helene, M. and Frene, J., 2003, "Theoretical analysis of the incompressible laminar flow in a macro-roughness cell," *ASME Journal of Tribology* **125**, pp. 309 – 318.
6. Sahlin, F., Glavatskih, S.B., Almqvist, T. and Larsson, R., 2005, "Two-dimensional CFD-analysis of micro-patterned surfaces in hydrodynamic lubrication," *ASME Journal of Tribology* **127**, pp. 96 – 102.
7. Brajdic-Mitidieri, P., Gosman, A.D., Loannides, E. and Spikes, H.A., 2005, "CFD analysis of a low friction pocketed pad bearing," *ASME Journal of Tribology* **127**, pp. 803 – 812.
8. Dobrica, M.B. and Fillon, M., 2009, "About the validity of Reynolds equation and inertia effects in textured sliders of infinite width," *Proceedings of the Institution of Mechanical Engineers, Part J: Journal of Engineering Tribology* **223**, 69 – 78.
9. Han, J., Fang, L., Sun, J. and Ge, S., 2010, "Hydrodynamic lubrication of microdimple textured surface using three-dimensional CFD," *Tribology Transactions* **53**, pp. 860 – 870.
10. Shi, X. and Ni, T., 2011, "Effects of groove textures on fully lubricated sliding with cavitation," *Tribology International* **44**, pp. 2022 – 2028.
11. Tønder, K., 2011, "Inlet roughness tribodevices: dynamic coefficients and leakage," *Tribology International* **34**, pp. 847 – 852.
12. Brizmer, V., Kligerman, T., Etsion, I., 2003, "A laser surface textured parallel thrust bearing," *Tribology Transactions* **46**, pp. 397 – 403.
13. Kligerman, Y., Etsion, I., Shinkarenko, A., 2005, "Improving tribological performance of piston rings by partial surface texturing,"

ASME Journal of Tribology **127**, pp. 632 – 638.

14. Fowell, M., Olver, A.V., Gosman, A.D., Spikes, H.A. and Pegg, I., 2007, "Entrainment and inlet suction: two mechanisms of hydrodynamic lubrication in textured bearings," *ASME Journal of Tribology* **129**, pp. 337 – 347.
15. Ausas, R., Ragot, P., Leiva, J., Jai, M., Bayada, G. and Buscaglia, G.C., 2007, "The impact of the cavitation model in the analysis of microtextured lubricated journal bearings," *ASME Journal of Tribology* **129**, pp. 868 – 875.
16. Rahmani, R., Shirvani, A. and Shirvani, H., 2007, "Optimization of partially textured parallel thrust bearings with square-shaped micro dimple," *Tribology Transactions* **50**, pp. 401 – 406.
17. Pascovici, M.D., Cicone, T., Fillon, M. and Dobrica, M.B., 2009, "Analytical investigation of a partially textured parallel slider," *Proceedings of the Institution of Mechanical Engineers, Part J: Journal of Engineering Tribology* **223**, pp. 151 – 158.
18. Dobrica, M.B., Fillon, M., Pascovici, M.D. and Cicone, T., 2010, "Optimizing surface texture for hydrodynamic lubricated-contacts using a mass-conserving numerical approach," *Proceedings of the Institution of Mechanical Engineers, Part J: Journal of Engineering Tribology* **224**, pp. 737 – 750.
19. Rahmani, R., Mirzaee, I., Shirvani, A. and Shirvani, H., 2010, "An analytical approach for analysis and optimization of slider bearings with infinite width parallel textures," *Tribology International* **43**, pp. 1551 – 1565.
20. Tala-Ighil, N., Fillon, M. and Maspeyrot, P., 2011, "Effect of texture area on the performances of a hydrodynamic journal bearing," *Tribology International* **44**, pp. 211 – 219.
21. Ma, C. and Zhu, H., 2011, "An optimum design model for textured surface with elliptical-shape dimples under hydrodynamic lubrication," *Tribology International* **44**, pp. 987 – 995.
22. Ma, M. and Hill, R.M., 2006, "Superhydrophobic surfaces," *Current Opinion in Colloid & Interface Science* **11**, pp. 193 – 202.
23. Fortier, A.E., Salant, R.F., 2005, "Numerical analysis of a journal bearing with a heterogeneous slip/no-slip surfaces, " *ASME Journal of Tribology* **127**, pp. 820 – 825.
24. Bayada, G. and Meurisse, M.H., 2009, "Impact of the cavitation model on the theoretical performance of heterogeneous slip/no-slip engineered contacts in hydrodynamic conditions," *Proceedings of the Institution of Mechanical Engineers, Part J: Journal of Engineering Tribology* **223**, pp. 371 – 381.
25. Rao, T.V.V.L.N., 2010, "Analysis of single-grooved slider and journal bearing with partial slip surface," *ASME Journal of Tribology*, pp. 014501-1–014501-7.
26. Aurelian, F., Patrick, M. and Mohamed, H., 2011, "Wall slip effects in (elasto) hydrodynamic journal bearing," *Tribology International* **44**, pp. 868 – 877.
27. Spikes, H.A., 2003, "The half-wetted bearing. Part 1: extended Reynolds equation," *Proceedings of the Institution of Mechanical Engineers, Part J: Journal of Engineering Tribology* **217**, pp. 1 – 14.
28. Spikes, H..A. and Granick, S., 2003, "Equation for slip of simple liquids at smooth solid surfaces," *Langmuir* **19**, pp. 5065 – 5071.
29. Salant, R.F. and Fortier, A.E., 2004, "Numerical analysis of a slider bearing with a heterogeneous slip/no-slip surface," *Tribology Transactions* **47**, pp. 328 – 334.
30. Wu, C.W., Ma, G.J. and Zhou, P., 2006, "Low friction and high load support capacity of slider bearing with a mixed slip surface," *ASME Journal of Tribology* **128**, pp. 904 – 907.
31. Choo, J.H., Glovnea, R.P., Forrest, A.K. and Spikes, H.A., 2007, "A low friction bearing based on liquid slip at the wall," *ASME Journal of Tribology* **129**, pp. 611 – 620.
32. Patankar, SV., 1980, *Numerical Heat Transfer and Fluid Flow*, Taylor & Francis, Levittown.
33. Watanabe, K., Yanuar and Udagawa, H., 1999, "Drag reduction of Newtonian fluid in a circular pipe with a highly water-repellant wall," *Journal of Fluid Mechanics* **381**, pp. 225 – 228.

34. Zhu, Y. and Granick, S., 2002, "Limits of the hydrodynamic no-slip boundary condition," *Physical Review Letters* **88**, pp. 106102–1–4.
35. Zhu, Y. and Granick, S., 2002, "No-slip boundary condition switches to partial slip when fluid contains surfactant," *Langmui*r **18** (26), pp. 10058 – 10063.
36. Granick, S., Zhu, Y. and Lee, H., 2003, "Slippery questions about complex fluids flowing past solids," *Nature Materials* **2**, pp. 221 – 227.
37. Wu, C.W. and Ma, G.J., 2005, "On the boundary slip of fluid flow," *Science in China Ser. G Physics, Mechanics & Astronomy* **48**, pp. 178 – 187.
38. Wu, C.W., Ma, G.J. and Sun, H.S., 2005, "Viscoplastic lubrication analysis in a metal-rolling inlet zone using parametric quadratic programming," *ASME Journal of Tribology* **127**, pp. 605 – 610.
39. Cameron, A., 1966, *The Principles of Lubrication*, Longman Green and Co, Ltd, London.

Paper C

M. Tauviqirrahman, Muchammad, Jamari, D.J. Schipper

Numerical study of the load carrying capacity of lubricated parallel sliding textured surfaces including wall slip

Accepted for publication in STLE Tribology Transactions.

Numerical Study of the Load Carrying Capacity of Lubricated Parallel Sliding Textured Surfaces including Wall Slip

M. Tauviqirrahman,[1,*)] Muchammad,[1)] Jamari,[2)] and D.J. Schipper[1)]

[1]Laboratory for Surface Technology and Tribology,
Faculty of Engineering Technology, University of Twente, The Netherlands
*Email: mtauviq99@gmail.com

[2]Laboratory for Engineering Design and Tribology,
Department of Mechanical Engineering, University of Diponegoro, Indonesia

Accepted for publication in STLE Tribology Transactions, 2013

Abstract **This paper analyzes the combined effect of surface texturing and wall slip on the load carrying capacity of parallel sliding systems. A new modified Reynolds equation with slip is proposed, based on the critical shear stress model, to reveal the hydrodynamic load carrying capacity. A range of parameters such as texturing zone, texture cell aspect ratio, critical shear stress and slip length are analysed. It is shown that the optimal texturing zone length oscillates around 75% of the slider length. A slight shift of the optimized texturing zone towards the inlet of the contact is observed when the critical shear stress is increased. The numerical analysis also shows that there is a unique threshold value of the critical shear stress for every texture cell aspect ratio. When this ratio is increased the threshold value increases thus influencing the slip considerably. Slip has a positive effect on the load carrying capacity for critical shear stress lower than the threshold value, whereas it has no effect on higher values. It is also found, that in comparison with a solely textured surface, the load carrying capacity of the combined textured/wall slip pattern can be increased by around 300% using the optimized slip parameters.**

Keywords: critical shear stress, load carrying capacity, surface texturing, wall slip

1. Introduction

The use of artificial surface texturing has already been a subject of several experimental and theoretical studies. Such a texturing is becoming popular in oil-lubricated devices because of its potential benefits in terms of load carrying capacity and friction. It has been shown that textured surfaces enhance load carrying capacity and reduce hydrodynamic friction in, for instance, systems with two parallel sliding surfaces [1-2], mechanical seals [3], and reciprocating (cylinder-liner) contacts [4].

Numerically, the use of the Reynolds equation and CFD (computational fluid dynamic) analysis based on the Navier-Stokes equation set emerged as two excellent ways of studying lubricant flow behaviour within lubricated textured surfaces. Two texture modes were used: macro-roughness and micro-roughness. The first mode is based on single cell texture configuration [5-8] and the second one is based on multiple cells pattern that provides a collective effect of the texture cells [9].

Full and partial texturing were two extreme cases of the artificial arrangement of textured area on the contact surface. It is worth mentioning the early work of Tonder [10] who analyzed the partial texturing mode by carrying out theoretical studies on the positive effect of a series of dimples or roughness at inlet of a sliding surface. A comparison of partially and fully textured surfaces comprising micro-roughness in parallel thrust bearings was made by Brizmer, *et al*. [11] by employing a numerical approach. They demonstrated that the

micro-dimple effect, which corresponds to full width texturing, is not useful for developing the large load support expected from a hydrodynamically lubricated contact. Subsequently, several studies were published in literatures [12-16] confirming the findings of reference [11]. One conclusion that emerges from these studies is that partial texturing has an advantage over full texturing. In addition, more attention has been paid to optimizing texturing parameters. Various surface texture models (elliptical model, sinusoidal model, rectangular model, cylindrical model, etc) were employed to conclude that the surface texture improves the tribological performance. Efforts were made in several works to establish the optimal texturing parameters such as texture depth, width, number of dimples and the location of dimples that would maximize the load carrying capacity. The aforementioned models and simulation results also provide an excellent set of guidelines for the optimum design of surface texture in some fields.

In most theoretical studies cited above, it was assumed that the lubricated contact was represented by no-slip planes. Doubtless, this assumption simplified the theoretical analysis and was successfully applied to engineering problems to some extent. However, with the continuous progress of the nano measurement techniques during recent years, a nano-scale measurement is possible for the wall slip [17-19]. Molecular dynamics simulations also reveal the occurrence of wall slip [20-21], depending on the roughness and the wettability of the surface. Nowadays, two main theoretical models of wall slip can be found in the literature: the slip length model [22-25] and the critical shear stress model [26-31]. The slip length model assumes that wall slip velocity is proportional to the shear rate at the solid surface and can be described by the following equation:

$$u_s = \beta \ \dot{\gamma}$$

where $\dot{\gamma}$ is the local shear rate, u_s is the slip velocity, and β is the slip length which is defined as the fictive distance beyond the liquid/solid interface at which the liquid velocity extrapolates to zero. At a small wall slip and small range of shear rate, some experimental observations [32-33] fit very closely to the slip length model. However, at high shear rate, some other experimental results [17, 34] show that the slip velocity increases in a strong nonlinear manner with the shear rate, thus wall slip can be described approximately by the critical shear stress model [27]. The critical shear stress model assumes that a critical shear stress, τ_c, exists at the solid/liquid interface. So wall slip takes place only after the surface shear stress exceeds the critical shear stress.

Many works have been dedicated to the study of the random slip influence on the hydrodynamic performance; the conclusion was that wall slip influences the performance of lubricated contact. The random slip in hydrodynamic system may be introduced due to the existence of the critical or limiting wall-shear stress while the wall slip boundary may be random or of an (artificial) deterministic nature. In a micro scale system such as MEMS (Micro-Electro-Mechanical System), the boundary condition of slip or no-slip plays a very important role in determining the fluid flow behaviour. Such a boundary condition allows a degree of control over the hydrodynamic pressure in confined systems and is important in a lubricated sliding contact. How to control wall slip with respect to lubrication was one of the challenging research questions in recent investigations. In addition to surface texturing, the use of an artificial slip surface was introduced deliberately in lubricated sliding contact. In practice, such a surface can be obtained by controlling its surface energy and its roughness to create a distinctive geometrical microstructure or nanostructure of the surface. Micro-structured pattern, which presents textured cells with wall slip conditions, can be made using lithographic techniques, plasma etching or metal assisted etching. This method is then followed by hydrophobic treatment which can be accomplished by techniques such as film or molecule deposition, solution coating or self-assembly of hydrophobic layers [35]. Introducing the concept of an artificial slip zone, several researchers such as Salant and Fortier [28-30] have explored the behaviour of the sliding contact with respect to load carrying capacity. The results of all these investigations show the existence of a lifting force (load carrying capacity), even if there is no wedge effect (two parallel sliding surfaces).

Very few researchers appear to have considered the interplay of surface texture and wall slip effect on lubrication. Bayada and Meurisse [36], using a relatively simple simulation, demonstrated that the pressure distribution induced by deterministic roughness is smaller than that induced by the artificial slip. Rao [37] employed an artificial slip on a stationary surface having a single-groove at a slider and a journal bearing and derived the pressure, the shear stress, stiffness and damping coefficients. The modified Reynolds equation based on the slip length model was solved. The author concluded that the non-dimensional pressure distribution was higher, compared with the conventional bearing. In a recent publication, Fatu *et al*. [38] investigated the influence of wall slip on load carrying capacity and power loss in hydrodynamic fluid bearings. Comparing with the textured bearings, wall slip conditions lead to better power loss improvement and higher carrying capacity. However, in their model the existence of the wall slip by exceeding a critical shear stress was neglected.

In previous works researchers demonstrated that, like artificially created microroughness (surface texturing), an artificial slip surface pattern can significantly improve the tribological performance. In the present paper, such a performance will be characterized not only by the physical surface texturing but also by the chemical modification of the surface (i.e. by adding boundary slip). For this reason the contribution of slip properties (critical shear stress and slip length) on the load carrying capacity at the parallel sliding textured surface is examined. In particular, the investigation is focused on defining which wall slip properties interact with the texture parameter (i.e. texture aspect ratio) with respect to the lubrication performance and how they interact. A modified Reynolds equation for a one-dimensional lubricated sliding contact is established based on the critical shear stress model taking into account of the wall slip of the stationary and moving surface.

2. Modified Reynolds equation

Let us consider a lubricated contact equivalent to a lower plane moving in the *x*-direction with surface velocity *U*, and an upper stationary surface, see Fig. 1. The governing equation in a full hydrodynamic lubrication region can be described by the Reynolds equation. In a one-dimensional case, considering the pressure in the lubricated sliding contact as a function of sliding direction (*x*), the momentum equation is simplified as

$$\frac{\partial^2 u}{\partial z^2} = \frac{1}{\mu}\frac{\partial p}{\partial x} \tag{1}$$

Since the hydrodynamic pressure does not vary through the film thickness, Eq. (1) can be integrated twice to obtain the velocity distribution. In order to obtain the velocity profile, it is necessary to define the velocity boundary conditions at the top and bottom surfaces. In this study the occurrence of slip in the lubricated sliding contact is determined by two criteria. Firstly, slip may occur in those areas where both stationary and moving surfaces have been treated to allow it. Secondly, the shear stress on the surfaces must exceed a critical shear stress value, referred to as τ_{cs} for the stationary surface and τ_{cm} for the moving surface. When both criteria are met the resulting slip velocity is proportional to the difference between the shear stress and the critical value, with proportionality factors referred to as α_s for the stationary surface and α_m for the sliding surface. This means that each of the sliding faces has a unique slip property. The product of the slip coefficient with viscosity, $\alpha\mu$, is commonly named ‘slip length’. The following surface boundary conditions are proposed:

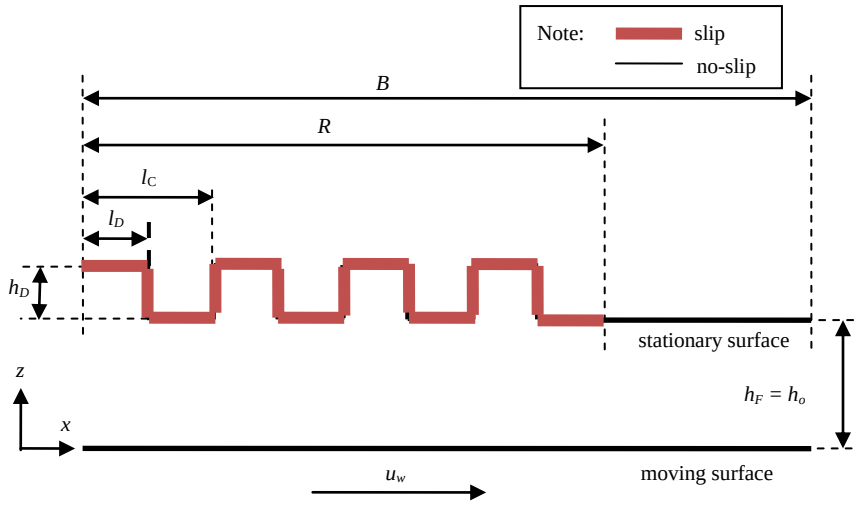

FIGURE 1: *Schematic representation of lubricated parallel sliding contacts with textured configuration combined with wall slip.*

$$\text{at } z = 0 \quad u = U + \alpha_m\left(\mu\frac{\partial u}{\partial z} + \tau_{cm}\right) \quad \text{for } \tau_m \geq \tau_{cm} \quad (2a)$$

$$u = U \quad \text{for } \tau_m < \tau_{cm} \quad (2b)$$

$$\text{at } z = h \quad u = \alpha_s\left(-\mu\frac{\partial u}{\partial z} - \tau_{cs}\right) \quad \text{for } \tau_s \geq \tau_{cs} \quad (2c)$$

$$u = 0 \quad \text{for } \tau_s < \tau_{cs} \quad (2d)$$

It is assumed that the fluid has constant viscosity, is incompressible and laminar, and the inertia effect of the lubricant is small. For the condition in which the shear stress exceeds the critical shear stress at the solid-liquid interface (Eqs. (2a) and (2c)), the corresponding velocity equation can be expressed as follows:

$$u = \frac{1}{2\mu}\frac{\partial p}{\partial x}z^2 - \left(\frac{h}{2\mu}\frac{\partial p}{\partial x}\frac{h+2\alpha_s\mu}{h+\mu(\alpha_s+\alpha_m)} + \frac{U}{h+\mu(\alpha_s+\alpha_m)} + \frac{\alpha_s\tau_{cs}+\alpha_m\tau_{cm}}{h+\mu(\alpha_s+\alpha_m)}\right)z + U\frac{h+\alpha_s\mu}{h+\mu(\alpha_s+\alpha_m)} - \frac{h}{2\mu}\frac{\partial p}{\partial x}\frac{\alpha_m\mu(h+2\alpha_s\mu)}{h+\mu(\alpha_m+\alpha_s)} + \frac{\alpha_m\tau_{cm}(h+\alpha_s\mu)-\alpha_m\alpha_s\mu\tau_{cs}}{h+\mu(\alpha_s+\alpha_m)} \quad (3)$$

The modified Reynolds equation is derived by integrating the continuity equations. Because the fluid density ρ is assumed to be constant across the film, it is convenient to express the continuity equation in integral form as follows [39]:

$$\int_0^h \frac{\partial}{\partial x}udz = -(u)_{z=h}\frac{\partial h}{\partial x} + \frac{\partial}{\partial x}\left(\int_0^h udz\right) = 0 \quad (4)$$

Therefore, the modified form of the one-dimensional Reynolds equation with slip reads:

$$\frac{\partial}{\partial x}\left(h^3\frac{h^2+4h\mu(\alpha_s+\alpha_m)+12\mu^2\alpha_s\alpha_m}{h(h+\mu(\alpha_s+\alpha_m))}\frac{\partial p}{\partial x}\right) = 6\mu U\frac{\partial}{\partial x}\left(\frac{h^2+2h\alpha_s\mu}{h+\mu(\alpha_s+\alpha_m)}\right) - 6\mu\tau_{cs}\frac{\partial}{\partial x}\left(\frac{\alpha_s h(h+2\alpha_m\mu)}{h+\mu(\alpha_s+\alpha_m)}\right) + 6\mu\tau_{cm}\frac{\partial}{\partial x}\left(\frac{\alpha_m h(h+2\alpha_s\mu)}{h+\mu(\alpha_s+\alpha_m)}\right) - 12\mu U\frac{\alpha_s\mu}{h+\mu(\alpha_s+\alpha_m)}\frac{\partial h}{\partial x} + 6h\frac{\partial p}{\partial x}\frac{\partial h}{\partial x}\frac{h\alpha_s\mu+2\alpha_s\alpha_m\mu^2}{h+\mu(\alpha_s+\alpha_m)} + 12\mu\tau_{cs}\left(\frac{\alpha_s(h+\alpha_m\mu)}{h+\mu(\alpha_s+\alpha_m)}\frac{\partial h}{\partial x}\right) - 12\mu\tau_{cm}\left(\frac{\alpha_s\alpha_m\mu}{h+\mu(\alpha_s+\alpha_m)}\frac{\partial h}{\partial x}\right) \quad (5)$$

When wall slip does not occur at both surfaces (stationary and moving surface), the Reynolds equation can be expressed as follows:

$$\frac{\partial}{\partial x}\left(h^3\frac{\partial p}{\partial x}\right) = 6U\mu\frac{\partial h}{\partial x} \quad (6)$$

For Eq. (6), the satisfied condition is when $\tau_m < \tau_{cm}$ and $\tau_s < \tau_{cs}$ as expressed in Eqs. (2b) and (2d). Under this condition, the slip coefficients, αs and αm are set to zero, thereby no-slip takes place.

It should be noted that the present model (Eq. (5)) can generally be used to solve the cases in which (1) the zero or non-zero critical shear stress is present, (2) wall slip occurs either at both surfaces (stationary and moving surface) or at one of the surfaces, and/or (3) no-slip takes place, by setting α_s, α_m, τ_{cs} and τ_{cm} to their specified value according to the appropriate boundary condition of the lubricated sliding contact. It must be pointed out that the modified form of the Reynolds equation presented in Eq. (5) is different from those used in the studies presented previously [28-30, 36-38]. The modified Reynolds equation includes the critical shear stress terms and the possibility of slip that may occur at both surfaces. Based on Eq. (5), it should be noted that if α_s, α_m, τ_{cs} and τ_{cm} are set to zero, the modified Reynolds equation developed becomes the classical Reynolds equation (Eq. (6)).

Figure 1 shows a schematic representation of a lubricated sliding contact with combined surface texturing and slip (texture/slip combination). In the present study, the numerical model is based on multiple dimples (without periodic boundary condition), instead of just a single dimple, allowing the effect of interaction between adjacent dimples on the hydrodynamic load carrying capacity can to be taken into account. Analysis of the combined textured/wall slip contact with uniform film thickness (two parallel surfaces) is of particular interest. An assumption is made that at the inlet and outlet of the domain the pressure is set to be ambient and the cavitation boundary condition is not used. In this study, a rectangular geometry for the texture cell shape is used. The parameter L_R for the non-dimensional texturing zone is introduced and categorized into three kinds of texturing: flat (L_R = 0), partial texturing (L_R < 1) and full texturing (L_R = 1). The texturing zone L_R may consist of a number of texture cells depending on the chosen texture cell aspect ratio. The texture cell can be described by three non-dimensional parameters: the texture density D_T (defined as the ratio between the dimple length l_D and the texture cell length l_C), relative dimple depth V (defined as the ratio between the dimple depth h_D and the land film thickness h_F), and the texture cell aspect ratio λ (defined as the ratio between the dimple length l_D and the dimple depth h_D). For the analysis of a lubricated contact with combined texture/wall slip condition, the slip boundary is employed on all sides of the texture cell (see Fig. 1). In the case of the present study, the lubricated sliding contact is operating under steady state conditions. The load carrying capacity is determined by integrating the calculated hydrodynamic pressure field along the surface contact.

3. Methodology

A numerical solution is required for solving Eq. (5). To this end, the finite difference equations obtained by means of the micro-control volume approach [40] were chosen. For all derivatives the central difference is used except at the boundaries. Appropriate one-sided difference is used at the boundaries.

Once Eq. (5) is solved for the hydrodynamic pressure distribution, the load carrying capacity can be calculated. The modified Reynolds equation is solved using TDMA (tri-diagonal matrix algorithm), [40]. In this study, an iterative procedure is used. Initially the slip coefficient α is set at zero everywhere, and the equations are solved. For textured surfaces where slip is employed, at locations where the critical shear stress is exceeded, the value of α is changed to its specified nonzero value according to the property of the surfaces, while in textured regions where the shear stress is below the critical shear stress, α is set at zero, and the equations are again solved. Iteration continues until the solution converges. It should be noted that the solution convergence is checked to an accuracy tolerance $\omega = 10^{-6}$ where

$$\max\left(\frac{\left|\phi_i^{new} - \phi_i^{old}\right|}{\left|\phi_i^{new}\right|}\right) \le \omega,$$

The iteration is also performed for $\omega = 10^{-7}$ and $\omega = 10^{-8}$, and it turned out that there is hardly any difference in the calculated values (< 0.1%).

To ensure grid independent results the numerical simulations have been conducted for the case of partially textured/wall slip contact having a texture cell aspect ratio λ of 30 and varying the grid numbers N. All conditions are evaluated for non-dimensional texturing zone L_R of 0.65. In this investigation the grid numbers varies from 100 to 8,000. Figure 2 and 3 show the effect of the number of nodes N on the non-dimensional load carrying capacity W^* and varying the non-dimensional slip length A. Analysing Figs. 2 and 3 in parallel one can see that after 4,000 nodes the solution becomes stable and thus produces a grid-independent solution. Therefore, the grid number used for the calculations in the present study is 4,000.

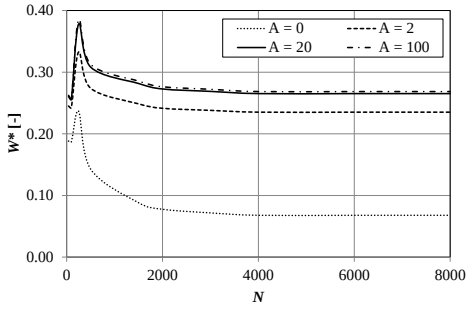

FIGURE 2: *Effect of the number of grid nodes N on the non-dimensional load carrying capacity W^* for different non-dimensional slip lengths A. All profiles are calculated using partial texturing zone (L_R = 0.65) with λ = 30.*

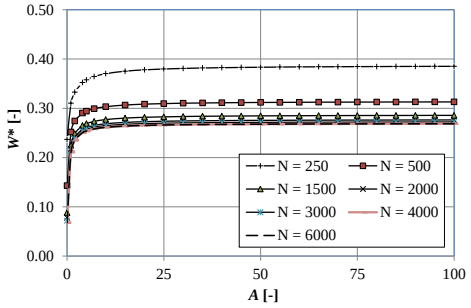

FIGURE 3: *Non-dimensional load carrying capacity W^* as a function of the non-dimensional slip length A for different number of grid nodes N. All profiles are calculated using partial texturing zone (L_R = 0.65) with λ = 30.*

The simulation results are presented in non-dimensional form, i.e. $p^* = ph_F^2 / \mu BU$ for the non-dimensional pressure, $W^* = Wh_F^2 / (U\mu B^2)$ for the non-dimensional load carrying capacity in which W is the load per unit length, $\tau_c^* = \tau_c h_F / \mu U$ for the non-dimensional critical shear stress. The non-dimensional slip length A is determined by normalizing the "slip length" ($\alpha\mu$) with the film thickness h_F.

Surface texturing, as mentioned in the previous section, seems to be a promising way of improving the performance of lubricated sliding contact. At this stage attention is drawn to one important practical design feature: the surface at which the textured/wall slip pattern must be applied so that it can generate more pressure and thus achieve the load carrying capacity.

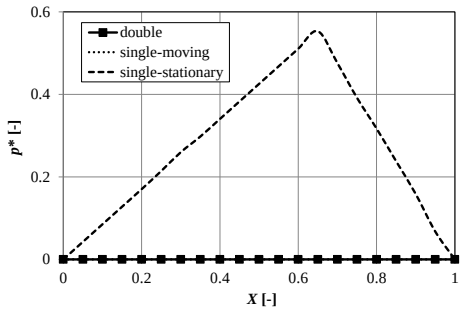

FIGURE 4: *Non-dimensional pressure distribution along the contact surface for parallel moving surfaces with various boundary conditions. All conditions are calculated using partial texturing zone (L_R = 0.65) combined with slip (i.e. zone which covers only a specific zone of the surface) for non-dimensional slip length A = 100 and texture cell aspect ratio λ = 30.*

Figure 4 shows the comparison of the non-dimensional pressure distribution with various boundary conditions on the two parallel surfaces. The term "double" is used for the situation in which the combined textured/wall slip pattern is present on both the stationary and the moving surface, whereas the term of "single-stationary" surface and "single-moving" surface are addressed to the contact situation in which the combined textured/wall slip situation occurs only on the stationary surface and the moving surface, respectively. From Fig. 4, it can be observed that by applying the combined

textured/wall slip pattern only on the stationary surface, pressure is generated and thus load carrying capacity can be achieved. If, however, the combined textured /wall slip pattern is applied to the moving surface, the system has no load carrying capacity and is therefore not of interest for engineering applications from a tribological point of view. Therefore, for all following computations, in order to permit the more generation of the load carrying capacity, the moving surface is designed as a smooth surface with no-slip condition, whereas the stationary surface is designed as textured surface with artificial wall slip. From the point of view of smooth lubricated contacts, this result is comparable with the findings of previous studies [29-30]. Furthermore, it is shown that in order to prevent the system from operating in an unstable manner, the moving surface should be designed as a no-slip surface, while the mixed slip boundary is applied at the stationary surface.

4. Results and discussion

In general, there are two main parameters in the combined textured/wall slip pattern, potentially having a significant effect on the load carrying capacity: firstly, the texture parameters (i.e. texturing zone, texture cell aspect ratio) and secondly the slip parameters (i.e. slip length, critical shear stress). The variations of all these parameters are considered here. Another parameter of the utmost importance is the texture density. However, a parametric study of this parameter is out of the scope of the present paper. This is because, as discussed by Dobrica, *et al*. [15], the maximum texture density will always yield the best results, so the texture cannot be optimized as a function of this parameter.

Various parameters were set up to investigate the effect of the slip parameters and texturing characteristics on the lubrication performance of sliding surfaces with respect to the improvement of the load carrying capacity. The primary parameters of the lubricated sliding contact are given as follows: the total length of lubricated contact B is $20\text{x}10^{-3}$ m, the land film thickness h_F is $1\text{x}10^{-6}$ m, the dynamic viscosity μ is 0.001 Pa.s and it is assumed that the fluid density ρ_l is 1,000 kg/m^3. The range of Reynolds numbers tested is from 0.001 to 20. In the following simulations, the critical shear stresses range from 0-1,000 Pa, reasonable values based on literature [17-18, 41-43] are used, and the slip coefficient α varies from 0 to 0.1 m^{2}s/kg (the corresponding slip length is $1\text{x}10^{-4}$ m) based on the results published in literature [25, 28, 31, 37]. All parameters and the range in which they are varied for all cases investigated in the present study are summarized in Table 1.

TABLE 1. *Simulated parameters list*

Parameter	Data setting	Unit
Slip coefficient α	0 – 0.1	m^{2}s/kg
Critical shear stress τ_c	0 – 1,500	Pa
Reynolds number	0.001 – 20	[-]
Texture density D_T	0.5	[-]
Relative dimple depth V	1	[-]
Dimple aspect ratio λ	30 – 300	[-]

The validity of the Reynolds equation in lubricated contacts with surface texturing was discussed in published literature. The limits of this equation were well established based on [44]. In this study, care has been taken to ensure that the configurations considered here fall within the established Reynolds validity domain. Here, the texture cell aspect ratio λ varies from 20 to 300 and the Reynolds number R_e varies from 0.001 to 20.

4.1. Effect of Texturing Zone

As mentioned in the previous section, partial texturing leads to positive effects. Therefore, in the present study the texture parameter of the non-dimensional texturing zone length L_R is briefly discussed first. In order to determine the optimal value of L_R (equivalent to the best configuration of a parallel textured slider), a parametric study is conducted in which this parameter is varied over a large range of values (0-1) for each slip condition (i.e. several values of non-dimensional critical shear stress τ_c^*). In

previously published work, Salant and Fortier [28] met a numerical instability problem when the critical shear stress is nonzero and therefore concluded that the lubricated contact is an unstable condition in the case of nonzero critical shear stress. The present work is able to obtain stable solutions for any value of the critical shear stress for a one-dimensional sliding contact. A numerical analysis for a two-dimensional sliding contact was also conducted (not presented in this study), and numerical instability problem was not found.

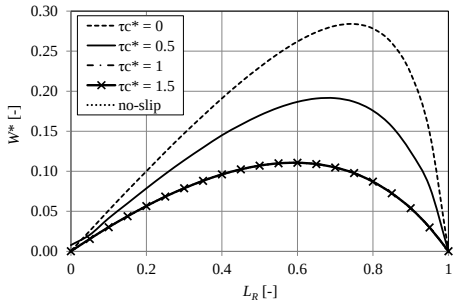

(a)

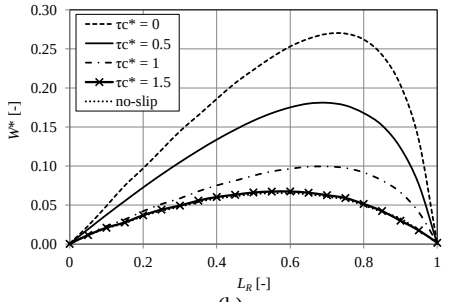

(b)

FIGURE 5: *Effect of the non-dimensional texturing zone L_R on the non-dimensional load carrying capacity W^* for several values of the non-dimensional critical shear stress τ_c^* for (a) λ = 30 and (b) λ = 300. The slip profiles are calculated for A = 100.*

Figure 5 shows the effect of the non-dimensional length of the texturing zone L_R (simulating flat, partial texturing, and full texturing) on the non-dimensional load carrying capacity W^* for several values of non-dimensional critical shear stresses τ_c^*. In this discussion, pure texturing surface (without slip) is also investigated by setting the non-dimensional slip length $A = 0$. It is assumed that the texture density D_T is constant and equal to 0.5, and the relative texture cell depth V is fixed at a value of 1. Thus, the variation of λ is achieved by modifying the dimple length l_C while keeping a constant land film thickness h_F and the dimple depth h_D.

Several specific features can be found based on Fig. 5. Firstly, the load carrying capacity grows and then decreases rapidly as the length of the texturing zone L_R increases. This trend prevails especially when wall slip with low critical shear stress is combined with textured pattern. It is easy to observe that partially textured sliders are superior to fully textured sliders. Full texturing (L_R = 1), as well as no texturing at all (L_R = 0) is unable to generate hydrodynamic lift in parallel sliders. This means that such configurations cause lubrication failure. This result is in a good agreement with recent literature [14-15]. Obviously, as can be seen from Fig. 5, there is an optimum value for non-dimensional texturing zone L_R for each value of τ_c^*, which decreases as τ_c^* increases. It is therefore evident that increasing the τ_c^* would make a shift of the optimum texturing zone towards the leading edge of the contact (left hand side of the curve). This indicates that with respect to the improvement in the load carrying capacity, the texturing zone in the case of combined textured/slip configuration needs to be sufficiently extended. An interesting thing to note is that when λ is increased by a factor of 10, no shift of the optimum value for L_R is found. In other words, this optimum value is practically independent of the texture cell aspect ratio. It can be seen that the optimum non-dimensional (inlet) partially textured length occurs within the interval L_{R_opt} = (0.6, 0.75), depending on the non-dimensional critical shear stress. For example, in the case of combined textured/slip configuration, for both λ considered here, the optimum length of the texturing zone occurs when L_R = 0.60 and 0.75, respectively for very high τ_c^* (i.e. τ_c^* = 1.5) and very low τ_c^*

(i.e. $\tau_c^* = 0$ or perfect slip). In the solely texturing case, the optimum length of the texturing zone L_R of 0.60 is noted. If the length of the texturing zone is higher or lower than these optimum values, the hydrodynamic response goes down abruptly. Secondly, for solely textured surfaces with low λ the prediction of the non-dimensional load carrying capacity is higher than that with high λ. However, the improvement in W^*at textured surfaces with high λ can be obtained more easy by employing slip in the textured zone (up to 270 % for $\tau_c^* = 0$ at the same L_R), see also Fig. 6. One can remark that the presence of engineered wall slip on textured surface expecially with low τ_c^* creates a significant effect on increasing the load carrying capacity in textured parallel sliding surfaces. Thirdly, employing the wall slip with high τ_c^* (for example $\tau_c^* > 1$) on a textured surface having low λ (in this case λ = 30) is less beneficial because the load carrying capacity is less sensitive to the slip. Under such conditions, few or no improvements are obtained: the solutions of the combined textured/wall slip pattern are similar to the pure texturing for the whole range of L_R. Thus, the use of combined textured/slip configuration with very low τ_c^* is recommended. However, textured surfaces with high λ (i.e. λ = 300) show a different trend, namely that combining slip on a textured surface for high τ_c^* (in the case $\tau_c^* = 1$) still increases W^* significantly (43 % for λ = 300 for the same L_R). Compared with a pure texturing case, the case $\tau_c^* = 0$, which corresponds to perfect slip, produces a significant improvement in W^* (up to 250 % for same L_R). Only for the case τ_c^* = 1.5 does it appear that adding slip to the textured surface is ineffective in generating more hydrodynamic load carrying capacity in the contact. This indicates that in relation to a combined textured/slip pattern there are unique thresholds of τ_c^* for every λ. These thresholds are explored in the following section. In general the partially textured surface combined with slip boundary, especially for low τ_c^*, is more effective than the solely textured one with respect to the tribological performance of lubricated contact.

4.2. Effect of Texture Cell Aspect Ratio

In the case of a parallel sliding surface, in order to improve the hydrodynamic effect, it is accepted that the most important process of surface texture design is to maximize the additional hydrodynamic pressure and thus increase the load carrying capacity. For traditional (flat, no-slip) parallel contact, no load carrying capacity takes place. In the textured surfaces, in addition to the texturing zone, it is believed that the texture cell aspect ratio can affect the hydrodynamic performance of lubricated sliding contact. Therefore, in this section in order to investigate the effect of texture aspect ratio λ, computations have been conducted by comparing several conditions, that is, different critical shear stress and slip length. The plotted results have been selected for the case L_{R_opt} = 0.75, a reasonable value of optimum partial texturing zone as described in the previous section.

Figure 6 shows an in-depth analysis of the effect of texture cell aspect ratio λ on the non-dimensional load carrying capacity W^* for various τ_c^* and A. Two observations can be made based on Fig. 6 (a) and (b). Firstly, in the case of the partial texturing with the optimized texturing zone (L_R = 0.75), increasing the texture cell aspect ratio shows a reduction in the load carrying capacity, while increasing the texture cell aspect ratio by more than a specified number would not make any variations in that performance. As can be seen, an increase in the texture aspect ratio from 20 to 70 gives a reduction in the non-dimensional load carrying capacity both for A = 2 and for A = 100. However, after λ reaches 70, the load carrying capacity is barely influenced by a further increase in the value of the λ. This condition also prevails in the case of a solely textured surface. It should be noted that the discrepancy in the load carrying capacity of the solely textured surface predicted by high λ (in this case λ = 300) is around 33% lower than that by low λ (i.e λ = 30), whereas for the case of combined textured/slip configuration with perfect slip (i.e.

τ_c^* = 0), the discrepency is just about 6%. This is to say that the load carrying capacity of the combined textured/slip pattern is weakly dependent on the texture aspect ratio. From Fig. 6, it is also shown that for the combined textured/slip pattern with a high non-dimensional critical shear stress (i.e. τ_c^* = 1.5), slip does not influence the load carrying capacity W^* very much. Such a pattern behaves similarly with a solely texturing surface (no-slip condition) for the whole of λ. Therefore, again, making (inlet) partial texturing on a surface combined with a slip property having very low τ_c^* (close to zero) will be very beneficial to the load carrying capacity.

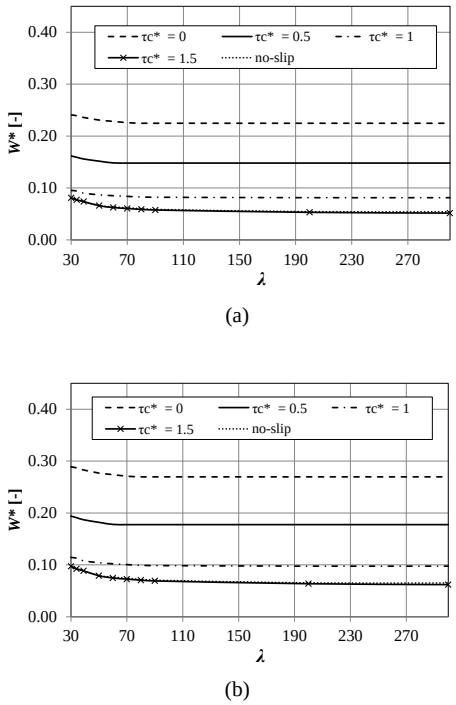

(a)

(b)

FIGURE 6: *Effect of the texture cell aspect ratio λ on the non-dimensional load carrying capacity W^* for several values of the non-dimensional critical shear stress τ_c^* calculated at a non-dimensional texturing zone L_R = 0.75 for (a) A = 2 and (b) A = 100.*

Secondly, with respect to the non-dimensional slip length *A*, combining slip at a textured surface with high *A* is more pronounced than with low *A*. For example, in the case of textured/wall slip configuration with a low slip length (*A* = 2), the prediction of W^* is 0.225 for λ = 300 and τ_c^* = 0. This can be compared to the one with a high slip length (*A* = 100) which predicts W^* of 0.269, that is about 16% higher for the same situation. However, it should be noted that the beneficial effect of the use of high slip length in the combined textured/slip pattern is only for a particular case, i.e. the case for a slip property with low τ_c^* (τ_c^* < 1). The non-dimensional load carrying capacity W^* predicted by combined textured/slip pattern with τ_c^* > 1, whatever the value of *A*, is the same for the whole of λ.

4.3. Effect of Slip Length

Numerous works have shown that a chemical treatment of the surface generates a slip length in the order of 1 μm [47], whereas a longer slip length up to 100 μm can be obtained through a combination of a hydrophobic material with an deterministic rough structure [25, 31, 48]. It is usually postulated that a large value of slip length implies greater slip. Therefore, the effect of wettability (represented by the slip length in this case) is also of particular interest. In the present study, the slip length of a hydrophobic textured surface is assumed as uniform in space. In order to investigate the effect of the non-dimensional slip length *A* for lubricated contacts using texturing combined with slip, computations have been made using an optimized non-dimensional texturing zone (L_R = 0.75) by comparing two conditions: low and high λ and displayed in Fig. 7(a) and (b).

As can be seen in Fig. 7, at a low non-dimensional critical shear stress $\left(\tau_c^* < 1\right)$ for non-dimensional slip lengths *A* lower than – for example – 10, the increase of *A* leads to a large improvement in the non-dimensional load carrying capacity of the lubricated contact, whereas for *A* greater than 10, the variation in *A* has an insignificant effect on the performance.

This trend prevails for two values of λ (in this case, for λ = 30 and 300). However, when τ_c^* is increased to 1.5, the benefit of employing slip on the textured surface will vanish for the texturing both with low λ (i.e. λ = 30) and with high λ (i.e. λ = 300), which is similar to the prediction of the no-slip (pure texturing) lubrication situation. It is interesting to observe that the optimal values of the non-dimensional slip length A are noted. These values are identical for the texturing both with λ = 30 and λ = 300. So, a A of 10 can be considered as an optimal value for inducing the (perfect) slip effect on a textured surface for all values of λ considered here.

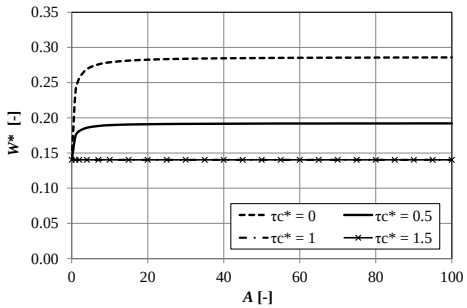

(a)

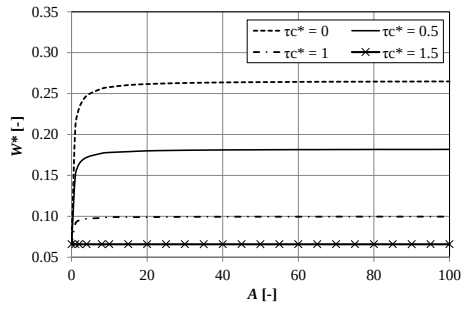

(b)

FIGURE 7: *Effect of the non-dimensional slip length A on the non-dimensional load carrying capacity W^* for several values of the non-dimensional critical shear stress τ_c^* calculated at a non-dimensional texturing zone L_R = 0.75 for (a) λ = 30 and (b) λ = 300.*

From Fig. 7, it is also shown that for λ = 30, employing slip with τ_c^* = 1 on a textured surface has no effect on the performance. But for a combined textured/slip surface with high λ and adding slip using the same τ_c^* (i.e. τ_c^* = 1), an improvement in W^* can still be obtained for the whole range of A (up to 50% for A > 20). Again, it indicates that there is a threshold value of the non-dimensional critical shear stress which is unique for every λ as mentioned before.

In relation to the slip property, in the case of (inlet) partial texturing pattern with slip, it is found that by setting the τ_c^* to zero the highest W^* can be achieved for the whole range of A. The predicted load carrying capacity enhancement is in some cases spectacular, especially for the high texture cell aspect ratio case. In the study considered here, in the case of combined textured/wall slip pattern having λ = 300, the maximum improvement in W^* is up to 300% calculated for τ_c^* = 0 and A = 20 or larger. For a textured surface with low λ (i.e. λ = 30), computation predicts a mere 100% improvement for the same τ_c^* and A. It indicates that if attention is paid to the textured surface having high λ, employing artificial wall slip with high A and low τ_c^* is very advisable for improving the load carrying capacity. This result is consistent with what was described in the previous section.

4.4. Effect of Critical Shear Stress

Critical shear stress is a main parameter in the numerical computation of slip boundary. The critical shear stress model adopted in the present study assumes that wall slip occurs only after the surface shear stress reaches the critical shear stress. The focus of this section is to show the importance of the critical shear stress choice for contacts with a textured surface combined with wall slip boundary. It will be shown that the slip property on combined textured/wall slip pattern must be chosen with care, because an inappropriate choice can lead to a decrease in the load carrying capacity. The influence of wall slip will be investigated for a textured surface by varying the critical shear stress. In the

calculations the (inlet) partial texturing surface at the optimized non-dimensional texturing zone (L_R = 0.75) is used. This because, as discussed earlier, it is known that a (inlet) partially textured surface is superior to both a fully textured surface as well as a flat surface (no texturing at all) with respect to load carrying capacity.

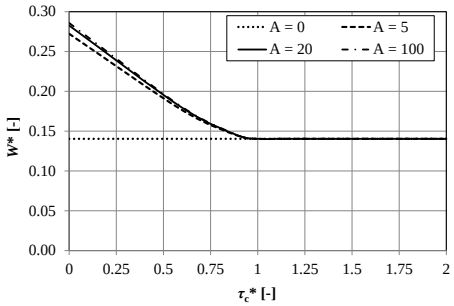

(a)

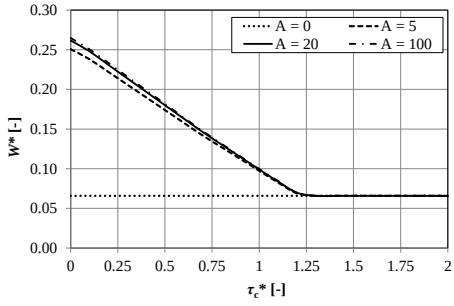

(b)

FIGURE 8: *Effect of the non-dimensional critical shear stress τ_c^* on the non-dimensional load carrying capacity W^* calculated at non-dimensional texturing zone L_R = 0.75 for different non-dimensional slip length values A for (a) λ = 30 and (b) λ = 300.*

Figure 8 shows the effect of the non-dimensional critical shear stress τ_c^* on the non-dimensional load carrying capacity W^* for different non-dimensional slip lengths A for (a) λ = 30 and (b) λ = 300. It can be found that combining slip on a textured surface is much more effective than without slip (i.e. pure texturing), and most effective when the critical shear stress is zero for both low λ and high λ. For optimized non-dimensional textured zone (L_R = 0.75), hydrodynamic load carrying capacity of the textured pattern combined with perfect slip results in an increase of a factor of 2 and 4, respectively for λ = 30 and λ = 300, greater than that predicted by the solely textured pattern. From Fig. 8 it can be seen that the non-dimensional hydrodynamic load carrying capacity decreases as the non-dimensional critical shear stress τ_c^* increases. However, as explained in the previous section, there will be a limit of τ_c^* after which an increase in τ_c^* will have no influence on W^*. It means that the combined textured/slip pattern will behave like a solely textured surface if the non-dimensional critical shear stress is higher than the threshold, otherwise the load carrying capacity may improve significantly until the perfect slip condition is achieved. It can also be seen based on Fig. 8 that for a combined textured/slip surface with λ = 30 and λ = 300, these threshold values are about 0.9 and 1.3 respectively. It is very interesting to note that the effect of A on the threshold of τ_c^* is rarely found either where λ = 30 or where λ = 300. For all values of A considered, the threshold refers to the same point. In addition, the difference in the prediction of W^* will decrease linearly with increasing τ_c^* until the threshold of τ_c^* is reached. On the other hand, from Fig. 8, if the variation of texture cell aspect ratio is considered, it is obvious that there is a clear shift for the threshold of τ_c^*, which directly results in a decrease in W^*. The larger the texture aspect ratio, the larger the threshold of τ_c^*. It can be said that the threshold of τ_c^* is affected only by λ. Moreover, to strengthen this result, the effect of the non-dimensional critical shear stress τ_c^* on the non-dimensional load carrying capacity W^* for a different texture cell aspect ratio λ is shown in Fig. 9. As expected, there is a shift of the threshold of τ_c^* with the increase of λ. For λ = 30, the threshold of τ_c^* occurs at τ_c^* = 0.9, while for λ = 100 the threshold of τ_c^* occurs somewhere between τ_c^* = 1.2 and τ_c^* = 1.3

which nearly coincides with the corresponding τ_c^* of λ = 300. This is also consistent with the results presented in Fig. 6: when λ is larger than around 70, the variation of λ will have very little effect on W^*. Based on Fig. 9, it may be concluded that for τ_c^* = 1, the textured/slip pattern with low λ (i.e. λ = 30 in this case) behaves like a solely textured surface. However, when λ is increased by a factor of 10, wall slip still has a significant effect on the increase in the load support (38 % higher than pure texturing). Generally speaking, for the same value of the critical shear stress, wall slip may or may not occur depending on the characteristics of the surface texturing (represented by texture aspect ratio λ in this case).

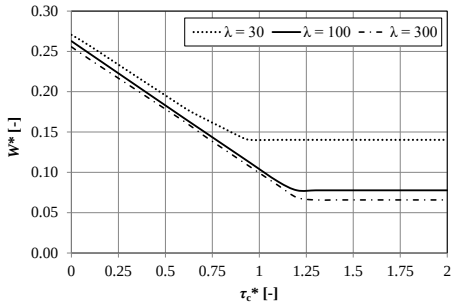

FIGURE 9: *Effect of the non-dimensional critical shear stress τ_c^* on the non-dimensional load carrying capacity W^* for different texture cell aspect ratios λ. All profiles are evaluated for A = 100.*

The critical shear stress was found to depend on surface wettability, surface roughness, fluid viscosity, etc. The wettability (sometimes quoted as hydrophobicity) is a critical surface property for materials or devices in micro-applications. The surface wettabilty is generally presented in terms of a slip length, which quantifies the extent to which the fluid elements near the wall are affected by corrugation of the surface energy [45]. As is well-known, the roughness effect on the critical shear stress is not so clear. Some researchers [17, 32, 44] reported that surface roughness inhibits wall slip or increases the critical shear stress, but others [46] reported that it increases wall slip. In this section, through numerical simulation, it is shown that in the case of the deterministic roughness combined with artificial slip, the threshold value of the critical shear stress depends in practice on physical roughness (i.e. texture parameter) instead of chemical roughness (i.e. slip length). This finding may bring us a new idea for controlling such stress to obtain an expected performance in both the scientific research and engineering design for microfluidics and MEMS-based devices.

4.5. Effect of Reynolds Number

The interest in varying the Reynolds number ($R_e = \rho U h_F / \mu$) is quite clear due to the practical applications of combined textured/slip may function at various Reynolds numbers. In the present work, the variation of R_e was made by dividing the sliding velocity while multiplying the viscosity by the same factor. In this way the factor μU which is part of the non-dimensional pressure factor $\left(p^* = p h_F^2 / \mu U l_c\right)$ was kept constant. The lubricant density ρ was also kept constant. The range of R_e values considered in the simulations varies from 0.001 to 20: values that are in the domain of validity of the Reynolds equation as demonstrated in [44]. However, for such range of R_e, the texture cell aspect ratio λ which can be chosen covers a large range, i.e. as long as λ is greater than 20.

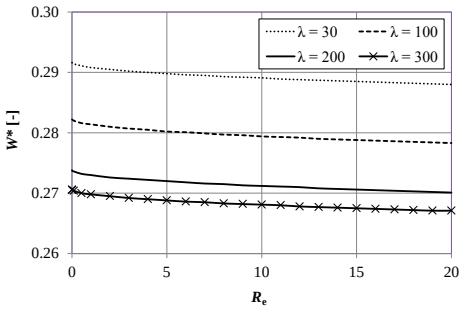

FIGURE 10: *Effect of the Reynolds number Re on the non-dimensional load carrying capacity W* for several values of the texture cell aspect ratio λ. All profiles are calculated for non-dimensional texturing zone L_R = 0.75, non-dimensional critical shear stress τ_c^* = 0 and non-dimensional slip length A = 100.*

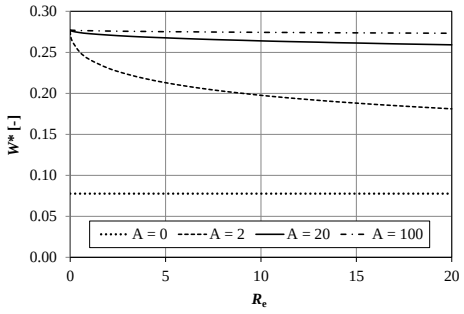

FIGURE 11: *Effect of Reynolds number R_e on the non-dimensional load carrying capacity W* for several values of non-dimensional slip lengths A. All profiles are calculated for a texturing zone $L_R = 0.75$, non-dimensional critical shear stress $\tau_C^* = 0$ and texture cell aspect ratio $\lambda = 100$.*

Figures 10 and 11 show the effect of the Reynolds number on the non-dimensional load carrying capacity by varying the texture cell aspect ratio and non-dimensional slip length respectively. All conditions are evaluated using a partially textured surface. As can be seen in Fig. 10, the load carrying capacity decreases as R_e increases for all λ values. A loss in the overall hydrodynamic load carrying capacity can be observed. The same trend (reduction in W^*) can be found in Fig. 11. Looking at the non-dimensional slip length, for high A values (in this case $A = 20$ and 100) the non-dimensional load carrying capacity W^* is not very sensitive to the increase of R_e. Contrary to the results for high A, the W^* predicted for low A (i.e. $A = 2$) turns out to be sensitive to R_e, especially to the range of R_e that is less than 4. In the case of pure texturing ($A = 0$), as expected, the non-dimensional load carrying capacity seems to show negligible variation for the whole range of R_e values considered. Generally speaking, adding wall slip to a textured pattern has a very positive effect on the load carrying capacity for the range of Reynolds numbers considered here. It should be noted that because *Re* is relatively small, the combined textured/wall slip pattern can be a very promising way to enhance the performance of liquid lubricated MEMS.

5. Conclusions

A hydrodynamic lubrication model for a textured surface combined with wall slip was proposed, and it was shown that the combined textured/wall slip pattern can give many advanced properties compared with solely textured contact (without slip). A parametric analysis with respect to the texturing zone, texture cell aspect ratio, slip length, and critical shear stress was performed in order to find optimum parameters for maximum load carrying capacity. The following conclusions summarize the results of the present study:

1. Partial texturing is much more effective than flat (no-texturing) surface as well as full texturing with respect to the load carrying capacity. Adding the slip to a textured surface is preferable.
2. The greatest improvement of the load carrying capacity is observed when the configuration of the combined textured/slip pattern having low texture cell aspect ratio, low critical shear stress and high slip length is employed. Compared with solely textured contact, the predicted maximum improvement is around 300% using optimized slip parameters.
3. The load carrying capacity of the lubrication film on combined textured/slip pattern decreases with the increase of the Reynolds number. However, for high A the load carrying capacity generation with the increase in R_e is not very sensitive.
4. The most significant finding is that there is are threshold values of the non-dimensional critical shear stress that depend on the texture cell aspect ratio. Larger texture cell aspect ratio, the larger the corresponding threshold value becomes. If the non-dimensional critical shear stress at the interface is higher than the threshold, adding slip will have no influence. This finding guide a new way to control the interfacial critical shear stress and surface (deterministic) roughness.

Nomenclature

D_T	texture density, l_D / l_C
h	film thickness
h_i	inlet film thickness
h_o	outlet film thickness
h_D	dimple depth
h_F	land film thickness
l_D	dimple length
l_C	cell length
B	slider length
T_R	textured zone length
p	fluid film pressure
R_e	Reynolds number, $(\rho_l U h_F) / \mu$
U	sliding velocity
V	relative dimple depth, h_D / h_F
W	load carrying capacity
z	cross-film coordinate
α_s , α_m	slip coefficient at surface *s* (stationary) and *m* (moving)
ρ_l	lubricant density
λ	texture cell aspect ratio
τ_{cs} , τ_{cm}	critical shear stress at surface *s* and *m*
τ_s , τ_m	shear stress at surface *a* and *b*
μ	dynamic viscosity

Non-dimensional parameters

$$A = \alpha\mu / h_o$$

$$L_R = T_R / B$$

$$p^* = p h_F^2 / \mu B U$$

$$W^* = W h_F^2 / (U \mu B^2)$$

$$\tau_c^* = \tau_c h_F / \mu U$$

References

1. Etsion, I., Halperin, G., Brizmer, V. and Kligerman, Y., 2004, "Experimental investigation of laser surface textured parallel thrust bearing," *Tribology Letters* **17**, pp. 295 – 300.
2. Kovalchenko, A., Ajayi, O., Erdemir, A., Fenske, G. and Etsion, I., 2005, "The effect of laser surface texturing on transitions in lubrication regimes during unidirectional sliding contact," *Tribology International* **38**, pp. 219 – 225.
3. Etsion, I. and Halperin, G., 2002, "A laser surface textured hydrostatic mechanical seal," *Tribology Transactions* **45**, pp. 430 – 434.
4. Ryk, G., Kligerman, Y. and Etsion, I., 2002, "Experimental investigation of laser surface texturing for reciprocating automotive components," *Tribology Transactions* **45**, pp. 444 – 449.
5. Arghir, M., Roucou, N., Helene, M. and Frene, J., 2003, "Theoretical analysis of the incompressible laminar flow in a macro-roughness cell," *ASME Journal of Tribology* **125**, pp. 309 – 318.
6. Sahlin, F., Glavatskih, S.B., Almqvist, T. and Larsson, R., 2005, "Two-dimensional CFD-analysis of micro-patterned surfaces in hydrodynamic lubrication," *ASME Journal of Tribology* **127**, pp. 96 – 102.
7. Han, J., Fang, L., Sun, J. and Ge, S., 2010, "Hydrodynamic lubrication of microdimple textured surface using three-dimensional CFD," *Tribology Transactions* **53**, pp. 860 – 870.
8. Ma, C. and Zhu, H., 2011, "An optimum design model for textured surface with elliptical-shape dimples under hydrodynamic lubrication," *Tribology International* **44**, pp. 987-995.
9. Kligerman, Y., Etsion, I. and Shinkarenko, A., 2005, "Improving tribological performance of piston rings by partial surface texturing," *ASME Journal of Tribology* **127**, pp. 632 – 638.
10. Tønder, K., 2011, "Inlet roughness tribodevices: dynamic coefficients and leakage," *Tribology International* **34**, pp. 847 – 852.
11. Brizmer, V., Kligerman, T. and Etsion, I., 2003, "A laser surface textured parallel thrust bearing," *Tribology Transactions* **46**, pp. 397 – 403.
12. Rahmani, R., Shirvani, A. and Shirvani, H., 2007, "Optimization of partially textured parallel thrust bearings with square-shaped micro dimple," *Tribology Transactions* **50**, pp. 401 – 406.
13. Rahmani, R., Mirzaee, I., Shirvani, A. and Shirvani, H., 2010, "An analytical approach for analysis and optimization of slider bearings with infinite width parallel textures," *Tribology International* **43**, pp. 1551 – 1565.

14. Pascovici, M.D., Cicone, T., Fillon, M. and Dobrica, M.B., 2009, "Analytical investigation of a partially textured parallel slider," *Proceedings of the Institution of Mechanical Engineers, Part J: Journal of Engineering Tribology* **223**, pp. 151 – 158.
15. Dobrica, M.B., Fillon, M., Pascovici, M.D. and Cicone, T., 2010, "Optimizing surface texture for hydrodynamic lubricated-contacts using a mass-conserving numerical approach," *Proceedings of the Institution of Mechanical Engineers, Part J: Journal of Engineering Tribology* **224**, pp. 737 – 750.
16. Tala-Ighil, N., Fillon, M. and Maspeyrot, P., 2011, "Effect of texture area on the performances of a hydrodynamic journal bearing," *Tribology International* **44**, pp. 211 – 219.
17. Zhu, Y. and Granick, S., 2002, "Limits of the hydrodynamic no-slip boundary condition," *Physical Review Letters* **88**, pp. 106102–1 – 4.
18. Zhu, Y. and Granick, S., 2002, "No-slip boundary condition switches to partial slip when fluid contains surfactant," *Langmui*r **18** (26), pp. 10058 – 10063.
19. Bonaccurso, E., Kappl, M. and Butt, H.J., 2002, "Hydrodynamic force measurement: boundary slip of water on hydrophilic surfaces and electrokinetic effects, " *Physical Review Letters* **88**, 076103–1-076103 – 4.
20. Barrat, J.L. and Bocquet, L., 1999, "Large slip effect at a nonwetting fluid-solid interface," *Physical Review Letters* **8**2(23), pp. 4671 – 4674.
21. Jabbarzadeh, A., Atkinson, J.D. and Tanner, R.I., 1999, "Wall slip in the molecular dynamics simulation of thin films of hexadecane," *Journal of Chemical Physics* **110**(5), pp. 2612 – 2620.
22. Navier, C.L.M.H., 1823, "Mémoire sur les lois du Mouvement des Fluides, " Memoires de l'Académie Royale des Sciences de l'Institut de France **1**, pp. 414 – 416.
23. Maxwell, J.C., 1879, "On stresses in rarified gases arising from inequalities of temperature," *Philosophical transactions of the Royal Society of London* **170**, pp. 231 – 256.
24. Pit, R., Hervet, H. and Leger L., 1999, "Friction and slip of a simple liquid at a solid surface," *Tribology Letters* **7**, pp. 147 – 152.
25. Watanabe, K., Yanuar and Udagawa, H., 1999, "Drag reduction of Newtonian fluid in a circular pipe with a highly water-repellant wall," *Journal of Fluid Mechanics* **381**, pp. 225 – 228.
26. Spikes, H.A., 2003, "The half-wetted bearing. Part 1: Extended Reynolds equation," *Proceedings of the Institution of Mechanical Engineers, Part J: Journal of Engineering Tribology* **217**, 1 – 14.
27. Spikes, H.A. and Granick, S., 2003, "Equation for slip of simple liquid at smooth solid surfaces," *Langmuir* **19**, pp. 5065 – 5071.
28. Salant, R.F. and Fortier, A.E., 2004, "Numerical analysis of a slider bearing with a heterogeneous slip/no-slip surface," *Tribology Transactions* **47**, pp. 328 – 334.
29. Wu, C.W., Ma, G.J. and Zhou, P., 2006, "Low friction and high load support capacity of slider bearing with a mixed slip surface," *ASME Journal of Tribology* **128**, pp. 904 – 907.
30. Ma, G.J., Wu, C.W. and Zhou, Z., 2007, "Wall slip and hydrodynamics of two-dimensional journal bearing," *Tribology International* **40**, pp. 1056 – 1066.
31. Choo, J.H., Glovnea, R.P., Forrest, A.K. and Spikes, H.A., 2007, "A low friction bearing based on liquid slip at the wall," *ASME Journal of Tribology* **129**, pp. 611 – 620.
32. Pit, R., Hervet, H. and Leger L., 2000, "Direct experimental evidence of slip in hexadecane: solid interfaces," *Physical Review Letters* **85**, 5, pp. 980 – 983.
33. Baudry, J. and Charlaix, E., 2001, "Experimental evidence for a large slip effect at a nonwetting fluid-solid interface," *Langmuir* **17**, pp. 5232 – 5236.
34. Craig, V.S.J., Neto, C. and Williams, D.R.M. (2001), "Shear-Dependent Boundary Slip in an Aqueous Newtonian Liquid," Phys. Rev. Lett. **87**, 054504.
35. Xiu, Y., 2008, *Fabrication of Surface Micro-and Nanostructures for Superhydrophobic Surfaces in Electric and Electronic Applications*, PhD thesis, Georgia Institute of Technology, Atlanta, GA.
36. Bayada, G. and Meurisse, M.H., 2009, "Impact of the cavitation model on the theoretical performance of heterogeneous

slip/no-slip engineered contacts in hydrodynamic conditions," *Proceedings of the Institution of Mechanical Engineers, Part J: Journal of Engineering Tribology* **223**, pp. 371 – 381.
37. Rao, T.V.V.L.N., 2010, "Analysis of single-grooved slider and journal bearing with partial slip surface," *ASME Journal of Tribology*, pp. 014501-1–014501-7.
38. Fatu, A., Maspeyrot, P. and Hajjam, M., 2011, "Wall slip effects in (elasto) hydrodynamic journal bearing," *Tribology International* **44**, pp. 868 – 877.
39. Hamrock, B.J., Schmid, S.R. and Jacobson, B., 2004, *Fundamental of Ftuid Film Lubrication*: *Second Edition*, Marcel Dekker, Inc.
40. Patankar, S.V., 1980, *Numerical Heat Transfer and Fluid Flow*, Taylor & Francis, Levittown.
41. Granick, S., Zhu, Y. and Lee, H., 2003, "Slippery questions about complex fluids flowing past solids," *Nature Materials* **2**, pp. 221 – 227.
42. Wu, C.W. and Ma, G.J., 2005, "On the boundary slip of fluid flow," *Science in China Ser. G Physics, Mechanics & Astronomy* **48**, pp. 178 – 187.
43. Wu, C.W., Ma, G.J. and Sun, H.S., 2005, "Viscoplastic lubrication analysis in a metal-rolling inlet zone using parametric quadratic programming," *ASME Journal of Tribology* **127**, pp. 605 – 610.
44. Dobrica, M.B. and Fillon, M., 2009, "About the validity of Reynolds equation and inertia effects in textured sliders of infinite width," *Proceedings of the Institution of Mechanical Engineers, Part J: Journal of Engineering Tribology* **223**, pp. 69 – 78.
45. Thompson, P.A. and Troian SM., 1997, "A general boundary condition for liquid flow at solid surfaces," *Nature* **389**, pp. 360 – 362.
46. Bonaccurso, E., Butt, H.J. and Craig, V.S.J., 2003, "Surface roughness and hydrodynamic boundary slip of a newtonian fluid in a completely wetting system," *Physical Review Letters* **90**, 14, 144501.
47. Tretheway, D.C. and Meinhart, C.D., 2002, "Apparent fluid slip at hydrophobic microchannel walls," *Physics of Fluids* **14,** L9-12.
48. Ou, J., Perot, B. and Rothstein, J.P., 2004, "Laminar drag reduction in microchannels using ultrahydrophobic surfaces," *Physics of Fluids* **16**, 4635.

Paper D

M. Tauviqirrahman, R. Ismail, Jamari, D.J. Schipper, 2013

Computational analysis of the lubricated sliding contact with artificial slip boundary

International Journal of Applied Mathematics and Statistics,
Volume 35, Issue 5, pp. 67 – 80.

Computational Analysis of the Lubricated-Sliding Contact with Artificial Slip Boundary

M. Tauviqirrahman,[1,*)] R. Ismail,[1)] Jamari,[2)] and D.J. Schipper[1)]

[1]Laboratory for Surface Technology and Tribology,
Faculty of Engineering Technology, University of Twente, The Netherlands
*Email: mtauviq99@gmail.com

[2]Laboratory for Engineering Design and Tribology,
Department of Mechanical Engineering, University of Diponegoro, Indonesia

International Journal of Applied Mathematics and Statistics, 2013, Volume 35, Issue 5

Abstract **The hydrodynamic lubrication performance (load support, friction force, friction coefficient, and volume flow) at lubricated sliding contact is influenced by boundary condition. In the present paper, the effect of artificial slip boundary on the sliding surfaces is explored based on modified Reynolds equation using computational analysis. A design idea for an infinite sliding contact with the optimized artificial slip area is proposed. It is found that the generation of the artificial slip at the leading edge on the stationary surface of the contact gives the highest load support, which is helpful to improve the operation stability of the system. Optimization of the size of the slip area on the stationary surface can give many advanced properties compared with the classical no-slip surface, i.e. a reduction of friction and an increase of load support. It is also shown that if the artificial slip is employed on the moving surface, the system is in an unsteady state and no great importance exists in engineering applications.**

Keywords: computational analysis, lubrication, slip boundary.

1. Introduction

During recent years, in classical lubrication mechanics, the assumption of no-slip at the interface of solid and fluid is used as the boundary condition of fluid flow over a solid surface. This assumption has been widely used in various macro-engineering designs and experiments. However, for flows at micro-scales such as microfluidics and MEMS (micro-electro-mechanical-system) based devices, this assumption may no longer be accurate. The development of MEMS devices has recently prompted the research interests in this area [1-7]. In MEMS based devices, the boundary condition will play a very important role in determining the fluid flow behaviour. Control of the boundary condition will allow a degree of control over the hydrodynamic pressure in confined systems and be important in a lubricated sliding contact of MEMS. How to control the wall slip in the application of lubricated-MEMS is one of the challenging tasks in the future. One of the main challenges on the design and performance of MEMS devices is the effective lubrication of their moving parts, since their low inertia and nanoscale smoothness mean that the surface forces can overwhelm the very small external applied force, making 'stiction' a major problem. Therefore, it is a necessary to propose a new surface technology to reduce friction and adhesion in such machines.

Slip boundary has received more and more attention in hydrodynamic lubrication systems either experimentally [8, 9] or numerically [10-15]. Their attention have been paid to the utilization of the slip phenomenon in practical applications. Recently, in order to get the

improvement of the performance of the lubrication, the concept of heterogeneous slip/no-slip pattern was proposed by some authors [12, 13, 16, 17]. It is believable that slip can reduce the friction and improve the load support. Salant and Fortier [12] described an increase in load support by designing an artificial slip in the finite slider bearing using a modified slip length model and difference method in the numerical solution. However, an instability problem in numerical simulation has been met when the limiting shear stress is nonzero, and thus concluded that the bearing operated in unstable condition in some range of sliding velocity. Wu *et al*. [13] found that an optimized slip zone exists for one-dimensional slider bearing, giving a highest load support and smallest friction when the gap is slightly divergent. Tauviqirrahman *et al*. [17] compared artificial slip boundaries. i.e. between partial slip and full slip and their effects on the lubrication performance. They concluded that the choice of slip area on certain surface must be taken carefully in relation to such performances. On the other words, inappropriate slip area pattern on a certain surface or the election of inappropriate surface containing a slip situation leads to the deterioration of the lubrication performance and reduces the operation stability of the system.

In the present paper, finite volume method combined with tridiagonal matrix algorithm (TDMA) is used to address the nonlinear governing Reynolds equation for lubricated sliding contact based on the limiting shear stress model. According to the distribution of the fluid pressure, the artificial slip surface is optimized so that a maximum hydrodynamic load carrying capacity can be obtained. The artificial slip surface is a function of the coordinate of the location. In addition, friction force, friction coefficient and volume flow are also investigated.

2. Problem statement and method of analysis

The derivation of classical Reynolds equation with a Newtonian lubricant is based on assumption of no slip between the lubricant and the contacting surfaces. The model of lubrication presented here is based on the fact that slip in the lubricant will exist in the interface. The proposed wall-slip model leads to a modified Reynolds equation.

2.1. Theory

Figure 1 presents a schematic of lubricated sliding contacts in MEMS with artificial slip boundary condition. Slip may only occur in those areas where two contacting surfaces has been treated to allow it and where the shear stress exceeds a critical value. When both criteria are met, the resulting slip velocity is proportional to the difference between the shear stress and the limiting value, with constant factors referred as α_t for the top surface and α_b for the bottom surface.

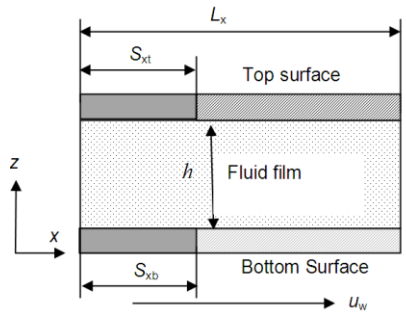

FIGURE 1: *Schematic of a parallel lubricated sliding contact with artifial slip boundary employed both on stationary and moving surfaces. The bottom surface moves with a tangential velocity u_w. L_x is the contact length and S_x is the artificial slip zone length (t and b are referred as top and bottom surface respectively).*

In the present study, the limiting shear stress is zero, and thus the slip length model [18] is used to address the modeling of the wall slip for the hydrodynamic analysis after the shear stress exceeds the limiting shear stress. The wall boundary conditions as depicted in Fig. 1 shows that on a part of the top and bottom surface, namely S_{xt} and S_{xb} respectively, a Navier slip boundary condition is adopted, which stipulates that the wall slip is proportional to the shear stress by the given constant. The bottom surface moves with a velocity u_w whereas the top surface is designed as the stationary surface. In the present study, both at the moving (bottom) surface and the stationary (top) surface the slip

boundary condition is allowed to make an artificial slip boundary. It means that slip partly covers on two surfaces and the others no-slip. Artificial slip surface is defined as the ratio of the slip area S_x to the contact length L_x (see Fig. 1). Such a lubrication system can be described with solving the new modified Reynolds equation as follows:

$$\frac{\partial}{\partial x}\left(\frac{h^3}{12\mu}\frac{h^2+4h\mu(\alpha_t+\alpha_b)+12\mu^2\alpha_t\alpha_b}{h(h+\mu(\alpha_t+\alpha_b))}\frac{\partial p}{\partial x}\right)= \frac{u_w}{2}\frac{\partial}{\partial x}\left(\frac{h^2+2h\mu\alpha_t}{h+\mu(\alpha_t+\alpha_b)}\right)-u_w\frac{\alpha_t\mu}{h+\mu(\alpha_t+\alpha_b)}\frac{\partial h}{\partial x} +\frac{h}{2\mu}\frac{\partial p}{\partial x}\frac{\partial h}{\partial x}\frac{h\alpha_t\mu+2\alpha_t\alpha_b\mu^2}{h+\mu(\alpha_t+\alpha_b)} \quad (1)$$

The physical meanings of the symbols in Eq. (1) are as follows: h the lubrication film thickness (gap) at location, p the lubrication film pressure, μ the lubricant viscosity, α the slip coefficient, subscripts t and b denote the top (stationary) and bottom (moving) surfaces, respectively. It can be seen that if the slip length α is set to zero (no-slip condition), Eq. (1) reduces to the classical Reynolds equation.

Equation 1 can be derived by considering the equilibrium of an element of fluid.

$$\frac{\partial^2 u}{\partial z^2}=\frac{1}{\mu}\frac{\partial p}{\partial x} \quad (2)$$

where z lies along the direction through the thickness of the film. To obtain the velocity profile, Eq. 2 can be integrated twice.

$$u=\frac{1}{2\mu}\frac{\partial p}{\partial x}Z^2+C_1Z+C_2 \quad (3)$$

To find the constants of integration, the boundary conditions are then used. The bottom and the top surfaces have the slip condition.

$$\left.\begin{array}{l}\text{at } z=0,\ u=u_w+\alpha_b\mu\left.\dfrac{\partial u}{\partial z}\right|_{z=0}\\ \text{at } z=h,\quad u=-\alpha_t\mu\left.\dfrac{\partial u}{\partial z}\right|_{z=h}\end{array}\right\} \quad (4)$$

This gives

$$u=\frac{1}{2\mu}\frac{\partial p}{\partial x}z^2 -\left(\frac{u_w}{h+\mu(\alpha_t+\alpha_b)}+\frac{h}{2\mu}\frac{\partial p}{\partial x}\frac{h+2\alpha_t\mu}{h+\mu(\alpha_t+\alpha_b)}\right)z +u_w\frac{h+\alpha_t\mu}{h+\mu(\alpha_t+\alpha_b)}-\frac{h}{2\mu}\frac{\partial p}{\partial x}\frac{\alpha_b\mu(h+2\alpha_t\mu)}{h+\mu(\alpha_t+\alpha_b)} \quad (5)$$

This velocity is used to compute the flow rate q in by integrating across the fluid film thickness, h. When q is differentiated to fulfill the continuity of flow, assuming μ is constant; this gives a modified Reynolds equation as stated in Eq. (1).

3. Numerical procedure

An assumption is made that the boundary pressures are zero at both sides of the contact. In the present study, no cavitation is modeled. For engineering an artificial slip on certain surface, an alternating slip (S_x) is moved from the inlet ($X = 0$) to the outlet ($X = 1$) with $X = x/L_x$, and then the maximum hydrodynamic load support is found. The simulation results will be presented in dimensionless form, i.e. p^* for dimensionless pressure ($p^* = ph^2/\mu L_x u_w$), w^* for dimensionless load support ($w^* = wh^2/(u_w\mu L_x^2)$ in which w is the load per unit length), f^* for dimensionless friction force ($f^* = fh/\mu u_w L_x$ where f is the unit width friction force), Ω for dimensionless friction coefficient ($\Omega = f^*/w^*$) and q^* for dimensionless volume flow ($q^* = q/hu_w$ where q is the unit width volume flow) and B for dimensionless slip length ($B = \alpha\mu/h$).

The modified Reynolds equation, Eq. (1) is solved numerically using finite volume method. By employing the discretization scheme, the computed domain is divided into a number of control volumes using a grid with uniform mesh size, ΔX. The calculation domain is $0 \le X \le L_x$. The mesh size is $\Delta X = L_x/n$. The uniform grid is applied on the slip face surface. The 100 meshes are employed in the computational domain. The grid independency was validated by various

numbers of mesh sizes. If the mesh number was above 101, the simulation results did not differ anymore. But obviously the computational cost increased. Considering the processing time limitation, 100 meshes was adopted for all simulation cases.

In order to maximize the performance of lubrication, the boundary conditions (slip zones S_{xa} and S_{xb}) of the model are optimized. The object of optimization is to maximize the hydrodynamic load support. The load support satisfies two main functional purposes: (a) to carry the applied external load, and (2) to minimize the contacting solids, and thus wear. The optimization analysis attempts to satisfy both functional requirements with a single design parameter, the area of the slip on two solid surfaces. The algorithm used in the present study is depicted on Fig. 2.

The optimization analysis is performed using developed computer code. The design variables, and objective function are referred to as the optimization variables. The design variables are slip zones S_{xa} and S_{xb} as indicated in Fig. 1. Design variables are independent quantities that are varied in order to achieve the optimum design. The objective function is the dependent variable that we are attempting to maximize and in this case the objective function is the maximum dimensionless load support w^*.

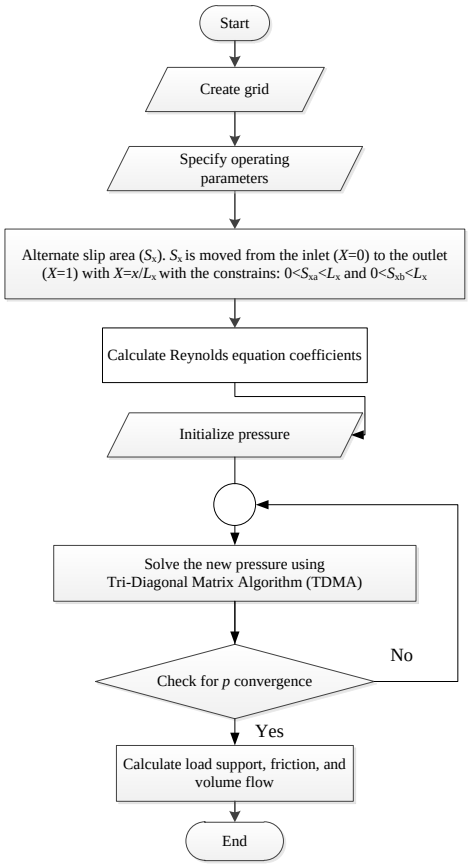

FIGURE 2: *Flow chart for numerical method.*

3. Results

In the present study, the concept of artificial slip boundary is introduced. It means that on chosen surface (may be stationary surface, moving surface, or both of them), slip is constructed to occur in certains regions and is absent in others. It is believed that the judicious choice of artificial slip boundary can alter the flow pattern in the liquid lubricating film so as it will lead to enhanced MEMS caharacteristics and improved operation stability. Therefore, the optimum ratio of slip to no-slip area will be examined by optimization for the case of the parallel lubricated sliding contact.

*3.1. Effects of the artificial slip on the load support w**

At first, a question in accordance with "at which wall" slip must be applied, at the stationary surface, moving surface, or both of them will be answered. A series of simulations were conducted with such boundaries to find the best possibility of artificial slip boundary application in terms of load support. Investigations are made for three kinds of slip boundaries, i.e. (1) slip is applied on both the stationary and moving surfaces is referred as “case I”, (2) slip applied on the stationary surface is referred as “case II”, (3) slip applied on the moving surface is referred as “case III”. These slip boundaries were also compared with “no-slip” case, i.e. no-slip condition applied on the both of surfaces. All of

the simulation results are in the dimensionless form. Figure 3 shows how the artificial slip surface (S_x/L_x) affects the hydrodynamic load support w^* of the lubrication film. As expected that no hydrodynamic pressure (and thus the load support) can be generated in parallel gap for traditional (no-slip) contact. It can also be observed that if the moving surface (case III) is designed as an artificial slip surface, whatever the values of S_{xb}/L_x, the system is in unsteady state because no load support occurs. The same result also happens if artificial slip is applied both at the moving surface and the stationary surface (case I), i.e. the load support abrupts whatever the value of S_{xb}/L_x. Only if the slip employed on the stationary surface (case II), the load support can be obtained for all values of S_{xa}/L_x except at $S_{xa}/L_x = 0$ (i.e. no-slip) and $S_{xa}/L_x = 1$ (i.e. full-slip). When $S_{xa}/L_x = 0.65$, i.e. the length of the slip zone is 0.65 times the contact length, the lubricated sliding contact gives the highest hydrodynamic load support. It should be pointed out that even though the slip model and the numerical method used are different, good agreement exists between the present theoritical prediction and the works of Wu *et al*. [13].

Secondly, the study is extended to explore the effect of the artificial the slip boundary on the load support, friction force and thus friction coefficient and volume flow at several slip length values. The slip boundary is only applied on the stationary surface due to the generation of the maximum load support as mentioned earlier by optimization. In the present study the dimensionless slip length A used are 1, 10, and 100 based on the works of Watanabe *et al*. [19]. As can be seen on Fig. 4, the higher the dimensionless slip length used, the higher the generated load support. The load support trend for all the variation of dimensionless slip length values is similar, i.e. the optimized artificial slip surface occurs when $S_x = 0.65$ for the highest load support. From this figure, when $S_x = 0.65$ it is also found that the prediction of the maximum load support for $B = 10$ and 100 is not too much different (only 4%). This is opposite with the generation of the load support when the B chosen is lower, i.e. 1. The difference can reach 32% if compared to that of $B = 10$. It indicates that in addition to the optimal artificial slip area, there is also an optimal value of dimensionless slip length B which can affect the performance of the lubrication. However, the optimization of B is beyond the scope of this study. The choose of B by optimization was described in detail by the authors in [15].

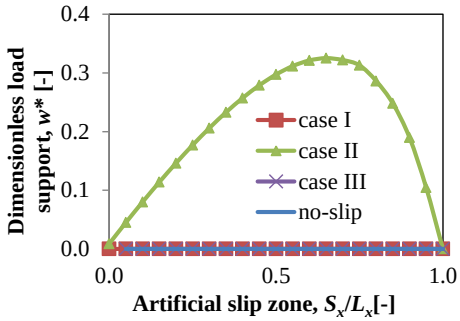

FIGURE 3: *Dimensionless load support versus artificial slip area (Note: slip is applied on both the stationary and moving surfaces (case I); slip applied on the stationary surface (case II); slip applied on the moving surface (case III).*

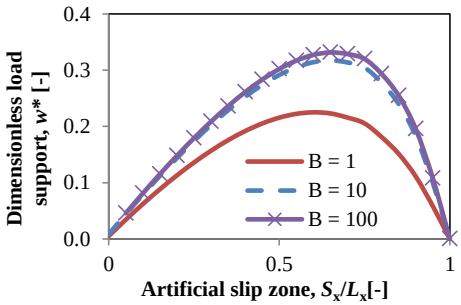

FIGURE 4: *Dimensional load support w* versus artificial slip area S_x at different dimensionless slip length values B.*

*3.2. Effects of the artificial slip on the friction f**

In Fig. 5 the effect of the length of slip area at several slip length values on the friction drag f^* is shown. It can be seen that the artificial slip surface leads to a reduction of the friction drag for all dimensionless slip length at all artificial slip values. The friction drag decreases with increasing the length of slip area (S_x). If the reduction of friction drag is of only particular interest, the full slip ($S_x/L_x = 1$) is very beneficial. However if the performance is also connected to the load support, full slip is not

recommended to use because no-load support yields at such slip pattern. It can be said that the lubricated sliding contacts with artificial slip produces lower friction than classical (no-slip) contact. Opposite to the hydrodynamic load support, the dimensionless friction drag becomes smaller for high dimensionless slip length. Therefore, the optimized artificial slip surface is a very promising way to increase the hydrodynamic performance and the stability of the lubricated MEMS system because it gives the advanced load support in combination with reduced friction force.

Figure 6 shows the effect of the length of slip area S_x on the dimensionless friction coefficient Ω. It should be noted that in the present study Ω is defined as the ratio of the dimensionless friction force f^* to the dimensionless load support w^*. Therefore, the contact with the uniform film thickness, for no-slip condition ($B = 0$), the friction coefficient can be infinite. It is shown that as the slip area S_x increases to around 0.2, the friction coefficient decreases significantly. However, for $S_x > 0.2$, increasing the slip area does not change the variation of the friction coefficient. Therefore, for the optimized slip area ($S_x/L_x = 0.65$), it is very beneficial to use the artificial slip boundary on the stationary surface with respect to the friction coefficient. Opposite to the friction coefficient, the dimensionless volume flow q^* increases with increasing the length of area due to the presence of the wall slip occurring the stationary surfaces (Fig. 7). The variation of slip length does not affect the volume flow significantly for the entire range of artificial slip values.

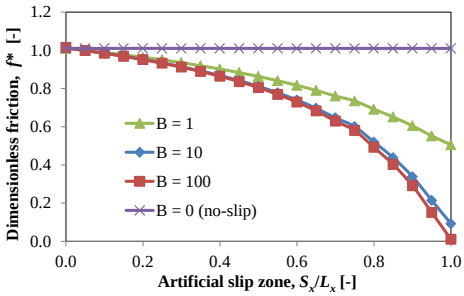

FIGURE 5: *Effect of the length of slip area, S_x on the friction drag f^* at various dimensionless slip length values B with slip applied on top surface.*

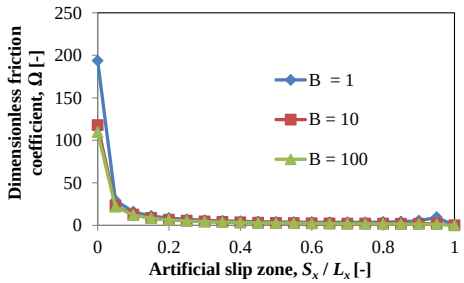

FIGURE 6: *Effect of the length of slip area, S_x on the friction coefficient Ω at various dimensionless slip length values B with slip applied on top surface.*

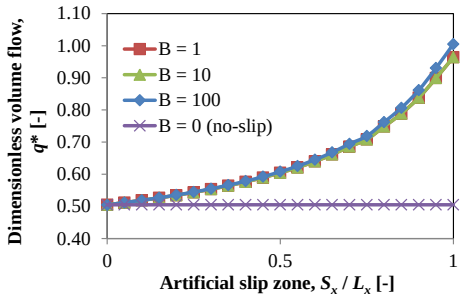

FIGURE 7: *Effect of the length of slip area, S_x on the dimensionless volume flow q* at various dimensionless slip length values B with slip applied on top surface.*

3.3. Effects of the slip length B on w, f* and q**

For infinite length slider contact, if the stationary surface has an artificial slip boundary consisting of two zones with slip and no-slip, a maximum load support can be achieved by optimizing the geometrical parameter, i.e. the slip zone. As discussed in the previous section, it was found that with respect to the load support, the optimized artificial slip boundary will yield the maximum load support when the slip area is 0.65 times the contact length. However, it is interesting to investigate the effect of slip length on the performance parameter including the load support, the friction, and the volume flow at such slip surface. Figure 8 shows the effect of the slip length on the load support. It is obvious that the load support increases with the increase of slip length. Load support can get a maximum when $B = 15$. However, when the dimensionless slip length B is larger than 15, load support does not change with the increase in the slip length. It

can be remarked that at the parallel sliding surfaces, there is no load support in the case of no-slip contact. Therefore, again, utilizing artificial slip boundary with an optimized geometry at lubricated-MEMS is very beneficial.

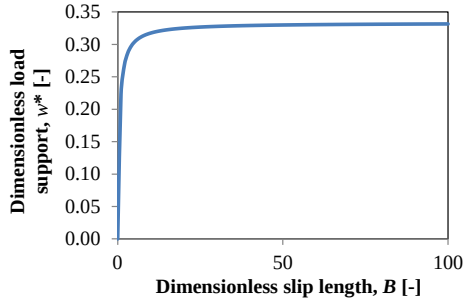

FIGURE 8: *Effect of the dimensionless slip length values B on the dimensionless load support w*.*

Figures 9-10 show the influence of the slip length on the friction and volume flow respectively. Similar to trend of the load support, there is an optimal value of B for each parameter, i.e. $B = 15$. It means that the decrease in friction as well as the increase in volume flow is not infinitely large. For example, when $B = 15$ and above it, the artificial slip boundary can reduce the friction drag by half of what Reynolds theory predict, whereas the volume flow can be increased to up 30% higher than that of no-slip ($B = 0$).

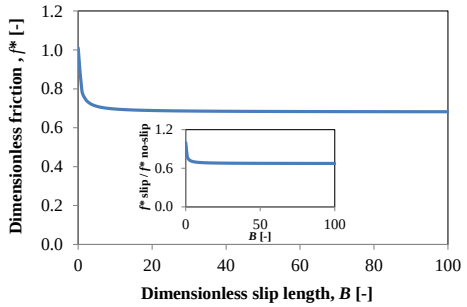

FIGURE 9: *Effect of the dimensionless slip length values B on the dimensionless friction force f*. The inset shows tha ratio of the friction with artifial slip area, f^*_{slip}, to that no-slip area, $f^*_{no\text{-}slip}$. ($S_x/L_x = 0.65$).*

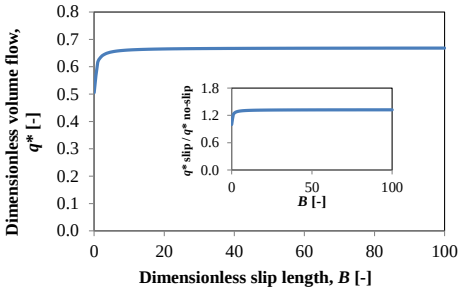

FIGURE 10: *Effect of the dimensionless slip length values B on the dimensionless volume flow q^*. The inset shows tha ratio of the volume flow with artifial slip area, q^*_{slip}, to that no-slip area, $q^*_{no\text{-}slip}$. ($S_x/L_x = 0.65$).*

From the inset of Figs. 9-10, it can also be seen that lubricated-MEMS with optimized artificial slip boundary gives an advantageous effect on the increase in the volume flow and the decrease in the friction.

4. Discussion and conclusion

An artificial slip surface at lubricated-MEMS was presented, and it was shown that the optimal artificial slip surface can give many advanced properties compared with the classical contact, i.e. high load carrying capacity and volume flow in combination with low friction coefficient. The conclusions can be summarized as follows:

1. The modified Reynolds equation for the artificial slip surface was established based on the limiting shear stress model considering the possibility of the occurence of slip at two contacting surfaces.
2. The system is in an unsteady state and no great importance exists in engineering applications if the moving surface is designed as a slip surface. Therefore, for an improved lubricated sliding contact, an artificial slip boundary is employed on the stationary surface.
3. The load support can get a maximum when $S_x = 0.65\ L_x$.
4. The optimized artificial slip surface with large slip length gives a large load support and volume flow, but gives a low friction which guide a new way to improve the operation stability of the system.

References

1. Craig, V.S.J., Neto, C. and Williams D.R.M., 2001, "Shear-dependent boundary slip in an aqueous Newtonian liquid," *Physical Review Letters* **87**(5), 054504.
2. 14. Zhu, Y. and Granick, S., 2001, "Rate-dependent slip of Newtonian liquid at smooth surfaces," *Physical Review Letters* **87** (9), 096105.
3. Zhu,Y. and Granick, S., 2002, "Limits of the hydrodynamic no-slip boundary condition," *Physical Review Letters* **88** (10), 106102. .
4. Hervet, H. and Léger, L., 2003, "Flow with slip at the wall: from simple to complex fluids," *C. R. Physique* **4** (2), pp. 241 – 249.
5. Pit, R., Hervet, H. and Leger, L., 2000, "Direct experimental evidence of slip in hexadecane: solid interfaces," *Physical Review Letters* **85** (5), pp. 980 – 983.
6. Bonaccurso, E., Kappl, M. and Butt, H.J., 2002, "Hydrodynamic force measurements: boundary slip of hydrophilic surfaces and electrokinetic effects," *Physical Review Letters* **88**, 076103.
7. Bonaccurso, E., Butt, H.J. and Craig, V.S.J., 2003, "Surface roughness and hydrodynamic boundary slip of a Newtonian fluid in a completely wetting system," *Physical Review Letters* **90** (14),144501.
8. Choo, J.H., Spikes, H.A., Ratoi, M., Glovnea, R. and Forrest, A., 2007, "Friction reduction in low-load hydrodynamic lubrication with a hydrophobic surface," *Tribology International* **40**, pp. 154 – 159.
9. Spikes, H.A., 2003, "The half-wetted bearing. Part 1: extended Reynolds equation," *Proceedings of the Institution of Mechanical Engineers, Part J: Journal of Engineering Tribology* **217**, pp. 1 – 14.
10. Choo, J.H., Glovnea, R.P., Forrest, A.K. and Spikes, H.A., 2007, "A low friction bearing based on liquid slip at the wall," *ASME Journal of Tribology* **129**, pp. 611 – 620.
11. Spikes, H.A., 2003, "The half-wetted bearing. Part 2: Potential application in low load contacts," *Proceedings of the Institution of Mechanical Engineers, Part J: Journal of Engineering Tribology* **217**, pp. 15 – 26.
12. Salant, R.F. and Fortier, A.E., 2004, "Numerical analysis of a slider bearing with a heterogeneous slip/no-slip surface," *Tribology Transactions* **47**, pp. 328 – 334.
13. Wu, C. W., Ma, G. J. and Zhou, P., 2006, "Low friction and high load support capacity of slider bearing with a mixed slip surface," *ASME Journal of Tribology* **128**, pp. 904 – 907.
14. Aurelian, F., Patrick, M. and Mohamed, H., 2011, "Wall slip effects in (elasto) hydrodynamic journal bearing," *Tribology International* **44**, pp. 868 – 877.
15. Tauviqirrahman, M., Ismail, R., Jamari, J. and Schipper, D.J., 2011, "Wall slip effects in a lubricated MEMS," *International Journal of Energy Machinery* **4**, pp. 13 – 22.
16. Fortier, A.E. and Salant, R.F., 2005, "Numerical analysis of a journal bearing with a heterogeneous slip/no-slip surfaces," *ASME Journal of Tribology* **127**, pp. 820 – 825.
17. Tauviqirrahman, M., Ismail, R., Jamari, J. and Schipper, D.J., 2011, "Optimization of partial slip surface at lubricated-MEMS," *Proceedings of 2nd International Conference on Instrumentation, Control and Automation*, ISBN: 978-1-4577-1460-3. IEEE Catalog Number: CFP1179P-DVD, doi: 10.1109/ICA.2011.6130190.
18. Navier, C.L.M.H., 1823, "Mémoire sur les lois du mouvement des fluides, " *Mémoires de l'Académie Royale des Sciences de l'Institut de France*. **6**, pp. 389 – 440.
19. Watanabe, K., Yanuar and Udagawa, H., 1999, "Drag reduction of Newtonian fluid in a circular pipe with a highly water-repellent wall," *Journal of Fluid Mechanics* **381**, pp. 225 – 228.

M. Tauviqirrahman, R. Ismail, Jamari, D.J. Schipper, 2011

Optimization of partial slip surface at lubricated-MEMS

Proceedings of 2nd International Conference on Instrumentation, Control and Automation, Issue date: 15-17 Nov., pp. 375 – 379.

Paper E

Optimization of Partial Slip Surface at Lubricated-MEMS

M. Tauviqirrahman,[1,*)] R. Ismail,[1)] Jamari,[2)] and D.J. Schipper[1)]

[1]Laboratory for Surface Technology and Tribology,
Faculty of Engineering Technology, University of Twente, The Netherlands
*Email: mtauviq99@gmail.com

[2]Laboratory for Engineering Design and Tribology,
Department of Mechanical Engineering, University of Diponegoro, Indonesia

Proceedings of 2nd International Conference on Instrumentation, Control and Automation, 2011, Issue date: 15-17 November

Abstract **This work reports the hydrodynamic performance (load support, friction force, friction coefficient, and volume flow) generated by a partial slip surface at lubricated-MEMS. The partial slip surface is optimized so that a maximum hydrodynamic load support could be obtained. The partial slip is applied on the stationary surface, the moving surface, and both of them. It is found that if the moving surface is designed as a partial slip surface, the system is in an unsteady state and no great importance exists in engineering applications. Controlling the partial slip surface of the stationary surface can give many advanced properties compared with the traditional no-slip contact, i.e. a large fluid load support in combination with low friction coefficient. It is also shown that partial slip surface gives the highest hydrodynamic pressure in a parallel slip gap, which is helpful to improve the operation stability of the system.**

Keywords: Finite volume analysis; lubrication; Micro-Electro-Mechanical-System (MEMS); wall slip

1. Introduction

The range of applications for Micro-Electro-Mechanical Systems (MEMS) is steadily increasing. For the last years, there has been a tremendous effort towards the development of Micro-Electro-Mechanical System (MEMS) for a wide variety of applications in the aerospace, automotive, biomedical, computer, and agricultural industries. Challenging new applications make use of micro devices with moving parts. The reliability of MEMS with moving parts is poor and do have a limited lifetime. The surfaces in contact are subjected to wear and as a result, the functionality of these systems fails. Applying a lubricant to these systems, to avoid wear, hampers the movement due to the adhesive/surface forces, leading to stiction.

The full-film lubrication situation is theoretically solved. The load support of such systems can be predicted as well as the separation (film thickness) between the opposing surfaces. Depending on the operational conditions one is able to determine if there will be physical contact between the surfaces (on roughness level). MEMS are widely in use, but MEMS in which moving components are present do have a short life-time. Using a lubricant could avoid direct contact between the surfaces; however, the surface forces become larger than the external applied force, i.e. stiction occurs. By modifying the contacting surfaces (coating or topography) and/or specific lubricant (so electro wetting can be applied) one is able to enhance, in a controlled way, hydrophobic / hydrophilic behavior of surfaces. If one surface is

hydrophobic (slip condition) and the other is hydrophilic (no-slip condition) the sliding velocity or displacement between the surfaces is accommodated by shear at the hydrophobic surface (the lubricant is kept in the contact by the hydrophilic surface). In this way wear of the surfaces is prevented and the surfaces are able to move because stiction is prevented.

In micro- or nano-scopic scales such as MEMS (Micro-Electro-Mechanical-System), the boundary condition will play a very important role in determining the fluid flow behavior. Control of the boundary condition will allow a degree of control over the hydrodynamic pressure in confined systems and is important in lubricated-MEMS. How to control the wall slip in the application of lubricated-MEMS is one of the challenging tasks in the future. It is because of large viscous drag forces on immersed, moving surfaces and also high hydrodynamic friction present in fluid film.

There is a large body of literature dealing with the analysis of lubricant flow in MEMS based on the analytical and numerical solution of Reynolds equation [1-3], molecular dynamic simulation method [4-5], and Lattice-Boltzman [6-7]. The accurate description of slip at the wall is very difficult and still remains a subject of intensive research. In fact, nearly two hundred years ago, Navier [8] proposed a general boundary condition that incorporates the possibility of fluid slip at a solid boundary. Navier's proposed boundary condition assumes that the velocity, u, at a solid surface is proportional to the shear stress at the surface. It reads: $u = b\,(\mathrm{d}u/\mathrm{d}z)$ where b is the slip length. If $b = 0$ then the generally assumed no-slip boundary condition is obtained. If b = finite, fluid slip occurs at the wall, but its effect depends upon the length scale of the flow. The Navier-slip boundary condition is the most widely used boundary condition with the methods based on the solution of continuum equations.

It is believable that slip can reduce the friction and improve the load support [9-14]. However, the choice of slip area on certain surface must be taken carefully in relation to such performances. On the other words, inappropriate slip area pattern on a certain surface or the election of inappropriate surface containing a slip situation leads to the deterioration of the lubrication performance and reduces the operation stability of the system.

This paper studies the optimization of hydrodynamic performance generated by the partial slip surface such as load support (load carrying capacity), friction force, friction coefficient, and volume flow based on the limiting shear stress model. According to the distribution of the fluid pressure, the partial slip surface is optimized so that a maximum hydrodynamic load carrying capacity can be obtained. The hydrodynamic contact with uniform film thickness is of particular interest.

2. Mathematical model

2.1. Modified Reynolds equation

Figure 1 presents a schematic of lubricated sliding contacts in MEMS with partial slip boundary condition. Slip may only occur in those areas where two contacting surfaces have been treated to allow it and where the shear stress exceeds a critical value τ_c. When both criteria are met, the resulting slip velocity is proportional to the difference between the shear stress and the limiting value, with constant factors referred as α_a for the top surface and α_b for the bottom surface. In the present study, the critical shear stress is zero, and thus the slip length model [8] is used to address the modeling of the wall slip for the hydrodynamic analysis after the shear stress exceeds the limiting shear stress. The wall boundary conditions as depicted in Fig. 1 shows that on a part of the top and bottom surface, namely T_{sa} and T_{sb}, respectively, a Navier slip boundary condition [8] is adopted, which stipulates that the wall slip is proportional to the shear stress by the given constant α. The bottom surface moves with a velocity U whereas the top surface is designed as the stationary surface. In the present study, both at the moving (bottom) surface and the stationary (top) surface the partial slip boundary condition is allowed to occur. It means that slip partly covers on two surfaces and the others no-slip. Partial slip surface is defined as the ratio of the slip area T_s to the contact length L. Such a lubrication

system can be described with solving the new modified Reynolds equation as follows:

$$\frac{\partial}{\partial x}\left(\frac{h^3}{12\mu}\frac{h^2+4h\mu(\alpha_a+\alpha_b)+12\mu^2\alpha_a\alpha_b}{h(h+\mu(\alpha_a+\alpha_b))}\frac{\partial p}{\partial x}\right) = \frac{U}{2}\frac{\partial}{\partial x}\left(\frac{h^2+2h\mu\alpha_a}{h+\mu(\alpha_a+\alpha_b)}\right)-U\frac{\alpha_a\mu}{h+\mu(\alpha_a+\alpha_b)}\frac{\partial h}{\partial x} + \frac{h}{2\mu}\frac{\partial p}{\partial x}\frac{\partial h}{\partial x}\frac{h\alpha_a\mu+2\alpha_a\alpha_b\mu^2}{h+\mu(\alpha_a+\alpha_b)} \quad (1)$$

The physical meanings of the symbols in Eq. (1) are as follows: h the lubrication film thickness (gap) at location, p the lubrication film pressure, μ the lubricant viscosity, α the slip coefficient, subscripts a and b denote the stationary and moving surfaces, respectively.

Eq. (1) is derived by following the usual approach to deduce the Reynolds equation from the Navier-Stokes system by assuming classical assumptions except that wall slip boundary is applied both on the stationary surface and moving surface as depicted in Fig. 1.

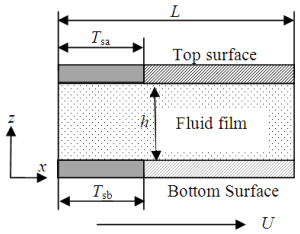

FIGURE 1: *Schematic of a lubricated sliding contact with slip boundaries both at stationary and moving surfaces. L is the contact length.*

2.2. Methodology

The modified Reynolds equation is discretized over the flow using the finite volume method, and is solved using alternating direction implicit method (ADI) with tridiagonal matrix algorithm (TDMA). By employing the discretization scheme, the computed domain is divided into a number of control volumes using a grid with uniform mesh size. The grid independency is validated by various numbers of mesh sizes. An assumption is made that the boundary pressures are null at both sides of the contact. However, the Reynolds cavitation model is adopted. In optimization process, alternating slip (T_s) is moved from the inlet (X=0) to the outlet (X=1) with $X = x/L$, and then, the maximum hydrodynamic load carrying capacity is found.

The simulation results will be presented in dimensionless form, i.e. $P^* = Ph^2/\mu LU$ for dimensionless pressure, $W = wh^2/(U\mu L^2)$ for dimensionless load support in which w is the load per unit length, $F = fh/\mu UL$ for dimensionless friction force (where f is the unit width friction force), $m = F/W$ for dimensionless friction coefficient and $Q = q/hU$ for dimensionless volume flow (where q is the unit width volume flow).

In order to maximize the performance of lubrication, the boundary conditions (slip zones T_{sa} and T_{sb}) of the model are optimized. The object of optimization is to maximize the hydrodynamic load support. The load support satisfies two main functional purposes: (1) carry the applied external load, and (2) to minimize the contacting solids, and thus wear. The optimization analysis attempts to satisfy both functional requirements with a single design parameter, the area of the slip on two solid surfaces.

The optimization analysis is performed in MATLAB using developed computer code. The design variables, and objective function are referred to the optimization variables. The design variables are slip zones T_{sa} and T_{sb} as indicated in Fig. 1. Design variables are independent quantities that are varied in order to achieve the optimum design. The objective function is the maximum dimensionless load support W. The objective function is the dependent variable that we are attempting to maximize.

Algorithm for optimization analysis used in the study are as follows:

1. Create grid.
2. Specify operating parameters.
3. Alternate the slip zone (T_s) by moving it from the inlet (X=0) to the outlet (X=1) of the contact where $X = x/L$ with the constrains: $0<T_{sa}<L$ and $0<T_{sb}<L$.
4. Calculate Reynolds equations coefficients.

5. Initialize pressure.
6. Solve the new pressure using TDMA.
7. Test for convergence.
8. Repeat steps 3-7 till convergence is obtained on all field variables.
9. Calculate load support W for various slip zone T_{sb} and T_{sa}.

3. Results and discussion

MEMS performance by lubrication as mentioned in previous section faces a great challenge due to the presence of stiction. It occurs because the surface force is much greater than external load. In order to eliminate the stiction and improve the load support in combination with reduced friction at the contacting surface, the concept of partial slip boundary is introduced. However, a big question emerges in accordance with "at which wall" slip must be applied, at the stationary surface, moving surface, or both of them. Series of simulations are conducted with such boundaries to find the best possibility of slip boundary application in terms of load support as indicated in Fig. 2. Investigations are made for four kinds of boundaries, i.e. (1) slip applied on both the stationary and moving surfaces is referred to as 'two-slip', (2) slip applied on the stationary (top) surface is referred to as 'one-slip top', (3) slip applied on the moving surface is referred to as 'one-slip bottom', and (4) no-slip condition applied on the both of surfaces is referred to as 'no-slip'. All of the simulation results are presented in the dimensionless form.

Figure 2 shows how the partial slip surface (T_s/L) affects the hydrodynamic load support W of the lubrication film. As expected, no hydrodynamic pressure (and thus the load support) can be built up in parallel gap for traditional (no-slip) contact. It can also be observed that if the moving surface (one-slip-bottom) is designed as a partial slip surface, whatever the values of T_s/L, the system is in unsteady state because no load support occurs. The same result also happens if partial slip is applied both at the moving surface and the stationary surface (two-slip), i.e. the load support goes off whatever the value of T_s/L. Only if the slip employed on the stationary surface (one-slip-top), the load support can be obtained for all values of T_s/L except at T_s/L = 0 (i.e. no-slip) and T_s/L = 1 (i.e. full-slip). When T_s/L = 0.65, the lubricated sliding contact gives the highest hydrodynamic load support. It is very interesting that the optimization result of partial slip surface is in a good agreement with the works of Wu *et al*. [9] even though the slip model and the numerical method are different.

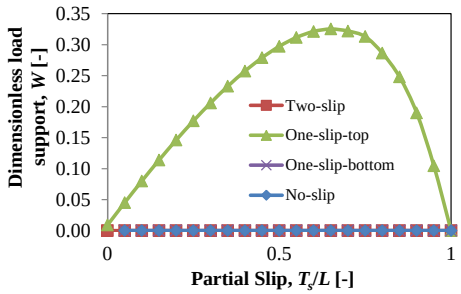

FIGURE 2: *Effect of the length of slip area, T_s on the dimensionless fluid load support W with several schemes of partial slip surface.*

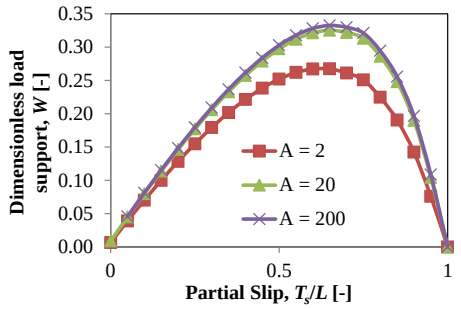

FIGURE 3: *Effect of the length of slip area, T_s on the dimensionless fluid load support W at various dimensionless slip length values A with slip applied on top surface.*

The study is extended to explore the effect of the variation of the slip boundary on the load support, friction force and thus friction coefficient, as well as volume flow at several slip length values. The slip boundary is only applied on the stationary surface due to the generation of the maximum load support as mentioned earlier. In the present study the dimensionless slip length A used are 2, 20, and 200 based on the works of Choo *et al*. [15]. As can be seen on Fig. 3 the higher the dimensionless slip length used, the higher the

generated load support. The load support trend for all the variation of dimensionless slip length values is similar, i.e. the optimized partial slip surface occurs when T_s = 0.65 for the highest load support.

In Fig. 4, the effect of the length of slip area at several slip length values on the friction force is shown. The partial slip surface leads to a reduction of the friction force for all dimensionless slip length at all partial slip values. The friction force decreases with increasing the length of slip area (T_s). If the reduction of friction force is of only particular interest, the fully slip (T_s/L = 1) is very advantageous. But if the performance is also related to the load support, fully slip is not beneficial because when T_s/L = 1, no-load support yields. This is to say that the lubricated sliding contacts with partial slip produces lower friction than traditional (no-slip) contact. Opposite to the hydrodynamic load support, the dimensionless friction force becomes smaller for high dimensionless slip length. Therefore, the optimized partial slip surface is a very promising way to increase the hydrodynamic performance and the stability of the lubricated MEMS system because it gives the advanced load support in combination with reduced friction force.

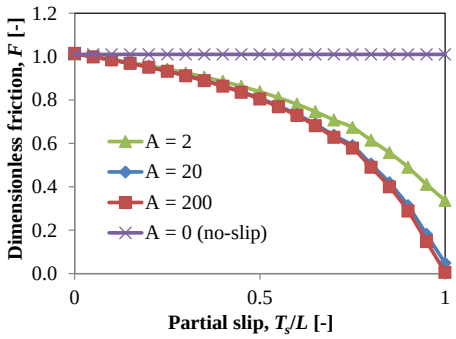

FIGURE 4: *Effect of the length of slip area, T_s on the friction force at various dimensionless slip length values A with slip applied on top surface.*

Figure 5 shows the effect of the length of slip area T_s on the dimensionless friction coefficient *m*. It should be noted that in the present study, *m* is defined as the ratio of the dimensionless friction force *F* to the dimensionless load support *W*. Therefore, the contact with the uniform film thickness, for no-slip condition (*A* = 0), the friction coefficient can be infinite. It is shown that when the slip area T_s increases to up 0.2, the friction coefficient decreases significantly. For T_s > 0.2, increasing the slip area will be less significant to the reduction in the friction coefficient. Therefore, for the optimized slip area (T_s/L = 0.65), it is very beneficial to use the partial slip boundary on the stationary surface. Opposite to the friction coefficient, the dimensionless volume flow increases with increasing length of area due to the presence of the wall slip occurring the stationary surfaces, see Fig. 6. The variation of slip length does not affect the volume flow significantly for all of partial slip values.

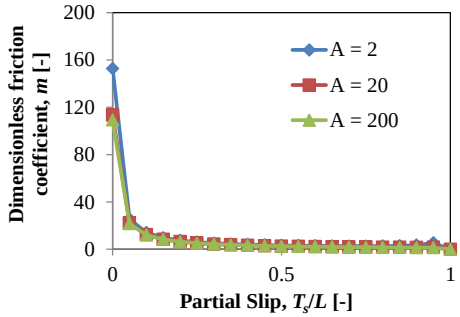

FIGURE 5: *Effect of the length of slip area, T_s on the friction coefficient m at various dimensionless slip length values A with slip applied on top surface.*

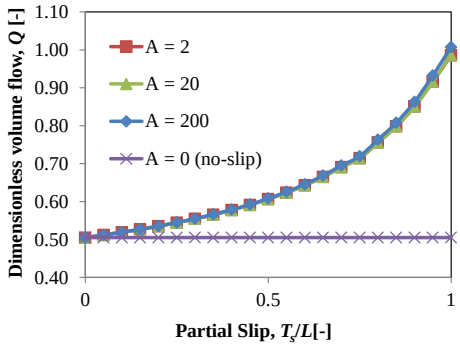

FIGURE 6: *Effect of the length of slip area, T_s on the dimensionless volume flow at various dimensionless slip length values A with slip applied on top surface.*

4. Conclusion

As a conclusion, this paper focused theoretically on the possibility of enhancing the hydrodynamic performance, i.e. high load carrying capacity in combination with low friction coefficient by optimizing partial slip surface. The simple geometrical model of a parallel sliding contact which exists mostly in MEMS is of particular interest. It was demonstrated that if the moving surface is designed as a partial slip surface, the system is in an unsteady state and no great importance exists in engineering applications. Controlling the partial slip surface of the stationary surface can give many advanced properties compared with the traditional no-slip contact, i.e. a large fluid load carrying capacity in combination with low friction coefficient. It is also shown that partial slip surface gives the highest hydrodynamic pressure in a parallel slip gap, which is helpful to improve the operation stability of the system.

References

1. Spikes, H.A., 2003, "The half-wetted bearing. Part 1: extended Reynolds equation," *Proceedings of the Institution of Mechanical Engineers, Part J: Journal of Engineering Tribology* **217**, pp. 1 – 14.
2. Spikes, H.A., 2003, "The half-wetted bearing. Part 2: Potential application in low load contacts," *Proceedings of the Institution of Mechanical Engineers, Part J: Journal of Engineering Tribology* **217**, pp. 15 – 26.
3. Choo, J.H., Spikes, H.A., Ratoi, M., Glovnea, R. and Forrest, A., 2007, "Friction reduction in low-load hydrodynamic lubrication with a hydrophobic surface," *Tribology International* **40**, pp. 154 – 159.
4. Priezjev, N.V., Darhuber, A.A. and Troian, S.M., 2005, "Slip behaviour in liquid films on surfaces of patterned wettability: comparison between continuum and molecular dynamics simulations," *Physical Review E* **71**, 041608, 2005.
5. Cottin-Bizonne, C., Barentin, C., Charlaix, E., Bocquet, L. and Barrat, J.L, 2004, "Dynamics of simple liquids at heterogeneous surfaces: molecular dynamics simulations and hydrodynamic description," *European Physical Journal E* **15**, pp. 427 – 438, 2004.
6. Harting, J., Kunert, C., and Herrmann, H.J., 2006, "Lattice Boltzmann simulations of apparent slip in hydrophobic channels," *Europhysics Letters* **75**, pp. 328 – 334.
7. Li, B.M. and Kwok, D.Y., 2003, "Discrete Boltzmann equation for microfluidics," *Physical Review Letters* **90**, 124502.
8. Navier, C.L.M.H., 1823, "Mémoire sur les lois du mouvement des fluides," *Mémoires de l'Académie Royale des Sciences de l'Institut de France* **6**, pp. 389 – 440.
9. Wu, C.W., Ma, G.J. and Zhou, P., 2006, "Low friction and high load support capacity of slider bearing with a mixed slip surface," *ASME Journal of Tribology* **128**, pp. 904 – 907.
10. Fortier, A.E. and Salant, R.F., 2005, "Numerical analysis of a journal bearing with a heterogeneous slip/no-slip surfaces," *ASME Journal of Tribology* **127**, pp. 820 – 825.
11. Salant, R.F. and Fortier, A.E., 2004, "Numerical analysis of a slider bearing with a heterogeneous slip/no-slip surface," *Tribology Transaction* **47**, pp. 328 – 334.
12. Tauviqirrahman, M., Ismail, R., Jamari, and Schipper, D.J., 2011, "Optimization of the complex slip surface and its effect on the hydrodynamic performance of two-dimensional lubricated contacts," submitted to *Computers and Fluids*.
13. Aurelian, F., Patrick, M. and Mohamed, H., 2011, "Wall slip effects in (elasto) hydrodynamic journal bearing," *Tribology International* **44**, pp. 868 – 877.
14. M. Tauviqirrahman, R. Ismail, J. Jamari, and D.J. Schipper, 2011, "Wall slip effects in a lubricated MEMS," *International Journal of Energy Machinery* **4** (1), pp. 13 – 22 (ISSN 1976-9954), 2011.
15. Choo, J.H., Glovnea, R.P., Forrest, A.K. and Spikes, H.A., 2007, "A low friction bearing based on liquid slip at the wall," *ASME Journal of Tribology* **129**, pp. 611 – 620.

Paper F

M. Tauviqirrahman, R. Ismail, Jamari, D.J. Schipper, 2011

Effect of boundary slip on the load support in a lubricated sliding contact

AIP (American Institute of Physics) Conference Proceedings, Volume 1415, Issue 51, pp. 51 – 54.

Effect of Boundary Slip on the Load Support in a Lubricated Sliding Contact

M. Tauviqirrahman,[1,*)] R. Ismail,[1)] Jamari,[2)] and D.J. Schipper[1)]

[1]Laboratory for Surface Technology and Tribology,
Faculty of Engineering Technology, University of Twente, The Netherlands
*Email: mtauviq99@gmail.com

[2]Laboratory for Engineering Design and Tribology,
Department of Mechanical Engineering, University of Diponegoro, Indonesia

AIP (American Institute of Physics) Conference Proceedings, 2011,
Volume 1415, Issue 51

Abstract **In recent years it has been shown experimentally by a number of researchers that, for certain engineered surfaces, the no-slip boundary condition is not a valid one. Moreover, researchers demonstrate that slip patterning can considerably improve the performance of lubricated contact. In nano-electro-mechanical-system (NEMS) devices containing moving components, there is a need to achieve low friction and high load support by lubrication. However, many researches were focused only on how to reduce the friction without paying much attention to the hydrodynamic pressure, i.e. load support. In this paper, the Reynolds model with slip boundary is presented for investigating the effect of slip boundary on the load support in a lubricated sliding contact. A finite volume method analysis is used to investigate the influence of boundary slip over the load support and friction. Numerical results of the extended Reynolds equation show that a homogeneously distributed slip boundary applied on a surface has a disadvantage with respect to the load support. It is found that in a lubricated system, if one of the lubricated surfaces is treated as homogeneous slip boundary, a lower load support with a reduced friction force is obtained. However, if that surface is designed as heterogeneous slip, i.e. partly boundary slip, the load support is about twice that of corresponding traditional sliding contact, even when there is no wedge effect.**

Keywords: hydrodynamic lubrication, numerical analysis, slip

1. Introduction

Nano-electro-mechanical-system (NEMS) devices are widely used, and nowadays, NEMS have become more sophisticated and more stringent design and longevity requirement. NEMS devices may contain rotating and/or sliding elements. Hence, the requirement for provision of adequate lubrication in NEMS became more than a casual interest.

In classical liquid lubrication, it is assumed that surfaces are fully wetted and no-slip occurs between the fluid and the solid boundary. In NEMS, this wetting is actually an unwanted process because it can encourage the occurrence of stiction and as a result, micro-parts can not be moved. Currently, many workers attempted to solve the stiction problem by introducing a slip boundary on the opposing surfaces when liquid lubrication is considered to use in NEMS. There were considerable studies in microsystem with the aim to utilize a slip boundary in order to reduce viscous drag [1-5]. Spikes [1-2] proposed a possible means of reducing the friction in liquid-lubricated bearings by making one nearing surface hydrophobic while the other hydrophilic, so that the liquid slips against the former under shear but adheres to the latter. Hild *et al.* [4] examined the influence of wettability on the friction force. It was shown that the Newtonian friction law breaks down for hydrophobic surfaces. The friction force becomes significantly smaller in the hydrophilic-hydrophobic interaction than in the same property interaction. The same result was shown by Choo *et al.* [5]. Their experiments were conducted using a tribometer to show the effect

of wettability on the friction coefficient between two shearing surfaces lubricated by an aqueous glycerol solution. The results obtained with two hydrophilic contacting surfaces were found to be consistent with hydrodynamic theory. It means that no-slip occur at these surfaces. From the experimental validation, they found that a reduction in the friction force occurs when one surface was made hydrophobic and the other was hydrophilic. It should be pointed out that these studies mainly focused only on one parameter, i.e. the friction force. Only little attention was paid to the effect of boundary slip on the load support [6-7]. In engineering application, there is very high possibility that boundary slip causes a friction force reduction, although at the same time the slip on a hydrophobic patterned surface may produce a small hydrodynamic response. In NEMS, by lubrication, low friction force and high load support are the goals which want to be achieved. In the present study, the effect of boundary slip on the load support in a lubricated sliding contact will be examined by means of numerical analysis. The hydrodynamic load support and the friction force will be investigated based on the analysis of the conventional lubricated sliding contacts and the homogeneous slip, as well as the heterogeneous slip.

2. Extended Reynolds equation

Figure 1 presents a schematic of an infinite width slider contacts. The lower surface moves with a velocity U whereas the upper surface is designed as the stationary surface. In the present study, both at the moving surface and the stationary surface the slip is allowed to occur. Such a lubrication system can be described with solving the extended Reynolds equation as follow:

$$\frac{\partial}{\partial x}\left(h^3\frac{\partial p}{\partial x}\frac{h^2+4h\mu(\alpha_a+\alpha_b)+12\mu^2\alpha_a\alpha_b}{h(h+\mu(\alpha_a+\alpha_b))}\right)+\frac{\partial}{\partial y}\left(h^3\frac{\partial p}{\partial y}\frac{h^2+4h\mu(\alpha_a+\alpha_b)+12\mu^2\alpha_a\alpha_b}{h(h+\mu(\alpha_a+\alpha_b))}\right)=6\mu U\frac{\partial}{\partial x}\left(\frac{h^2+2h\alpha_a\mu}{h+\mu(\alpha_a+\alpha_b)}\right) \quad (1)$$

It is assumed that the slip length model is used to address the modeling of the slip boundary for the hydrodynamic analysis. The physical meanings of the symbols in Eq. (1) are as follows: h the lubrication film thickness (gap) at location, p the lubrication film pressure, α the slip coefficient (subscripts a and b denote the stationary and moving surfaces, respectively) and μ the lubricant viscosity.

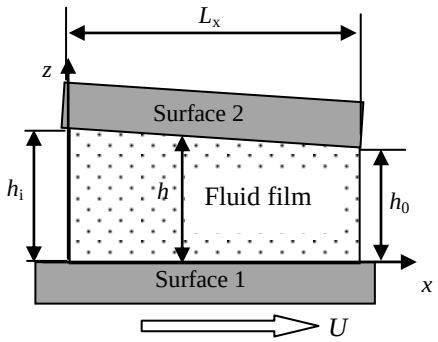

FIGURE 1: *Schematic of a lubricated sliding contact with wall slip (subscripts i and 0 denote the inlet and outlet, respectively).*

3. Methodology

In this work the extended Reynolds equation is solved numerically using a finite volume method. The entire computed domain is assumed as a full fluid lubrication. By employing the discretization scheme, the computed domain is divided into a number of control volumes using a grid with uniform mesh size. The grid independency is validated by various numbers of mesh sizes. An assumption is made that the boundary pressures are null at both sides of the contact. All of the following simulation results will be presented in the dimensionless forms.

4. Results and discussion

The slip boundary effects are investigated for steady state lubricated sliding contact with various surface boundary conditions, i.e. traditional no-slip surface, homogeneous slip surface, and heterogeneous slip surface. In the present study, they are compared each other with respect to the lubrication performance (load support). In all following computations, it is

considered that slip cannot occur on the moving surface ($\alpha_b = 0$ in Eq. (1)).

Since full film lubrication is assumed, the entire load *w* is carried by the lubricant film and the calculation is simply an integration of the lubricant film pressure *p*. The friction force *f* generated by the lubrication system is due to the fluid viscous shear. It is calculated by integrating the interface shear stress over the surface area.

4.1. Traditional no-slip

The behavior of traditional (no-slip) hydrodynamic lubrication between the opposing contact can be estimated by a classical form of the Reynolds equations which is obtained by switching α_a, α_b in Eq. (1) to zero. The derivation of the classical Reynolds equation is based on the assumption of no-slip between the lubricant and the contacting surfaces, i.e. the lubricant velocities at the surfaces are set equal to the surface velocities. In the classical Reynolds lubrication, the mechanism to generate a pressure is due to the wedge effect.

4.2. Homogeneous and heterogeneous slip

In real practice, slip area can be obtained by grafting or deposition of hydrophobic compounds on the initial surface at certain zone. The great challenge for a slip area applied on the surface from the perspective of a numerical simulation is choosing the slip area geometry. There are two kinds of slip area conditions. First, what called as a homogeneous slip and second, as a heterogeneous slip. Homogeneous slip means that slip is applied everywhere on a surface, while heterogeneous slip refers to a surface condition which have one region with slip and another region without slip. Sometimes in other published works, heterogeneous slip is called as mixed slip, complex slip and partial slip. In the present work, it is considered that slip area covers only at certain rectangular zone (ω x *l*) in the inlet as indicated in Fig. 2. Based on the optimization process using genetic algorithm (not shown in this study), the dimensionless geometry of slip zone (region I) of 0.777 x 0.635 is employed. It is assumed that the contact length L_x is set equal to the contact width L_y.

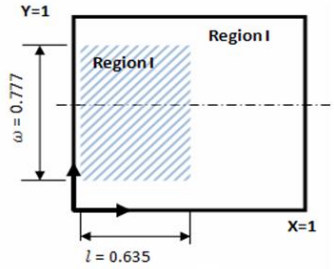

FIGURE 2: *Schematic of a heterogeneous slip surface.*

To explore the effect of wall slip as a function of the operational conditions, model calculations are performed to study the effect of a change in slope incline ratios H_i (where $H_i=h_i/h_o$), and dimensionless slip length *A* (where $A=\alpha\mu / h_0$) on the friction force and the load support.

Below (Figs. 3-5) are the computation results of the dimensionless hydrodynamic pressure distribution, P $\left(\text{where } P = p(h_0^2 / U\mu L_x)\right)$ for no-slip, homogeneous slip and heterogeneous slip analysis respectively in the presence of wedge effect. Computations are conducted with the following base values: dimensionless sliding velocity U^* = 100 where $U^* = 6U\mu L_x / p_e h_0^2$ and A = 20. Figure 3 shows the dimensionless pressure distribution for three cases. The dimensionless load support, W $\left(\text{where } W = w(h_0^2 / U\mu L_x^2 L_y)\right)$ and the dimensionless friction force, F $\left(\text{where } F = f(h_0 / U\mu L_x L_y)\right)$ computed for the no-slip boundary is 1.173 and 45.33 respectively. For the surface of the same configuration but with homogeneous slip (A=20) the corresponding dimensionless load support and the dimensionless friction force is 0.58 and 4.07 respectively. The same trend for friction, i.e. reduction, is found in the literature [1-5]. The reduction in pressure generation and as a result a lower load support, however, is often unwanted. In this case, the load support gained by the addition of slip decreases about an half compared to that of the no-slip surface. The slip

boundary shows a disadvantage over the surface if applied over the whole surface. However, using the heterogeneous slip with the optimized slip area, the improvement of the load support becomes more significant, i.e. 1.83 as indicated in Fig. 3 which shows the highest pressure peak than the other conditions. The friction force is also much lower than the no-slip condition, i.e. 34.30.

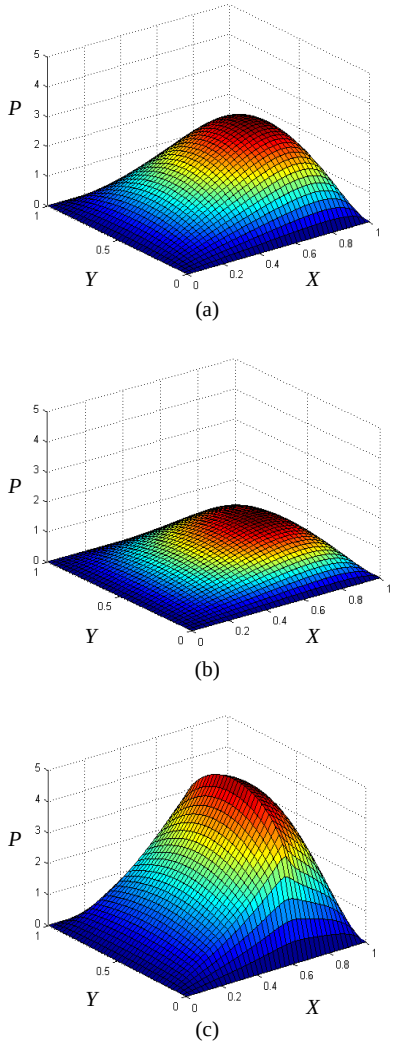

FIGURE 3: *Dimensionless pressure distribution for (a) no-slip analysis, (b) homogeneous sip analysis, and (c) heterogeneous slip analysis. These analyses are evaluated at the same convergent wedge (H_i=2.2).*

Figure 4 is a graph of the variation of the dimensionless load support W with respect to the dimensionless parameter of slope incline ratio H_i. H_i is the ratio of inlet to outlet film thickness and therefore starts at a value of 1, which represents parallel surfaces. Both homogeneous slip boundary and no-slip boundary show a similar trend. They have a zero load support when the surfaces are parallel. The load then increases until its maximum value is attained at H_i is approximately 2, then starts to decrease. It can be observed that the load support for the wall slip is about 0.5 times that of the surface with the no-slip boundary. Opposite with no-slip and homogeneous slip boundary conditions, the optimized heterogeneous slip surface gives more advantages. This boundary still produces high load support even in the absence of the wedge effect.

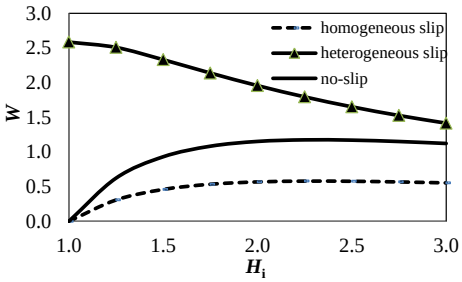

FIGURE 4: *Effect of the slope incline ratio, H_i on the dimensionless load support, W.*

Figure 5 shows the relationship between the dimensionless friction force F and the slope incline H_i. For no-slip and heterogeneous slip situation, as the ratio between the inlet and outlet film thickness increases, the friction force decreases. But for homogeneous slip boundary, as the slope incline increases, the friction force also increases slightly. Compared with the heterogeneous slip and no-slip surface, the homogeneous slip generates a lower friction force. It is as expected because the slip applied everywhere. However, if the load support is of interest, the heterogeneous slip is more advisable because the improvement of load support is more significant and thus as a consequence the friction coefficient will also reduce.

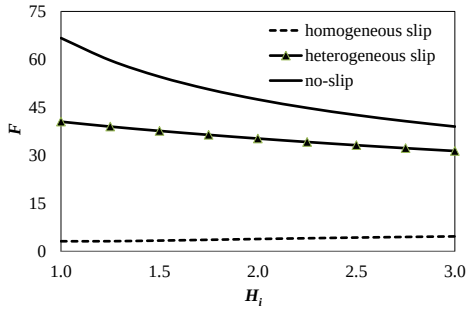

FIGURE 5: *Effect of the slope incline ratio, H_i on the dimensionless friction force, F.*

Figure 6 shows the effect of slip length *A* on the load support *W* of the sliding contact with a homogeneous slip surface (at H_i=2.2), and a heterogeneous slip surface condition (at H_i=1 and 2.2). It should be pointed out that when H_i=1, there is no load support for homogeneous slip for all of slip lengths. Different results will be obtained if heterogeneous slip is employed. The heterogeneous slip condition at parallel surfaces gives more load support than if H_i=2.2 in which at that slope incline, the classical Reynolds equation predicts the maximum achievable load support. This finding may bring us to the conclusion to design lubricated-NEMS which contains moving parts, at parallel contact, to generate hydrodynamic pressure by applying a heterogeneous slip surface.

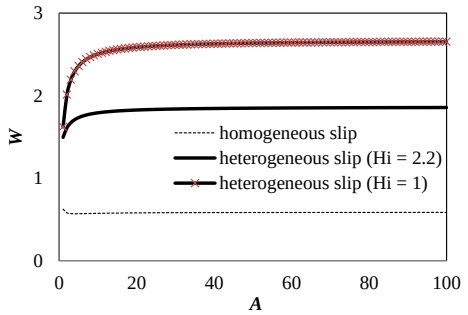

FIGURE 6: *Effect of the slip length, A on the dimensionless load support, W. Homogeneous slip is evaluated at the convergent wedge (H_i=2.2) while heterogeneous slip is evaluated both at H_i =1 and H_i=2.2.*

5. Conclusions

The hydrodynamic lubrication analysis with respect to the friction force and the load support with various surface boundary conditions (no-slip, homogeneous slip and heterogeneous slip) were investigated. It is found that a homogeneous slip boundary on one surface produces a lower hydrodynamic pressure in a lubricated sliding contact at various conditions (slope incline, and slip length), resulting in a reduced load support which reduces the positive effect of slip on friction. However, if the surface is designed as heterogeneous slip pattern, even when there is no wedge effect, the load support is about twice that of corresponding traditional sliding contact. Therefore, it is very advantage to make one of the contacting surfaces in lubricated-NEMS with heterogeneous slip surface for achieving ideal lubrication performance, i.e. reduced friction and increased load support.

References

1. Spikes, H.A., 2003, "The half-wetted bearing. Part 1: extended Reynolds equation," *Proceedings of the Institution of Mechanical Engineers, Part J: Journal of Engineering Tribology* **217**, pp. 1 – 14.
2. Spikes, H.A., 2003, "The half-wetted bearing. Part 2: Potential application in low load contacts," *Proceedings of the Institution of Mechanical Engineers, Part J: Journal of Engineering Tribology* **217**, pp. 15 – 26.
3. Spikes, H..A. and Granick, S., 2003, "Equation for slip of simple liquids at smooth solid surfaces," *Langmuir* **19**, pp. 5065 – 5071.
4. Hild, W., Opitz, A., Schaefer, J.A. and Scherge, M., 2003, "The effect of wetting on the microhydrodynamics of surfaces lubricated with water and oil," *Wear* **254**, pp. 871 – 875.
5. Choo, J.H., Glovnea, R.P., Forrest, A.K. and Spikes, H.A., 2007, "A low friction bearing based on liquid slip at the wall," *ASME Journal of Tribology* **129**, pp. 611 – 20.
6. Salant, R.F. and Fortier, A.E., 2004, "Numerical analysis of a slider bearing with a heterogeneous slip/no-slip surface," *Tribology Transactions* **47**, pp. 328 – 334.

7. Wu, C.W., Ma, G.J. and Zhou, P., 2006, "Low friction and high load support capacity of slider bearing with a mixed slip surface," *ASME Journal of Tribology* **128**, pp. 904 – 907.

M. Tauviqirrahman, Muchammad, Jamari, D.J. Schipper

CFD analysis of artificial slippage and surface texturing in lubricated sliding contact

Resubmitted to Tribology International.

Paper G

CFD Analysis of Artificial Slippage and Surface Texturing in Lubricated Sliding Contact

M. Tauviqirrahman,[1,*)] Muchammad,[1)] Jamari,[2)] and D.J. Schipper[1)]

[1]Laboratory for Surface Technology and Tribology,
Faculty of Engineering Technology, University of Twente, The Netherlands
*Email: mtauviq99@gmail.com

[2]Laboratory for Engineering Design and Tribology,
Department of Mechanical Engineering, University of Diponegoro, Indonesia

Resubmitted to Tribology International, 2013

Abstract **In this paper, based on a CFD model, the effect of slippage on the lubrication performance (load support and friction) of lubricated sliding contacts is discussed. In order to model hydrophobicity, i.e. slippage, the enhanced user-defined-function (UDF) in the FLUENT package is developed. The slippage in the liquid-lubricated sliding contact is controlled by applying a hydrophobic or hydrophilic property at the stationary smooth or textured surface. The results show that a hydrophobic textured surface is superior to a hydrophilic textured one. The results also suggest that the hydrophobicity of a lubricated surface (smooth or textured) enhances the load support and reduces the friction. It is demonstrated that, in comparison with a well-chosen complex slippage smooth surface, a textured surface is still a less efficient way to decrease the friction even if the hydrophobic property is used in the textured region.**

Keywords: hydrophilic, hydrophobic, MEMS (micro-electro-mechanical-system), slippage, surface texture

1. Introduction

In recent times, both miniaturization and the rapid development of micro-electro-mechanical-systems (MEMS) have attracted great attention [1-5]. MEMS-based devices have played a key role in many important areas, for example agricultural industries, transportation, telecommunication, automotive, environmental, monitoring, biomedical, defense systems and a wide range of consumer products. However, the use of MEMS is limited due to adhesion, friction and wear [1, 2]. From there on, every type of MEMS device is susceptible to stiction. The devices are said to suffer from stiction when the internal restoring forces of microstructures cannot overcome surface adhesive force.

As is well known, many MEMS devices include moving (sliding/rolling) surfaces and thus it is necessary to apply a lubricant between the contacting surfaces to reduce friction and wear. The general purpose of lubrication is to minimize friction, wear and heating of machine components which move relative to each other. Understanding lubricant film formation and its effect on load support and friction is one of the main factors. In MEMS, liquid lubrication has generally been omitted due to the high hydrodynamic friction force that occurs in the fluid film. In comparison with a solid coating, stiction prevention using liquid lubrication is less practical. However, recent studies have demonstrated that it is possible for Newtonian liquids to slip along very smooth solid walls [3-5] and this may make liquid lubricants for MEMS devices feasible. Control of the boundary condition will allow a degree of control over the hydrodynamic pressure in

confined systems and is important in lubricated MEMS. One of the treatments developed to eliminate stiction is the development of new materials or design of surfaces and interfaces with hydrophobic behaviour [6-7]. Non-wetting (hydrophobicity) is a critical surface property for materials or devices in micro-applications. The hydrophobicity of a surface is generally presented in terms of a slippage length, which quantifies the extent to which the fluid elements near the wall are affected by corrugation of the surface energy [8].

A number of excellent works have evinced the presence of boundary slippage on a hydrophobic surface [9-13]. It has been demonstrated that the slippage velocity on a hydrophobic surface results in a significant friction reduction in micro-scale flows [11, 12]. For most hydrophilic surfaces, however, no-slippage occurs. In a lubricated sliding contact one is able to enhance, in a controlled way, the hydrophobic/hydrophilic behaviour of the surfaces. If one surface is hydrophobic (slippage) and the other is hydrophilic (no-slippage), the sliding velocity or displacement between the surfaces is accommodated by shear at the hydrophobic surface (the lubricant is kept in the contact by the hydrophilic surface). In this way, wear of the surfaces is prevented and the surfaces are able to move because stiction is prevented. In general, it is feasible to expect promising utilization of boundary slippage in micro-devices such a Micro-Electro-Mechanical-Systems (MEMS) in order to solve the failure of MEMS.

The great challenge for a hydrophobic surface from the perspective of a numerical simulation is choosing a model for the boundary slippage. This is because the hydrodynamic behaviour of lubricated contacts is governed mainly by the boundary conditions of the lubricant that provides lubrication [14-17]. The Navier slippage boundary condition is the most widely used boundary condition to describe boundary slippage with methods based on the solution of the continuum equations. Recently, the use of artificial slippage of surfaces has become popular with respect to lubrication, since this type of surface enhancement would give better tribological performance. Several researchers such as [14-17] have explored the behaviour of the sliding contact using an artificial slippage surface with respect to load support. The results of all these investigations show the existence of a lifting force (load support) even there is no wedge effect (two parallel sliding surfaces) using such a slippage boundary condition.

Another attractive technique for tackling the stiction problem is patterning or texturing the surface with micro/nano-scale dimensions (sometimes referred to as "physical roughness" in this study). The hydrodynamic lubrication theory of textured surface has been studied with strong interest by researchers. This is basically because all surfaces are rough to some extent and generally the roughness asperity height is of the same order as the film thickness height between the lubricated surfaces. Under such conditions surface roughness of mechanical components such as MEMS significantly affects its performance. In recent years, artificial (deterministic) surface roughness (i.e. surface texturing) has been introduced as a surface engineering technique to reduce friction. The most promising technique, originating from investigations, is to modify the contacting surface in a controlled way by laser surface texturing (LST). Friction reduction is obtained by employing different patterns in the form of micro-textures on the surface.

Theoretical analysis of textured surface has generally been carried out using the Reynolds equation [18-26]. However, the increase of engineering problems in complex geometries for which Reynolds equation is unsuited and the increasing availability of user-friendly, commercial CFD codes based on the Navier-Stokes equations mean that the application of CFD simulation is quite effective [24, 27-31].

All the investigations mentioned above are confined to the study of deterministic physical roughness of surfaces with a hydrophilic property, i.e. no-slippage surface boundary condition. Very few researchers appear to have considered the interplay of the surface texture and slippage on lubrication performance. Aurelian *et al*. [32] studied the influence of texture and wall slippage in hydrodynamic bearings. In a recent publication, Rao *et al*. [33] evaluated the effects of texture/slippage configuration on improvement in load support and reduction in friction coefficient for partially

textured slippage slider and journal bearing. Even though major progress has been made in the lubrication of textured slippage surfaces, the majority of work is still based on the Reynolds equation, which means that the inertia-less approach was employed in their model. Therefore, to complement the previous findings by clarifying the interaction of slippage ("chemical treatment") with surface texture ("physical roughness"), it is necessary to make a distinct analysis, based on the CFD approach, of the lubrication property of hydrophobic textured surfaces. As is well known, a CFD approach certainly has advantages over a Reynolds approach when simulating hydrodynamically lubricated contacts. In the CFD approach, no assumptions are made with respect to thin lubricating films or inertia-less liquid flow which are necessary to obtain the Reynolds equation. In some cases, the inertia inside the fluid determines the accuracy of the predicted pressure - and the wall shear stress - profiles. It appears that there is no literature which explores the combined effect of slippage and surface texturing using the CFD technique.

Chemical treatment or physical roughness? This is not only an interesting question, but may also involve different fundamental mechanisms since it is clear that a different experimental set up and models might lead to different results. In the present paper, the two types of approaches (i.e. chemical treatment or physical roughness) are explored as well as the interaction between them with respect to the performance of a lubricated sliding contact. A hydrodynamic lubrication model of an incompressible Newtonian fluid with boundary slippage is proposed based on the Navier-Stokes equations. The model is solved using the finite volume method to obtain the pressure profile and the wall shear stress distribution. The hydrodynamic performance in terms of load support, friction force and friction coefficient is estimated using CFD. A user-defined-function (UDF) to model a boundary slippage in the FLUENT package is developed to simulate the effect of a hydrophobic surface in a deterministic way. To get results, it is intended to first investigate the artificial slippage of a smooth surface. The artificial physical roughness is then explored to obtain the optimum texture parameters. For more accurate results, an entire textured sliding contact (using multiple texture cells without periodic boundary condition) is modelled. Finally, the combination of artificial slippage and textured surface is investigated using CFD. As is known from previous research, the surface texturing as well as surface slippage are an effective means of controlling lubrication performance in lubricated sliding contact. In order to further improve this approach, in the following computations the predicted performance induced by slippage and surface texturing simultaneously will be evaluated in comparison with the performance of an optimum operating smooth (without texturing) sliding contact.

2. Numerical model

2.1. Governing equations of continuum mechanics

The Navier-Stokes equations are solved over the domain using a finite-volume method with the commercial CFD software package FLUENT®. The equations are applied with constant density and viscosity, without body force. The equations are steady and solved in the *x*- and *z*-direction only. With these properties the Navier-Stokes and the continuity equations can be expressed, respectively, as

$$\rho(\mathbf{u} \bullet \nabla)\mathbf{u} = -\nabla p + \eta \nabla^2 \mathbf{u} \quad (1)$$

$$\nabla \bullet \mathbf{u} = 0 \quad (2)$$

2.2. Slippage modeling

With the application of sliding surfaces in very narrow-gap conditions and the availability of hydrophobic materials, the classical no-slippage boundary condition can be broken down. When lubricant slips along a solid-liquid interface, the slippage length β is generally used to address the relation between slippage velocity and surface shear rate, i.e.

$$u_s = \beta \left. \frac{\partial u}{\partial z} \right|_{\text{surface}} \quad (3)$$

where u_s indicates the streamwise slippage velocity at the hydrophobic surface, β denotes the slippage length and $\partial u / \partial z|_{\text{surface}}$ is the surface shear rate. It is usually postulated that a large value of β implies greater slippage.

Furthermore, it is also conventionally implied that the large slippage is also associated with large friction force reduction. Numerous works have demonstrated that the chemical treatment of the surface generates a slippage length of around 1 μm [11], whereas a greater slippage length up to 100 μm can be obtained through a combination of a deterministic textured structure and a hydrophobic surface [4, 34, 35]. In the present study, the slippage length of a hydrophobic surface is assumed as uniform in space.

In order to model the Navier slippage behaviour in ANSYS-FLUENT, it is necessary to make an additional subroutine to enhance FLUENT's capability and customize its feature for a lubrication modelling analysis. This subroutine. known as User-Defined-Function (UDF), is a function that allows a user to define the boundary conditions, material properties and source terms for the flow regime, as well as to specify customized model parameters [36]. In this way the Navier slippage boundary condition can be applied to surfaces of the lubricated sliding contact.

2.3 Boundary conditions and solution procedure

For either a stationary smooth or textured surface, two different surface types are considered in this study: hydrophobic (slippage) and hydrophilic (no-slippage) surfaces. In addition to the smooth surface case, the artificial rough surface with and without boundary slippage condition is of particular interest. It means that at the solid walls, the "slippage" boundary condition was allowed to occur in a deterministic way in a certain region for the momentum equations. Cavitation is not considered in the present work. A main assumption of the CFD model presented here is the sole existence of full hydrodynamic lubrication (i.e. no contact between the surfaces is permitted). At the inlet and outlet of the domain, the pressure was set to atmospheric and a zero velocity gradient in the direction normal to sliding was assumed. This can also be thought of as a fully developed flow approximation.

A Newtonian laminar flow model was assumed for the solution. All the cases in this study will be regarded as isothermal and therefore the energy conservation equation is not included. The control volume-based technique was employed to numerically solve the Navier-Stokes equation. The second order upwind scheme was applied for momentum discretization and the SIMPLE procedure was used for pressure-velocity coupling in the calculations. All calculations have been performed with double-precision and the iterative error has been reduced to machine accuracy. Therefore, the numerical uncertainty is mainly due to the discretization error.

In the CFD approach, meshing of the computational domain is needed in order to solve the continuity and momentum equations over each grid cell. The high resolution scheme in FLUENT is used to discretize. It should be noted that the meshing process for the smooth and textured surfaces has been checked to ensure grid independent results. For the smooth surfaces a grid of 200x40 hexahedral elements in *x*- and *z*- direction respectively is used. For the textured surfaces the number of elements of the grid is higher than in the smooth case. The generated grid for these simulations is composed of around 500x100 elements since a finer mesh is used in the textured area. For partially textured surfaces several divisions in the textured region are used in the film direction in which a non-uniform mesh is employed, whereas a uniform mesh is applied in the untextured region.

3. Results and Discussions

The load support, the viscous friction force and the friction coefficient are a good measure of the effectiveness of the artificial slippage and deterministic rough surface. Load support of a lubrication film can be achieved by the integration of the hydrodynamic pressure on the bottom (moving) surface, and the friction force can be obtained by integrating the shear stress on the bottom surface of the lubrication film (see Fig. 1). In the present work, the friction coefficient is defined as the ratio of the friction force per unit length to the load support per unit length.

The boundary slippage effects are first investigated for the case of a lubricated sliding smooth surface by varying the slope incline ratio h^* (inlet over outlet film thickness) to introduce the wedge effect. A parameter is introduced in order to define the slippage region L_s as presented in Fig. 1a. For the slippage zone L_s which is set equal to the contact length L, the boundary slippage is termed as "homogenous slippage" ($L_s = L$) which means the slippage is applied everywhere along the contact length. For the slippage zone which covers only a specific zone of the surface, the term "artificial complex slippage" is used. In the present study, therefore, the complex slippage condition is preferred when the ratio of the slippage zone L_s to the contact length L is less than 1. Next, the study is extended to the influence of surface texturing with no-slippage (Fig. 1b). Finally, surface texturing combined with slippage (texture/slippage combination) as indicated in Fig. 1c is explored. In this study, the shape of the texture cell is chosen to be rectangular. As noted, most of the results from the literature review show that there is a little effect of the texture shape on the tribological performances of the LST (laser surface textured) surfaces. In addition, based on recent publications [37, 38], in relation to the orientation effect of the texture on sliding surfaces, it was stated that for non-circular texture shapes, which are similar to what is used in this study, the strongest hydrodynamic load support is offered when its main axis is perpendicular to the sliding direction.

To analyse the effect of slippage of a hydrophobic surface on lubrication, the simulation was performed for a value of the slippage length proportional to the slippage length in the experimental work of Choo *et al.* [3]. Hence, a slippage length of 20×10^{-6} m was considered for all following computations.

In the analysis of a textured parallel sliding surface, a texture cell is characterized by three non-dimensional parameters: the texture density α (defined as the ratio between the dimple length l_d and the texture cell length l_c), relative dimple depth K (defined as the ratio between the dimple depth h_d and the land film thickness h_f), and the texture aspect ratio λ (defined as the ratio between the dimple length l_d and the dimple depth h_d) as shown in Fig. 1b and 1c. It is assumed that h_f is set equal to h_o.

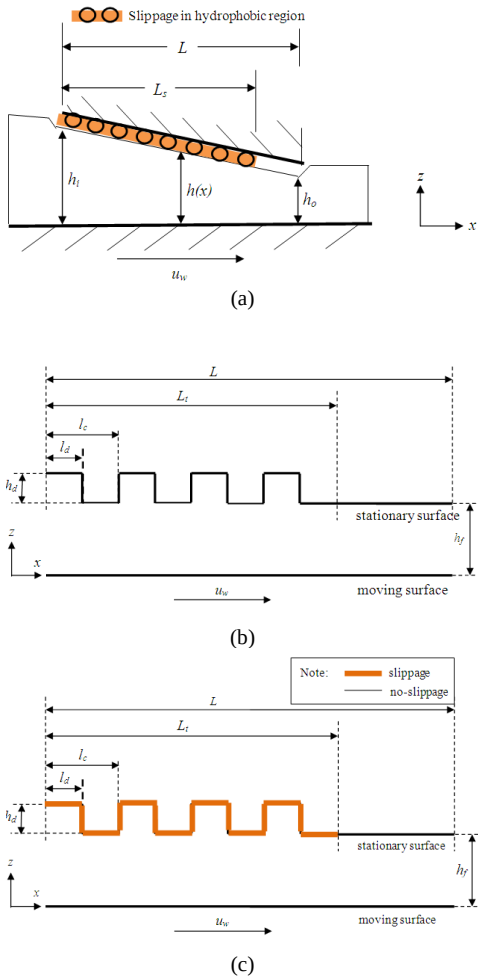

FIGURE 1: *Schematic of a lubricated parallel sliding contacts with: (a) artificial slippage, (b) artificial roughness ("hydrophilic textured pattern"), (c) artificial roughness combined with an artificial slippage ("hydrophobic textured pattern").*

The simulations have been carried out for various cases as described in Table 1. For the first case, i.e. smooth classical (no-slip) surface, the prediction of load support is conducted when the wedge effect is present ($h^* > 1$). As known, the converging wedge is considered as the first

important condition for producing hydrodynamic pressure in a lubrication film between two solid surfaces with a relative sliding/rolling motion. A maximum hydrodynamic load support can be obtained by adjusting some geometrical parameters, such as the slip region, texturing region and texture cell aspect ratio [17]. In the present study, the exploitation of the slip phenomena and the texturing characteristics to improve the performance of a sliding contact, with an emphasis on increasing load support and reducing friction coefficient, are examined by means of numerical analysis. Further, by comparing the results with the traditional (no-slip, smooth) lubricated contact at an optimal slope incline ratio, the optimized parameters of a pattern containing chemical treatment and physical roughness with respect to load support can be proposed. All parameters and the range in which they are varied for all cases investigated are summarized in Table 2. It should be pointed out that when h^* equals 1, the traditional (no-slip, smooth) contact has zero load support. In the present paper, simulation results will be presented in non-dimensional form.

TABLE 1: *Simulated type of contact.*

	Type of surface	Type of condition
Case 1	Traditional	No-slippage
Case 2	Artificial slippage	Homogeneous and complex slippage
Case 3	Hydrophilic textured	Partial texturing
Case 4	Hydrophobic textured	Partial texturing

TABLE 2: *Simulated parameters.*

Parameter	Data setting	Unit
Slip length β	$20\text{x}10^{-6}$	m
Slope incline ratio h^*	1 – 3	[-]
Non-dimensional slippage region S^+	0 – 1	[-]
Non-dimensional textured region T^+	0 – 1	[-]
Texture density α	0.7	[-]
Relative dimple depth K	1	[-]
Dimple aspect ratio λ	5 – 300	[-]

3.1. Validation of solution method

It is necessary to test that the CFD code developed generates the mesh density needed to obtain an accurate solution (especially for the cases of textured surfaces), to handle the elements reliably and to treat the slippage modelling of a hydrophobic surface. This was done in two steps: first by considering an infinitely long Rayleigh step bearing case with the known Reynolds solution and later by considering the lubricated case containing an artificial homogeneous slippage.

3.1.1. No-slippage case

For the first validation, an infinitely long, linear step bearing as shown in Fig. 2 was analysed. In this case, the sliding velocity of the lower surface u_w is 1 m/s (the corresponding Reynolds number R_e is 0.1 assuming a fluid density ρ of $1\text{x}10^3$ kg/m^3 and a dynamic viscosity η of $1\text{x}10^{-2}$ Pa.s), the total length of the lubricated contact L is $20\text{x}10^{-3}$ m, the length of the textured region L_t is $10\text{x}10^{-3}$ m and the inlet h_i and outlet film thickness h_o are $2\text{x}10^{-6}$ and $1\text{x}10^{-6}$ m respectively. The numerical results for such a case are compared with the analytical solution [39].

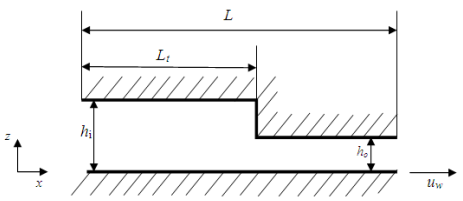

FIGURE 2: *Rayleigh step bearing.*

Table 3 shows the non-dimensional maximum hydrodynamic pressure, the total load support and the friction force, and their corresponding deviations, where the deviation is defined as the difference between the absolute values obtained from the analytical and the CFD solution divided by that of the analytical solution. It can be observed that the hydrodynamic profiles of load support, friction and friction coefficient are in close agreement. The prediction of the pressure distribution by the CFD calculation and the analytical solution are presented in Fig. 3.

TABLE 3: *Non-dimensional maximum hydrodynamic pressure p^+, load support w^+, and friction force f^+ predicted by analytical solution and CFD.*

Solution	p^+_{max} [-]	Deviation of p^+_{max} [%]	w^+ [-]	Deviation of w^+ [%]	f^+ [-]	Deviation of f^+ [%]
Analytic [39]	1.333	-	0.667	-	1.833	-
CFD [present]	1.333	0.030	0.665	0.225	1.833	0.033

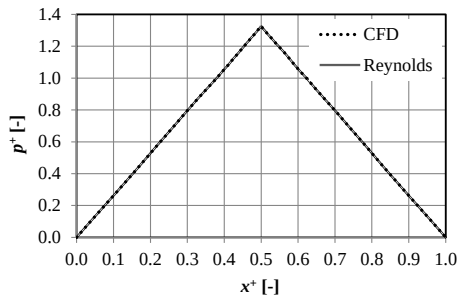

FIGURE 3: *Comparison between the pressure distribution predicted by CFD (present study) and Reynolds equation (analytical solution).*

3.1.2. Slippage case

The aim of this section is to examine whether the computational fluid dynamic (CFD) technique could be used to handle slippage in the hydrophobic region for the lubricated MEMS application. It will be shown that commercial CFD software can be modified to meet such requirements with enhanced UDF (User-Defined-Function) subroutines.

A number of different variants of the Reynolds equation have been proposed during the years to include slippage [14-17, 32, 33, 40, 41]. In this section, the CFD approach (based on the NS equation) containing a UDF slippage code is compared to the modified Reynolds solution where the slippage terms are taken into account (see Refs. [3, 4] for more details of the derivation of modified Reynolds equation).

The simple lubricated sliding contact shown in Fig. 1b is of particular interest. This is a linear wedge, with a hydrophilic smooth surface and moving with velocity $u = u_w$ against a hydrophobic stationary surface with a homogeneously distributed boundary slippage (in this case $L_s = L$, see Fig 1b). The lubricated contact slope is defined by the slope incline ratio $h^* = h_i/h_o$, where h_i and h_o are, respectively, the inlet and outlet film thickness. The primary parameters of the smooth lubricated contact are given as follows: the h_i and h_o are $2.2\text{x}10^{-6}$ m and $1\text{x}10^{-6}$ m, respectively, the overall contact length $L = 1\text{x}10^{-3}$ m and the slippage length β is $20\text{x}10^{-6}$ m. In this simulation, the Reynolds number R_e is 1 (the the corresponding sliding velocity u_w is 1 m/s) assuming the fluid density ρ_l is $1\text{x}10^3$ kg/m^3 and the dynamic viscosity η is $1\text{x}10^{-3}$ Pa.s, a value that is in the domain of validity of the Reynolds equation as explained in [24]. For the same calculation conditions of references [3, 4], it is shown that the numerical results based on CFD solution for smooth lubricated sliding contact with slippage are right.

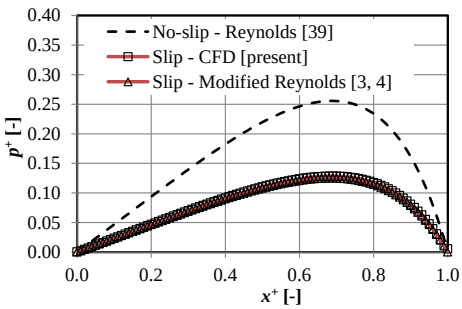

FIGURE 4: *Comparison between the pressure distribution obtained with CFD (Navier-Stokes equation) and the modified Reynolds solution* [3, 4] *in the case of homogeneous slippage condition. The profiles are calculated for $h^* = 2.2$ and $R_e = 1$. The solid curves with symbols are the theoretical predictions for the slippage pattern; the dashed line are those predicted by the analytical solution* [39] *for the no-slippage situation*

In Fig. 4, the pressure distribution has been plotted as a function of the spatial dimension for the Navier-Stokes and the Reynolds solutions, respectively. Comparison is also made to the classical (no-slippage, smooth) case where the analytical solition has been given in [39] so that the effect of homogeneous slippage on the hydrodynamic pressure of the lubricated sliding contact can be investigated. As shown in Fig. 4, the results presented here are in general agreement with the reference result. With the value of *Re* = 1 in Fig. 4, the Navier-Stokes and the modified Reynolds equation are much alike. The results clearly show that in case of a homogeneous slippage, the hydrodynamic pressure decreases. The maximum pressure for slippage situation is half of the pressure of the corresponding classical (i.e. no-slippage) lubricated contact. The boundary slippage will reduce the pressure through the reduction of the velocity gradients at the surface as shown in Fig. 5. The hydrodynamic pressure gradient of the homogeneous slippage case is continuous as well as in the no-slippage case. This confirms findings of the study made by other researchers [15, 17, 40].

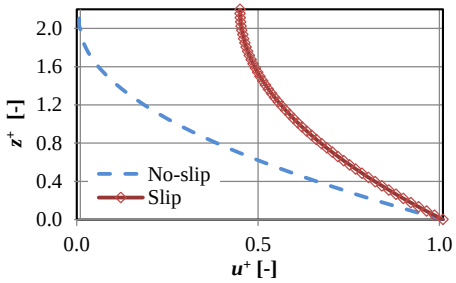

(a)

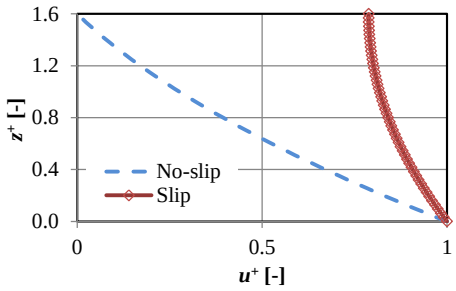

(b)

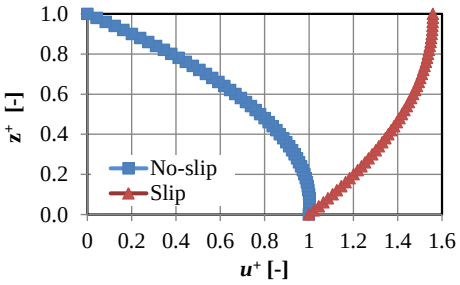

(c)

FIGURE 5: *Velocity distribution at (a) the beginning, (b) the middle and (c) the end of lubricated sliding contact. All slippage profiles are calculated by CFD simulation.*

Figure 6 summarizes the ratio of the hydrodynamic performance parameters (load support *W*, friction *F*, and friction coefficient μ) with a homogeneous boundary slippage to that without slippage predicted by the CFD model and the modified Reynolds solution. In the following computations, the performance ratio is defined as the ratio of hydrodynamic parameter (w, f, μ) predicted for the engineered surface to that by classical (no-slippage, smooth) surface calculated for $h^*_{opt\_w}$ of 2.2. It is shown that the load support decreases to about a half compared to that of the no-slippage surface. Compared to the traditional no-slippage surfaces, the friction force is decreased significantly when a homogeneously distributed slippage boundary is employed (by 80% lower). It is interesting to note that the value of w^+/w^+_{ns} and f^+/f^+_{ns} are similar with those given in Refs. [15, 40] although the slippage model and the numerical method used are different. The numerical calculations also show that, under the running conditions chosen, only a small deviation in predicting the μ^+/μ^+_{ns} between the two approaches can be observed. The deviation is within 3 %. Globally, the deviation is in the permissible range, which validates that the CFD based calculation method is correct. The results are encouraging from two viewpoints: verification of the CFD code and justification of using a CFD approach. In addition, from a CFD viewpoint, the results are encouraging because of the possibilities of extending the simulations

of the hydrodynamic lubrication conjunction to include more inertia for simulating lubrication in high speed MEMS.

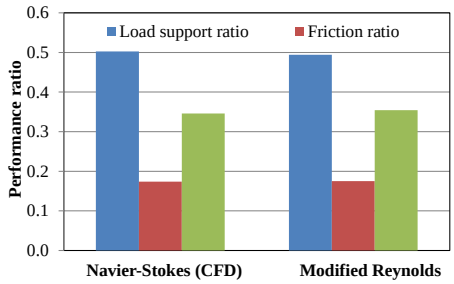

FIGURE 6: *Effect of homogeneous slippage in the hydrophobic region on the performance ratio for two different approaches, i.e. the Navier-Stokes equation (left) and the modified Reynold equation (right). Both slip and no-slip results are obtained for the same h^* (i.e. $h^* = 2.2$).*

3.2. Artificial slippage on smooth surface

Recently, the use of artificial (deterministic) slippage has become popular with respect to lubrication, since this type of surface enhancement would give a better tribological performance. Two artificial slippage modes are used: homogeneous slippage and complex slippage. In this study, the artificial complex slippage is of particular interest. This because of the fact that it is known that a complex slippage is superior to a homogeneous slippage with respect to load support as discussed in the previous section and literature [15, 17]. The geometry of the lubricated sliding contact is presented in Fig. 1a. The slippage region L_s is varied to create an optimal complex slippage with respect to the load support. The complex slippage condition is referred when the ratio of the slippage zone L_s to the contact length L is less than 1. In this computation, based on the work of [41], with respect to the maximum load support, it is considered that hydrophilic property is applied to the moving surface so that slippage does not occur on that surface. Reynolds number R_e of 1 indicating laminar flow was chosen.

Figure 7 shows the effect of the non-dimensional length of slippage region, s^+ on the ratio of the non-dimensional load support of a complex slippage surface, w^+ to that of a no-slippage surface, w^+_{ns} for several slope incline ratios h^*. w^+_{ns} is evaluated at $h^* = 2.2$. It is found that the complex slippage surface gives the highest load support when a slippage zone covers 0.65 times the length of the contact ($S^+ = 0.65$) and the the wedge effect is absent (i.e. $h^* = 1$). However, the classical (smooth, no-slip) contact ($S^+ = 0$) predicts that only when $h^* > 1$ the hydrodynamic pressure can be built up, and the maximum load support occurs when $h^* = 2.2$, which agrees with the exact solution [38]. An artificial complex slip surface with parallel moving surfaces can increase the maximum load support by approximately two times when compared to what a classical (no-slip) contact predicts for an optimal slope incline ratio (i.e. $h^* = 2.2$).

Figure 7 clearly shows that two parallel moving surfaces with an optimized complex slippage surface can also provide load support. It is interesting that this value is similar with those given in Ref. [15, 33] although the slippage models and numerical methods used are different. The maximum load support for such complex slippage surface is over twice that of the corresponding traditional lubricated contact. However, it must be underlined that for $h^* = 1$, if the stationary surface is designed as a homogeneous slippage surface ($L_s/L = 1$), the numerical results show that there is no load support for parallel sliding surfaces. If the stationary (top) surface is a homogeneous slip surface ($S^+ = 1$), the numerical solution suggests that the load support is only 50% of that of the corresponding conventional sliding contact. This agrees with other numerical analysies [15, 17, 40].

The relationship between the friction force, the slope incline ratio, and the length of slippage region is given in Fig. 8. It can be seen that in the investigated slope incline ratio range, for $S^+ < 0.65$, the decrease in the friction force is not sensitive to the length of the slippage region especially for high h^* (in this case $h^* = 2.2$ and 3.0). However, for values of S^+ larger than 0.65 the friction force decreases significantly for all values of h^*. In comparison to the optimum classical (no-slip) contact, for $S^+ < 0.65$, the artificial slippage gives a little improvement of the friction force reduction when a high slope incline ratio is employed. It indicates that the

wedge effect has a small effect in reducing the friction force. For example, for the artificial complex slippage contact with a slippage region of 0.50 and a slope incline ratio of 3.0, the friction force differs from the optimum classical (smooth, no-slip) surface by only 6 % (lower). As the h^* is decreased to 1 (i.e. parallel moving surfaces), at the same length of the slippage region (i.e. S^+ = 0.5) the difference in friction force increases (it is up 10 % higher). For all values of h^*, the friction force becomes smaller than that of a traditional sliding contact after S^+ is larger than about 0.65. However, from Fig. 8, for parallel sliding surfaces, the advantage of employing an optimized artificial slippage is clear. The decrease in friction force becomes larger when S^+ is larger than 0.65. This has also been confirmed by literature [15]. Generally, it indicates that the wedge effect weakens the hydrodynamic effect by slippage.

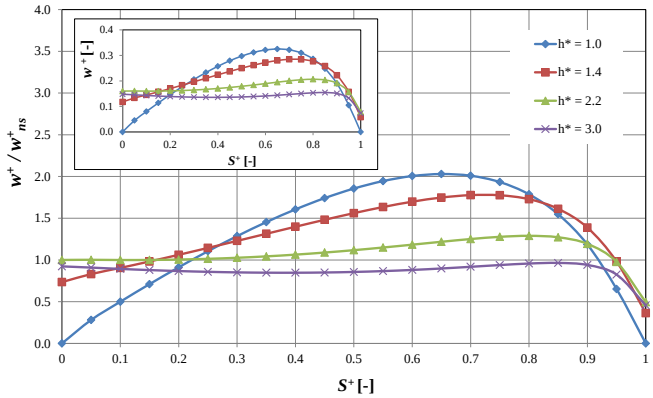

FIGURE 7: *Effect of the length of the non-dimensional slippage region, S^+ on the ratio of the non-dimensional load support of a artificial slippage surface, w^+, to that of a no-slippage surface, w^+_{ns}, for several slope incline ratios, h^*. w^+_{ns} is evaluated at $h^*_{opt\_w^+}$ = 2.2. The insert shows the corresponding non-dimensional load support, w^+, for complex slippage.*

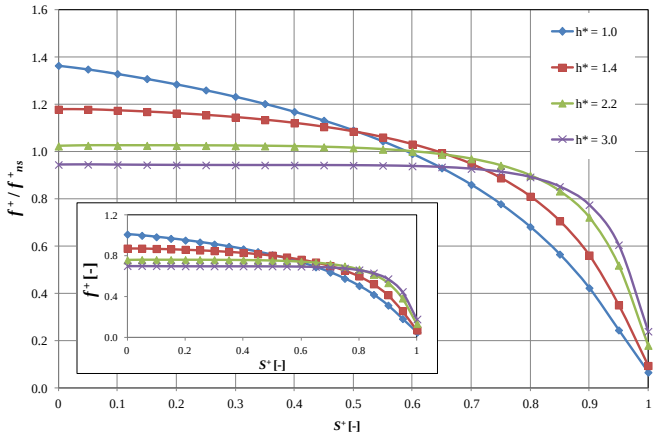

FIGURE 8: *Effect of the length of the non-dimensional slippage region, S^+, on the ratio of the non-dimensional friction force of a artificial slippage surface, f^+, to that of a no-slippage surface, f^+_{ns}, for several slope incline ratios, h^*. f^+_{ns} is evaluated at the optimized slope incline ratio ($h^*_{opt\_w^+}$ = 2.2). The insert shows the corresponding non-dimensional friction force, f^+, for complex slippage.*

The effect of the slippage parameter on the load support and the friction force can be better analysed using the non-dimensional friction coefficient. Figure 9 demonstrates the effects of the non-dimensional length of the artificial slippage region on the friction coefficient for different slope incline ratios. As can be seen in Fig. 9, in the case of paralell sliding surfaces, increasing the length of the slippage region S^+ from 0.05 to 0.6 has a significant effect on the friction coefficient. However, for S^+ is, say, 0.6 and above, the friction coefficient is not influenced considerably with further increase of the value of the slippage region. It can be said that the optimum value of S^+ = 0.65, which maximizes the load support, see Fig. 7, is close to those corresponding minimum friction coefficient. One can remark that for parallel sliding surface (i.e. h^* = 1), when S^+ = 0 and S^+ = 1, the predicted friction coefficient are very large, not shown in Fig. 9, due to the inability of such surfaces in generating the load spport (w^+ = 0). In comparison to the optimum classcical (no-slip, smooth) contact, the benefit of the artificial slippage with a large slope incline ratio (h^* = 3.0) is not as effective as that with a very low slope incline ratio (h^* = 1.0). This is consistent with the result presented in Figs. 7-8 which shows that for high h*, the improvement of the lubrication performance is not very significant and such contact behaves like the convenional no-slip moving surface situation.

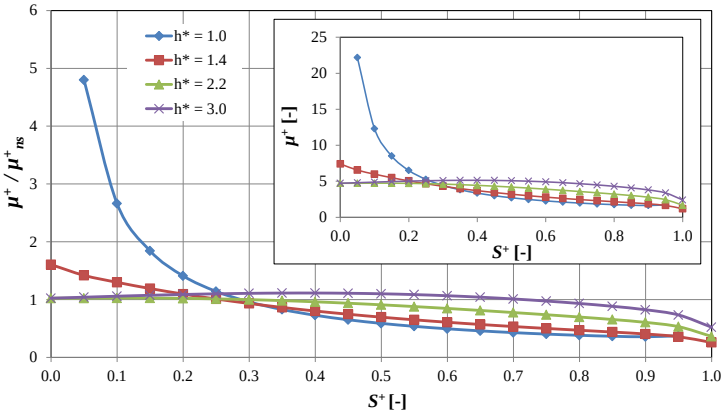

FIGURE 9: *Effect of the length of the non-dimensional slippage region, S^+, on the ratio of the non-dimensional friction coefficient of a complex slippage surface, μ^+, to that of a no-slippage surface, μ^+_{ns}, for several slope incline ratios, h^*. μ^+_{ns} is evaluated at the optimized slope incline ratio ($h^*_{opt\_w^+}$ = 2.2). The insert shows the corresponding non-dimensional friction coefficient, μ^+, for complex slippage.*

Figure 10a shows the non-dimensional pressure p^+ related to the non-dimensional spatial location x^+ and variable slope incline ratio h^*, where the typical slippage parameter, S^+ = 0.65. It can be seen that the maximum pressure distribution for parallel sliding surfaces is approximately three times as large as the maximum pressure obtained from a no-slippage wedge when h^* = 2.2. One can remark that when the slope incline ratio is 2.2 or larger, the benefit of employing an artificial complex slippage surface will vanish. In other words, the configuration of the surface with high slope incline ratio (h^* = 3.0 in this case) is not advisable for improving the load support: a classical configuration with optimized slope incline ratio ($h^*_{opt\_w^+} = 2.2$) is recommended. Therefore, for maximum load support, it is very beneficial to construct the parallel sliding surface configuration.

The non-dimensional shear stress distribution, τ^+_{xz}, with artificial slippage (S^+ = 0.65) is shown in Fig. 10b. The variation of the non-

dimensional shear stress distribution in the hydrophobic region is not significant for all values of the slope incline ratio. However, in the hydrophilic region (no-slip), the non-dimensional shear stress decreases significantly for small h^* (h^* = 1 in this case). It indicates that in addition to the improvement of the load support, the artificial slippage with uniform film thickness is also effective for reducing the friction force.

The conclusion of this section is that the right choice of the arrangement of the length of the slippage region on one of the lubricated surfaces has a very positive effect with respect to the lubrication performance as summarized in Fig. 11.

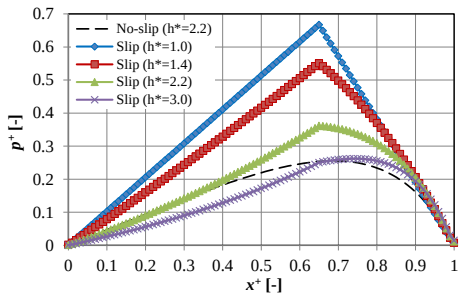

(a)

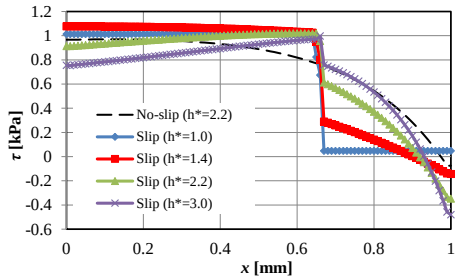

(b)

FIGURE 10: *(a) Non-dimensional hydrodynamic pressure distribution, p^+, and (b) non-dimensional surface shear stress, τ_{xz}^+, for several slope incline ratios, h^*, generated by a complex slippage surface ($S_{opt\_w^+}^+ = 0.65$).*

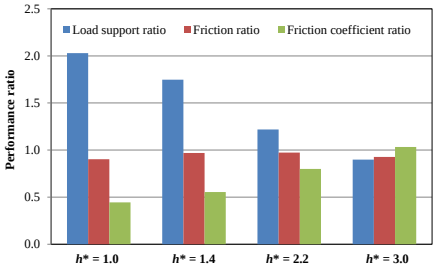

FIGURE 11: *The effect of an optimized complex slippage in the hydrophobic region ($S_{opt\_w^+}^+ = 0.65$) on the performance ratio for several slope incline ratios, h*. (Note : The performance ratio is defined as the ratio of hydrodynamic parameter (w+, f+, μ+) predicted for slippage surface at the corresponding h* to that by a no-slippage surface at h* of 2.2).*

3.3. Interaction of boundary slippage with artificial surface roughness

In addition to the artificial chemical surface treatment, it is believed that the artificial physical roughness can lead to an improved hydrodynamic performance and has attracted researchers to study this more deeply. It is interesting to study the combination of the artificial slippage and the artificial roughness at lubricated parallel sliding contacts. A parametric analysis, in non-dimensional form, is performed in order to investigate the effect of various texture parameters on the lubrication performance. In this analysis, to obtain an estimate of the performance benefit of boundary slippage (hydrophobic) on artificial surface roughness (surface texture), the comparison should be made between a hydrophilic textured surface and a hydrophobic textured surface having the same texture parameter.

3.3.1. Hydrophilic textured surface

In the case of a parallel sliding surface, in order to improve the hydrodynamic effect, it is accepted that the most important process of surface texture design is to maximize the additional hydrodynamic pressure and thus the load support. For traditional (smooth, no-slip) parallel contact, no load support takes place. Therefore, the parameters that have been found most important in affecting the load support will

be investigated, i.e. the texture density α, relative dimple depth K, texture cell aspect ratio λ, and non-dimensional textured region T^+. In this study, the first two parameters are fixed. Relative dimple depth K of 1 was chosen, a reasonable value for an optimium lubrication performance of textured contact (i.e. the maximum load support and the minimum friction force) based on the work of Shi and Ni [31], while the texture density α chosen is 0.7. The variation in texture cell aspect ratio is achieved by modifying the dimple length l_C while keeping a constant land film thickness h_F and dimple depth h_D.

Figure 12 shows the non-dimensional load support which is plotted against the textured region T^+ for large and small texture cell aspect ratio, i.e. λ = 40 and 5. It should be noted that for small λ used in this study, according to Dobrica and Fillon [24], the Reynolds theory approach is inapplicable whatever the R_e number due to the violation of the assumption of small variations in film thickness compared to the feature length. Two observations can be made based on Fig. 12. At first, for reasonable values of the texture aspect ratio and dimple density, the optimum non-dimensional textured length $T^+_{\text{opt\_}w^+}$ is around 0.55. This result corresponds to the one obtained by Etsion and Halperin [42], based on a numerical solution of two-dimensional Reynolds equation, for textured parallel thrust bearings, and later by Pascovici *et al.* [23], based on an analytical solution of the one dimensional Reynolds equation, for partially textured parallel sliding contact. Secondly, full texturing (in this case T^+ = 1) gives the lowest non-dimensional load support which is close to zero for all values of texture aspect ratio λ. This has also been confirmed by recent work [24, 43]. It means that the presence of a texturing zone at the leading edge of the contact produces this positive effect. From the insert of Fig. 12, one can remark that for λ > 80, the load support no longer varies significantly with λ. It indicates that compared to the optimum classical (smooth, no-slip) contact, the textured surface with high λ gives no improvement of load support.

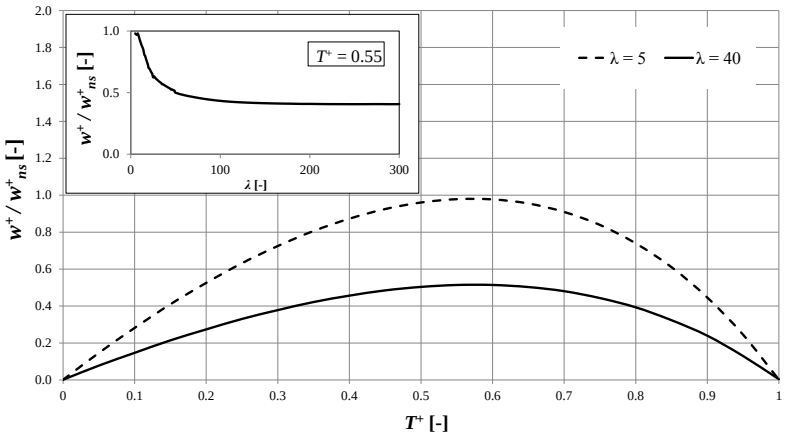

FIGURE 12: *Effect of the non-dimensional length of the textured region, T^+, on the ratio of non-dimensional load support of a textured surface, w^+, to that of a no-slippage surface, w^+_{ns}, for low and high texture cell aspect ratio λ. w^+ is evaluated for two parallel sliding surfaces, whereas w^+_{ns} is evaluated for the optimized slope incline ratio ($h^*_{opt\_w^+}$ = 2.2). The insert shows the effect of the texture cell aspect ratio λ on the non-dimensional load support.*

The combined effect of texture parameters (T^+ and λ) on load-support and friction force can be better analyzed using the non-dimensional friction coefficient. Its variation as a function of the non-dimensional length of the textured region for two values of the texture cell aspect ratio is presented in Fig. 13. It is shown that extending the length of the textured region results in a decrease-then-increase behaviour of the friction coefficient. This trend prevails for

high and low values of texture cell aspect ratio. Also shown in Fig. 13 is that the non-dimensional friction coefficient reaches a minimum value of 6.29 and 11.61, respectively, for λ = 5 and 40 for textured region T^+ = 0.60. Analyzing Figs. 12 and 13, one can remark that the optimum length of the textured region has very close optima for both criteria (minimum friction coefficient and maximum load support respectively), which agrees with literature [23] very well.

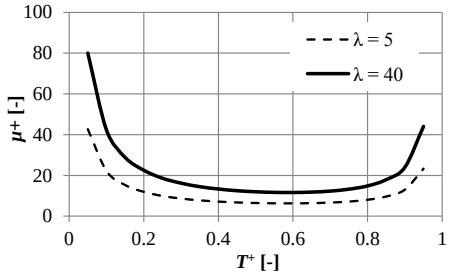

FIGURE 13: *Non-dimensional friction coefficient μ^+ versus non-dimensional length of the texture region T^+ in the case of hydrophilic textured pattern.*

Given the non-dimensional texture cell aspect ratio T^+ equal to 0.55, Fig. 14 examine the surface normal pressure distributions and the wall shear stress corresponding to different texture cell aspect ratios λ. It is clear that with the decrease of λ, the hydrodynamic pressure continuously increases, whilst the wall shear stress decreases especially in the untextured region. As depicted in Fig. 15, compared to the hydrophilic textured pattern with high λ, the textured one with low λ can improve the load support and decrease the friction force, and thus reduce the friction coefficient. However, this configuration is less effective for reducing the load support compared to the optimum classical contact.

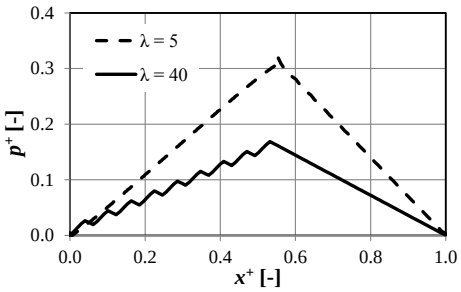

(a)

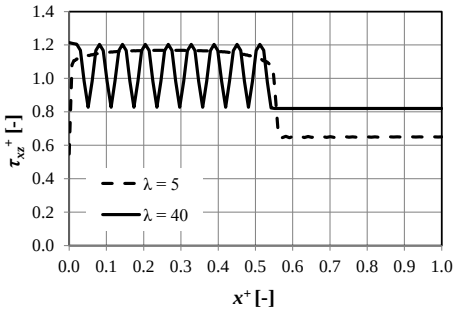

(b)

FIGURE 14: *Hydrophilic textured surface: (a) non-dimensional hydrodynamic pressure distribution, p^+, (b) non-dimensional surface shear stress, τ_{xz}^+, for two values of λ. All profiles are calculated at the optimized texturing region ($T^+_{opt\_w^+}$ = 0.55).*

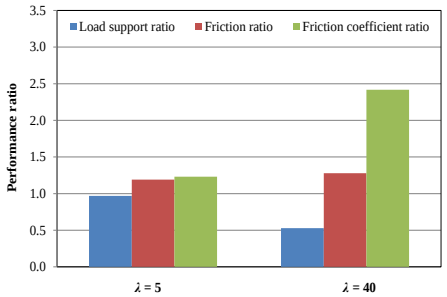

FIGURE 15: *Effect of the texture cell aspect ratio on the hydrodynamic performance parameters of lubricated sliding contacts evaluated for a parallel partially textured sliding contact with T^+ = 0.55.*

3.3.2. Hydrophobic textured surface

In real application, a slippage pattern can be obtained by treating the surface with a hydrophobic chemical treatment. This can be accomplished by techniques such as film or molecule deposition, solution coating or self-assembly of hydrophobic layers. In this section, with respect to the lubrication performance, the combination of the artificial physical roughness and chemical treatment is investigated numerically in terms of load support, friction force, and friction coefficient. Again, their predicted performance is compared to the optimum conventional (no-slip, without texture) contact. In the present work, the optimum texture parameters of the textured surface (with hydrophilic condition) discussed in the previous section ($T^+ = 0.55$ and $\lambda = 5$) are used.

It is interesting to check whether a different arrangement of the slippage boundary on the texture cell has a significant effect on the tribological performance. In this section, four arrangements of slippage, applied to create four hydrophobic textured configurations (see Fig. 16), are proposed and compared with each other.

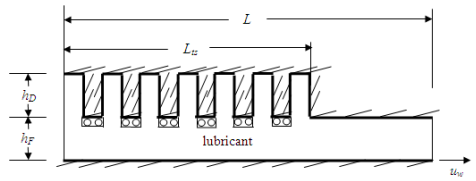

(a)

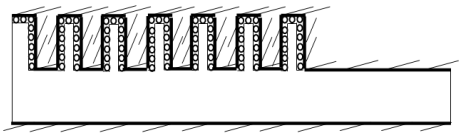

(b)

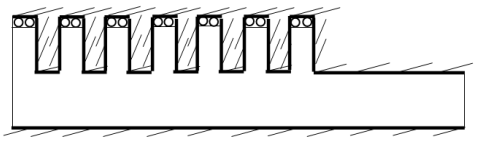

(c)

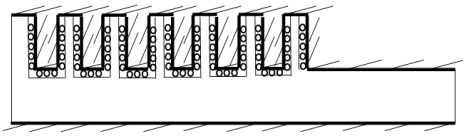

(d)

FIGURE 16: *Four configurations of boundary slippage of hydrophobic textured surface: (a) "bottom slip", (b) top-multiple slip (c) "top slip", (d) "bottom-multiple slip".*

The results, as indicated in Fig. 17a, suggest that for the same textured region and texture cell aspect ratio, a surface with "bottom-multiple slip" (i.e. configuration *d*) generates a larger non-dimensional hydrodynamic pressure profile compared to the others.

Figure 17b shows the non-dimensional wall shear stress for all hydrophobic (slippage) partially textured configurations. As shown in Fig. 17b, the results show that the variation of shear stress distribution for all configurations is not significant. However, configuration *d* gives a lower non-dimensional shear stress distribution especially in the untextured region compared to other configuration. It means that configuration *d* generates a lower friction force, and thus a lower friction coefficient. It is worth noting that all shear stress curves do not vary much. It indicates that the friction force is not that sensitive to the arrangement of boundary slippage. However, for the untextured part of the sliding contact ($x^+ > 06$), configuration *d* gives lower values, and as a result the friction force is reduced. Obviously, this trend can also be observed in Fig. 18. The predicted friction force ratio f^+ / f_{ns}^+ ranges from 1.01 to 1.10, which means that compared to the optimum classical contact, no significant change in friction force is obtained using artificial physical roughness no matter how the slip is applied.

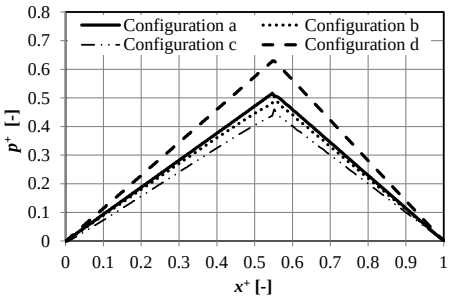

(a)

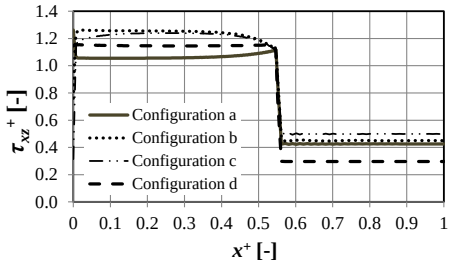

(b)

FIGURE 17: *Hydrophobic textured surface: (a) Non-dimensional hydrodynamic pressure distribution, p^+, and (b) non-dimensional surface shear stress, τ_{xz}^+, for several configurations. All curves are calculated for the optimum texturing parameters $T^+ = 0.55$ and $\lambda = 5$.*

In order to shows the true benefits of the chemical/physical roughness combined pattern over the optimum classical contact for all configurations, the performance ratio (non-dimensional load support, friction force, and friction coeffient) is summarized in Fig. 18. Note that the performance values were calculated for $T^+ = 0.65$ and $\lambda = 5$.

From Fig. 18, it is clear that for all configurations considered with respect to hydrophobic textured surfaces presented here, a significantly enhanced load support can be generated in comparison with optimum classical contact (i.e. no-slip and $h^* = 2.2$). For example, an improvement of 97% in load support is obtained when configuration *d* is employed, and an improvement of 38% (lowest value) when configuration *c* is used. It indicates that combining artificial physical roughness with chemical treatment wherever the arrangement of slippage is put, is beneficial with respect to the lubrication performance. However, a well-chosen slippage within the texture cell is important for an optimal improvement.

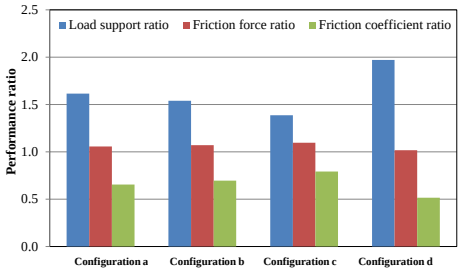

FIGURE 18: *Effect of the arrangement of boundary slippage on the texture cell on the lubrication performance ratio.*

Figure 17b shows the non-dimensional wall shear stress for all hydrophobic (slippage) partially textured configurations. It is worth noting that there is very little difference between the shear stress curves. This indicates that the friction force is not very sensitive to the arrangement of boundary slippage. However, for the untextured part of the sliding contact ($x^+ > 0.6$), configuration *d* gives lower values, and as a result the friction force is reduced. Obviously, this trend can also be observed in Fig. 18. The predicted friction force ratio f^+ / f_{ns}^+ ranges from 1.01 to 1.10, which means that in comparison with the optimum classical contact no significant change in friction force is obtained using artificial physical roughness no matter how the slip is applied.

However, a hydrophobic textured surface results in a lower friction coefficient than when optimum traditional contact is used, due to the high load support. Because of the presence of boundary slippage effect on the texture cells this has a more dominant effect than in the case of a hydrophilic textured surface, see Figs. 12-13 and thus results in an increase of the load support.

Finally, the comparison is made on the basis of the hydrodynamic performance for various possible surface boundary conditions. In this section, all parameters including the length of the slip region L_s, length of the texturing zone L_t,

and the texture cell aspect ratio λ, have been initially optimized based on previous results as discussed before. Table 3 shows the optimized sliding contact configurations of the traditional (smooth, no-slip) contact, the complex slip surface, the hydrophilic textured surface, the hydrophobic textured surface.

As can be seen in Table 4, the maximum improvement in load support, w^+, is obtained for the artificial complex slip surface (about 100% larger). For the hydrophobic partially textured pattern, the computation predicts a 95% improvement. The partially hydrophilic textured surface (without slippage) produces just slightly less load support, $w^+ = 0.155$ which means that a decrease in w^+ is noticed ($\approx$ 3% lower). So, with respect to the load support, while the hydrophobic textured surface with boundary slip is superior to the textured surface alone, it is not as effective as the smooth configuration with a complex slip. It is interesting to note that in a real application, for example in lubricated-MEMS containing moving surfaces, the fact that load support can be produced by artificial complex slippage surface on perfectly smooth surface seems to be a very promising way for designing very high load support lubricated mechanisms. The comparison of the predicted pressure generation is presented in Fig. 19. It is shown that the highest pressure is found for the smooth slippage surface condition in which the value is approximately three times as large as the maximum pressure obtained from those without slip.

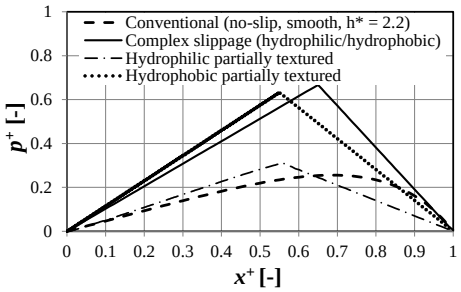

(a)

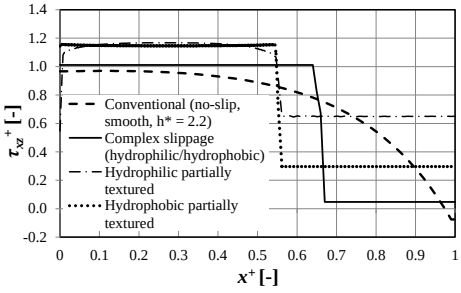

(b)

FIGURE 19: *(a) Non-dimensional pressure distribution, and (b) non-dimensional shear stress for four contact types. All configurations are calculated based on the optimized values as indicated in Table 3.*

TABLE 4: *Optimized lubricated contact characteristics*.

Contact type	Type	h^*	S^+	T^+	λ	w^+	f^+	μ^+
Classical (no-slip, smooth)	1	2.2	-	-	-	0.16	0.76	4.72
Complex slippage	2	1	0.65	-	-	0.33	0.68	2.04
Hydrophilic textured	3	1	-	0.55	5	0.16	0.88	5.68
Hydrophobic textured (Configuration *d*, see Fig. 16)	4	1	0.55	0.55	5	0.32	0.77	2.44

As shown in Table 4 and Fig. 20, with respect to the friction force, the smooth lubricated surface with artificial slip surface has an obvious friction reduction effect compared to the textured contact (either with the hydrophylic or hydrophobic condition). At the non-dimensional length of the textured region S^+ of 0.65, compared to the optimum conventional contact, the friction reduction could be 10 %. For all textured patterns, the friction forces tend to be larger than the optimum classical contact (i.e. type 4). It is as expected, because the textured contact cases were evaluated at $h^* = 1$, while the optimum traditional contact was calculated for the slip incline ratio in which the wedge effect is dominant to reduce the friction. However, once the load support generated by the textured surface is not large enough, while the friction force do not reduce, the friction coefficient become also large. The best result of friction coefficient reduction (57% lower) was obtained by the artificial complex slippage. The findings

in this study serve as a useful guide for designing lubricated-MEMSs which frequently exhibits parallel gaps.

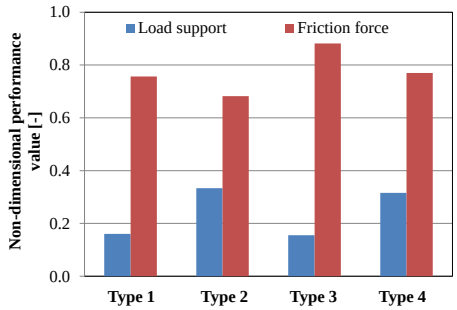

(a)

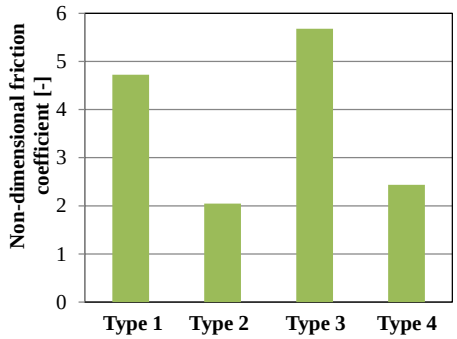

(b)

FIGURE 20: *(a) Non-dimensional performance value (w^+ and f^+) and (b) the coressponding non-dimensional friction coefficient, μ^+, for the four contact types: (1) hydrophilic (no-slippage) smooth surface, (2) complex slippage (hydrophobic/hydrophilic) smooth surface, (3) hydrophilic textured surface and (4) hydrophobic textured surface.*

4. Conclusions

The aim of the investigation was to examine if CFD software could be modified to handle hydrophobic simulations in full film hydrodynamic lubrication. Based on the findings, it can be concluded that the CFD software can be modified to handle a slippage boundary and thus able to model surface slippage in the hydrophobic region succesfully.

Furthermore, the effect of the hydrophobic surfaces combined with deterministic rough surface is solved. The present results can explain the connection between the surface roughness and the hydrophobicity in a deterministic way. A well-chosen slippage arrangement within the texture cell is important for an optimal improvement in the parallel lubricated sliding contact. Indeed, an effective hydrophobic textured surface, as indicated in this paper, can be utilized as a guideline for the fabrication of modified sliding surfaces, for instance, in lubricated-MEMS.

Based on the simulation results, a 48% reduction occurs in the friction coefficient for a hydrophobic textured parallel sliding surface when compared with the optimum conventional contact. However, this reduction is not as effective as the artificial complex slip prediction with uniform film thickness which is able to reduce it by 57%. The interesting outcome of this study is that the results can be considered as a good evaluation tool for the tribological performance of the surface "slippage" concept.

Nomenclature

f	=	friction force
h_d	=	dimple depth
h_f	=	land film thickness
h_i	=	inlet film thickness
h_o	=	outlet film thickness
K	=	Relative dimple depth
L	=	length of lubricated surface
L_t	=	length of textured region
L_s	=	length of hydrophobic (slippage) region
p	=	fluid film pressure
R_e	=	Reynolds number
u	=	local fluid velocity
u_s	=	slippage velocity
u_w	=	wall velocity
w	=	load support
x	=	coordinate direction
z	=	cross-film coordinate
α	=	texture density
β	=	slippage length
λ	=	texture aspect ratio
η	=	dynamic viscosity
ρ_l	=	lubricant density

τ_{xz} = surface shear stress

Non-dimensional parameters

$f^+ = fh_o / (u_w \eta L)$

$h^* = h_i / h_o$

$p^+ = ph_o^2 / (u_w \eta L)$

$S^+ = L_s / L$

$T^+ = L_t / L$

$u^+ = u / u_w$

$w^+ = wh_o^2 / (u_w \eta L^2)$

$x^+ = x / L$

$z^+ = z / h_o$

$\tau_{xz}^+ = \tau_{xz} h_o / (u_w \eta)$

Subscripts

cs	complex slippage
max	maximal value
ns	no-slippage
opt	optimum value
$\_w^+$	corresponding to maximum load support

References

1. Henck, S.A., 1997, "Lubrication of digital micromirror devices," *Tribology Letters* **3**, pp. 239 – 247.
2. de Boer, M.P. and Mayer, T.M., 2001, "Tribology of MEMS," *MRS Bulletin* **26**, pp. 302 – 304.
3. Choo, J.H., Spikes, H.A., Ratoi, M., Glovnea, R. and Forrest, A., 2007, "Friction reduction in low-load hydrodynamic lubrication with a hydrophobic surface," *Tribology International* **40**, pp. 154 – 159.
4. Choo, J.H., Glovnea, R.P., Forrest, A.K. and Spikes, H.A., 2007, "A low friction bearing based on liquid slip at the wall," *ASME Journal of Tribology* **129**, pp. 611 – 620.
5. Ku, I.S.Y., Reddyhoff, T., Wayte, R., Choo, J.H., Holmes, A.S. and Spikes, H.A, 2013, "Lubrication of microelectromechanical devices using liquids of different viscosities," *ASME Journal of Tribology* **134**, pp. 012002-1 – 7.
6. Jung, Y.C. and Bhushan B., 2006, "Contact angle, adhesion and friction properties of micro and nanopatterned polymers for superhydrophobicity," *Nanotechnology* **17**, pp. 4970 – 4980.
7. Zou, M., Cai, L. and Wang, H., 2006, "Adhesion and friction studies of a nanotextured surface produced by spin coating of colloidal silica nanoparticle solution," *Tribology Letters* **21**, pp. 25 – 30.
8. Thompson, P.A. and Troian, S.M., 1997, "A general boundary condition for liquid flow at solid surfaces," *Nature* **389**, pp. 360 – 362.
9. Pit, R., Hervet, H. and Leger L., 2000, "Direct experimental evidence of slip in hexadecane: solid interfaces," *Physical Review Letters* **85**, 5, pp. 980 – 983.
10. Zhu, Y. and Granick, S., 2002, "Limits of the hydrodynamic no-slip boundary condition," *Physical Review Letters* **88**, pp. 106102–1–4.
11. Tretheway, D.C. and Meinhart, C.D., 2002, "Apparent fluid slip at hydrophobic microchannel walls," *Physics of Fluids* **14**, L9-12.
12. Choi, C.H., Westin, K.J.A. and Breuer, K.S., 2003, "Apparent slip flows in hydrophilic and hydrophobic microchannels," *Physics of Fluids* **15**, pp. 2897 – 2902.
13. Cottin-Bizonne, C., Cross, B., Steinberger, A. and Charlaix, E., 2005, "Boundary slip on smooth hydrophobic surfaces: intrinsic effects and possible artifacts," *Physical Review Letters* **94**, 056102.
14. Salant, R.F. and Fortier, A.E., 2004, "Numerical analysis of a slider bearing with a heterogeneous slip/no-slip surface," *Tribology Transactions* **47**, pp. 328 – 334.
15. Wu, C.W., Ma, G.J. and Zhou, P., 2006, "Low friction and high load support capacity of slider bearing with a mixed slip surface," *ASME Journal of Tribology* **128**, pp. 904 – 907.
16. Ma, G.J., Wu, C.W. and Zhou, Z., 2007, "Wall slip and hydrodynamics of two-dimensional journal bearing," *Tribology International* **40**, pp. 1056 – 1066.
17. Tauviqirrahman, M., Ismail, R., Jamari, J., Schipper, D.J., 2013, "Study of surface texturing and boundary slip on improving the load support of lubricated sliding contacts," *Acta Mechanica* 224, pp. 365 – 381.

18. Tønder, K., 2011, "Inlet roughness tribodevices: dynamic coefficients and leakage," *Tribology International* **34**, pp. 847 – 852.
19. Brizmer, V., Kligerman, T. and Etsion, I., 2003, "A laser surface textured parallel thrust bearing," *Tribology Transactions* **46**, pp. 397 – 403.
20. Kligerman, Y., Etsion, I. and Shinkarenko, A., 2005, "Improving tribological performance of piston rings by partial surface texturing," *ASME Journal of Tribology* **127**, pp. 632 – 638.
21. Fowell M, Olver AV, Gosman AD, Spikes HA and Pegg I., 2007, "Entrainment and inlet suction: two mechanisms of hydrodynamic lubrication in textured bearings," *ASME Journal of Tribology* **129**, pp. 337 – 347.
22. Rahmani, R., Shirvani, A. and Shirvani, H., 2007, "Optimization of partially textured parallel thrust bearings with square-shaped micro dimple," *Tribology Transactions* **50**, pp. 401 – 406.
23. Pascovici, M.D., Cicone, T., Fillon, M. and Dobrica, M.B., 2009, "Analytical investigation of a partially textured parallel slider," *Proceedings of the Institution of Mechanical Engineers, Part J: Journal of Engineering Tribology* **223**, pp. 151 – 158.
24. Dobrica, M.B. and Fillon, M., 2009, "About the validity of Reynolds equation and inertia effects in textured sliders of infinite width," *Proceedings of the Institution of Mechanical Engineers, Part J: Journal of Engineering Tribology* **223**, pp. 69 – 78.
25. Dobrica, M.B., Fillon, M., Pascovici, M.D. and Cicone, T., 2010, "Optimizing surface texture for hydrodynamic lubricated-contacts using a mass-conserving numerical approach," *Proceedings of the Institution of Mechanical Engineers, Part J: Journal of Engineering Tribology* **224**, pp. 737 – 750.
26. Ma, C. and Zhu, H., 2011, "An optimum design model for textured surface with elliptical-shape dimples under hydrodynamic lubrication," *Tribology International* **44**, pp. 987-995.
27. Arghir, M., Roucou, N., Helene, M. and Frene, J., 2003, "Theoretical analysis of the incompressible laminar flow in a macro-roughness cell," *ASME Journal of Tribology* **125**, pp. 309 – 318.
28. Sahlin, F., Glavatskih, S.B., Almqvist, T. and Larsson, R., 2005, "Two-dimensional CFD-analysis of micro-patterned surfaces in hydrodynamic lubrication," *ASME Journal of Tribology* **127**, pp. 96 – 102.
29. Brajdic-Mitidieri, P., Gosman, A.D., Loannides, E. and Spikes, H.A., 2005, "CFD analysis of a low friction pocketed pad bearing," *ASME Journal of Tribology* **127**, pp. 803 – 812.
30. Han, J., Fang, L., Sun, J. and Ge, S., 2010, "Hydrodynamic lubrication of microdimple textured surface using three-dimensional CFD," *Tribology Transactions* **53**, pp. 860 – 870.
31. Shi, X. and Ni, T., 2011, "Effects of groove textures on fully lubricated sliding with cavitation," *Tribology International* **44**, pp. 2022 – 2028.
32. Aurelian, F., Patrick, M. and Mohamed, H., 2011, "Wall slip effects in (elasto) hydrodynamic journal bearing," *Tribology International* **44**, pp. 868 – 877.
33. Rao, T.V.V.L.N., Rani, A.M.A., Nagarajan, T. and Hashim, F.M., 2012, "Analysis of slider and journal bearing using partially textured slip surface," *Tribology International* **56**, pp. 121 – 128.
34. Watanabe, K., Yanuar and Udagawa, H., 1999, "Drag reduction of Newtonian fluid in a circular pipe with a highly water-repellant wall," *Journal of Fluid Mechanics* **381**, pp. 225 – 228.
35. Ou, J., Perot, B. and Rothstein, J.P., 2004, "Laminar drag reduction in microchannels using ultrahydrophobic surfaces," *Physics of Fluids* **16**, 4635.
36. ANSYS FLUENT 12 UDF Manual 2009.
37. Ren, N., Nanbu, T., Yasuda, Y., Zhu, D. and Wang, Q., 2007, "Micro textures in concentrated-conformal-contact lubrication: effect of distribution patterns," *Tribology Letters* **28**, pp. 275 – 285.
38. Yu, H., Wang, X. and Zhou, F., 2010, "Geometric shape effects of surface texture on the generation of hydrodynamic pressure between conformal contacting surfaces," *Tribology Letters* **37**, pp. 123 – 130.
39. Cameron, A., 1966, *The Priciples of Lubrication*, Longman Green and co,ltd, London.
40. Spikes, H.A., 2003, "The half-wetted bearing. Part 1: extended Reynolds

equation," *Proceedings of the Institution of Mechanical Engineers, Part J: Journal of Engineering Tribology* **217**, pp. 1 – 14.
41. Bayada, G. and Meurisse, M.H., 2009, "Impact of the cavitation model on the theoretical performance of heterogeneous slip/no-slip engineered contacts in hydrodynamic conditions," *Proceedings of the Institution of Mechanical Engineers, Part J: Journal of Engineering Tribology* **223**, pp. 371 – 381.
42. Etsion, I. and Halperin, G., 2002, "A laser surface textured hydrostatic mechanical seal," *Tribology Transactions* **45**, pp. 430 – 434.
43. Tala-Ighil, N., Fillon, M. and Maspeyrot, P., 2011, "Effect of texture area on the performances of a hydrodynamic journal bearing," *Tribology International* **44**, pp. 211 – 219.

Paper H

M. Tauviqirrahman, R. Ismail, Jamari, D.J. Schipper, 2013

Combined effects of texturing and slippage in lubricated parallel sliding contact

Tribology International, Volume 66, pp. 274 – 281

Combined Effect of Texturing and Boundary Slippage in Lubricated Sliding Contacts

M. Tauviqirrahman,[1,*)] R. Ismail,[1)] Jamari,[2)] and D.J. Schipper[1)]

[1]Laboratory for Surface Technology and Tribology,
Faculty of Engineering Technology, University of Twente, The Netherlands
*Email: mtauviq99@gmail.com

[2]Laboratory for Engineering Design and Tribology,
Department of Mechanical Engineering, University of Diponegoro, Indonesia

Published in: Tribology International, 2013, Volume 66, pp. 274 – 281

Abstract **High level of friction limits the reliability of lubricated micro-electro-mechanical-systems (MEMS) devices. The current paper explores the possibility of employing slippage combined with a textured surface in MEMS in order to improve performance characteristics. A modified Reynolds equation based on the limiting shear stress model is developed. It is confirmed that compared to an untextured surface as well as a solely textured surface, the textured surface employing a slippage has a much lower coefficient of friction, which is not affected by the texture cell aspect ratio. The results indicate that the combined textured/slippage pattern has a beneficial effect by increasing the load capacity and decreasing the friction.**

Keywords: hydrodynamic lubrication, micro-electro-mechanical-system (MEMS), performance characteristic, slippage, surface texturing

1. Introduction

Today, promising research on the development of micro-electro-mechanical-systems (MEMS) is proceeding. The MEMS field affects a wide swath of chemists, engineers, biologists, and physicists. As a result, the MEMS products range from biological, physical sensors, radio frequency (RF), and optical to robotic devices. However, one main factor that limits the widespread use and reliability of MEMS is strong adhesion with subsequent friction, and wear [1, 2]. From there on, every type of MEMS device is susceptible to stiction. The devices are said to suffer from stiction when the restoring forces are unable to overcome the interface forces.

As is well known, many MEMS devices include moving (sliding/rolling) surfaces and thus, it is necessary to apply a lubricant between the contacting surfaces to reduce friction and wear. The general purpose of lubrication is to minimize friction, wear, and heating of machine components which move relative to each other. A main factor is the understanding of lubricant film formation and its effect on load carrying capacity and friction force. However, a significant barrier to the development of MEMS lubrication is the problem of achieving effective tribological performance of their moving parts. In MEMS, liquid lubrication has generally been omitted due to the high hydrodynamic friction force that occurs due to shearing the fluid film. Compared to a solid coating, stiction prevention using liquid lubrication is less practical. However, recent studies have demonstrated that

it is possible for Newtonian liquids to slip along very smooth solid walls [3-5] and this result may make liquid lubricants for MEMS devices feasible. One of the developed treatments to eliminate stiction is the development of new materials or design of surfaces and interfaces with hydrophobic behavior [6, 7]. Non-wetting (hydrophobicity, stiction resistance) is a critical surface behavior for materials or devices in micro-applications. The hydrophobicity of a surface is generally presented in terms of a slippage length, which quantifies the extent to which the fluid elements near the wall are affected by corrugation of the surface energy [8].

A number of excellent works have evinced the presence of boundary slippage on a hydrophobic surface [9-13]. It has been demonstrated that the slippage velocity on hydrophobic surface results in a significant friction reduction in micro-scale flows [11, 12]. For most hydrophilic surfaces, however, no-slippage occurs. In general, it is feasible to expect promising utilization of slippage in micro-devices such MEMS in order to solve the failure of MEMS due to stiction.

The great challenge with respect to a hydrophobic surface from the perspective of a numerical simulation is choosing a model for the slippage. This is because the hydrodynamic characteristics of lubricated contacts are mainly controlled by the boundary conditions of the lubricant that provide lubrication. Currently, the use of artificial slippage of surfaces has received a great deal of attention in the relevant literature, since this type of surface enhancement would give a better tribological performance [14-16]. The results of all these investigations show the existence of a lifting force (load carrying capacity) in the absence of the wedge effect (uniform film thickness) using such slippage surface.

Another attractive technique to tackle the stiction problem is by texturing a surface with a micro/nano-scale dimension. The hydrodynamic lubrication theory of textured rough surfaces has been studied widely. The most promising technique originates from investigations by modifying the contacting surface in a controlled way by laser surface texturing (LST). Friction reduction was obtained with the employment of different patterns in the form of micro-textures at the surface. Partial and full texturing were two extreme cases of artificial arrangement of a textured area on the contact surface. It is worth mentioning the early work of Tonder [17] who analyzed the partial texturing mode by theoretical studies to show the positive effect of a series of dimples or roughness at inlet of a sliding surface. A comparison of partial and full texturing comprising micro-roughness in parallel thrust bearings was given by Brizmer *et al*. [18] through employing a numerical approach. Subsequently, several studies were published in literature [19-23] confirming the findings of Brizmer *et al*. [18]. One emerging conclusion of these studies is that there is an advantage of partial texturing over full texturing. In addition, more attention has been paid to the optimization of the texturing parameters. The previously-mentioned models and simulation results also provide an excellent set of guidelines for the optimum design of a surface texture in some fields. However, in all the investigations mentioned to study the effect of surface texturing, the no-slippage surface boundary condition was used. Very few researchers appear to have considered the interplay of surface texturing and slippage effect on lubrication performance characteristics [24, 25].

In general, the previous studies have shown that surface texturing as well as surface slippage is an effective means of controlling friction in lubricated sliding contacts. In order to further improve this approach, it is necessary to reduce the hydrodynamic friction (and thus stiction) by combining the slippage and the texturing effect. The present work is focused on analyzing the interaction of slippage and texturing in a hydrodynamic lubrication model to find the optimum parameters based on the load carrying capacity and the coefficient of friction.

2. Mathematical model

In a hydrodynamic lubrication problem, the governing equation in the full hydrodynamic lubrication regime can be described by the well-known Reynolds equation. For the one-dimensional analysis, the isoviscous Newtonian Reynolds equation is derived from a simple form of the x-component of the Navier-Stokes

equation, that assumes an incompressible flow and neglecting the inertia effects in the film:

$$\frac{\partial^2 u}{\partial z^2} = \frac{1}{\eta}\frac{\partial p}{\partial x} \tag{1}$$

In order to obtain the velocity distribution by integration of Eq. [1], it is necessary to define the surface boundary conditions. Let us consider a lubricated contact equivalent to a lower plane moving in the *x*-direction with surface velocity u_w, and an upper stationary surface, see Fig. 1. In this study, the occurrence of slippage in the lubricated sliding contact is determined by two criteria. At first, slippage may only occur in those areas where both the stationary and moving surface have been treated to allow it. Second, the shear stress on the surfaces must exceed a limiting shear stress value, referred to as τ_{cs} for the stationary surface and τ_{cm} for the moving surface. When both criteria are met, the resulting slippage velocity is proportional to the difference between the shear stress and the limiting value, with proportionality factors referred to as α_s for the stationary surface and α_m for the sliding surface. It means that each of the sliding surfaces has a unique slippage property. The product of the slippage coefficient with viscosity, $\alpha\eta$, is commonly named 'slippage length'. The surface boundary conditions are proposed as follows:

at $z = 0$ $\quad u = u_w + \alpha_m\left(\eta\frac{\partial u}{\partial z} + \tau_{cm}\right)$ for $\tau_m \geq \tau_{cm}$

$\qquad u = u_w$ for $\tau_m < \tau_{cm}$ (2b)

at $z = h$ $\quad u = \alpha_s\left(-\eta\frac{\partial u}{\partial z} - \tau_{cs}\right)$ for $\tau_s \geq \tau_{cs}$

$\qquad u = 0$ for $\tau_s < \tau_{cs}$ (2a)

The solution of Eq. (1) yields the distribution of the fluid velocity, subject to the boundary equations, Eq. (2). It reads:

$$u = \frac{1}{2\eta}\frac{\partial p}{\partial x}z^2 - \left(\frac{h}{2\eta}\frac{\partial p}{\partial x}\frac{h+2\alpha_s\eta}{h+\eta(\alpha_s+\alpha_m)} + \frac{U}{h+\eta(\alpha_s+\alpha_m)} + \frac{\alpha_s\tau_{cs}+\alpha_m\tau_{cm}}{h+\eta(\alpha_s+\alpha_m)}\right)z + U\frac{h+\alpha_s\eta}{h+\eta(\alpha_s+\alpha_m)} - \frac{h}{2\eta}\frac{\partial p}{\partial x}\frac{\alpha_m\eta(h+2\alpha_s\eta)}{h+\eta(\alpha_s+\alpha_m)} + \frac{\alpha_m\tau_{cm}(h+\alpha_s\eta)-\alpha_m\alpha_s\eta\tau_{cs}}{h+\eta(\alpha_s+\alpha_m)} \tag{3}$$

The modified Reynolds equation is derived by integrating the continuity equation. If the fluid density ρ is assumed to be the mean density across the film, it is convenient to express the continuity equation in integral form as follows:

$$\int_0^h \frac{\partial}{\partial x}u\,dz = -(u)_{z=h}\frac{\partial h}{\partial x} + \frac{\partial}{\partial x}\left(\int_0^h u\,dz\right) = 0 \tag{4}$$

Therefore, the modified form of the one-dimensional Reynolds equation with slip reads:

$$\frac{\partial}{\partial x}\left(h^3\frac{h^2+4h\eta(\alpha_s+\alpha_m)+12\eta^2\alpha_s\alpha_m}{h(h+\eta(\alpha_s+\alpha_m))}\frac{\partial p}{\partial x}\right) = 6\eta U\frac{\partial}{\partial x}\left(\frac{h^2+2h\alpha_a\eta}{h+\eta(\alpha_s+\alpha_m)}\right) - 6\eta\tau_{ca}\frac{\partial}{\partial x}\left(\frac{\alpha_s h(h+2\alpha_m\eta)}{h+\eta(\alpha_s+\alpha_m)}\right) + 6\eta\tau_{cm}\frac{\partial}{\partial x}\left(\frac{\alpha_m h(h+2\alpha_s\eta)}{h+\eta(\alpha_s+\alpha_m)}\right) - 12\eta U\frac{\alpha_s\eta}{h+\eta(\alpha_s+\alpha_m)}\frac{\partial h}{\partial x} + 6h\frac{\partial p}{\partial x}\frac{\partial h}{\partial x}\frac{h\alpha_s\eta+2\alpha_s\alpha_m\eta^2}{h+\eta(\alpha_s+\alpha_m)} + 12\eta\tau_{ca}\left(\frac{\alpha_s(h+\alpha_m\eta)}{h+\eta(\alpha_s+\alpha_m)}\frac{\partial h}{\partial x}\right) - 12\eta\tau_{cm}\left(\frac{\alpha_s\alpha_m\eta}{h+\eta(\alpha_s+\alpha_m)}\frac{\partial h}{\partial x}\right) \tag{5}$$

It must be pointed out that the modified form of the Reynolds equation presented in Eq. [5] is different from those used in the studies discussed previously [14-16, 24-26]. The modified Reynolds equation includes the limiting shear stress terms and the possibility of slippage that may occur on both surfaces.

In the case of the present study, the lubricated sliding contact is operating under steady state conditions. The load carrying capacity is determined by integrating the calculated hydrodynamic pressure field along the contact surface. The coefficient of friction is obtained by dividing the friction force by the load carrying

capacity, while the friction force is calculated by integrating the shear stress over the surface area.

3. Methodology

The global contact geometry considered in this work is that of a parallel sliding contact with multiple texture cells (without periodic boundary condition). For the analysis of a lubricated contact with combined texture/slippage condition, the boundary slippage is employed on all sides of the texture cell (see Fig. 2). Here, it is assumed that slippage, which is employed on the textured surface, has a superhydrophobic property (fully non-wetted), and the limiting shear stress is ideal and equal to zero. For all following computations, the stationary surface is designed as a textured surface.

A numerical method is required for solving Eq. [5]. To this end, the finite difference equations obtained by means of the micro-control volume approach [27] was chosen, on account of its advantages in analyzing a complex domain. In addition, its stability is unaffected by changes in flow direction. The entire computed domain is assumed as full fluid lubrication. By employing the discretization scheme, the computed domain is divided into a number of control volumes. The mesh number is obtained from a mesh refinement study and is approximately 4,000 nodes. For all derivatives the central difference is used except at the boundaries. Appropriate one-sided difference is used at the boundaries [27]. The assumption made is that at the inlet and outlet of the domain, the pressure is set to be zero and the cavitation boundary condition is not used.

The modified Reynolds equation is solved using TDMA (tri-diagonal matrix algorithm), [27]. Once Eq. (5) is solved for the hydrodynamic pressure distribution, the load support can be calculated, as well as the friction force and finally the coefficient of friction. It should be noted that the solution convergence is checked to an accuracy of tolerance $\varepsilon = 10^{-6}$ where

$$\max\left(\frac{\left|\phi_i^{new} - \phi_i^{old}\right|}{\left|\phi_i^{new}\right|}\right) \le \varepsilon,$$

is the variable field. The iteration is also performed for $\varepsilon = 10^{-5}$ and $\varepsilon = 10^{-7}$, and there is hardly any difference in the calculated values (i.e < 0.1%). The simulation results will be presented in dimensionless form, i.e. $W^* = Wh_F^2/(u_w \eta L^2)$ for the dimensionless load carrying capacity, $F^* = Fh_F/(u_w \eta L)$ for the dimensionless friction force, and $\mu^* = F^*/W^*$ for the dimensionless coefficient of friction. The dimensionless slippage length B^* is determined by normalizing the "slippage length" ($\alpha\eta$) with the film thickness h_F.

In this study, a rectangular geometry for the texture cell shape is used. In order to avoid "inlet suction" at the leading edge of the contact, the texture surface starts with a dimple. The parameter R^* for the dimensionless textured region length is introduced and categorized into three kinds of textured surface, i.e. untextured surface ($R^* = 0$), partially textured surface ($R^* < 1$) and fully textured surface ($R^* = 1$). The texturing zone R^* may consist of a number of texture cells depending on the chosen texture cell aspect ratio. The texture cell can be described by three dimensionless parameters: the texture density S^* (defined as the ratio between the dimple length D_l and the texture cell length D_C), relative dimple depth M^* (defined as the ratio between the dimple depth D_h and the land film thickness h_F), and the texture cell aspect ratio D^* (defined as the ratio between the dimple length D_l and the dimple depth D_h). In the present paper, it is assumed that the texture density, S^* is constant and equal to 0.5, and the relative dimple depth, M^* is fixed at a value of 1. Thus, the variation of D^* is accomplished by modifying the dimple length, D_l while keeping a constant land film thickness, h_F and dimple depth, D_h.

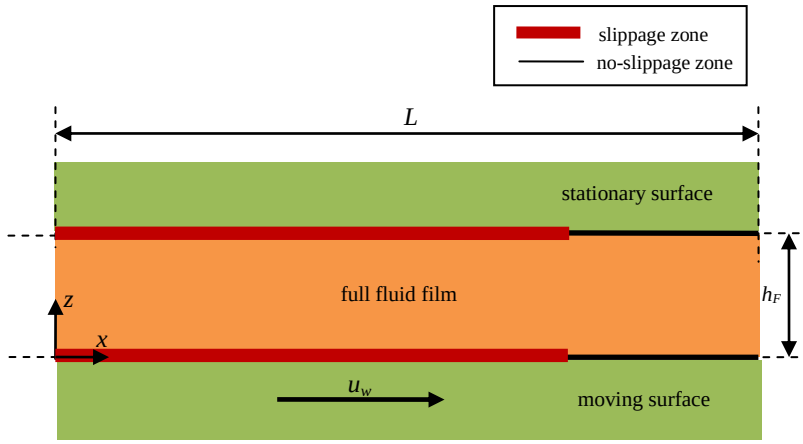

FIGURE 1: *Schematic of a lubricated untextured parallel sliding contact with slippage.*

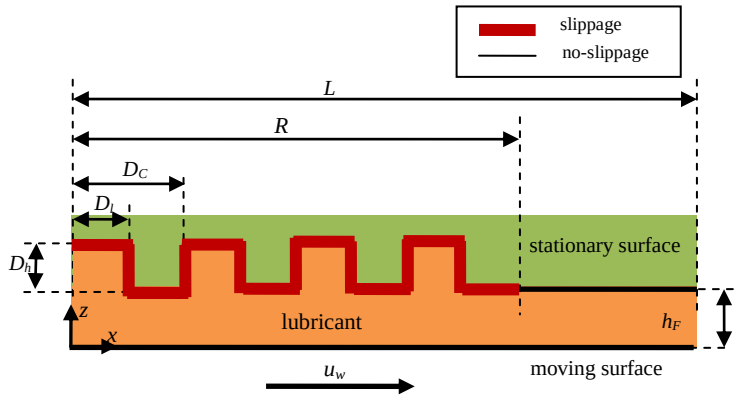

FIGURE 2: *Schematic of a lubricated parallel sliding contact with partially textured stationary surface combined with slippage at all sides of the texture cell.*

4. Results and discussions

Surface texturing, as is known, seems to be a promising way of improving the performance of lubricated sliding contacts. At this stage, one important practical design feature will be pointed out, i.e. the slippage effect at the textured surface such that it can induce a more positive effect on the performance characteristic.

2.1. Effect of textured region length

As reported by other researchers, partially (purely) textured surfaces could lead to positive effects. Therefore, in the present study, in the case of combined textured/slippage configuration, the texture parameter of the dimensionless textured region length, R^* is briefly discussed first. In order to determine the optimum value of R^* (equivalent to the best configuration of a partially textured slider), a parametric study is conducted, in which the R^* is varied between 0 and 1 for several slippage conditions (i.e. several values of dimensionless slippage length, B^*). It is usually postulated that a large value of B^* implies greater slippage. Therefore, the effect of wettability (represented by B^* in this case) is also of particular interest. Numerous works have demonstrated that a chemical treatment of the surface generates a slippage length in the order of 1 μm [11],

whereas a longer slippage length up to 100 μm can be obtained through a combination of an artificial rough structure with a hydrophobic surface [4, 28, 29]. In the present study, the slippage length of a hydrophobic surface is assumed as uniform in space.

Figure 3 shows the effect of the dimensionless textured region length, R^* (simulating untextured surface, partially textured surface or fully textured surface) on the dimensionless load carrying capacity, W^*, and varying the dimensionless slippage length, B^*. It should be noted that a solely textured surface (without slippage) is obtained by setting the dimensionless slippage length $B^* = 0$. Several specific features can be found in Fig. 3. First, the load carrying capacity increases and then decreases rapidly with the increase in textured region length. This trend prevails especially when a boundary slippage is combined with a textured surface. It is easy to observe that partial texturing is preferred over full texturing. It is worth noting that for all values of B^*, when $R^* = 0$ (untextured) or $R^* = 1$ (full texturing), the generated load carrying capacity goes off, which means that such configurations cause lubrication failure. This result is consistent with recent literature [21, 22].

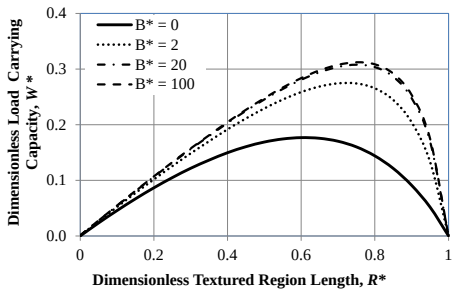

FIGURE 3: *Dimensionless load carrying capacity, W*, versus dimensionless textured region length, R*, for various values of the dimensionless slippage length, B* (Note: D* = 20).*

Obviously, as can be seen from Fig. 3, there is an optimum value for the dimensionless textured region length, R^*, at each value of B^*, which increases with increasing B^*. It is therefore evident that decreasing B^* would make a shift of the optimum texturing region length towards the leading edge of the contact (left-hand side of the curve). It means that for improving the load carrying capacity significantly, the texturing zone in the combined textured/slippage pattern needs to be sufficiently extended. One can remark that in the case of a solely textured slider (i.e. $B^* = 0$), partial texturing pattern is most effective for $R^* = 0.6$. In the case of combined textured/slippage configuration, the optimum dimensionless (inlet) partially textured region length occurs within a narrow interval $R^*_{opt\_W^*} = (0.7, 0.75)$ depending on the dimensionless slippage length. The optimum textured region combined with slippage situation occurs when $R^* = 0.7$ and 0.75, respectively, for low B^* (in this case $B^* = 2$) and high B^* (i.e. $B^* = 20$ and $B^* = 100$). If the textured region length is higher or lower than these optimum values, the hydrodynamic response goes down abruptly.

Secondly, adding slippage to the textured surface appears effective to generate more hydrodynamic load carrying capacity. The dimensionless load carrying capacity, W^* predicted by combined textured/slippage patterns is higher than that by pure texturing. For example, the improvement in W^* for a textured surface with slippage (when $B^* = 20$ and $R^*_{opt\_W^*} = 0.75$) is up to 75% compared to the solely textured surface (when $R^*_{opt\_W^*} = 0.6$). That is to say that the presence of boundary slippage in texture cells creates a more dominant effect and results in an increase in the load carrying capacity in textured parallel sliding surfaces. However, when B^* is increased by a factor 5 (i.e. $B^* = 100$), no significant improvement in W^* is found (in this case, it is just up 76% for the same R^*). It indicates that in relation to the combined textured/slippage pattern, there is an optimum slippage length B^*. In the next subsection, the investigation of this value will be explored. As a concluding remark, it can be noted that the partially textured surface combined with boundary slippage for high B^* is more effective than the solely textured one with respect to the load carrying capacity.

When the lubricant slips along the solid-liquid interface, as reported by other researchers, a large slippage is also associated with large friction force reduction. However, in an engineering application, in addition to the friction force reduction effect, at the same time,

the slippage may reduce the hydrodynamic pressure and thus the load carrying capacity. However, in MEMS, by lubrication, a low friction force and a high load carrying capacity is wanted. Therefore, the combined effect of slippage and texture parameters on the load carrying capacity and the friction force can be better analyzed using the dimensionless coefficient of friction.

The dimensionless coefficient of friction variation as a function of the textured region length for several values of the dimensionless slippage length, B^* is presented in Fig. 4. It is shown that extending the length of the textured region, R^* results in the decrease-then-increase behavior of the coefficient of friction. This trend prevails for both combined textured/slippage pattern and purely textured pattern. The optimal (pure) texturing zone with respect to the minimum coefficient of friction occurs when $R^* = 0.65$ which is very close to the optimum for the maximum load carrying capacity criteria as discussed before. This result matchs very well with Ref. [21]. However, as can be seen in Fig. 4, compared to the purely textured surface, there is a large shift of the minimum dimensionless coefficient of friction if slippage is employed on the textured surface. The optimal dimensionless textured region length, R^* in the case of a combined textured/slippage pattern is around 0.8 and 0.9, for a low slippage length (i.e. $B^* = 2$), and a high slippage length (i.e. $B^* = 20$ and 100), respectively. It is worth noting that as well as the solely textured surface case, the optimal texturing region length in the case of the combined textured/slippage pattern corresponding to a minimum coefficient of friction is very close to the one leading to a maximum load carrying capacity. The simulation results, showing the performance characteristics and the corresponding optimized textured region length for the cases considered here, are summarized in Table 1. Therefore, for reasonable values of texture cell aspect ratio in the following computations, the textured region length, R^* is considered to be 0.60 and 0.80, respectively, for the case of the solely textured pattern and the combined textured/slippage pattern.

Figure 4 also shows the superiority of a combined textured/slippage pattern against a solely textured surface in reducing the coefficient of friction. For example, the optimized partially textured surface (without slippage) at $R^*_{opt\_\mu^*} = 0.65$ produces a dimensionless coefficient of friction, $\mu^* = 5.18$, which is 53% higher than that by the combined textured/slippage pattern (at $R^*_{opt\_\mu^*} = 0.85$ and $B^* = 20$). If the prediction of the coefficient of friction is evaluated at the same textured length, i.e. $R^*_{opt\_\mu^*} = 0.65$ which is the optimal value of the textured length for the pure texturing case, the decrease in μ^* predicted by the combined textured/slippage case is still high, that is, 40% lower compared to that for the purely textured one. That is to say that adding slippage to textured surface gives a lower coefficient of friction than a purely textured configuration for all values of R^* and B^*.

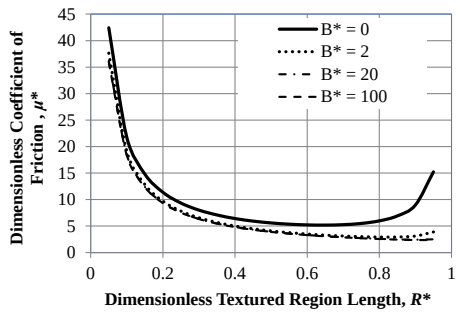

FIGURE 4: *Dimensionless coefficient of friction, μ^*, versus dimensionless textured region length, R^*, for various values of the dimensionless slippage length, B^* (Note: $D^* = 20$).*

TABLE 1: *Lubricated contact characteristics and the corresponding textured region length, R^*.*

Textured contact type	$R^*_{opt\_W^*}$	W^*	$R^*_{opt\_\mu^*}$	μ^*
Solely textured pattern	0.60	0.177	0.65	5.18
Combined textured/slippage pattern ($B^* = 2$)	0.70	0.274	0.80	2.93
Combined textured/slippage pattern ($B^* = 20$)	0.75	0.308	0.85	2.43
Combined textured/slippage pattern ($B^* = 100$)	0.75	0.312	0.85	2.37

4.2. Effect of texture cell aspect ratio

As explained in the previous section, the optimum textured region length corresponding to a minimum coefficient of friction is quite identical to the one leading to a maximum load carrying capacity. Dobrica and Fillon [30] were interested in the theoretical modeling of the flow in hydrodynamic lubricated parallel textured sliders. They took into account the texture cell aspect ratio, D^* as well as the Reynolds number, R_e when analyzing such textured sliders. It was shown that the dimensionless load carrying capacity (which is equivalent to the dimensionless hydrodynamic pressure) decreases with the increase in the texture cell aspect ratio, D^*, which agrees well with our simulation results as shown in Fig. 5 in the case of the solely textured pattern. Figure 5 shows the effect of the texture cell aspect ratio, D^* on the dimensionless load carrying capacity, W^* for various dimensionless slippage length B^*. The plotted results have been calculated using the optimized textured region length, i.e. $R^*_{opt} = 0.6$ and 0.8, respectively, for the pure texturing and the combined textured/slippage configuration, which are reasonable values for the optimum partial texturing zone as described in the previous section.

Two observations can be made based on Fig. 5. At first, concerning the load carrying capacity, the combined textured/slippage solution leads to an improvement compared to the solely textured slider. It is also shown that the effect of the dimensionless slippage length, B^*, combining slippage on textured surface with a high B^* is more pronounced than with a low B^*. Compared to the solely textured pattern, the improvement in W* of the combined textured/slippage pattern is 123% and 170%, respectively, predicted by B^* of 20 (low slippage) and B^* of 100 (high slippage) at the same D^* (the chosen $D^* = 20$ in this case). Secondly, for both cases (i.e. partially textured/slippage surface and purely textured surface), increasing the texture cell aspect ratio shows a reduction in the load carrying capacity, while increasing the texture cell aspect ratio more than a specified number hardly changes that performance. As can be seen, an increase in the texture aspect ratio from 20 to, say, 150 gives a significant reduction in the dimensionless load carrying capacity for all values of B*. However, after D^* reaches 150 and above, the load carrying capacity is hardly influenced anymore with a further increase in the value of the D^*. This condition also prevails in the case of a solely textured surface. For example, in the case of a combined textured/slippage configuration having a low texture aspect ratio ($D^* = 20$), the prediction of the dimensionless load carrying capacity, W* is 0.30 for $B^* = 100$. This can be compared to the one having a high texture aspect ratio ($D^* = 200$) which predicts W^* of 0.26, which is about 0.8 times lower, for the same slippage length. In conclusion, making (inlet) partial texturing with a low texture aspect ratio on a surface combined with a high slippage will be very beneficial with respect to the load carrying capacity.

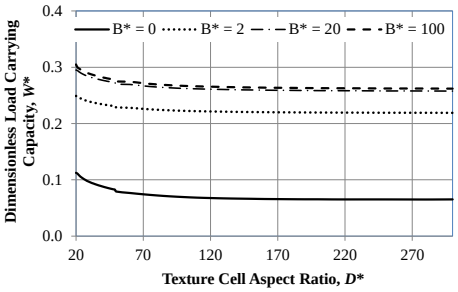

FIGURE 5: *Dimensionless load carrying capacity, W*, versus texture cell aspect ratio, D*, for various values of dimensionless slippage length, B* (Note: $R^*_{opt} = 0.6$ and 0.8, respectively, for the pure texturing and the combined textured/slippage configuration).*

Figure 6 shows the variation of the coefficient of friction with the texture aspect ratio for various values of slippage length. Based on Fig. 6, some specific features of the hydrodynamic coefficient of friction are found. Firstly, it can be observed that there is a significant reduction in dimensionless coefficient of friction, μ^* for the combined textured/slippage surface for all values of slippage length considered here. Compared to the solely textured pattern, an improvement in μ^* is predicted whatever the value of slippage length. This is to say that adding the slippage condition on the texture cells even with small slippage effect can lead to a significant reduction in coefficient of friction (up to 65% for $B^* = 2$ and $D^* = 20$). However, increasing the slippage property (i.e. the B^* is increased by a factor 5, for example) induces a little improvement in the coefficient of friction

for the same D^*. In this case, the maximal reduction in coefficient of friction (70% for B^* = 20 and D^* = 20) is slightly larger than the friction reduction in the previous case. Once again, it indicates that there is an optimum slippage length as mentioned in the previous section.

Secondly, in the case of a combined textured/slippage configuration, the sensitivity of the coefficient of friction on the texture aspect ratio is very small for all values of B^*. Opposite to these results, in the case of pure texturing, the predicted μ^* turns out to be sensitive to D^* especially for values of D^* which are less than 150. It is found that an increase in texture aspect ratio leads to an increase in the predicted coefficient of friction. For D^* > 150, the coefficient of friction seems to show negligible variation. Recalling the discussion on the load carrying capacity mentioned earlier, see Fig. 5, it can be deduced that the texture aspect ratio inducing the maximum coefficient of friction of the solely textured sliding contact is identical to that generating the minimum load carrying capacity, that is, D^* = 150. However, this trend is not found in the case of textured pattern combined with slippage. The explanation is that the slippage parameter (i.e. B^*) has a more dominant effect in determining the coefficient of friction than texture parameter (i.e. D^*). It is more clear if the friction force, F^* is plotted along the texture cell aspect ratio as shown in Fig. 7. From Fig. 7, it can be seen that for the combined textured/slippage pattern, there is a variation in the dimensionless friction force in the range of D^* from 20 to 120. This phenomenon also occurs for the load carrying capacity profiles as a function of D^* (see Fig. 5). Consequently, the variation of the friction force will compensate the variation of the load carrying capacity to generate a relatively unchanged coefficient of friction. A contradictive result is found in the case of a purely textured surface. The predicted friction force remains unchanged, especially for D^* > 120. For D^* < 120, the reduction in load carrying capacity is larger than the reduction in the friction force so there is a net overall increase in the coefficient of friction. From Fig. 7, it is worth noting that for the case of pure texturing, the friction force does not depend on the texture cell aspect ratio, and thus the number of texture cells. This result agrees well with the analytical work of Pascovici *et al*. [21].

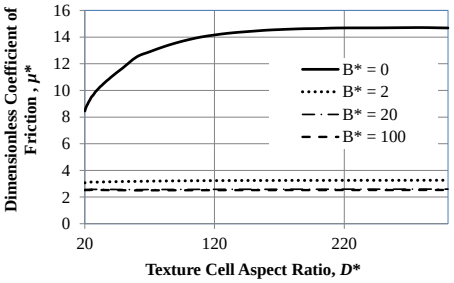

FIGURE 6: *Dimensionless coefficient of friction, μ^*, versus texture cell aspect ratio, D^*, for various values of dimensionless slippage length, B^*.*

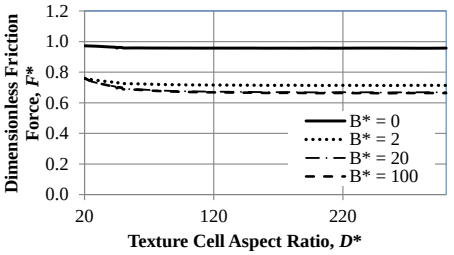

FIGURE 7: *Dimensionless friction force, F^*, versus texture cell aspect ratio, D^*, for various values of dimensionless slippage length, B^*.*

4.3. Effect of slippage length

In order to investigate the effect of the dimensionless slippage length, B^* for lubricated contacts using texturing combined with slippage, computations have been performed using an optimized dimensionless texturing region length by comparing several conditions, that is, different texture cell aspect ratios, D^* and the results are displayed in Fig. 8.

As can be seen in Fig. 8, a well-chosen partially textured configuration with slippage leads to a greater improvement in load carrying capacity, compared with a simple partially textured surface for all values of texture cell aspect ratio. The maximum improvement by adding wall slippage on the textured surface is up to 116 % and 158 %, respectively, for low slippage (for example B^* = 2) and high slippage (B^* = 100) at

D^* = 20. It indicates that the calculated results are strongly affected by the slippage length but weakly sensitive to the texture aspect ratio, which are consistent with previous results as mentioned earlier. The higher the value of the slippage length, the higher the predicted load carrying capacity. Specifically, for B^* lower than 10, the increase in B^* leads to a large improvement in the load carrying capacity of the lubricated contact (see insert of Fig. 8), whereas for B* greater than say 10, the variation in B* has an insignificant effect on the performance. It is interesting to observe that optimal values of the dimensionless slippage length, B* are noted. These values are identical for all D^*. So, a B^* of 10 can be considered as an optimal value for inducing the slippage effect on a textured surface for all values of D^* considered.

In relation to the texture cell aspect ratio effect, as is shown in Fig. 8, it can be observed that the smaller the texture cell aspect ratio, the higher the predicted load carrying capacity, which matches well with the previous results, see Fig. 5. This trend prevails for the case of pure texturing as well as for the combined textured/slippage pattern. However, the discrepancy in W* for the textured pattern with slippage between the case with low D^* (i.e. D^* = 20) and with high D^* (i.e. D^* = 300) is not as big as the case without slippage. For example, for the partially textured contact with slippage subject to B^*_{opt} of 10, the load carrying capacity at D^* of 300 is just 1.2 times lower than that at D^* of 20. With respect to the utilization of the slippage property (i.e. B^*_{opt} = 10) on the textured surface, the load carrying capacity can be improved by 148 % (at D^* = 20) and 287 % (at D^* = 300) higher than the solely textured surface. The results of this study are summarized in Table 2. Once again, it means that the slippage effect has a much higher contribution in inducing the pressure distribution and thus the load carrying capacity than the texturing effect.

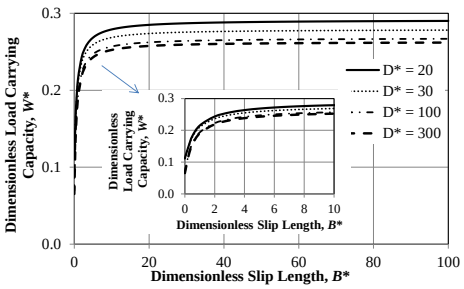

FIGURE 8: *Dimensionless load carrying capacity, W*, versus dimensionless slippage length, B*, for various values of texture cell aspect ratio, D*. The insert shows the predicted W* for low values of B* (i.e. 1 to 10).*

TABLE 2: *Effect of texture aspect ratio on the load carrying capacity at the textured/slippage pattern.*

	Dimensionless load carrying capacity, W^*		Change in load carrying capacity (%)
	$B^* = 0$	$B^*_{opt} = 10$	
$D^* = 20$	0.1125	0.2791	148
$D^* = 30$	0.1106	0.2686	143
$D^* = 100$	0.0694	0.2569	270
$D^* = 300$	0.0652	0.2524	287

Note: Change (%) =

$$100 * \left(\left| \frac{(\text{solely textured pattern} - \text{combined textured/slippage pattern})}{\text{solely textured pattern}} \right| \right)$$

In Fig. 9, the coefficient of friction of the optimized partially textured contact (R^*_{opt} = 0.6 and 0.8, respectively, for the pure texturing and the combined textured/slippage configuration) versus the slippage length is presented. The results are evaluated for different texture aspect ratios. Figure 9 shows that for the whole range of texture aspect ratios, the partially textured/slippage combination is advisable for reducing the coefficient of friction rather than the classical texturing (without slippage). The increase in the dimensionless slippage length leads to a decrease in the predicted coefficient of friction. However, the decrease in μ^* is limited, which indicates an optimum slippage length. As shown in Figs. 8 and 9, the optimum dimensionless slippage length reveals a high load carrying capacity and a low coefficient of friction. A value of 10 is chosen as an optimum for B^* because a further increase in B^* does not affect the performance anymore (see insert of Fig 9). If B^* decreases below this value, W^* and μ^* attains to its no-slippage value, which means

that the combined textured/slippage contact behaves like a traditional one (without slippage). For B^*_{opt} larger than 10, the coefficient of friction prediction by employing slippage is 3 to 5 times lower compared to the classical textured surface in the range of D^* considered here. From Fig. 9, it can also be concluded that, unlike the pure texturing that is sensitive to the variation of texture aspect ratio, the coefficient of friction of the combined textured/slippage pattern is very weakly dependent on the texture aspect ratio. The discrepancy in the coefficient of friction of the solely textured surface predicted by D^* of 300 is around 42% higher than that by D^* of 20, whereas for the case of combined textured/slippage pattern, the discrepancy is just about 3%.

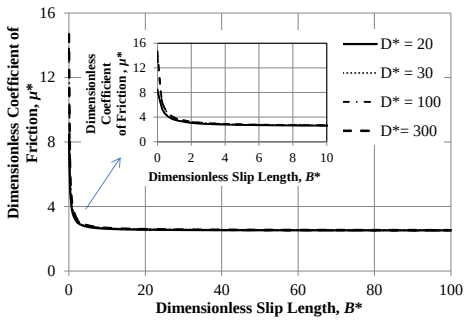

FIGURE 9: *Dimensionless coefficient of friction, μ*, versus dimensionless slippage length, B*, for various values of texture cell aspect ratio, D*. The insert shows the predicted μ* for low values of B* (i.e. 1 to10).*

5. Conclusion

This paper focused on the possibility of improving the hydrodynamic performance characteristic (high load carrying capacity combined with low coefficient of friction) of lubricated parallel sliding contacts by texturing the surface with and without boundary slippage. A model of a lubricated sliding contact with boundary slippage has been developed and the effect of the slippage parameter on the textured configuration on the hydrodynamic lubrication property has been analyzed. The following conclusions summarize the results of the present study:

1. The texturing region has a huge impact on performance characteristics both for the combined textured/slippage pattern and the purely textured one. Partial texturing is much more effective than an untextured surface as well as full texturing with respect to the load carrying capacity and the coefficient of friction.
2. All the results demonstrate the superiority of combined textured/slippage surface in terms of load carrying capacity and friction coefficient, when compared to purely textured sliders.
3. For partial texturing combined with slippage, increasing the texture cell aspect ratio does not help in improving the system, i.e. reducing the coefficient of friction.
4. The best characteristic performance can be achieved when the configuration of the combined textured/slip pattern has a high slip length. Compared with the solely textured contact, the predicted improvement in the load carrying capacity is around 150-300%, while the reduction in the coefficient of friction is about 70-80% depending on the texture cell aspect ratio. This finding may have useful implications for reducing friction and thus the stiction in liquid-lubricated-MEMS devices.

Nomenclature

D^*	texture cell aspect ratio
D_c	cell length
D_h	dimple depth
D_l	dimple length
F	Friction force per unit width
h	film thickness
h_F	land film thickness
L	slider length
M^*	relative dimple depth, D_h / h_F
R	textured region length
S^*	texture density, D_l / D_c
u_w	sliding velocity
W	load carrying capacity per unit width
z	cross-film coordinate
α_s , α_m	slippage coefficient at surface s (stationary) and m (moving)
η	dynamic viscosity
μ	Coefficient of friction, F / W

τ_{cs}, τ_{cm} limiting shear stress at surface *s* (stationary) and *m* (moving)

Dimensionless parameters

$B^* = \alpha\eta / h_F$

$D^* = D_l / D_h$

$R^* = R / L$

$W^* = Wh_F^2 / (u_w \eta L^2)$

$F^* = Fh_F / (u_w \eta L)$

$\mu^* = F^* / W^*$

Subscripts

opt optimum value

$\_W^*$ corresponding to maximum load carrying capacity

$\_\mu^*$ corresponding to minimum coefficient of friction

References

1. Henck, S.A., 1997, "Lubrication of digital micromirror devices," *Tribology Letters* **3**, pp. 239 – 247.
2. de Boer, M.P. and Mayer, T.M., 2001, "Tribology of MEMS," *MRS Bulletin* **26**, pp. 302 – 304.
3. Choo, J.H., Spikes, H.A., Ratoi, M., Glovnea, R. and Forrest, A., 2007, "Friction reduction in low-load hydrodynamic lubrication with a hydrophobic surface," *Tribology International* **40**, pp. 154 – 159.
4. Choo, J.H., Glovnea, R.P., Forrest, A.K. and Spikes, H.A., 2007, "A low friction bearing based on liquid slip at the wall," *ASME Journal of Tribology* **129**, pp. 611 – 620.
5. Ku, I.S.Y., Reddyhoff, T., Wayte, R., Choo, J.H., Holmes, A.S. and Spikes, H.A, 2013, "Lubrication of microelectromechanical devices using liquids of different viscosities," *ASME Journal of Tribology* **134**, pp. 012002-1 – 7.
6. Jung, Y.C. and Bhushan B., 2006, "Contact angle, adhesion and friction properties of micro and nanopatterned polymers for superhydrophobicity," *Nanotechnology* **17**, pp. 4970 – 4980.
7. Zou, M., Cai, L. and Wang, H., 2006, "Adhesion and friction studies of a nanotextured surface produced by spin coating of colloidal silica nanoparticle solution," *Tribology Letters* **21**, pp. 25 – 30.
8. Thompson, P.A. and Troian, S.M., 1997, "A general boundary condition for liquid flow at solid surfaces," *Nature* **389**, pp. 360 – 362.
9. Pit, R., Hervet, H. and Leger L., 2000, "Direct experimental evidence of slip in hexadecane: solid interfaces," *Physical Review Letters* **85**, 5, pp. 980 – 983.
10. Zhu, Y. and Granick, S., 2002, "Limits of the hydrodynamic no-slip boundary condition," *Physical Review Letters* **88**, pp. 106102–1 – 4.
11. Tretheway, D.C. and Meinhart, C.D., 2002, "Apparent fluid slip at hydrophobic microchannel walls," *Physics of Fluids* **14**, L9-12.
12. Choi, C.H., Westin, K.J.A. and Breuer, K.S., 2003, "Apparent slip flows in hydrophilic and hydrophobic microchannels," *Physics of Fluids* **15**, pp. 2897 – 2902.
13. Cottin-Bizonne, C., Cross, B., Steinberger, A. and Charlaix, E., 2005, "Boundary slip on smooth hydrophobic surfaces: intrinsic effects and possible artifacts," *Physical Review Letters* **94**, 056102.
14. Salant, R.F. and Fortier, A.E., 2004, "Numerical analysis of a slider bearing with a heterogeneous slip/no-slip surface," *Tribology Transactions* **47**, pp. 328 – 334.
15. Wu, C.W., Ma, G.J. and Zhou, P., 2006, "Low friction and high load support capacity of slider bearing with a mixed slip surface," *ASME Journal of Tribology* **128**, pp. 904 – 907.
16. Ma, G.J., Wu, C.W. and Zhou, Z., 2007, "Wall slip and hydrodynamics of two-dimensional journal bearing," *Tribology International* **40**, pp. 1056 – 1066.
17. Tønder, K., 2011, "Inlet roughness tribodevices: dynamic coefficients and leakage," *Tribology International* **34**, pp. 847 – 852.
18. Brizmer, V., Kligerman, T. and Etsion, I., 2003, "A laser surface textured parallel thrust bearing," *Tribology Transactions* **46**, pp. 397 – 403.
19. Rahmani, R., Mirzaee, I., Shirvani, A. and Shirvani, H., 2010, "An analytical approach for analyses and optimization of slider bearings with infinite width parallel textures," *Tribology International* **43**, pp. 1551 – 1565.

20. Rahmani, R., Shirvani, A. and Shirvani, H., 2007, "Optimization of partially textured parallel thrust bearings with square-shaped micro dimple," *Tribology Transactions* **50**, pp. 401 – 406.
21. Pascovici, M.D., Cicone, T., Fillon, M. and Dobrica, M.B., 2009, "Analytical investigation of a partially textured parallel slider," *Proceedings of the Institution of Mechanical Engineers, Part J: Journal of Engineering Tribology* **223**, pp. 151 – 158.
22. Dobrica, M.B., Fillon, M., Pascovici, M.D. and Cicone, T., 2010, "Optimizing surface texture for hydrodynamic lubricated-contacts using a mass-conserving numerical approach," *Proceedings of the Institution of Mechanical Engineers, Part J: Journal of Engineering Tribology* **224**, pp. 737 – 750.
23. Tala-Ighil, N., Fillon, M. and Maspeyrot, P., 2011, "Effect of texture area on the performances of a hydrodynamic journal bearing," *Tribology International* **44**, pp. 211 – 219.
24. Aurelian, F., Patrick, M. and Mohamed, H., 2011, "Wall slip effects in (elasto) hydrodynamic journal bearing," *Tribology International* **44**, pp. 868 – 877.
25. Rao, T.V.V.L.N., Rani, A.M.A., Nagarajan, T. and Hashim, F.M., 2012, "Analysis of slider and journal bearing using partially textured slip surface," *Tribology International* **56**, pp. 121 – 128.
26. Bayada, G. and Meurisse, M.H., 2009, "Impact of the cavitation model on the theoretical performance of heterogeneous slip/no-slip engineered contacts in hydrodynamic conditions," *Proceedings of the Institution of Mechanical Engineers, Part J: Journal of Engineering Tribology* **223**, pp. 371 – 381.
27. Patankar, S.V., 1980, *Numerical Heat Transfer and Fluid Flow*, Levittown: Taylor & Francis.
28. Watanabe, K., Yanuar and Udagawa, H., 1999, "Drag reduction of Newtonian fluid in a circular pipe with a highly water-repellant wall," *Journal of Fluid Mechanics* **381**, pp. 225 – 228.
29. Ou, J., Perot, B. and Rothstein, J.P., 2004, "Laminar drag reduction in microchannels using ultrahydrophobic surfaces," *Physics of Fluids* **16**, 4635.
30. Dobrica, M.B. and Fillon, M., 2009, "About the validity of Reynolds equation and inertia effects in textured sliders of infinite width," *Proceedings of the Institution of Mechanical Engineers, Part J: Journal of Engineering Tribology* **223**, pp. 69 – 78.

Acknowledgements

I am enormously grateful to Prof. Dik Schipper, my promoter and Dr. Jamari, my daily supervisor. I would like to thank them for sharing their ideas and knowledge, their encouragement and their generosity. They supported me throughout the whole process of my study, ranging from the correction of typing errors, valuable comments/suggestions and numerous other things which always helped me to more in the right direction. I might not have survived my study and would not have produced these scientific results without their help and support.

Next, I would like to thank the graduation committee members: G.P.M.R. Dewulf, D.J. Schipper, J. Jamari, Huis in ‘t Veld, J.G.E. Gardeniers, R. Larsson and S. Franklin for reading the final thesis draft and subsequently giving me their valuable advice and suggestions to improve the quality of my thesis.

I am indebted to Pak Jamari, Pak Soegiyanto, and Pak Rifky for introducing me to the Engineering Design and Tribology Group, University of Diponegoro which leads to the opportunity to carry out the PhD research project at University of Twente.

I would also like to thank Nur Hidayah and Belinda for the help with many administrative matters. Not to forget, I also want to thank Adib for helping me to design a nice cover of this thesis.

And last, but certainly not least, I would like to thank my lovely wife, Farida Nur Ifada for her patience, her support, her great understanding and her unfailing love. Closest to my heart are my friends and family. Especially my parents for their never ending care and my brothers for the all the inspiring energy they provides me with.